Characterization of factors affecting synaptic transmission in *C. elegans*

Dissertation

zur Erlangung des Doktorgrades

der Naturwissenschaften

vorgelegt beim Fachbereich 14

der Johann Wolfgang Goethe-Universität

in Frankfurt am Main

von

Barbara Jánosi

aus Budapest, Ungarn

Frankfurt am Main, 2023

D30

Vom Fachbereich 14

der Johann Wolfgang Goethe-Universität als Dissertation angenommen.

Dekan: Prof. Dr. Clemens Glaubitz

Gutachter: Prof. Dr. Alexander Gottschalk, Prof. Dr. Clemens Glaubitz

Datum der Disputation: 14.12.2023

Contents

Declaration 8

Abstract 10

Zusammenfassung 12

1. Introduction 18

1.1 Neurobiology 18

1.1.1 Synaptic vesicle cycle 18

1.1.1.1 SV trafficking toward the active zone and exocytosis 19

1.1.1.2 SV endocytosis and recycling 21

1.1.1.3 The presynaptic active zone 24

1.2 *C. elegans* as a subject of study in neurobiology 27

1.2.1 *C. elegans* as a model organism 27

1.2.2 *C. elegans* nervous system 30

1.2.3 Optogenetics in *C. elegans* 32

1.2.4 Channelrhodopsin-2 (ChR2) variants 34

1.3 Objectives 36

1.3.1 ERP-1 project 36

1.3.2 RIMB-1 project 37

1.3.3 pOpsicle project 39

2. Materials and methods 41

2.1 Materials 41

2.1.1 Equipment 41

2.1.2 Consumables 43

2.1.3 Chemical substances 45

2.1.4 Buffers and Media 46

2.1.5 Kits....48
2.1.6 Enzymes....48
2.1.7 Plasmids....49
2.1.8 Oligonucleotides....49
2.1.9 Organisms....52
2.1.10 Transgenic *C. elegans* strains....52
2.1.11 Software....55
2.2 Methods....56
2.2.1 Molecular and Microbiological methods....56
2.2.1.1 Polymerase chain reaction (PCR)....56
2.2.1.2 Genomic DNA extraction of *C. elegans*....57
2.2.1.3 Site-directed mutagenesis....58
2.2.1.4 Agarose gel electrophoresis....58
2.2.1.5 DNA gel extraction....58
2.2.1.6 PCR product purification....59
2.2.1.7 DNA restriction digest....59
2.2.1.8 DNA dephosphorylation....59
2.2.1.9 DNA fragment ligation....59
2.2.1.10 Heat-shock transformation of *E. coli* cells....60
2.2.1.11 Plasmid DNA preparation....60
2.2.1.12 DNA sequencing....61
2.2.1.13 Cloning strategies....61
2.2.2 *C. elegans* methods....62
2.2.2.1 Cultivation of *C. elegans*....62
2.2.2.2 Male generation and crosses....62
2.2.2.3 Genotyping....63
2.2.2.4 Decontamination....63

2.2.2.5 Microinjection into *C. elegans* 63
2.2.2.6 *C. elegans* behavioural and pharmacological assays 65
2.2.2.7 Swimming assay 65
2.2.2.8 Contraction assay 65
2.2.2.9 Aldicarb and levamisole assays 66
2.2.3 Microscopy 66
2.2.3.1 Stereo microscopy 66
2.2.3.2 Fluorescence microscopy 66
2.2.3.2.1 Expression pattern analysis of ERP-1 and RIMB-1 67
2.2.3.2.2 Quantitative analysis of GFP::UNC-2 67
2.2.3.2.3 pOpsicle assay 68
2.2.3.3 Electronmicroscopy of *C. elegans* – performed mainly by Dr. Szi-chieh Yu 69
2.2.4 Electrophysiology of *C. elegans* – performed by Dr. Jana F. Liewald 70
2.2.5 Voltage imaging of *C. elegans* – performed by Amelie Bergs 71
2.2.6 Statistical analysis 71
3. Results 72
3.1 Characterization of synaptic vesicle recycling factors 72
3.1.1 *sad-1* 73
3.1.2 *eel-1* 74
3.1.3 *let-60* 74
3.1.4 *inx-8, inx-10* 74
3.1.5 *itsn-1* 76
3.2 A novel player in SV recycling: endophilin B cooperates with endophilin A and clathrin to promote the regeneration of SVs 79
3.2.1 ERP-1 is expressed in cholinergic motor neurons 79
3.2.2 *erp-1* mutants exhibit reduced cholinergic transmission 80
3.2.3 ERP-1 participates in the same pathway as UNC-57 83

3.2.4 Animals that lack both ERP-1 and UNC-57 are still capable of SV recycling 85

3.2.5 *chc-1* mutants have a moderate SV recycling defect.....87

3.2.6 CHC-1 has a role in the breakdown of large endosomal vesicles 88

3.2.7 The cooperation of endophilins and CHC-1 enables SV recycling.....89

3.3 New insights into a known player: RIMB-1 affects the localization of VGCCs and the excitation/inhibition balance in *C. elegans* 94

3.3.1 RIMB-1 is expressed in cholinergic and GABAergic motor neurons.....95

3.3.2 Cholinergic transmission is reduced in *rimb-1* mutants 96

3.3.3 Unexpectedly, *rimb-1* mutants exhibit increased evoked postsynaptic currents...100

3.3.4 Direct stimulation of GABAergic neurons led to decreased ePSCs in *rimb-1* mutants 102

3.3.5 Increased ePSCs of *rimb-1* mutants are gone in the absence of GABA transmission 104

3.3.6 RIMB-1 and ELKS-1 do not have redundant functions.....106

3.3.7 RIMB-1 is essential for the precise localisation of SV release 108

3.3.8 Unfastening VGCCs affects cholinergic transmission and counterweights the mutation of RIMB-1 110

3.3.9 VGCC distribution is strongly altered in animals lacking both RIMB-1 and the PDZ ligand of UNC-2 115

3.4 A new method for directly assessing synaptic vesicle fusion and recycling events 117

3.4.1 The construct of the new tool – the pOpsicle method 117

3.4.2 First microscopy results.....118

4. Discussion.....120

4.1 ERP-1 supports SV recycling at the PM and at the LV membrane in cooperation with UNC-57 and CHC-1.....120

4.2 RIMB-1 is responsible for the precise localization of VGCCs and for maintaining the excitation-inhibition balance between cholinergic and GABAergic neurons.....124

4.3 pOpsicle enables the direct visualization of SV recycling.....129

4.4 Outlook 129
References 131
List of Publications 167
Acknowledgements 168

Declaration

Except where stated otherwise by reference or acknowledgment, the work presented was generated by myself under the supervision of my advisor during my doctoral studies. All contributions from colleagues are explicitly referenced in the thesis. The material listed below was obtained in the context of collaborative research:

Figure 21: Spontaneous and evoked postsynaptic currents at the NMJ of *erp-1*, *unc-57* and *erp-1; unc-57* double mutants. Collaboration partner: Dr. Jana F. Liewald, Buchmann Institute of Molecular Life Sciences (BMLS), Goethe University, Frankfurt, Germany. Dr. Jana F. Liewald performed the experiment and analysed the data

Figure 22: Large vesicle (LV) analysis via transmission electron microscopy (TEM) in *erp-1*, *unc-57* and *erp-1; unc-57* mutants. Collaboration partner: Dr. Szi-chieh Yu, Princeton Neuroscience Institute, Princeton University, Princeton, NJ, USA. Dr. Szi-chieh Yu performed the experiment and analysed the data.

Figure 24: Large vesicle (LV) analysis in mutants lacking CHC-1 indicates a role in the breakdown of synaptic endosomes during SV recycling. Collaboration partner: Dr. Szi-chieh Yu, Princeton Neuroscience Institute, Princeton University, Princeton, NJ, USA. Dr. Szi-chieh Yu performed the experiment and analysed the data.

Figure 27: Large vesicle (LV) analysis via transmission electron microscopy (TEM) in *chc-1*, *chc-1; erp-1*, and *chc-1; unc-57* mutants. Collaboration partner: Dr. Szi-chieh Yu, Princeton Neuroscience Institute, Princeton University, Princeton, NJ, USA. Dr. Szi-chieh Yu planned the experiment and performed the experiments with the *chc-1* mutants, whereas we performed the experiments with the double mutants together.

Figure 35: *rimb-1* mutants exhibit increased evoked postsynaptic currents at the NMJ. Dr. Jana F. Liewald, Buchmann Institute of Molecular Life Sciences (BMLS), Goethe University, Frankfurt, Germany. Dr. Jana F. Liewald performed the experiment and analysed the data.

Figure 36: Photostimulation of cholinergic neurons led to reduced muscle depolarization in *rimb-1* mutants. Collaboration partner: Amelie Bergs, Buchmann Institute of Molecular Life

Sciences (BMLS), Goethe University, Frankfurt, Germany. Amelie Bergs performed the experiment and analysed the data.

Figure 38: Photostimulation of GABAergic neurons resulted in reduced postsynaptic currents in *rimb-1* mutants. Collaboration partner: Dr. Jana F. Liewald, Buchmann Institute of Molecular Life Sciences (BMLS), Goethe University, Frankfurt, Germany. Dr. Jana F. Liewald performed the experiment and analysed the data.

Figure 40: Increased ePSCs of *rimb-1* mutants are gone in *rimb-1; unc-47* double mutants. Collaboration partner: Dr. Jana F. Liewald, Buchmann Institute of Molecular Life Sciences (BMLS), Goethe University, Frankfurt, Germany. Dr. Jana F. Liewald performed the experiment and analysed the data.

Figure 42: Electron microscopy analysis of photostimulated, cholinergic synapses in *rimb-1* mutants. Collaboration partner: Dr. Szi-chieh Yu, Princeton Neuroscience Institute, Princeton University, Princeton, NJ, USA. Dr. Szi-chieh Yu performed the experiment and analysed the data, which was re-analysed by me for Figure 42, D.

Figure 46: UNC-2-ΔPDZ mutants exhibited altered synaptic transmission in electrophysiological experiments. Collaboration partner: Dr. Jana F. Liewald, Buchmann Institute of Molecular Life Sciences (BMLS), Goethe University, Frankfurt, Germany. Dr. Jana F. Liewald performed the experiment and analysed the data.

Whenever a figure, table or text is identical to a previous publication, it is stated explicitly in the thesis that copyright permission and/or co-author agreement has been obtained. The following parts of the thesis have been previously published:
Introduction - Figures: 1, 2, 3, 4, 5, 6, 7, 8.
Results - Figure: 10.
The following figures of the thesis have been published in an own article:
16, 17, 18, 19, 20, 21, 22, 23, 24, 27.
The following figures of the thesis have been published in an own preprint article:
28, 29, 30, 31, 32, 33, 34, 35, 36, 37, 38, 39, 40, 42, 43, 44, 45, 46, 47, 48.

Abstract

Synaptic transmission is a fundamental process that involves the transfer of information from a presynaptic neuron to a target cell through the release of neurotransmitters. The SV cycle is a complex series of events that enables the recycling of SVs, allowing for the sustained release of neurotransmitters. This process is mediated by a variety of proteins and enzymes, and its regulation is critical for maintaining proper synaptic function. Despite extensive research efforts, many aspects of the SV cycle and the underlying synaptic proteins remain poorly understood, highlighting the need for continued investigation into this important process. During this work, multiple aspects of synaptic transmission were studied by performing behavioural, pharmacological, optogenetic, electrophysiological and ultrastructural assays on *Caenorhabditis elegans*. First, the role of two proteins (ERP-1 and RIMB-1) were analysed in the synaptic vesicle cycle. Second, a new optogenetic tool, the pOpsicle assay was described, which enables the direct visualization of synaptic vesicle (SV) release.

Activity-dependent bulk endocytosis (ADBE) enables the endocytosis of SV membrane and proteins in a fast manner during intense stimulation, resulting in bulk endosomes (also so-called large vesicles, LVs). Recycling proteins can be characterized by its site of action, whether they act at the plasma membrane (participating at the LV formation), or at the LV membrane (participating at the SV formation). ERP-1 (the *C. elegans* ortholog of Endophilin B) was recently identified as a possible SV recycling factor, its contribution to synaptic transmission has not been analysed before. During this project the function and possible cooperation of three proteins, ERP-1, UNC-57 (the *C. elegans* ortholog of Endophilin A) and CHC-1 (the *C. elegans* ortholog clathrin heavy chain) were studied, with a special emphasis of the site of action. It has been confirmed that these proteins participate together in synaptic vesicle recycling. Endophilins (ERP-1 and UNC-57) act both at the PM and the LV level, but while UNC-57 has been identified as the main player, ERP-1 rather has a minor role and acts as a back-up protein. CHC-1 functions the LV level in the first place, but it can compensate for the loss of UNC-57 and acts as a back-up protein at the PM.

RIM-binding protein is an evolutionarily conserved active zone protein, which interacts directly with RIM and N, P/Q, as well as L-type Ca^{2+} channels. RIM-BP and RIM have redundant functions in different model organisms including *C. elegans,* however, while the loss of UNC-10 (the *C. elegans* ortholog of RIM) led to drastic behavioural defects, the loss of RIMB-1 (the *C. elegans* ortholog of RIM-BP) led only to mild phenotypes. During this work the synaptic function of RIMB-1 and its interaction with UNC-10 and UNC-2 (*C. elegans*

ortholog of the CaV2 α1 subunit) were extensively investigated. It has been shown that RIMB-1 contributes to the precise localization of VGCCs in cooperation with UNC-10. Furthermore, it has been demonstrated, that RIMB-1 plays different roles in cholinergic and GABAergic neurons, thus it contributes to maintain a proper excitation/inhibition balance.

There are numerous available assays, which enable the indirect analysis of synaptic transmission, however, a tool, that enables the direct visualization of SV release, is highly desired. pOpsicle is a method which combines the optogenetic stimulation of cholinergic neurons with real-time visualization of SV release. A pH-sensitive fluorescence protein, pHuji, was inserted into the second intravesicular loop of the synaptic vesicle membrane protein, synaptogyrin (SNG-1). The fluorescence of pHuji is quenched inside the vesicles, but once they are released, the pH increases and pHuji can be detected. pOpsicle enables not only the direct visualization of SV exo-, and endocytosis events, but also the identification of putative SV recycling proteins.

Zusammenfassung

Synaptische Übertragung ermöglicht die Kommunikation zwischen einem präsynaptischen Neuron und einer postsynaptischen Zielzelle. Bei chemischen Synapsen wird das Signal, das als präsynaptische Aktionspotential ankommt, in ein chemisches Signal umgewandelt, die Erregungsübertragung erfolgt über Transmitter. Das Aktionspoteintial depolarisiert das synaptische Endknöpfchen, spannungsgesteuerte Calciumkanäle öffnen und Ca^{2+} Ionen strömen ein. Dies hat zur Folge, dass die mit Neurotransmittern gefüllten synaptischen Vesikel (SV) mit der präsynaptischen Membran verschmelzen. Der freigesetzte Transmitter tritt in den synaptischen Spalt ein und bindet an Rezeptoren der Postsynapse. Die de-novo Synthese von synaptischen Vesikeln ist nicht schnell genung, um den hohen Bedarf zu unterstützen. Daher werden Vesikel durch den synaptischen Vesikelzyklus regeneriert.

Die Freisetzung von Neurotransmittern erfolgt in der präsynaptischen aktiven Zone (AZ). AZs variieren morphologisch zwischen verschiedenen Arten: zentrale Synapsen von Wirbeltieren sind typischerweise scheibenförmig, während einige sensorische Neuronen von Wirbeltieren Bandsynapsen mit einem großen AZ und einem elektronendichten synaptischen Band bilden. Die markanten elektronendichten Projektionen in den AZs von *Drosophila* sind T-Balken, während der zentrale Teil der *C. elegans* AZ die sogenannte „dense projektion“ (DP) ist. All diese bestehen aus evolutionär konservierten Proteinen. Der Kern der aktiven Zone wird typischerweise von fünf von diesen Proteinen gebildet, nämlich RIM, Munc13, RIM-BP, liprin−α und ELKS. Diese Proteine sind unter anderem am Docking und Priming der Vesikel oder an der Rekrutierung von Ca^{2+}-Kanälen beteiligt.

Der Fadenwurm *Caenorhabditis elegans* hat ein relativ kleines, aber gut charakterisiertes Nervensystem, das ein hervorragendes Modell zur Untersuchung neuronaler Schaltkreise und Verhaltensweisen ist. Der erwachsene *C. elegans* Hermaphrodite ist etwa 1 mm lang und besteht aus 959 somatischen Zellen, von denen genau 302 Neuronen sind. Das Tier hat einen transparenten Körper, der nicht nur die Visualisierung einzelner Zellen (mit einem Lichtmikroskop) oder fluoreszierender Marker (mit einem Fluoreszenzmikroskop) sondern auch die optogenetische Manipulation ermöglicht.

Optogenetik ermöglicht die nicht-invasive Manipulation von Neuronen. Lichtempfindliche Proteine wie Ionenkanäle, Pumpen oder Enzyme können durch Lichtzufuhr aktiviert werden, wodurch die Aktivität von Neuronen, die diese Proteine exprimieren, durch Licht gesteuert werden kann. *C. elegans* war der erste vielzellige Organismus, dessen Verhalten durch

Optogenetik kontrolliert werden konnte. Channelrhodopsin-2 war das erste lichtempfindliche Protein, das erfolgreich in *C. elegans* exprimiert wurde.

Channelrhodopsine sind Sieben-Transmembran (7-TM)-Helixproteine, die das Chromophor all-trans-Retinal binden. Channelrhodopsin-2 (ChR2) ist ein lichtgesteuerter, nicht selektiver Kationenkanal, der für mono- (Na^+, K^+, H^+) und divalente Kationen (Ca^{2+}) durchlässig ist. ChR2 kann durch blaues Licht schnell gesteuert werden: Es kann durch Lichtbeleuchtung geöffnet werden, während es sich im Dunkeln schließt. Das Anregungsspektrum von ChR2 ähnelt dem von GFP, sein Anregungspeak liegt bei 460 nm.

Die hier vorliegende Arbeit charakterisiert Mechanismen und insbesondere neue Proteine, die das Recycling von Synaptischen Vesikeln in neuronalen Endköpfen ermöglichen. Die Rolle von zwei Proteinen beim SV-Recycling, ERP-1 und RIMB-1 wurde unter Verwendung der cholinergen neuromuskulären Verbindungen des Nematoden *C. elegans* analysiert. Weiterhin, ein optogenetisches Instrument, der sogenannte pOpsicle-Assay, wurde beschrieben, der neben der direkten Visualisierung von SV-Exo- und Endozytoseereignissen auch die Identifizierung neuer SV-Recycling-Proteine ermöglicht.

ERP-1 (das *C. elegans*-Ortholog von Endophilin B), wurde kürzlich als potenzieller SV Recyclingfaktor identifiziert, sein möglicher Beitrag zur SV-Endozytose wurde zuvor nicht untersucht. Bei Wirbeltieren gibt es zwei Endophilin-Varianten. Das andere, Endophilin-A (UNC-57 in *C. elegans*), spielt eine wesentliche Rolle bei der SV-Endozytose und Recycling: es rekrutiert andere essentielle Proteine und hat eine membranbiegende Funktion. Clathrin (schwere Kette von Clathrin, kodiert durch *chc-1* in *C. elegans*) spielt eine Rolle bei der Clathrin-vermittelten Endozytose und auch bei der ultraschnellen Endozytose, wo es nicht an der Plasmamembran (PM), sondern auf der Ebene der Endosomen eine Rolle spielt und unterstützt dadurch die Regeneration von SVs.

Die aktivitätsabhängige Bulk-Endozytose (ADBE) ermöglicht es, SV-Membran und -Proteine während intensiver Stimulation schnell wiederzugewinnen, was zu Bulk-Endosomen führt (auch als "large Vesikel", LVs bezeichnet), aus denen SVs durch ein Abknospungsprozess reformiert werden. Während der Arbeit wurde die Funktion und ein mögliches Zusammenwirken von UNC-57, ERP-1 und CHC-1 untersucht, mit besonderem Augenmerk auf den Wirkort (an der PM oder an der Membran der LVs) dieser Proteine. Dazu wurden verhaltens-, pharmakologische, optogenetische, elektrophysiologische und ultrastrukturelle Assays mit *C. elegans* durchgeführt.

UNC-57 wirkt an der PM und an der LV-Membran, während CHC-1 in Anwesenheit von UNC-57 an der LV-Membran wirkt. Sobald UNC-57 fehlt, kann CHC-1 seinen Verlust auch

am PM kompensieren. ERP-1 spielt im Vergleich zu den beiden anderen Proteinen eine untergeordnete Rolle, ermöglicht jedoch ein basales SV-Recycling, auch wenn sowohl UNC-57 als auch CHC-1 fehlen, und es funktioniert sowohl an der PM- als auch an der LV-Membran. Durch das Zusammenwirken dieser Proteine entsteht ein robustes System: Fehlen zwei Proteine, kann das dritte dies kompensieren und so eine ausreichende synaptische Aktivität und ein Überleben ermöglichen.

Das evolutionär konservierte Protein der aktiven Zone, RIM-binding protein (RIM-BP), besteht aus drei „Src-homology type III“ (SH3) und drei „Fibronectin type III“ (FN3) Domänen. SH3-Domänen interagieren direkt mit RIM und mit N-, P/Q- und auch L-Typ-Ca^{2+}-Kanälen. Es ist bekannt, dass der Verlust von UNC-10 (das *C. elegans*-Homolog von RIM) zu drastischen Verhaltensstörungen führt. Im Gegensatz dazu führte der Verlust von RIMB-1 (das *C. elegans*-Homolog von RIM-BP) nur zu milden Phänotypen, jedoch scheinen RIMB-1 und UNC-10 auch in *C. elegans* eine redundante Rolle zu spielen. Ähnlich wie frühere Ergebnisse von anderen Modellorganismen, spielt RIMB-1 auch bei der Clusterbildung von spannungsgesteuerten Calciumkanälen (VGCCs, voltage-gated calcium channels) in *C. elegans* eine Rolle; UNC-2 (der *C. elegans*-Ortholog von CACNA1B – die spannungsabhängige Calciumkanal-Untereinheit Alpha-1B) zeigte eine veränderte, diffusere Verteilung an den präsynaptischen Stellen in *rimb-1; unc-10* Doppelmutanten. Während dieses Projekts wurde die synaptische Funktion von RIMB-1 und seine Interaktion mit UNC-10 und UNC-2 durch verhaltens-, pharmakologische, optogenetische, elektrophysiologische und ultrastrukturelle Assays unter Verwendung von *C. elegans* untersucht.

rimb-1-Mutanten zeigten leichte Verhaltensfehler in Schwimm- und Aldicarb-Assays, ähnlich den zuvor vorgestellten Ergebnissen, und einen leichten Recycling-Phänotyp im Kontraktionsassay. Diese cholinergen Defizite waren in den elektrophysiologischen Experimenten nicht erkennbar, wo die cholinerge Stimulation durch ChR2 zu einer erhöhten Übertragung in *rimb-1*-Mutanten führte. Reduzierte Depolarisationswerte von *rimb-1*-Mutanten in der Muskelspannungsbildgebung konnten jedoch unsere bisherige Interpretation, basierend auf den Verhaltensassays bestätigen. Die gesamte Acetylcholin (ACh)-Freisetzung von *rimb-1*-Mutanten war nicht reduziert, sondern verzögert und höchstwahrscheinlich nicht so synchron, wie es erforderlich ist, um Muskelströme hervorzurufen. Um dies auszugleichen, wurde eine erhöhte Menge an ACh freigesetzt, aber aufgrund des ungenauen Timings war die muskuläre Depolarisation unwirksam, was durch die verringerte postsynaptische Muskelkontraktion von *rimb-1*-Mutanten gezeigt werden konnte.

Dies war bei *rimb-1*-Mutanten ohne GABA, bei denen die ACh-Freisetzung nicht so hochreguliert war, wie bei *rimb-1*-Einzelmutanten, nicht der Fall. Darüber hinaus führte die direkte Stimulation von GABAergen Neuronen von *rimb-1*-Mutanten zu keinen Verhaltensstörungen, jedoch elektrophysiologische Messungen zeigten, dass diese Tiere reduzierten evozierten postsynaptischen Strom (ePSCs-evoked postsynaptic currents) produzierten und die SV-Freisetzung verzögert war. Die vergrößerten cholinergen ePSCs von *rimb-1*-Mutanten repräsentieren höchstwahrscheinlich eine homöostatische Kompensationsreaktion; *rimb-1*-Mutanten, denen GABA fehlt, besitzen einen geringeren homöostatischen Antrieb, das cholinerge-GABAerge System durch Hochregulierung der ACh-Freisetzung auszugleichen, daher sind die erhöhten Ströme in diesen Mutanten verschwunden. All dies weist darauf hin, dass RIMB-1 unterschiedliche Rollen in GABAergen und cholinergen Synapsen spielt und dass dieses Protein zum normalen Erregungs-/Hemmungsgleichgewicht an der neuromuskulären Synapse von *C. elegans* beiträgt.

Nicht nur die elektrophysiologischen Experimente von *rimb-1*-Mutanten, sondern auch die Ultrastrukturanalyse deuteten auf eine veränderte SV-Übertragung bei diesen Tieren hin. Angedockte SVs zeigten eine veränderte Verteilung in *rimb-1*-Mutanten; Diese waren nicht nur in unmittelbarer Nähe der dichten Projektion sichtbar, sondern auch in größerer Entfernung. Vergleich der mit/ohne ATR aufgezogenen Tiere, außerdem größere evozierte Ströme weisen darauf hin, dass diese distalen SVs ebenfalls freigesetzt wurden; Die optogenetische Stimulation ist viel stärker als eine physiologische und führt zu größeren Ca^{2+}-Domänen mit der Möglichkeit, mehr angedockte SVs zu erreichen.

Während dieses Projekts haben wir *rimb-1*-Mutanten mit *rimb-1; unc-10* Doppelmutanten verglichen. Die Ergebnisse zeigten, dass RIMB-1 und UNC-10 kooperieren, aber da die Phänotypen von *rimb-1; unc-10*-Doppelmutanten von der *unc-10*-Mutation dominiert werden, die Analyse dieser Mutanten nicht geeignet ist, die reine Wirkung der unverankerten VGCCs zu untersuchen; daher wurde hierfür eine umgekehrte Strategie verwendet. RIM bindet über seine PDZ-Domäne an die C-Termini von VGCCs. Die Analyse von *unc-2*-Mutanten mit einer C-terminalen Deletion (die letzten zehn Aminosäuren – die Stelle des Liganden der PDZ-Domäne – wurden gelöscht: von nun an als UNC-2-ΔPDZ -Mutanten bezeichnet) ermöglichte uns die Untersuchung der Beitrag von UNC-10 zur Rekrutierung von VGCCs, wodurch UNC-10 vollständig intakt bleibt.

UNC-2-ΔPDZ-Mutanten zeigten teils schwächeren (Aldicarb-Assay), teils stärkeren (Kontraktions-Assay) Phänotyp als *rimb-1*-Mutanten, jedoch wirkten sich die Phänotypen bei

Doppelmutanten in fast allen Experimenten entgegen. Diese ziemlich unerwarteten Ergebnisse können durch redundante Proteinwechselwirkungen erklärt werden; es ist durchaus sehr wahrscheinlich, dass UNC-2 durch mehr als zwei (RIMB-1 und UNC-10) Proteine gebunden ist.

In Mutanten, denen sowohl der RIMB-1- als auch der UNC-2-PDZ-Ligand fehlte, war die Fluoreszenzintensität von GFP::UNC-2 signifikant verringert, während einzelne Mutanten Wildtyp-ähnliche Intensitäten zeigten. Dies zeigt, dass bei Mutanten, denen sowohl RIMB-1- als auch UNC-2-PDZ-Ligand fehlt, die VGCC-Verteilung tatsächlich verändert ist, während dieser Effekt bei Mutanten, denen nur RIMB-1- oder UNC-2-PDZ-Ligand fehlt, nicht so deutlich ist. Daher sind RIMB-1 und der UNC-2-PDZ-Ligand sehr wichtige Akteure und zusammen für die korrekte Anbindung von VGCC-Kanälen verantwortlich.

Zusammenfassend wurde in diesem Projekt gezeigt, dass RIMB-1 – in Zusammenarbeit mit UNC-10 – zur genauen Lokalisierung der VGCCs an der Präsynapse in *C. elegans* beiträgt. Darüber hinaus wurde gezeigt, dass RIMB-1 unterschiedliche Rollen in cholinergen und GABAergen Neuronen spielt und damit ein angemessenes Erregungs-/Hemmungsgleichgewicht unterstützt.

SV-Recyclingproteine können durch indirekte Assays wie Ca^{2+}-Imaging oder Kontraktionsassay identifiziert werden, jedoch ist die Interpretation der Ergebnisse oft nicht eindeutig und es sind weitere Experimente erforderlich, um die Funktion der Proteine zu bestätigen. Zeitaufwändigere Experimente, wie elektrophysiologische oder elektronenmikroskopische Assays, ermöglichen genauere Schlussfolgerungen, allerdings ist es nicht realistisch, eine Hochdurchsatzanalyse mit diesen Methoden durchzuführen. Daher wird ein Assay benötigt, der die direkte Visualisierung von SV-Exo- und Endozytose ermöglicht. Während dieser Arbeit wurde eine neue Methode, das sogenannte pOpsicle eingeführt, das die optogenetische Stimulation cholinerger Neuronen mit der Echtzeit-Visualisierung der SV-Freisetzung kombiniert. Dazu wurde ein pH-sensitives Fluoreszenzprotein, pHuji, in die zweite intravesikuläre Schleife des synaptischen Vesikelmembranproteins Synaptogyrin (SNG-1) eingefügt. Ruhende Vesikel haben einen pH-Wert von 5,5, während der extrazelluläre pH-Wert mit pH 7,4 höher ist. Die Fluoreszenz von pHuji wird bei pH 5,5 gequencht, aber sobald die Vesikel freigesetzt werden und der pH-Wert ansteigt, kann pHuji detektiert werden. Nach SV-Endozytose werden die Vesikel schnell wieder angesäuert, wodurch die Fluoreszenz wieder gequencht wird.

Der Nachweis spontaner Freisetzungsereignisse war nicht möglich, daher wurde die SV-Freisetzungsvisualisierung von pHuji mit der Stimulation cholinerger Neuronen kombiniert.

Dafür wurde ChR2 in cholinergen Neuronen exprimiert. ChR2 kann über blaues Licht stimuliert werden; durch kontinuierliche Visualisierung von pHuji-, SV-Exo- und Endozytoseereignissen können während und nach der Blaulichtstimulation erkannt werden. Durch die Analyse des Fluoreszenzsignals von pHuji einige Sekunden lang nach der Blaulichtstimulation, können SV-Endozytose und -Recycling untersucht werden und SV-Recycling-Mutanten können durch eine veränderte Fluoreszenzspur identifiziert werden; somit ermöglicht das pOpsicle-Tool die Identifizierung neuartiger SV-Recyclingproteine auf direktem Weg.

1. Introduction

1.1 Neurobiology

1.1.1 Synaptic vesicle cycle

Synaptic transmission enables the communication between a presynaptic neuron and a postsynaptic target cell. During chemical synaptic transmission, neurotransmitter-filled synaptic vesicles (SVs) fuse with the presynaptic membrane. The released neurotransmitter enters the synaptic cleft and binds to the postsynaptic receptors. The *de novo* synthesis of SVs would not be fast enough to support the high demand of neurotransmitter-filled SVs, thus, vesicles are reconstituted through the synaptic vesicle cycle (Figure 1) (Chanaday et al., 2019; Südhof, 2004). At the beginning of the cycle, SVs are filled with neurotransmitters. Filled SVs approach the presynaptic active zone (the site of neurotransmitter release) and after docking and priming, neurotransmitters are released. This is followed by the endocytosis and recycling of the SVs (Südhof, 2004).

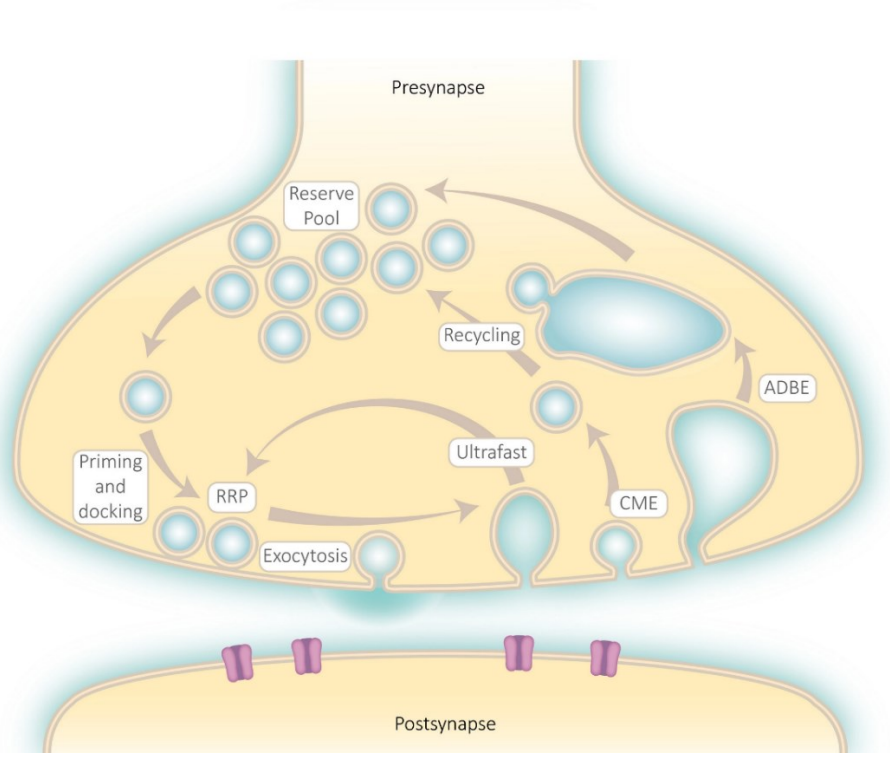

Figure 1: The synaptic vesicle cycle (from: (Bonnycastle et al., 2021)). During synaptic activity, synaptic vesicles (SVs) from the reserve pool are mobilized and approach the presynaptic membrane. Once docked and primed, these vesicles become fusion-competent and can be immediately released upon Ca^{2+} influx, which is defined as the readily releasable pool (RRP). Upon exocytosis, neurotransmitters enter the synaptic cleft and bind to postsynaptic receptors. This is followed by the endocytosis of the SV membrane and proteins, and the recycling of the SVs can occur via different pathways (such as ultrafast endocytosis, clathrin-mediated endocytosis, and activity-dependent bulk endocytosis).

1.1.1.1 SV trafficking toward the active zone and exocytosis

SVs are filled with neurotransmitter through active transport. A vesicular ATPase with proton pump activity creates an electrochemical gradient, which drives the uptake of neurotransmitters (Maycox et al., 1988). Dependent on the state of releasability, filled SVs can be classified into three distinct pools, the cooperation of which is crucial for fast and repeated rounds of neurotransmission. These are the readily releasable pool (RRP), the recycling pool and the reserve pool (Rizzoli & Betz, 2005). SVs of the RRP are already docked and primed, thus when an action potential arrives at the presynaptic nerve terminal, these can be released immediately (Holderith et al., 2012). For a constant availability of releasable SVs, the RRP needs to be replenished (Guo et al., 2015). For this, dependent of the strength of the stimulation, SVs of the recycling (moderate stimulation) or the reserve pool (intense stimulation) can be used (Rizzoli & Betz, 2005). SV clusters and vesicle pool turnover is regulated by multiple proteins. One of these is synapsin, a protein which is associated with SVs in a phosphorylation-dependent manner (Chi et al., 2001). Synapsin cooperates with the actin cytoskeleton and clusters SVs maintaining the reserve pool (Bloom et al., 2003; De Camilli et al., 1983), but regulates SV clustering also through other protein interactions (Atias et al., 2019; Giovedì et al., 2004; Pavlos & Jahn, 2011).

Filled SVs approach, and dock to, the active zone (Figure 2). Next, SVs are primed to fusion competence, which is controlled by the cooperation of several distinct proteins. Three crucial members of these are the SNARE proteins; synaptobrevin/VAMP (a SV associated membrane protein), syntaxin and SNAP-25 (presynaptic membrane proteins) (Söllner, Whiteheart, et al., 1993), which together form the SNARE complex. To support the proper assembly of this complex, other proteins, such as Munc18 or Munc13, are required. Munc18 is responsible for blocking SNARE formation by binding syntaxin (Burkhardt et al., 2008). Munc13 supports the proper local protein configuration of syntaxin and synaptobrevin, furthermore it cooperates with Munc18 promoting a proper syntaxin/SNAP-25 subconfiguration (Y. Lai et al., 2017). The synaptic core complex forms an unstable intermediate, where the SV and presynaptic membranes are pulled close together but are not fused yet. In the next step a fusion pore is formed (Südhof, 2004). Once the complex is assembled, a small cytosolic protein, complexin, also binds to it (McMahon et al., 1995) activating the SNARE complex into a metastable state (Tang et al., 2006).

The arrival of an action potential leads to the depolarization of the presynaptic nerve terminal. This is followed by the opening of voltage gated Ca^{2+} channels which leads to local Ca^{2+}

concentration increase, triggering fast SV release. Since the assembly of the SNARE complex itself is not Ca^{2+} sensitive, an additional Ca^{2+} sensor, synaptotagmin is required (Geppert et al., 1994). Synaptotagmins are SV membrane proteins with two cytoplasmic C2 (Ca^{2+} binding) domains (Perin et al., 1990), which act as an inhibitor of membrane fusion in the absence of Ca^{2+} (Söllner, Bennett, et al., 1993). Upon Ca^{2+} binding, this inhibition releases and synaptotagmin further supports the fusion by active membrane remodelling (Brunger et al., 2018).

Another important regulator of SV exocytosis is Rab3. This protein has a GTP and a GDP bound state: it is localized on the SVs in its active, GTP-bound state, whereas following Ca^{2+}-influx and GTP hydrolysis, it dissociates from the SV membrane in its GDP-bound form (von Mollard et al., 1991). Its GDP-bound state binds to other effector proteins such as RIM (Rab3-interacting molecule), participating at the formation of the docking complex (Y. Wang et al., 1997). The GTP hydrolysis is catalysed by the Rab-3 GAP, which is localized also on the SVs and binds to synaptotagmin, as long as Ca^{2+} is not present (Cheng et al., 2015). Ca^{2+} influx dissociates synaptotagmin and Rab-3 GAP, which is followed by GTP hydrolysis and the complete disassembly of the docking complex. Finally, Rab3 and Rab3 effectors can be recycled (Y. Wang et al., 1997, 2000).

For the disassembly of the SNARE complex, first, alpha-SNAP displaces synaptotagmin and another protein, NSF, binds to the alpha-SNAP-SNARE complex. NSF possesses ATPase activity; ATP hydrolysis dissociates the alpha-SNAP-SNARE complex and the components can be recycled (Söllner, Bennett, et al., 1993).

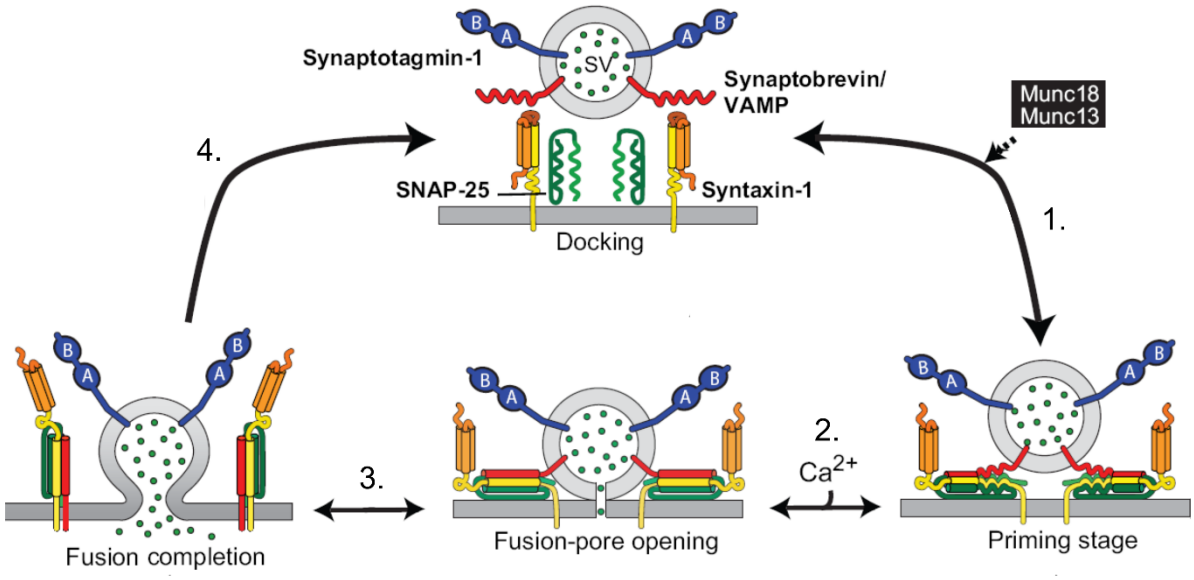

Figure 2: Model of synaptic vesicle exocytosis (modified from: (Pang & Südhof, 2010)). Synaptic vesicles are docked to the presynaptic active zone. SNARE-complex assembly and priming is supported by Munc-18, Munc-

13 and RIM (step 1.). Ca^{2+}-influx is followed by fusion-pore opening (step 2). Once the fusion is completed, neurotransmitter can be released (step 3.). After the disassembly of SNARE-complex, proteins can be recycled, which can be followed by a new round of SV exocytosis.

1.1.1.2 SV endocytosis and recycling

During SV exocytosis, the SV membrane fuses with the presynaptic membrane. This excess membrane, as well as the integral SV proteins, need to be retrieved via endocytosis which is followed by subsequent steps that enable SV recycling. There are, at least, four different SV recycling pathways: clathrin-mediated endocytosis (CME), "kiss-and-run" endocytosis, bulk endocytosis and ultrafast endocytosis (Figure 3) (Chanaday et al., 2019).

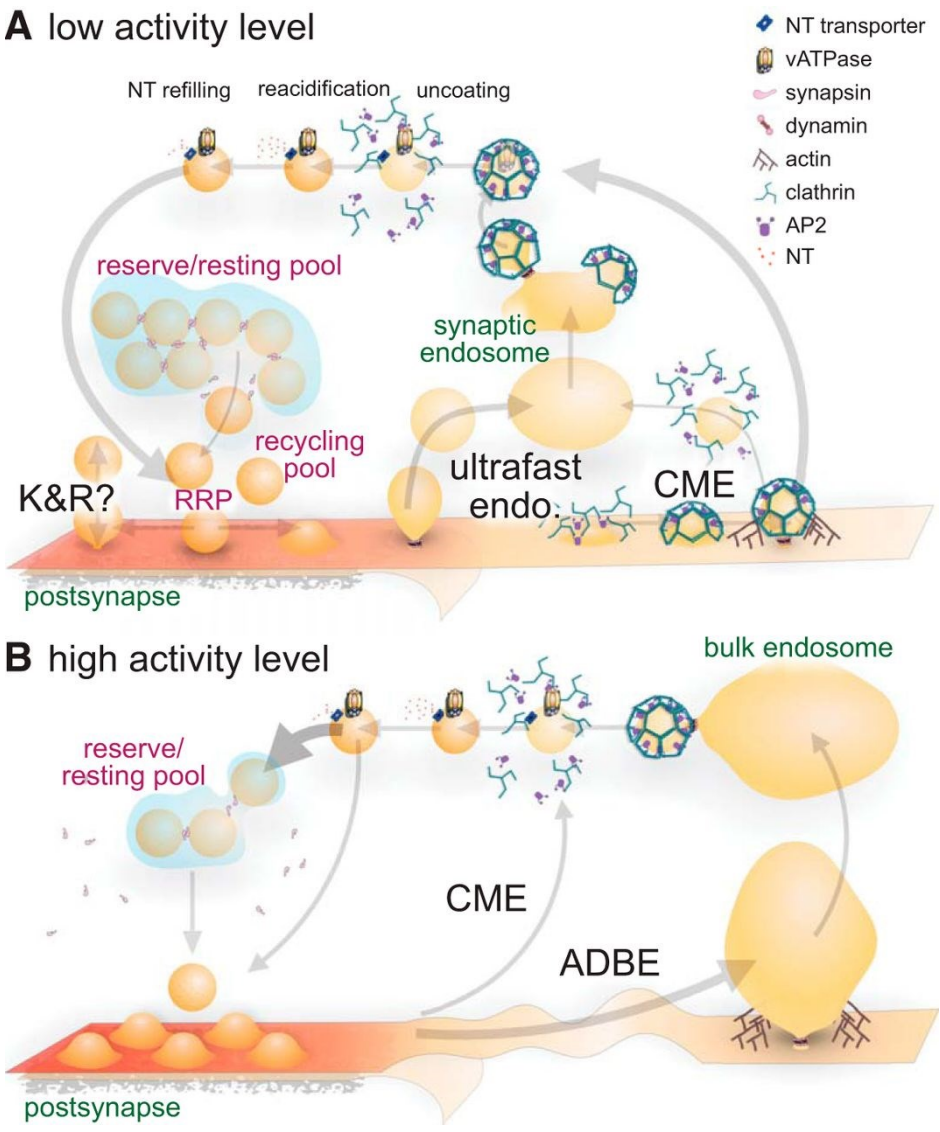

Figure 3: SV cycle and different ways of SV recycling (from: (Chanaday et al., 2019)). A, At low activity levels, vesicles of the RRP are released at the active zone. SV membrane and proteins can be retrieved via 1, kiss-and-run (K&R) pathway (although this pathway is highly controversial), via 2, ultrafast endocytosis or under certain

circumstances via 3, clathrin mediated endocytosis (CME). Vesicles retrieved by ultrafast endocytosis fuse with synaptic endosomes, from which SVs are reformed via clathrin-dependent budding. **B,** At high activity level, numerous vesicles, also directly from the reserve pool are released. For the recycling, the activity dependent bulk endocytosis (ADBE) pathway is used, vesicles are reformed via clathrin-dependent budding. **A, & B,** All clathrin-coated vesicles are subsequently uncoated, reacidified (via the vATPase) and refilled with neurotransmitter (NT).

Clathrin-mediated endocytosis (CME) was first described in classic experiments at the frog neuromuscular junction (Heuser & Reese, 1973). In these experiments, clathrin-coated vesicles were visualized at the periactive zone of the plasma membrane. The "kiss-and-run" pathway was described around the same time under similar experimental conditions, when clear, uncoated, partly internalized vesicles were identified directly at the active zone (Ceccarelli et al., 1973). A few years later large, uncoated endosomal structures were visualized at the pre-synapse, in response to strong stimulation; bulk endocytosis was identified (T. M. Miller & Heuser, 1984). Ultrafast endocytosis was described recently, when following a single stimulation, rapid SV endocytosis was observed (Watanabe, Liu, et al., 2013; Watanabe, Rost, et al., 2013).

CME is the most characterized recycling pathway, which requires the so-called clathrin-associated proteins and, in average, 20-30 s time after stimulation (Saheki & De Camilli, 2012). The inner layer of the clathrin coat is formed by adaptor proteins such as AP-2 (Bonifacino & Traub, 2003) and AP180 (Morgan et al., 2000), whereas the outer layer is formed by clathrin. Once the clathrin-coat is fully assembled, proteins such as synaptojanin (McPherson et al., 1996) and endophilin (Ringstad et al., 1999) are recruited at the neck of the endocytosed vesicles and regulate SV fission and uncoating of vesicles. For the vesicle scission another protein, the GTPase dynamin is required (Hinshaw & Schmid, 1995). This is followed by the shedding of the coat proteins, which finally results uncoated, regenerated vesicles (Saheki & De Camilli, 2012).

Exocytosed SVs reconstituted via CME are "full-collapsed" upon fusion. On the contrary, during "kiss-and-run" type exo/endocytosis, the SV membrane is completely retained, thus, SVs can be reused without any molecular sorting (Saheki & De Camilli, 2012). This recycling pathway is highly controversial, however, numerous indirect evidence suggest its existence. These are based on incomplete discharge of FM dyes (Aravanis et al., 2003; Petrov et al., 2022) and of a combination of large vs. small dyes (Wen et al., 2017), capacitance recordings of giant synapses (He et al., 2006) and tracking of individual SVs labelled with quantum dots (Qin et al., 2019; Q. Zhang et al., 2009). The time constant of this type of endocytosis is 1-10 s (Rizzoli & Jahn, 2007). Several years ago, capacitance measurements described very fast endocytic

events (Sun et al., 2002) and this type of evidence has also been used to prove the existence of the "kiss-and-run" pathway. However, novel techniques in electron microscopy allowed to identify another recycling pathway: the ultrafast endocytosis.

Ultrafast endocytosis was described recently in *C. elegans* and cultured murine hippocampal neurons (Watanabe, Liu, et al., 2013; Watanabe, Rost, et al., 2013). In these studies, mild stimulation was coupled with physiological temperature and rapid freezing strategy, which enabled to capture endocytic events within 50-1000 ms after stimulation. The molecular machinery is not completely discovered yet, but it is known that the polymerization of actin is essential (Watanabe, Rost, et al., 2013), furthermore synaptojanin and endophilin are responsible for the neck formation and dynamin is required for the fission of the vesicle at the plasma membrane (Watanabe et al., 2018). These endocytic vesicles fuse and form large synaptic endosomes. Synaptic vesicles are regenerated from these large vesicles with the help of synaptojanin and endophilin in a clathrin-dependent way (Watanabe et al., 2014, 2018). Upon prolonged, intense stimulation numerous SVs are released, thus the surface of the pre-synapse grows immensely and the excess plasma membrane needs to be retrieved rapidly through bulk endocytosis (Clayton et al., 2008). This results in large (100-500 nm) bulk endosomes (also termed 'large vesicles', LVs) (Chanaday et al., 2019; Kittelmann et al., 2013), from which SVs are then reproduced. The process is rather fast; bulk endosome formation takes about 1-2 seconds, whereas its disintegration is complete within 8-10 s (Kittelmann et al., 2013; Teng et al., 2007). Similar to ultrafast endocytosis, polymerized actin is essential for bulk endocytosis as well (X.-S. Wu et al., 2016). Furthermore, endophilin, synaptojanin and dynamin are required for the endocytosis and also for the resolution of the LVs (Kittelmann et al., 2013).

To summarize, SVs can be recycled via distinct pathways, dependent on the temperature, stimulus intensity and synapse type (Chanaday et al., 2019). Whereas according to the classic view, CME was the major recycling pathway, currently it seems to be more likely that SV endocytosis predominantly occurs via clathrin-independent pathways, as long as samples are kept at physiological temperatures. However, clathrin and clathrin-associated proteins play an essential role beyond the endocytosis at the plasma membrane; they participate at the resolution of synaptic endosomes (Chanaday et al., 2019; Gan & Watanabe, 2018). SV recycling is more complex, than thought before and so far, a lot of questions remain unanswered. Novel techniques such as 'flash-and-freeze' electron microscopy (Watanabe, Liu, et al., 2013) enable to analyse the synaptic ultrastructure directly after stimulation. The discovery of the pH sensitive fluorescence proteins, such as pHluorin (Miesenböck et al., 1998), enable to

investigate SV exocytosis *in vivo* (Ventimiglia & Bargmann, 2017), under near physiological conditions. These and other strategies help to unravel the molecular mechanisms of SV recycling, to which I also aimed to contribute to, with this work.

1.1.1.3 The presynaptic active zone

Neurotransmitter release occurs at the presynaptic active zone (AZ). AZs vary morphologically among different species: central synapses of vertebrates are typically disc-shaped, whereas some sensory neurons of vertebrates form ribbon synapses with a large AZ and an electron-dense synaptic ribbon. T-bars are the prominent electron-dense projections in the AZs of *Drosophila*, while the central part of the *C. elegans* AZ is the so-called dense projection (DP) (Ackermann et al., 2015). All of these are composed of evolutionarily conserved proteins. The core of the active zone is formed typically by five of them, which are RIM, Munc13, RIM-BP, liprin-α and ELKS (Figure 4). These proteins participate besides others in the docking and priming of the vesicles or in Ca^{2+} channel recruiting (Südhof, 2012).

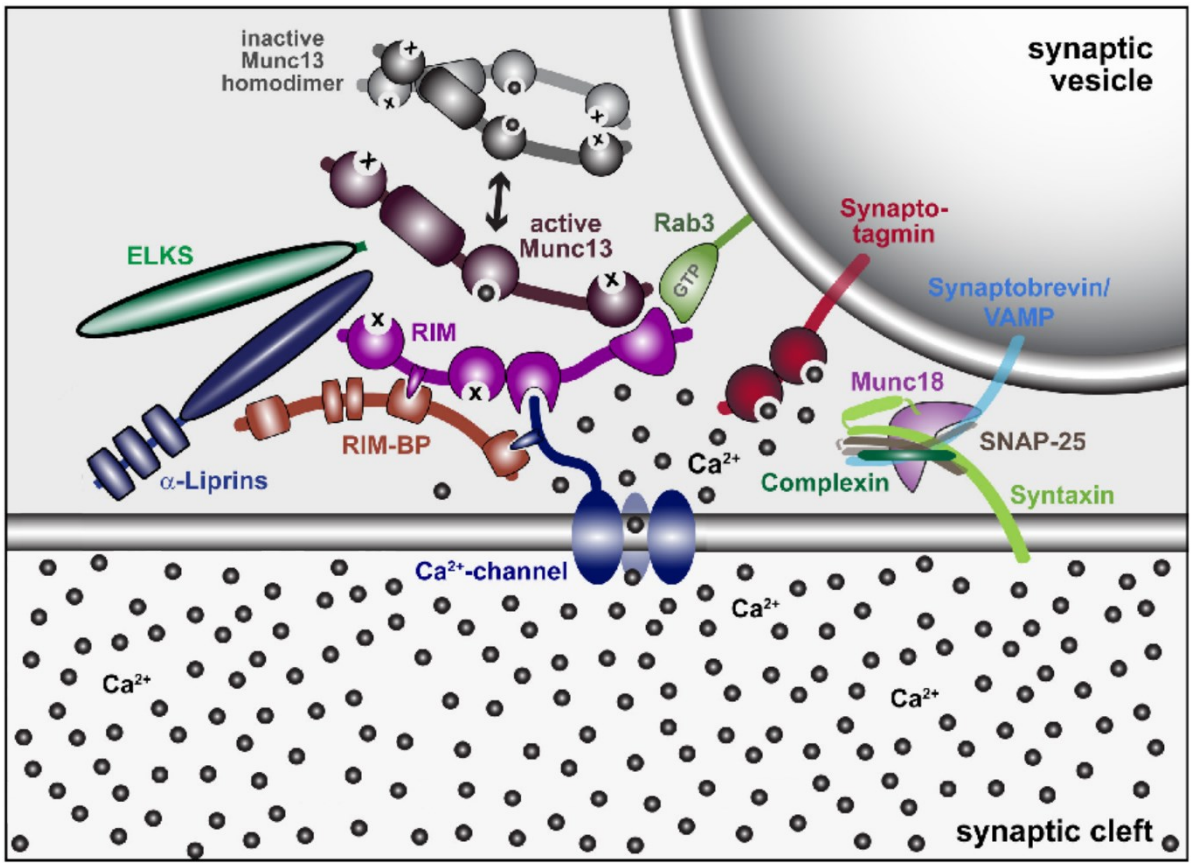

Figure 4: Model of the presynaptic active zone (modified from: (Südhof, 2012)). Depicted are the five core proteins (RIM, Munc13, RIM-BP, liprin–α and ELKS) of the active zone, a docked SV (with the SV membrane

associated Rab3 protein and the SV membrane proteins synaptotagmin and synaptobrevin) furthermore proteins of the SNARE complex and a voltage-gated Ca^{2+}-channel (VGCC).

RIM (short of Rab3 interacting molecule (Y. Wang et al., 1997)) consist of an N-terminal zinc-finger domain surrounded by α helices, a central PDZ domain and two C-terminal C2 domains with a prolin-rich sequence between them (Y. Wang & Südhof, 2003). RIM has a crucial role in SV docking and priming (Schoch et al., 2002) furthermore in Ca^{2+} channel recruiting (Kaeser et al., 2011). The zinc-finger domain binds to Munc13 (Betz et al., 2001), whereas the α helices bind to Rab3 (Y. Wang et al., 1997), forming a tripartite complex with an important role in SV priming (Dulubova et al., 2005). The central PDZ domain binds to ELKS (Ohtsuka et al., 2002; Y. Wang et al., 2002) and also to N and P/Q-type Ca^{2+} channels (Kaeser et al., 2011). The prolin-rich sequence of RIM directly interacts with the second SH3 domain of RIM-BP (Y. Wang et al., 2000), and the third SH3 domain of RIM-BP also binds to the voltage-gated Ca^{2+} channels (Hibino et al., 2002), forming a threepartite complex responsible for Ca^{2+} channel recruiting to the AZ. The C2 domains associate with synaptotagmin, SNAP-25, N-type Ca^{2+} channels (Coppola et al., 2001) and α-liprin (Schoch et al., 2002), further pointing out the importance of RIM in SV transmission.

RIM-BP consists of three central FN3 (fibronectin III) domains surrounded by three (one central and two C terminal) SH3 domains (Y. Wang et al., 2000). As already mentioned above, its SH3 domains directly interact with RIM (Y. Wang et al., 2000) as well as with N, P/Q and also L-type Ca^{2+} channels (Hibino et al., 2002). RIM-BP has an essential role in the coupling between Ca^{2+} channels and SV exocytosis (Acuna et al., 2015). It has been also shown that RIM and RIM-BP are redundant organizers of the AZ. In mutants lacking both proteins not only Ca^{2+} channel anchoring, and docking and priming of SVs was impaired but also postsynaptic specializations were affected (Acuna et al., 2016). RIM-BP seems to have a role in the homeostatic modulation of SV release (Müller et al., 2015), in the replenishment of the RRP (Krinner et al., 2017) and also in SV guidance toward release sites (Petzoldt et al., 2020).

UNC-13 was discovered first in *C. elegans* (Maruyama & Brenner, 1991) and its mammalian orthologue, Munc13 was later identified as an important factor of SV priming (Augustin et al., 1999). In total, there are five *munc-13* genes in mammals responsible for expressing the different isoforms of this protein (Brose et al., 1995; Koch et al., 2000). All of them have two Ca^{2+} independent C2 domains (C2B and C2C) with a MUN domain between them, furthermore the long isoforms have an additional N-terminal C2 domain (C2A), a central calmodulin binding sequence, and a C1 domain (Brose et al., 1995). The MUN domain binds to the SNARE

complex, thus its presence is essential for SV priming (Stevens et al., 2005). This function can be inhibited by homodimerization of the N-terminal C2A domains, while the zinc-finger domain of RIM can also bind to C2A, promoting synaptic transmission (Dulubova et al., 2005). Liprin-α consists of an N-terminal coiled-coil domain and three C-terminal SAM domains (Serra-Pagès et al., 1995). This protein can form homodimers (Taru & Jin, 2011), can bind to the C2B domain of RIM (Schoch et al., 2002), or can attach to ELKS (Dai et al., 2006) via the N-terminal half. On the other side, the C-terminal SAM domains can form heterodimers, with a related protein, β-liprin (Serra-Pagès et al., 1995). α-liprin (SYD-2 in *C. elegans*) was discovered as an AZ protein in *C. elegans*. Mutant animals possessed an elongated AZ with mislocalized presynaptic proteins (Zhen & Jin, 1999) and disrupted SV accumulation (Dai et al., 2006). While in *C. elegans* there is only one isoform, in vertebrates there are four isoforms (liprin-α1, α2, α3, α4) present (Spangler & Hoogenraad, 2007). Liprin-α2 is responsible for the recruitment of presynaptic proteins, such as RIM and CASK (Spangler et al., 2013), whereas liprin-α3 is necessary for SV docking and exocytosis (M. Y. Wong et al., 2018).

ELKS-1 was first identified in a human papillary thyroid carcinoma where *elks-1* fused to the RET (a receptor-type tyrosin kinase) through gene rearrangement (Nakata et al., 1999). Later it was rediscovered as a binding partner of Rab6 (Monier et al., 2002) and as an active zone protein called CAST (Ohtsuka et al., 2002) or ERC (Y. Wang et al., 2002). The protein consist of coiled-coil domains and a PDZ-binding motif (Ohtsuka et al., 2002). Although it has been known that ELKS directly binds to RIM ((Ohtsuka et al., 2002; Y. Wang et al., 2002), *elks-1* mutants in *C. elegans* did not show any deficiencies at the behavioural or the synaptic physiological level (Deken et al., 2005). ELKS also directly binds to liprin-α (Ko et al., 2003) and it has been shown that a gain of function mutation of liprin-α (in *C. elegans syd-2*) is able to rescue the *syd-1* mutation (another protein which is essential for localizing presynaptic components), but only in the presence of ELKS-1 (Dai et al., 2006). According to subsequent studies, ELKS-1 has a function in controlling of voltage-gated Ca^{2+} channel density (Dong et al., 2018) and RRP size (Dong et al., 2018; Held et al., 2016).

The function of these five core proteins is extended by other proteins, such as Piccolo or Bassoon. These proteins are essential in vertebrates and play a redundant role in SV clustering (Mukherjee et al., 2010), besides, Piccolo is crucial for SV recycling (Ackermann et al., 2019). Clarinet-1 is an AZ protein in *C. elegans* with homology to vertebrate Piccolo, which is involved is SV clustering and release (Xuan et al., 2017). CASK is a protein with various binding partners such as neurexins (Hata et al., 1996) and liprin-α (Wei et al., 2011), thus

besides others, it forms a link between the AZ proteins and the presynaptic adhesion molecule neurexin (LaConte et al., 2016).

Voltage-gate Ca^{2+} channels (VGCCs) are also localized to the AZ. Presynaptic neurotransmission depends mostly on P/Q (CaV2.1) and N-type (CaV2.2) Ca^{2+} channels, but R-type (CaV2.3) channels may also be present (L. Li et al., 2007). These all consist of a pore forming $Ca_v\alpha_1$ subunit, furthermore a cytosolic $Ca_v\beta$ and an extracellular $Ca_v\alpha_2\delta$ subunit. The pore-forming subunit consists of four domains, all of which comprising six transmembrane helices (S1-S6). S5 and S6 are the actual pore-forming helices, whereas S1-S4 are responsible for voltage-sensing (Gandini & Zamponi, 2022).

Besides VGCCs, neurotransmitter receptors, which act as autoreceptors or that respond to axo-axonic inputs to modulate neurotransmission, can also be localized at the presynaptic AZ. It has been shown that a group III metabotropic glutamate receptor, mGluR7, is restricted to the AZ. Furthermore, dependent of the postsynaptic cell type, distinct levels of this protein were present at the pre-synapse (Shigemoto et al., 1996). Subsequent studies showed that other metabotropic glutamate receptors (Corti et al., 2002; Kogo et al., 2004), as well as presynaptic $GABA_B$ (Luján et al., 2004) and nicotinic acetylcholine receptors (Garção et al., 2014) can also be found at the AZ.

1.2 *C. elegans* as a subject of study in neurobiology

1.2.1 *C. elegans* as a model organism

The nematode *Caenorhabditis elegans* is nowadays one of the most important model species. Researchers, such as Emile Maupas and Victor Nigon started to use this animal already around 1900, but the large breakthrough started in the 1960s, when Sydney Brenner and his collaborators began to study *C. elegans* (Frézal & Félix, 2015). This nematode was the first multicellular organism whose complete genome was sequenced (The *C. elegans* Sequencing Consortium*, 1998), which made it an attractive model organism of choice for a growing number of researchers.

The adult *C. elegans* hermaphrodite is about 1 mm long and consists of 959 somatic cells, of which exactly 302 are neurons (J. E. Sulston & Horvitz, 1977). The animal has a transparent body which enables not only the visualization of individual cells (using a light microscope) or fluorescent markers (using a fluorescence microscope) (Corsi et al., 2015) but also the optogenetic manipulation (Husson et al., 2013). It can be easily grown in the laboratory using

agar plates seeded with *E. coli* bacterium and the animals on the Petri dishes can be easily observed with a dissecting microscope.

Another major advantage is the short life cycle of *C. elegans* (Figure 5). Its reproductive cycle takes about 3 days at room temperature, the average life span of wild type animals is 18 days (S. Zhang et al., 2020). The life cycle starts with the embryonic stage which is followed by four larval (L1-L4) and the adult stages (Fielenbach & Antebi, 2008). Under unfavourable environmental conditions, such as overcrowding, absence of food or high temperature, animals can enter an alternative L3 stage, which is called the dauer or L3d stage (Cassada & Russell, 1975). This non-aging dauerlarva stage can last for months, during which feeding is arrested and locomotion is reduced. Normal development continues with the L4 stage when favourable conditions return.

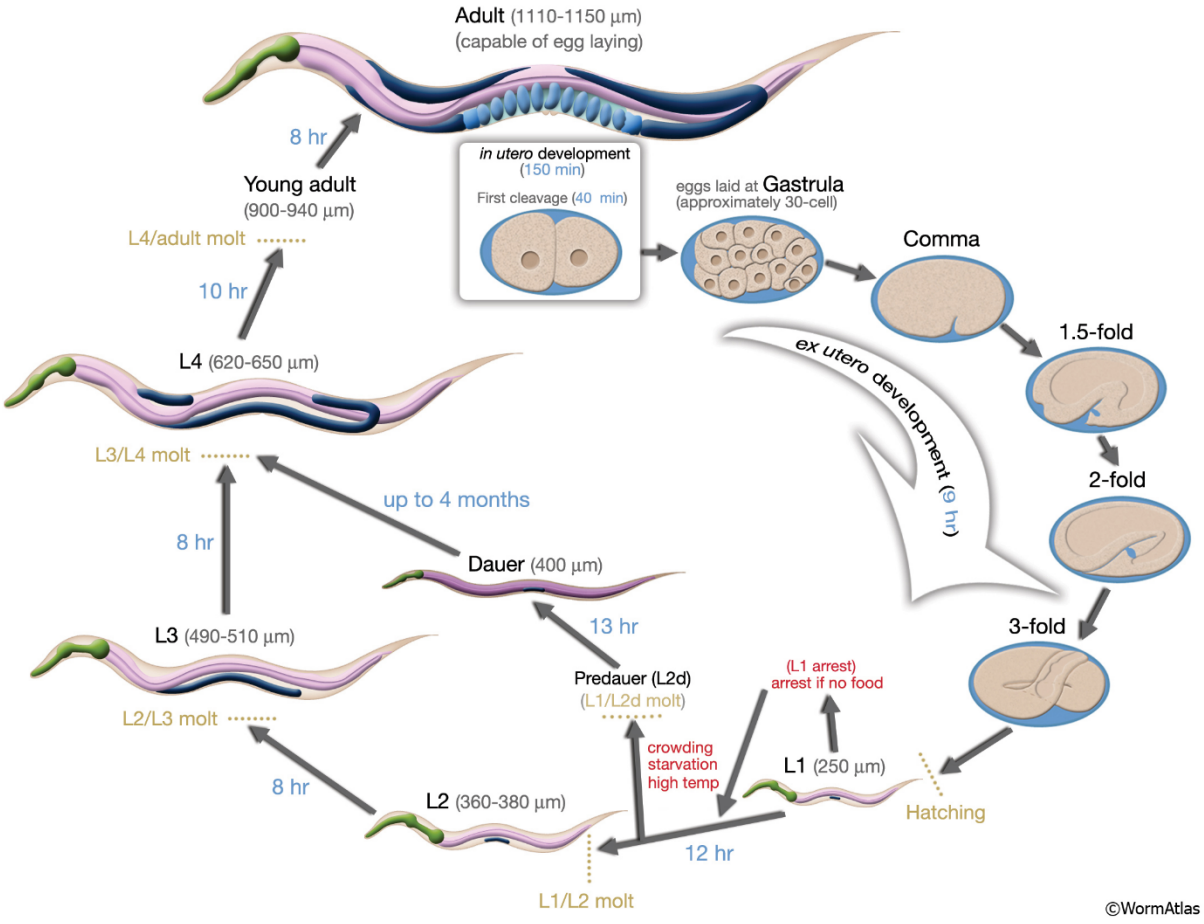

Figure 5: Life cycle of *C. elegans* at 22°C (from: (Z. F. Altun & Hall, 2006)). After egg laying, animals need about 3 days to reach adulthood under favourable conditions at 22°C. In case conditions are unfavourable, animals can develop *via* the dauer stage, which can last up to 4 months. The length of the animal (in µm) at the different stages is marked in black, the time (in hr) the animal spends in a stage is marked with blue colour.

C. elegans can be grown between 16 and 25 °C. By adjusting the temperature, the growth rate of the animals can be influenced, which can be advantageous when working with these animals (Byerly et al., 1976). Another useful feature is, that *C. elegans* can be frozen, and after gradually cooling the temperature to – 80 °C, samples can moved to liquid nitrogen for long-term storage (Brenner, 1974).

There are two sexes of *C. elegans*, the XX hermaphrodites and the XO males, which differ in their morphology, anatomy and behaviour (Lints & Hall, 2004). Under normal conditions male proportion is low (0.01 - 0.1 %); male genesis occurs upon X-chromosome loss in hermaphrodite gametogenesis which is an infrequent event (Hodgkin & Doniach, 1997). The proportion of males can be increased through mating (~50 %) or in the laboratory through heat-shock treatment (J. Sulston & Hodgkin, 1988) or ethanol exposure (Lyons & Hecht, 1997). The self-fertilizing hermaphrodite can produce about 300 progeny (Hodgkin & Barnes, 1991), male mating increases this number to 1200-1400 (Z. F. Altun & Hall, 2006). Self-fertilization enables to maintain genetically identical homozygous worms, whereas mating increases the genetic diversity and can be used in the laboratory to generate double- or multiple mutant strains.

The ~100 MB *C. elegans* genome including ~20.000 protein-coding genes (The *C. elegans* Sequencing Consortium*, 1998) is encoded within 5 pair of autosomes and one or two (in males and hermaphrodites, respectively) X chromosomes (Nigon, 1949). It has numerous evolutionary conserved genes in its genome with human orthologs (C.-H. Lai et al., 2000; Shaye & Greenwald, 2011) and a lot of proteins participating for example in apoptosis, or being involved in human neurodegenerative diseases, were first identified in *C. elegans* (Silverman et al., 2009).

A wide range of gene alteration techniques are available to modify the genome of *C. elegans*. As already mentioned above, crossing can be used to create strains with multiple mutations, but also new mutations can be introduced. Non-directed mutagenesis creates random mutations in the genome and it can be accomplished via chemical (Thompson et al., 2013) or radiation mutagenesis (Muller, 1927), or by using transposons (Bessereau et al., 2001). Gene-targeted mutagenesis enables the modification of specific genes. This can be also done by using transposons (Barrett et al., 2004), but also by using zinc finger nuckleases (ZFNs), transcription activator-like effector nucleases (TALENs) (Wood et al., 2011), or the CRISPR/Cas system (Dickinson et al., 2013). A major advantage is that ~ 22.000 mutant strains are available and can be ordered from the Caenorhabditis Genetics Center (CGC at the University of Minnesota, Twin Cities).

Besides working with mutant strains, gene expression can be also controlled by RNA interference (RNAi) (Fire et al., 1998). This mechanism regulates gene expression in plants, animals, and humans, but can be used as a gene-silencing technique in the laboratory. With the introduction of double stranded RNA (dsRNA), mRNA molecules with identical sequences to the dsRNA can be degraded. dsRNA can be introduced to *C. elegans* in different ways, such as injection or through feeding the animals with dsRNA expressing bacteria (Conte et al., 2015). This method enables to create animals with loss-of-function phenotypes in a rapid way, thus it helps to perform high-throughput experiments as well (Wabnig et al., 2015).

1.2.2 *C. elegans* nervous system

C. elegans has a relatively small, but well-characterized nervous system, which is an excellent model for investigating neural circuits and their role in driving behaviour. Its 302 neurons belong in two distinct categories: a large somatic nervous system consists of 282, and a small pharyngeal nervous system of 20 neurons (Z. F. Altun & Hall, 2005). As in other organisms, *C. elegans* neurons can be categorized as motor-, sensory-, and interneurons, but also a more sophisticated classification exists. Neurons of the somatic nervous system can be characterized based on morphology and connectivity, and this a total of 118 such classes can be distinguished. Beyond ~5000 chemical synapses, these neurons communicate through at least ~600 gap junction and ~2000 neuromuscular junctions (White et al., 1986; Witvliet et al., 2021).

The most synapse-rich part of the *C. elegans* nervous system is the nerve ring. It is localized in the head around the center of the foregut (pharynx) and consists of the axons of more than 50 % of the neurons. The *en passant* synapses between these neurons are responsible for governing the major part of the animal's behaviours (Z. Altun, 2017).

The locomotory behaviours of *C. elegans* are controlled by motor neurons (Figure 6). This category consists of 113 neurons, 75 of which innervate 79 body wall muscles (neck and body muscles) and form 8 distinct (AS, DA, DB, DD, VA, VB, VC, and VD) groups. VA, VB, DA, DB, AS classes are the stimulatory A and B-type neurons, their neurotransmitter is acetylcholine (ACh). VD and DD motor neurons are the inhibitory D-type neurons. These release γ-aminobutyric acid (GABA) and are postsynaptic to other motor neurons (as depicted also in Figure 6). VC motor neurons secrete ACh as well as serotonin, and these innervate primarily vulval muscles. Ventral muscles are innervated by VA, VB, VC, and VD whereas dorsal muscles are innervated by DA, DB, DD, and AS classes. The cell bodies of all these 8

classes are localized at the ventral side along the VNC (ventral nerve chord), the dorsal side is innervated by dorsal commissures sent by the respective motor neurons (White et al., 1976, 1986).

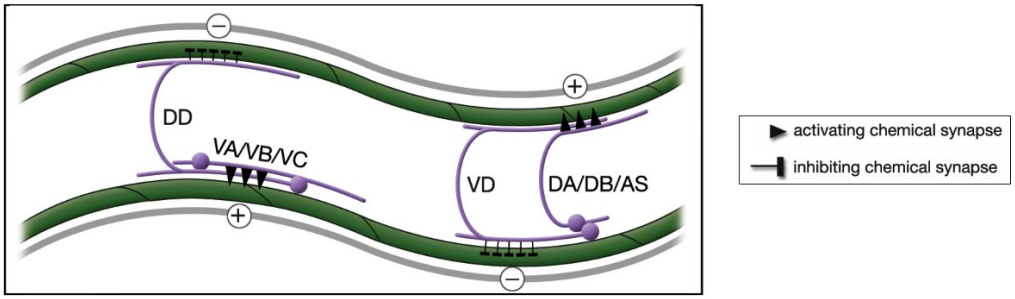

Figure 6: Motor neuron classes of *C. elegans* (modified from: (Z. F. Altun & Hall, 2005)). Ventral muscles are innervated by VA, VB, VC, and VD, whereas dorsal muscles are innervated by DA, DB, AS, and DD motor neuron classes. VA, VB, DA, DB, AS and VC are stimulatory, whereas VD and DD are inhibitory neurons. D.type neurons are exclusively postsynaptic receiving input from the stimulatory neurons: this enables the reciprocal inhibition of muscles and with this, the sinusoidal locomotion.

Motor neurons innervate muscle cells at specialised chemical synapses called neuromuscular junctions (NMJs). In *C. elegans* NMJs elongated muscle arms grow toward motor neurons and synapses are formed *en passant* (White et al., 1986). The majority of the NMJs are located at the VNC or at the DNC (dorsal nerve chord) (Zhen & Samuel, 2015), where the above mentioned cholinergic and GABAergic motor neurons form synapses.

The most important neurotransmitters in *C. elegans* are ACh, GABA and glutamate but there are also a few aminergic neurons. ACh is the most widely used neurotransmitter, 52 of the 118 classes of nerve cells are cholinergic (Pereira et al., 2015). ACh has mainly excitatory effects, but can also work as an inhibitor through ACh-gated anion channels (Putrenko et al., 2005). GABA is the most broadly used inhibitor in *C. elegans*, however, only 9 neuron classes are GABAergic (Gendrel et al., 2016; McIntire et al., 1993). 28 neuron classes use glutamate as excitatory transmitter (Serrano-Saiz et al., 2013) and in total 26 neurons employ octopamine, tyramine, dopamine or serotonin as neurotransmitter (Chase & Koelle, 2007).

The characteristic sinusoidal locomotion of *C. elegans* is controlled by A, B, D (McIntire et al., 1993) and AS-type motor neurons (Tolstenkov et al., 2018). A, B and D-type motor neurons form synapses in a way, that upon activation of cholinergic A or B type motor neurons, GABAergic D-type motor neurons are also stimulated. The special architecture of synapses enables the reciprocal inhibition of muscles: once dorsal muscles are activated, ventral muscles are inhibited or vica versa (McIntire et al., 1993). AS-type motor neurons contribute to this

locomotion by innervating muscles and other motor neurons assymetrically (Tolstenkov et al., 2018).

1.2.3 Optogenetics in *C. elegans*

Optogenetics enables the manipulation of neurons in a non-invasive manner. Light-sensitive proteins, such as ion-channels, pumps or enzymes can be activated with the administration of light, thus the activity of neurons which express these proteins can be controlled by light. *C. elegans* with its transparent body is the perfect organism for optogenetic manipulation; it was the first multicellular organism whose behaviour could be controlled by optogenetics. Channelrhodopsin-2 was the first light-sensitive protein successfully expressed in *C. elegans* (Nagel et al., 2005). Since 2005, *C. elegans* have been used extensively in optogenetics and nowadays a wide range of optogenetic tools is available.

Some of the most widely used optogenetic tools are Channelrhodopsin-2 (ChR2), Halorhodopsin (NpHR), Archaerhodopsin-3 (Arch) and the photoactivated adenylate cyclase (PAC) (Figure 7). ChR2 is a light-gated cation channel derived from the green alga *Clamydomonas reinhardtii* (Nagel et al., 2003). In the early years, *X. laevis* oocytes (Nagel et al., 2003), cultured mammalian neurons (Boyden et al., 2005) and *C. elegans* (Nagel et al., 2005) were stimulated using this optogenetic tool. Neurons can be inhibited with the help of NpHR or Arch. NpHR is a yellow light driven Cl^- pump and is endogenous in the archaeon *Natronomonas pharaonis*. This was the first available optogenetic tool for inhibiting neuronal activity (X. Han & Boyden, 2007; F. Zhang et al., 2007) and it is frequently used in *C. elegans* as well (Bergs et al., 2018; Husson et al., 2012; Kuhara et al., 2011; Q. Liu et al., 2009; F. Zhang et al., 2007). Arch was isolated from the archaebacterium *Halorubrum sodomense.* It is a light-driven outward proton pump; thus it enables also the inhibition of neuronal activity (Husson et al., 2012; Okazaki et al., 2012). All of the above-mentioned tools aim to manipulate the ion-flow through the membrane and with this, the modulation of membrane potential. On the contrary, PAC enables intracellular manipulation through the modulation of the second messenger cAMP: with the administration of blue light, cAMP production can be stimulated (Schröder-Lang et al., 2007). PAC was derived from the single-celled alga *Euglena gracilis* (Iseki et al., 2002) and is a combination of a photoreceptor and an adenylyl cyclase. Using this tool enabled the manipulation of cAMP in *X. laevis* oocytes, HEK293 cells and *Drosophila*

melanogaster (Schröder-Lang et al., 2007) and enhanced SV release in *C. elegans* (Steuer Costa et al., 2017; Weissenberger et al., 2011).

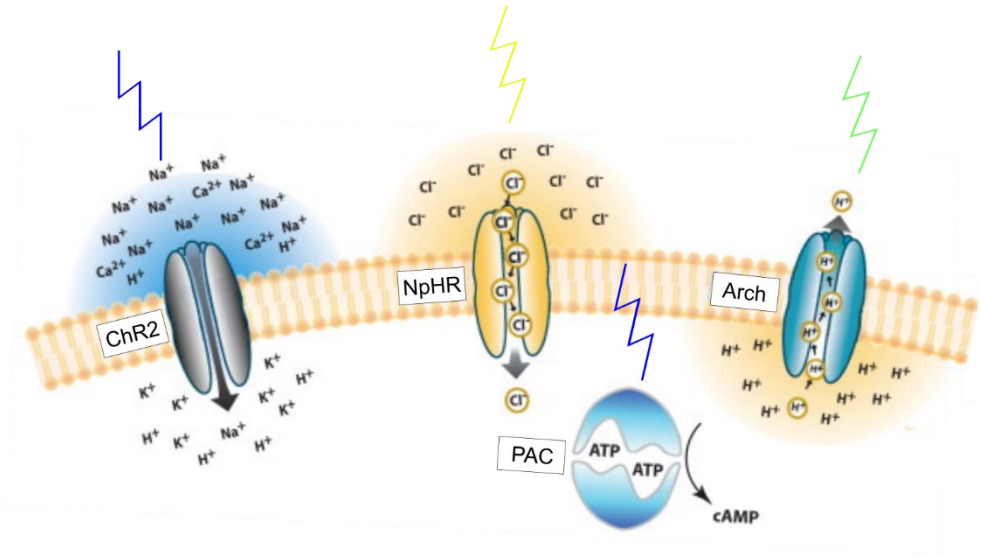

Figure 7: Model of optogenetic tools (modified from: (Yizhar et al., 2011)). Some of the most widely used optogenetic tools are Channelrhodopsin-2 (ChR2), Halorhodopsin (NpHR), Archaerhodopsin-3 (Arch) and the Photoactivated adenylate cyclase (PAC). Neurons can be stimulated via ChR2, which is permeable to cations upon blue light stimulation. NpHR and Arch are inhibitory tools: NpHR is a yellow light gated inward Cl^- pump, whereas Arch is a green-yellow light activated outward proton pump. PAC enables intracellular manipulation: it can be activated by blue light and produces cAMP from ATP.

Optogenetics tools also enable to monitor distinct biochemical parameters of neurons such as pH (Miesenböck et al., 1998), Ca^{2+} concentration (Zhao et al., 2011) or membrane potential (Dimitrov et al., 2007). There are several pH-sensitive fluorescent proteins available, one of the most commonly used is pHluorin, which is a modified green fluorescent protein (GFP) with high pH-sensitivity (Miesenböck et al., 1998), which has been successfully used in neurobiology for monitoring SV exo- and endocytosis events in various modell organisms (Bozza et al., 2004; Paquin et al., 2016; Sankaranarayanan et al., 2000; D. Yu & Davis, 2012). Besides green, several red pH-sensitive fluorescent proteins were described during the past years such as pHTomato (Y. Li & Tsien, 2012), pHRed (Tantama et al., 2011) or pHuji (Shen et al., 2014). pHuji was engineered using mApple (Shaner et al., 2008) as a template. It has a high pH sensitivity; more than a 20-fold intensity change was observed when raising the pH from pH 5.5. to pH 7.5 (Shen et al., 2014).

The traditional way of monitoring the activity of excitable cells is electrophysiology. However, during the past years novel imaging methods have been published and a wide range of genetically encoded Ca^{2+}-, and voltage indicators (GECIs and GEVIs) were described (Lin & Schnitzer, 2016). While GECIs enable to measure the neuronal activity indirectly through Ca^{2+}

imaging, GEVIs enable the direct measurement of voltage properties by analysing fluorescent changes. Besides other model organisms, these tools were successfully expressed and used also in *C. elegans* (Azimi Hashemi et al., 2019; Wabnig et al., 2015).

1.2.4 Channelrhodopsin-2 (ChR2) variants

Channelrhodopsins are seven-transmembrane (7-TM) helix proteins which bind the chromophore *all-trans* retinal. Channelrhodopsin-2 (ChR2) is a light-gated non-selective cation-channel, which is permeable by mono- (Na^+, K^+, H^+) and divalent cations (Ca^{2+}) (Nagel et al., 2003). ChR2 can be rapidly controlled by blue light: it can be opened by light illumination, while in the dark it closes (Boyden et al., 2005). The excitation spectrum of ChR2 is similar to GFP, its excitation peak is at 460 nm (Nagel et al., 2003).

In the first experiments wild type ChR2 (ChR2(wt)) was investigated. The expression of this construct induced light-activated currents in *X. laevis* oocytes and HEK293 cells (Nagel et al., 2003). Similar results could be obtained by using a fusion construct of ChR2(wt) and YFP. During illumination of cultured ChR2-positive rat neurons, fast depolarizing currents were observed (Boyden et al., 2005).

For the *C. elegans* experiments, the original sequence of ChR2(wt) was optimized to obtain a gain-of-function variant: in ChR2(H134R) an arginine is found at position 134 instead of the original histidine (Nagel et al., 2005). The expression of ChR2(H134R)::YFP in muscle cells or in mechanosensory neurons of *C. elegans* induced remarkable behavioural changes during illumination. Expression in body-wall muscles caused a strong contraction with a reduced body length (up to 13 % contraction was visible compared to the original length) during light stimulation. Animals contracted rapidly (maximal contraction was reached 500-600 ms after light-on) and this contraction was sustained by constant illumination (up to 1 min). After the end of the light stimulation, muscles relaxed in a fast manner (within 1 s). For a functional ChR2, the presence of the co-factor *all-trans* retinal (ATR) is necessary. *C. elegans* can be grown on NGM plates supplemented with ATR, animals raised without this supplement were tested as negative controls and showed no contraction at all.

Tapping the Petri dish of *C. elegans* results in simultaneous activation of the mechanosensory neurons ALM, PLM, AVM and PVM, which induces withdrawal behaviour. This behaviour could be evoked also by using optogenetics (Nagel et al., 2005). ChR2(H134R)::YFP was expressed in the above mentioned mechanosensory neurons and transgenic animals were

illuminated repeatedly 1-s-long with blue-light. Withdrawal behaviour significantly increased in animals raised with ATR.

Besides ChR2(H134R), other ChR2 variants have also been generated. Creating the ChR2(C128X) variants aimed to increase the operational light-sensitivity of the protein. While for the opening of the original ChR2 higher light-intensities were required, for the stimulation of ChR2(C128A) or ChR2(C128S) 300-fold lower stimulation was sufficient (Berndt et al., 2009). The closing time constant of these variants changed significantly: this value was 11.9 ms for wild type ChR2, whereas for C128T, C128A and C128S it changed to 2, 52, 106 s, respectively. These slow ChR2 variants were also tested in *C. elegans* (Schultheis, Liewald, et al., 2011). Brief (1 s) blue-light stimulation of animals, expressing ChR2(C128X) in body wall muscles, induced rapid, long-lasting body contraction (Figure 8). Mutants expressing the ChR2(H134R) reached its initial length 1 s after light-off, whereas mutants expressing the C128T, C128A and C128S variants, reached this state of relaxation after 5 s, 3 min, >5 min, respectively.

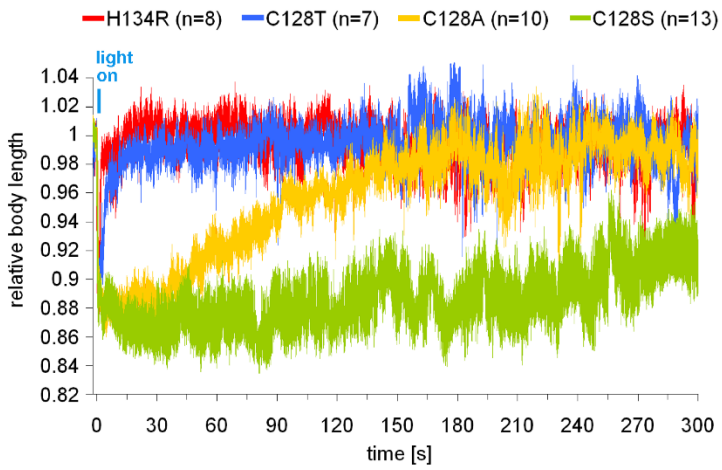

Figure 8: Comparison of ChR2(H134R) and ChR2(C128X) variants in contraction assay using *C. elegans* (from: (Schultheis, Liewald, et al., 2011)). Different variants of ChR2 were expressed in body wall muscles of *C. elegans*. Animals were stimulated using blue light (0.69 mW/mm^2; 450–490 nm; given at t=0 s 1-s-long), depicted is the relative body length (normalized to the initial length). Mutants expressing the ChR2(H134R) variant reached its initial length 1 s after light stimulus, while mutants expressing the C128T, C128A or C128S variants needed more time for reaching this state of relaxation.

1.3 Objectives

The major objectives of this work were (1) to describe and characterize novel SV recycling proteins and (2) to introduce a novel optogenetic tool which enables the direct monitoring of SV exo-, and endocytosis, and the identification of undescribed SV proteins.
The first experiments aimed to characterize proteins which were classified as promising SV recycling candidates based on a previous publication from the Gottschalk Lab (Wabnig et al., 2015). In this high-throughput all-optical analysis, optogenetic muscle stimulation was coupled with muscular Ca^{2+} imaging. Ca^{2+} traces of positive controls (mutants and RNAi knockdown animals of known SV recycling genes) were compared with the traces of RNAi knockdown animals of 95 in cholinergic synaptic transmission defective genes and further controls. Following cluster analysis, the most promising SV recycling candidates were chosen from the publication, and respective mutants were analysed through behavioural assays such as swimming-, and contraction assay. According to the original plans, we would have chosen a few promising candidates following the analysis of the behavioural experiments and these candidates would have been extensively analysed using techniques such as electron microscopy or electrophysiology. However, the mutant phenotypes were not as strong as we hypothesised before, and the interpretation of the results was more difficult than previously thought. Thus, we needed to change our strategy. The new goal was to extensively analyse two proteins which were known to have a role in the SV cycle, but the exact function of these remained unknown: ERP-1 (the *C. elegans* ortholog of Endophilin B) and RIMB-1 (the *C. elegans* ortholog of RIM-BP). Furthermore, I aimed to develop a new optogenetic tool which enables the direct analysis of SV release activity and thus helps to identify novel SV recycling proteins: the pOpsicle assay.

1.3.1 ERP-1 project

Synaptic vesicle (SV) recycling is crucial to maintain sustained neurotransmission. During the past years, multiple recycling pathways have been identified, distinguished by the kinetics and the mediating molecular machinery (Chanaday et al., 2019). One of the essential proteins is clathrin, which not only plays the key role in the clathrin-mediated endocytosis (CME) (Heuser & Reese, 1973), but it is also required for another, recently-identified recycling pathway, the ultrafast endocytosis (Watanabe et al., 2014). While the CME is a relatively slow process (10-

30 s) (T. M. Miller & Heuser, 1984) and enables to form new SVs right at the plasma membrane (PM) with the help of clathrin and clathrin associated proteins (Saheki & De Camilli, 2012), ultrafast endocytosis is fast (50-100 ms) (Kittelmann et al., 2013; Watanabe, Liu, et al., 2013) and produces large, clear-core vesicles in a clathrin independent manner. New SVs are formed from these via clathrin mediated budding (Kittelmann et al., 2013; Watanabe et al., 2014). Thus, SVs can be reformed not only at the PM but also at the membrane of the large endocytic vesicles (LVs).

Besides clathrin, many other proteins - such as dynamin, synaptojanin or the endophilins-, are required for SV recycling, the function of which was extensively investigated during the past years. Endophilin is required for the recruitment of synaptojanin (Schuske et al., 2003) and dynamin (Sundborger et al., 2011), furthermore it functions as a membrane-bending molecule (Bai et al., 2010). Endophilin is required for CME (Milosevic et al., 2011) and ultrafast endocytosis (Watanabe et al., 2018). In vertebrates there are two subgroups of endophilins present, endophilin A and endophilin B (Modregger et al., 2003). Endophilin A (encoded by *unc-57* in *C. elegans*) is responsible for the endocytosis at the PM (Farsad et al., 2001) and is also involved in clathrin-independent endocytosis in non-neuronal cells (Boucrot et al., 2015), whereas the less well understood B isoform (encoded by *erp-1* in *C. elegans*) seems to contribute to the intracellular membrane trafficking (Modregger et al., 2003). In endophilin A triple knockout (endophilin A is encoded by three different genes) mice CME was impaired: coated synaptic vesicles accumulated but a low level of synaptic transmission was sustained (Milosevic et al., 2011). According to a previous publication in *C. elegans*, synaptic transmission was only partially maintained when UNC-57/endophilin A was tethered to the PM (Bai et al., 2010), which suggests a role for this protein also at the large vesicle level. A possible contribution of ERP-1 to SV endocytosis was not investigated yet; this protein was recently identified as a possible SV recycling factor (Wabnig et al., 2015). It has been previously demonstrated that clathrin has a role in SV biogenesis in *C. elegans* (Sato et al., 2009) as well, however, the site of action remained unclear.

The ‘ERP-1 project’ aimed to analyse the function of UNC-57, ERP-1 and CHC-, furthermore the site of action (at the PM or at the membrane of the LVs) of these proteins.

1.3.2 RIMB-1 project

RIM-binding protein (RIM-BP) is an evolutionarily conserved active zone protein, with three

src-homology type III (SH3), and three fibronectin type III (FN3) domains (Hibino et al., 2002). There is a single gene expressing RIM-BP in invertebrates, whereas in vertebrates there are RIM-BP1 and RIM-BP2 and in mammals also a third protein, RIM-BP3 (mainly expressed outside the nervous system) (Mittelstaedt & Schoch, 2007) . RIM-BP interacts with RIM via the second (Y. Wang et al., 2000), and with voltage gated Ca^{2+} channels (VGCCs) (Hibino et al., 2002) preferentially via the second or third SH3 domain (Davydova et al., 2014; Petzoldt et al., 2020)(Figure 28, B). In *Drosophila*, the loss of RIM-BP impaired Ca^{2+} channel clustering, lead to decreased Ca^{2+} influx, and markedly reduced the SV release probability (K. S. Y. Liu et al., 2011). Further investigation of the same mutant revealed the role of RIM-BP in homeostatic plasticity through modulating the Ca^{2+} influx and supporting the access to the RRP SVs (Müller et al., 2015). RIM-BP was shown to have a role in the coupling of Ca^{2+} influx and SV exocytosis in RIM-BP1, RIM-BP2 double mutant mice (Acuna et al., 2015), while the combined loss of RIM and the two RIM-BPs demonstrated that these proteins are essential, redundant organizers of the active zone (Acuna et al., 2016). Liquid-liquid phase separation (LLPS) experiments also demonstrated that RIM and RIM-BP can effectively cluster VGCCs and are central organizers of the active zone (X. Wu et al., 2019). Mutation of RIMB-BP2 disrupted the precise Ca^{2+} channel localization and altered short term plasticity (Grauel et al., 2016). Similar findings were published investigating the inner hair cells of RIM-BP2 mutant mice: according to this, RIM-BP2 has a role in VGCC clustering and supports the replenishment of the RRP (Krinner et al., 2017). Further analysis of *Drosophila* RIM-BP revealed that the N-terminal region of these protein is responsible for promoting SV recruitment (Petzoldt et al., 2020)

It is known that the loss of UNC-10 (the *C. elegans* homolog of RIM) leads to drastic behavioural defects (Koushika et al., 2001). On the contrary, the loss of RIMB-1 (the *C. elegans* homolog of RIM-BP) led only to mild phenotypes, however, RIMB-1 and UNC-10 seems to have redundant roles also in *C. elegans* (Kushibiki et al., 2019). Similar to previous findings in other model organism, RIMB-1 has a role in VGCC (in *C. elegans* UNC-2) clustering in *C. elegans* as well; UNC-2 showed an altered, more diffuse distribution at the presynaptic sites in *rimb-1; unc-10* double mutants (Kushibiki et al., 2019). A previous publication described two distinct localization mechanisms of UNC-2: a SYD-2 dependent and a SYD-2 independent one. According to the first one, SYD-2 plays a central role in the localization of UNC-10, ELKS-1, and RIMB-1 proteins, which contribute to the localization of UNC-2. Furthermore, UNC-10 and ELKS-1 are able to localize UNC-2 in a SYD-2 independent-manner as well (Oh et al., 2021).

The ‘RIMB-1 project’ aimed to analyse the function of RIMB-1, with a special emphasis on its contribution to the localization of UNC-2 (in cooperation with UNC-10) and its contribution to the excitation/inhibition balance of *C. elegans*.

1.3.3 pOpsicle project

SV recycling proteins, such as ERP-1, can be identified through indirect assays such as Ca^{2+}-imaging (Wabnig et al., 2015) or an assay that measures optogenetically induced muscle contraction (Liewald et al., 2008), however, the interpretation of the results is often ambiguous and further experiments are needed confirming the function of the proteins. More time-consuming experiments, such as electrophysiological or electron microscopical assays, enable to draw more precise conclusions, however, it is not realistic to perform high-throughput analysis via these methods. Thus, a tool, which enables the direct visualization of SV exo-, and endocytosis, is needed. pOpsicle is a method which combines the optogenetic stimulation of cholinergic neurons (Liewald et al., 2008) with real-time visualization of SV release. For this, a pH-sensitive fluorescence protein, pHuji (Shen et al., 2014), was inserted into the second intravesicular loop of the synaptic vesicle membrane protein, synaptogyrin (SNG-1) (Abraham et al., 2011) (Figure 9). Resting vesicles have a luminal pH of 5.5 (Atluri & Ryan, 2006), whereas the extracellular pH is higher, i.e. 7.4. The fluorescence of pHuji is quenched at pH 5.5 but once the vesicles are released and the pH increases, pHuji can be detected (Shen et al., 2014). After SV endocytosis, vesicles are quickly reacidified, thus the fluorescence is quenched again.

The detection of spontaneous release events was not possible, therefore, SV release visualization of pHuji was combined with the stimulation of cholinergic neurons. For this, ChR2 was expressed is cholinergic neurons. ChR2 can be stimulated via blue light; by continuous visualization of pHuji, SV exo-, and endocytosis events can be detected during and after blue light stimulation. By analysing the fluorescent signal of pHuji a few-seconds-long after blue light stimulation, SV endocytosis and recycling can be investigated, and SV recycling mutants can be identified through an altered fluorescent trace; with this the pOpsicle tool enables the identification of novel SV recycling proteins in a direct way.

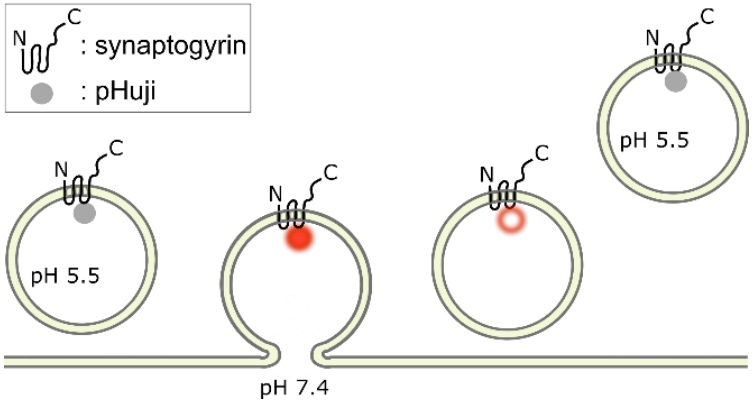

Figure 9: pHuji as an SV release indicator. SVs of *C. elegans*, which express the SNG-1::pHuji construct, contain the pH-sensitive fluorescence marker, pHuji. Fluorescence of pHuji is quenched at pH 5.5 but once the vesicles are released, the pH increases and pHuji can be detected. Following SV exocytosis, SV membrane and proteins are retrieved and quickly reacidified: fluorescence is quenched again.

2. Materials and methods

2.1 Materials

2.1.1 Equipment

Table 1: Equipment used

Description	Type	Manufacturer
Autoclaves	Line FVS 5075 ELVC	Fedgari Tuttnauer
Automated freeze substitution unit	Reichert AFS	Leica
Bunsen burner	Labogaz 470	Campingaz
Cameras	PowerShotG9 ORCA-Flash4.0 Evolve 512 Delta Rolera EM-C2	Canon Hamamatsu Teledyne Photometrics Teledyne Photometrics
Camera for TEM	Erlangshen ES500W	Gatan
Centrifuges	Rotanta 460 Pico 17 Microcentrifuge	Hettich Heraeus Carl Roth
ddH2O equipment	Milli-Q Plus	Millipore
Electrophoresis chamber	Varia 1	Carl Roth
Filters	F49-470 F48-495 F37-520 F74-423 F38-605 F37-647 F47-700	AHF Analysetechnik AHF Analysetechnik AHF Analysetechnik AHF Analysetechnik AHF Analysetechnik AHF Analysetechnik AHF Analysetechnik
Gas cartridge	C206	Campingaz
Gel documentation system	Felix 6040 EOS 500D Dark Hood DH-40	Biostep Canon Biostep

Heating block	Rotilabo- Block Heater H 250	Carl Roth
High power LED	460 nm 590 nm	Prior Scientific Prior Scientific
High pressure freezer	HPM010	BAL-TEC
Incubator, shaking	INB400 (37 °C)	Memmert
Incubators	DF8528 Slim Vip (-80 °C) FSK 3600 Index 20B (20 °C) Vinothek (15 °C) Ecotron (37 °C)	Skadi Liebherr Liebherr Infors HAT
Laser, 470 nm		
Laser, 637 nm	OBIS FP 637LX	Coherent
Laser beam splitter	HC BS R594 lambda/2 PV flat	AHF Analysentechnik
Lamps	HBO 50 Mercury-vapor HBO 100 Mercury-vapor	Osram Osram
LED lamp	KSL-70	Rapp OptoElectronic
Magnetic stirrer	Stuart CB162	Bibby Scientific
Micromanipulator	MMJ	Marzhauser
Micropipette puller	Modell P97	Sutter
Microscopes	Axio Observer Z1 Axiovert 200 Leica MZ 16F Zeiss Cell Observer SD Spinning Disc Confocal Microscope Axiovert 40 CFL SMZ 645 stereo microscope	Carl Zeiss Carl Zeiss Leica Carl Zeiss Carl Zeiss Nikon
Microwave	MM 41580	Micromaxx
Monochromator	Polychrome V	Till Photonics
Optical power meter	PM100 PM100D	Thor Labs Thor Labs
Patch clamp amplifier	EPC-10	HEKA

Photometer	Genova TrayCell (1:10, 1:50 virtual dilution factor)	Jenway Hellma Analytics
Piezo Z stage	NanoScanZ	Prior Scientific
Pipette	0.5 µL, 1 µL, 100 µL, 1000 µL	Eppendorf
Scales	Analysewaage 770 EMB 600-2	Kern Kern
Shutter	Shutter	Shutter Instrument Company
Shutter control system	Lambda SC	Shutter Instrument Company
Thermocycler	MyCycler Personal Thermal Cycler T1 Thermocycler Biometra TOne	Bio-Rad Biometra Analytik Jena GmbH
Transmission electron microscope	CM12	Philips
Ultramicrotom	EM UC6	Leica
UV lightbox	BioView	BioView
Vortex shaker	Vortex Genie 2	Scientific Industries

2.1.2 Consumables

Table 2: Consumables used

Description	**Type**	**Manufacturer**
Beem capsules	size 3	Science Services
Blade	Stirrup-shaped	Carl Roth
Borosilicate glass capillaries	1B100F-4	Worcester Polytechnic Institute
Centrifuge tube	15 mL and 50 mL	Greiner Bio-One
Collagenase	C5138	Sigma-Aldrich
Cover slip	Squared cover slip 22x22 mm	Carl Roth
Cryogenic vial	2 ml	BioCision
Diamond knives	Trim 45° Ultra 45°	DIATOME DIATOME
Disposable pipete tips	1 µL, 100 µL, 1000 µL	Carl Roth

Disposable syringe	With luer fitting, 5, 10 and 20 ml	B. Braun
Dust-off	XL	EMS
Flow-through ring		Leica microsystems
Glass capillary	1B 100 F-4	World Precision Instruments
Glass pipettes	5 mL, 10 mL and 25 mL	Brand
Histoacryl glue		B. Braun
HPF Carrier	3mm diameter, Standard, Typ A, Aluminium	Science Services
Instant glue	CA 221	Carl Roth
Microcentrifuge tube	200 µL Row of 8x 200 µL 1.5 mL and 2 mL	Sarstedt neoLab Carl Roth
Microcentrifuge plate	96x 200 µL	Carl Roth
Microscope slide		Carl Roth
Objective immersion oil	Immersol 518F	Carl Zeiss
Perfect loop		EMS
Petri dish	60/15 mm, 100/20 mm and 150/20 mm	Greiner Bio One
Plastic capsules	D5 x H15 mm	Leica Microsystems
Plastic solvent container with screw top	12.5 ml	Leica Microsystems
Protective gloves	Rotiprotect latex and nitrile	Carl Roth
Parafilm	Parafilm M	VWR
Sapphire disc	3 x 0.16 mm	Engineering Office M.
Spacer ring	0.4 mm	Engineering Office M.
Specimen forcep	305 mm	SEM
Syringe filter	ROTILABO, 0.22 µm	Roth selection
TEM grid	Formvar/Carbon film coated, 2 x 1 mm slot, Cu	Science Services
Transfer pipets	graduated, 15.5 cm	EMS
Tweezer	Style 2A SA/DR	EMS

2.1.3 Chemical substances

Table 3: Chemical substances

Substance	Manufacturer
Aceton, glass distilled	EMS
Agar	AppliChem
Agarose	Invitrogen
Aldicarb	Sigma-Aldrich
All-*trans* retinal	Merck
Ampicillin sodium salt	AppliChem
Calcium chloride	Carl Roth
Cholesterol	Merck
Desoxy nucleotide triphosphate (dNTP)	Invitrogen
Dipotassium phosphate	Carl Roth
Disodium phosphate	Carl Roth
Epoxy resin, AGAR 100 Premix kit hard	Agar Scientific
Ethanol 94 %	Carl Roth
Ethanol 99 % (AR grade)	AppliChem
Ethidium bromide 5 %	Carl Roth
Gealtine	Carl Roth
GeneRuler 100bp DNA Ladder	Thermo Fisher Scientific
GeneRuler 1 kb DNA Ladder	Thermo Fisher Scientific
GeneRuler 1 kb Plus DNA Ladder	Thermo Fisher Scientific
Glycerin	Carl Roth
Halocarbon oil	Halocarbon
Isopropanol	Carl Roth
Kobe Agar	Carl Roth
Lead Citrate 3%, ready to use solution	Science Services
Magnesium chloride	Carl Roth
Magnesium sulfate	Carl Roth
Monopotassium phosphate	Carl Roth
Nitrogen	Linde
Nystatin	Merck

Oligonucleotides	Eurofins MWG
Osmium Tetroxide (0.25 g)	EMS
Polyethylen glycol (PEG) 6000 g/mol	Carl Roth
Polystyrene beads (0.1 µm)	Polysciences
Potassium chloride	Carl Roth
Potassium hydroxid	Carl Roth
Sodium chloride	Carl Roth
Sodium hydroxide	Carl Roth
Sodium hypochlorite 12 %	Carl Roth
Streptomycin	AppliChem
Tannin	Carl Roth
Tris-(hydroxymethyl)-aminomethane (TRIS)	Carl Roth
Tetramisole-hydrochlorid	Sigma-Aldrich
Tryptone/Peptone from Casein	Carl Roth
Tween-20	Carl Roth
Uranyl Acetate Solution	Science services
Yeast extract	Carl Roth

2.1.4 Buffers and Media

Table 4: Buffers and media

Buffer/Media	**Manufacturer/Content**
Bleach solution	1:1 solution of 1 N NaOH and 5% NaClO (v/v)
Gel loading dye, blue (6x)	New England Biolabs
Gel loading dye, purple (6x)	New England Biolabs
Gibson Assembly Master Mix	New England Biolabs
dNTP Mix	10 mM dATP 10 mM dCTP 10 mM dGTP 10 mM dTTP
Injection buffer (10x)	20 % (w/v) PEG

	200 mM Potassium phosphate 0.33 mM Calcium chloride 0.33 mM Magnesium sulfate
Lysogeny broth (LB) medium	0.5 % (w/v) Yeast extract 1 % (w/v) Tryptone/Peptone 1 % Sodium chloride Optional 1.5 % (w/v) Agar Optional after autoclaved: 100 µg/µL Ampicillin 200 µg/µL Streptomycin
M9 buffer	1 mM Magnesium sulfate 20 mM Monopotassium phosphate 40 mM Disodium phosphate 85 mM Sodium chloride
NEB CutSmart buffer (10x)	New England Biolabs
NEBuffer 2.1 (10x)	New England Biolabs
Nematode growth medium (NGM)	0.25 % (w/v) Tryptone/Peptone 0.3 % (w/v) Sodium chloride 1.7 % (w/v) Agar 1 mM Calcium chloride 1 mM Magnesium sulfate 25 mM Potassium phosphate buffer 0.0005 % (w/v) Cholesterol (in ethanol) 0.001 % (w/v) Nystatin (in ethanol)
Phusion HF buffer (5x)	New England Biolabs
Potassium phosphate buffer (1 M, pH 7.5)	1 M Monopotassium phosphate 1 M Dipotassium phosphate
Quick Ligase Reaction Buffer (2x)	New England Biolabs
Single egg/worm lysis buffer (SEWLB)	2.5 mM Magnesium chloride 10 mM Tris-HCl (pH 8.3) 50 mM Potassium chloride 0.05 % (w/v) Gelatin 0.45 % (v/v) Tween-20

S buffer (pH 6)	6.5 mM Monopotassium phosphate 43.5 mM Dipotassium phosphate 100 mM Sodium chloride
TAE (TRIS acetate EDTA) buffer (50 x)	40mM TRIS/Acetic acid 2mM EDTA at pH 8.5
T4 DNA ligase buffer (10x)	New England Biolabs
ThermoPol buffer (10x)	New England Biolabs

2.1.5 Kits

Table 5: Used kits

Kit	**Manufacturer**
QIAquick Gel Extraction Kit	Qiagen
QIAquick PCR & Gel Cleanup Kit	Qiagen
Roti-Prep Plasmid Mini	Carl Roth
NucleoBond PC 100	Macherey-Nagel
TOPO TA Cloning Kit	Life Technologies

2.1.6 Enzymes

Following restriction enzymes were used during this work: *Bbs*I, *Dpn*I, *Nhe*I, *Psi*I, *Sap*I. All restriction enzymes were obtained from New England Biolabs and were used according to the supplier's protocols. All further enzymes used during this work are listed in Table 6.

Table 6: Enzymes used

Enzyme	**Manufacturer**
Antarctic phosphatase	New England Biolabs
Proteinase K	Thermo Fisher Scientific
Phusion DNA Polymerase	New England Biolabs
Quick Ligase	New England Biolabs
Taq DNA Polymerase	New England Biolabs
T4 DNA Ligase	New England Biolabs

2.1.7 Plasmids

Plasmids, which were used during this work, are listed in Table 7.

Table 7: Plasmid created/used during this work

Name	Description	Source
	pmyo-2::CFP	
	pmyo-::myc::ChR2	Dr. N. Azimi Hashemi
pRM348	punc-17::syntintron::3'UTR::AmpR	Prof. J. Rand
pCS178	pflp-1 (trc)::mCherry	Dr. C. Schultheis
pCS179	pflp-1 (trc)::GFP	Dr. C. Schultheis
pAG52	psng-1::sng-1::CBP	Prof. Dr. A. Gottschalk
pAH03	punc-17::ccb-1::tagRFP-atLOV2_cODC1	Anke Hermann
pJB10	punc-17::syntintron::sng-1::unc-54-3'UTR::Amp	This work
pJB16	primb-1::GFP::AmpR	This work
pJB17	punc-17::mCherry::AmpR	This work
pJB22	pDisplay::pHuji	Addgene
pJB24	pDisplay::pHuji*	This work
pJB25	punc-17::syntintron::sng-1-pHuji*::unc-54-3'UTR::Amp	This work
pJB26	punc-17::ChR-2(H134R)_myc	This work
pJB29	TOPO vector::pHuji*	This work

* original AddGene plasmid with point mutation in pHuji – BbsI restriction-site was removed without any amino-acid change

2.1.8 Oligonucleotides

Oligonucleotids, which were used during this work, are listed in Table 8. Oligonucleotids, which were designed during this work, are named as oBJX.

Table 8: Used oligonucleotids

Name	Sequence	Description
	GGTAACTCGGTGGAGTCATTTG	punc-17 fwd
oFB176	GTTCGTTTTAGACCGGACAG	unc-2 fwd_SunyBiotech
oFB177	AAAAATTTGGCAGACATGGG	unc-2 rev_SunyBiotech
oBJ16	GCGGAATTCGAGGAGTTACAG	rimb-1 fwd
oBJ17	ACGTAGTTCGGGTGGTGAG	rimb-1 rev
oBJ18	GGTCCGTCGTTTGCCAATATC	rimb-1 del. rev
oBJ28	GTCTCACGGCTCTGTTACGC	Insertseq_punc17
oBJ30	TGGAGGATACGGACAATG	eel-1 fwd
oBJ31	ACCTGAAATCGCTCTCA	eel-1 del. rev
oBJ32	CAGTTGCCGTTAATCCTG	eel-1 rev
oBJ33	GACTGATCGAGATGACAAATC	let-60 N2 fwd
oBJ34	GACTGATCGAGATGACAAATT	let-60 mut. fwd
oBJ35	CGATAAACCAGCATGCCTG	let-60 rev
oBJ36	TGTCGAAAGAAGCGCGAAAG	sad-1 rev
oBJ37	TAGAGGATAACGCCACAACTCC	sad-1 N2 fwd
oBJ38	TCATTGCCCGCAGTAAACTC	sad-1 seq
oBJ39	TGGAACGGAAACAACGCTTTC	erp-1 fwd
oBJ40	AGTGGCTCAAACGGAAAACC	erp-1 rev
oBJ41	CGGGAATTGAGCGGGTAAGT	erp-1 del rev
oBJ42	TCCAGAGCCTAAACGATGCTG	unc-57 fwd
oBJ43	TGTGCGGTGGTGCTGAATAA	unc-57 rev
oBJ44	TCCAGACAGCTATCGAATCTCA	itsn-1 fwd
oBJ45	GCAGCAAAATGCTCTCCACC	itsn-1 rev
oBJ46	GCTGTCTCACTGACTGTTC	let-60 seq
oBJ58	tcaggaggacccttggctagATGGAGAACGTGCGTGCTTATG	sng-1_fwd_Gibson
oBJ59	atgactcgagctaATAACCATATCCTTCCGACTGAG	sng-1_rev_Gibson
oBJ60	atatggttattagCTCGAGTCATGGTCGACAAG	unc54_3'UTR_fwd_Gibson

oBJ61	aaacgcgcgagacgaaagggcccAAACAGTTATGTTTGGTATATTGGG	unc54_3'UTR_rev_Gibson
oBJ76	TAGCTCTTCCAGCGAGAGGACCTCCTCCTC	fwd primb-1
oBJ77	AGCGCTGTTGGTGACTAGGTGGTCC	rev primb-1
oBJ78	TATAGCTCTTCGAGCCTTCCGGCTCGTATGTTG	fwd punc-17_Sap1
oBJ79	AGCGCTTACCTTTGGGTCCTTTGG	rev punc-17
oBJ80	GGCTTAGGCTTGAACATAGG	punc-17 seq 2/4
oBJ81	CCGCGAACAATCCCAATCAG	punc-17 seq 3/4
oBJ82	TCCTTACCCGCCGTGAATCC	punc-17 seq 4/4
oBJ83	CTCGGTGGAGTCATTTGAAC	punc-17 insert seq
oBJ88	CCCTGTCGGCGCCAATTAAC	primb-1 middle seq
oBJ98	GTGGGACGCACTGAATGTCT	sng-1_fwd
oBJ99	TTTTAGGGAGGTGCCGCATT	sng-1_fwd_del
oBJ100	TACGAGATCTACAAGTGCTCAGG	sng-1_rev
oBJ101	AGAGGATGGTTCAGTCGGGA	elks-1 fwd
oBJ102	CGCATCCACATCACCCTGTA	elks-1 rev. del.
oBJ103	TGTTGCTCCATCGCATCCTT	elks-1 rev
oBJ104	GCAGAAGAAAACCATGGGCTG	pHuji_Bbs1mut_fwd
oBJ105	CAGCCCATGGTTTTCTTCTGC	pHuji_Bbs1mut_rev
oBJ107	ATATCGAAAAGTCTTCAGGTGGAGGTGGAAGTATGGTGAGCAAGGGCGAG	pHuji_Bbs1site_fwd
oBJ108	TATATTCGCCGTCTTCGGTGGAGGTGGAAGTCTTGTACAGCTCGTCCATG	pHuji_Bbs1site_rev
oBJ113	GAACGCTAGCACCACTAGATCCATCTAGAG	chop-2(H134R)fwd_NheIsite
oBJ114	GCATGCTAGCCACCAGACAAGTTGGTAA	chop-2(H134R)rev_NheIsite
oBJ115	TTGGTGGCACTGAGATTG	myc tag fwd
oBJ116	CAGGGAGAAAGAGCATGTAG	myc tag rev
oBJ130	CGCGGATAAGCTCATGTGGA	snb-1(md247)_fwd
oBJ131	TCCAGCAGACACAAGCTCAG	snb-1(md247)_rev
oBJ138	ATCAGCAGAGTTGATTGCTCT	unc-47 fwd

oBJ139	CCGCTGCTGTGTTCAAAGTT	unc-47 rev
oBJ140	GCCCATCGAGGATCATCTTC	unc-2 rev. del.
oBJ141	GTCATTCTTATTACGCTATCGTC	snb-1(md247)_del_rev

2.1.9 Organisms

Table 9: Organisms used during this work

Species	**Strain**	**Source**
Caenorhabditis elegans	Bristol N2 (wild type)	*Caenorhabditis* Genetics Center (CGC)
Escherichia coli	OP50-1	CGC
Escherichia coli	DH5α	Invitrogen

2.1.10 Transgenic *C. elegans* strains

Table 10: Transgenic *C. elegans* strains generated/used during this work

Strain	**Genotype**	**Generated in this thesis**
	wild type	
	rimb-1(tm5964)	
CB406	*unc-57(e406)I*	
DH1230	*chc-1(b1025ts)III*	
RB700	*erp-1(ok462)X*	
BC12478	*dpy-5(e907)I; sIs10597[rCes F35A5.8a::GFP + pCeh361]*	
ZM9583	*unc-2(hp858[GFP::UNC-2])*	
VC201	*itsn-1(ok268)IV*	
VC116	*inx-8 (gk42)IV*	
RB2051	*inx-10 (ok2714)V*	
CX5156	*sad-1(ky289)*	
VC1100	*eel-1 (ok1575)*	

PS436	*let-60(sy93)*	
NM1657	*unc-10(md1117)X*	
EG5027	*oxIs353[pmyo-3::ChR2::mCherry::unc-54 3'-UTR; lin15+]V*	
ZX460	*wild type; zxIs6[punc-17::ChR2(H134R)::YFP; lin-15+]V*	
ZX498	*snb-1(md247) V.; zxIs6[punc-17::ChR2(H134R)::YFP; lin-15+]V*	
ZX531	*unc-47(e307)III; zxIs6[punc-17::ChR2(H134R)::yfp; lin-15+]*	
ZX634	*unc-57(e406)I; zxIs6[punc-17::ChR2(H134R)::YFP; lin-15+]V*	
ZX1602	*erp-1(ok462)X; zxIs6[punc-17::ChR2(H134R)::YFP; lin-15+]V*	
ZX1605	*unc-2(pk95::Tc1); zxIs6[punc-17::ChR2(H134R)::yfp; lin-15+]*	
ZX1611	*inx-10 (ok2714)V; zxis58[pmyo-3::RCamp35, punc-17::ChR2]*	
ZX1617	*inx-8 (gk42)IV; zxis58[pmyo-3::Rcamp35, punc-17::ChR2]*	
ZX1636	wild type; *zxis58[pmyo-3::RCamp35, punc-17::ChR2]*	
ZX1778	*chc-1(b1025ts)III; zxIs6[punc-17::ChR2(H134R)::YFP; lin-15+]V*	
ZX1799	*itsn-1(ok268)IV; zxis58[pmyo-3::RCamp35, punc-17::ChR2]*	
ZX2025	*rimb-1(tm5964)III; zxIs6[punc-17::ChR2(H134R)::yfp; lin-15+]*	
ZX2088	*erp-1(ok462)X; unc-57(e406)I*	X
ZX2227	*unc-57(e406)I; erp-1(ok462)X; zxIs6[punc-17::ChR2(H134R)::YFP; lin-15+]V*	X
ZX2340	*unc-10(md1117); rimb-1(tm5964)*	X

ZX2342	*chc-1(b1025ts)III; unc-57(e406)I; zxIs6[punc-17::ChR2(H134R)::YFP; lin-15+]V*	X
ZX2343	*chc-1(b1025)III; erp-1(ok462)X; zxIs6[punc-17::ChR2(H134R)::YFP; lin-15+]V*	X
ZX2412	*unc-10(md1117); rimb-1(tm5964); zxIs6[punc-17::ChR2(H134R)::yfp; lin-15+]*	X
ZX2413	*unc-10(md1117); zxIs6[punc-17::ChR2(H134R)::yfp; lin-15+]*	X
ZX2474	*zxEx1137[primb-1::GFP; punc-17::mCherry]*	X
ZX2532	*elks-1(js816)IV ; rimb-1(tm5964) III.*	X
ZX2562	*rimb-1(tm5964)III; oxIs353[pmyo-3::ChR2::mCherry::unc-54 3'-UTR; lin15+]V*	X
ZX2574	*rimb-1(tm5964)III; zxIs3[punc-47::ChR2(H134R)::yfp; lin-15+]*	X
ZX2623/PHX1749	*unc-2(syb1749[UNC-2-ΔPDZ]) (UNC-2-ΔPDZ CRISPR deletion of 10 C-terminal amino acids)*	
ZX2624	*unc-2(syb1749[UNC-2-ΔPDZ]); zxIs6[punc-17::ChR2(H134R)::yfp; lin-15+]*	X
ZX2625	*unc-2(syb1749[UNC-2-ΔPDZ]); rimb-1(tm5964)III; zxIs6[punc-17:: ChR2(H134R)::yfp; lin-15+]*	X
ZX2626	*rimb-1(tm5964) III.;unc-47(e307) III.; zxIs6[punc-17::chop-2(H134R)::yfp;lin-15+]*	X
ZX2627	*snb-1(md247)V; oxIs353[pmyo-3::ChR2::mCherry::unc-54 3'-UTR; lin15+]V 17::ChR2(H134R)::yfp; lin-15+]*	X
ZX2691/PHX2088	*unc-2(syb2088[UNC-2-ΔPDZ]); unc-2(hp858[GFP::UNC-2]) (UNC-2-ΔPDZ CRISPR deletion of 10 C-terminal amino acids in GFP::UNC-2 insertion)*	
ZX2741	*unc-38(x20) I; zxIs6[punc-17::chop-2(H134R)::yfp;lin-15+]*	

ZX2742	*sng-1(ok234) X; zxEx1257[punc-17::sng-1-pHuji; punc-17::ChR2(H134R)::myc; pmyo2::CFP]*	X
ZX2757	*unc-2(syb1749[UNC-2-ΔPDZ]) 3x outcrossed*	X
ZX2758	*unc-2(syb1749[UNC-2-ΔPDZ]); zxIs6[punc-17:: ChR2(H134R)::yfp; lin-15+]*	X
ZX2759	*unc-2(syb1749[UNC-2-ΔPDZ]); rimb-1(tm5964)III; zxIs6[punc-17::ChR2(H134R)::yfp; lin-15+]*	X
ZX2824	*rimb-1(tm5964) III; unc-2(syb2088[UNC-2-ΔPDZ]); unc-2(hp858[GFP::UNC-2])*	X
ZX2825	*rimb-1(tm5964) III; unc-2(hp858[GFP::UNC-2])*	X

2.1.11 Software

Table 11: Used software

Name	Version	Manufacturer
Arduino	1.8	Arduino Team
Argus X1	3	Biostep
Axio Vision	4.5	Carl Zeiss
Clone Manager	9	Sci Ed Central
FIJI		Fiji contributors
Graphpad Prism	8.02	Graphpad Software
Inkscape	0.92.5	The Inkscape Team
ImageJ		National Institutes of Health
KNIME Desktop	2.12	KNIME.com
Micro-Manager	1.4	Open Imaging
Microsoft Office	365	Microsoft
MiniAnalysis	6.0.7	Synaptosoft, Decatur
NEBioCalculator	1.12.0	New England Biolabs
NEBcloner	1.8.1	New England Biolabs
OriginPro2015		OriginLab
Patchmaster software		HEKA
VirtualDub	1.10.4	Avery Lee

ZEN	2 blue edition	Carl Zeiss
ZEN lite	3.2 blue edition	Carl Zeiss

2.2 Methods

2.2.1 Molecular and Microbiological methods

2.2.1.1 Polymerase chain reaction (PCR)

The polymerase chain reaction (PCR) is one of the most widely used molecular methods, which enables the exponential amplification of a specific DNA fragment *in vitro*. The reaction can be divided into three distinct steps: denaturation, annealing and elongation. During denaturation the double-stranded template DNA is separated into single strands. Next, two complementary oligonucleotides, the primers, bind to the template, which are extended by the DNA polymerase in the elongation step. Primers are designed in a way, that they flank the target region. The forward and reverse primers are complementary to the antisense and sense strand of the DNA, respectively.

Primers, used during this work, were designed with the Clone Manager 9 software. Depending on the purpose of the amplification, different DNA polymerases were chosen to work with. *Taq* polymerase was used for genotyping, whereas the high-fidelity *Phusion* polymerase was used for cloning purposes. The PCR components and the thermocycling conditions are listed in Table 12, 13 and 14.

Table 12: PCR components using Taq (for *C. elegans* genotyping) or Phusion polymerase.

Component	***Taq* polymerase - genotyping**	**Phusion polymerase**
Template DNA	2.5 µl	variable
dNTPs (10 mM)	1 µl	1 µl
Forward primer	0.6 µl (100 µM)	2.5 µl (10 µM)
Reverse primer	0.6 µl (100 µM)	2.5 µl (10 µM)
Buffer	2.5 µl 10x ThermoPol buffer	10 µl 5x Phusion HF buffer

Polymerase	0.25 µl	0.5 µl
ddH_2O	to 25 µl	to 50 µl

Table 13: Thermocycling conditions using *Taq* polymerase.

Step		**Time**	**Temperature**
Initial denaturation		30 s	95 °C
Denaturation	32 Cycles	15 s	95 °C
Annealing		30 s	T_m – 5 °C
Elongation		60 s / kb	68 °C
Final Extension		10 min	68 °C
Pause		10 min	4 °C

Table 14: Thermocycling conditions using Phusion polymerase.

Step		**Time**	**Temperature**
Initial denaturation		30 s	98 °C
Denaturation	32 Cycles	10 s	98 °C
Annealing		30 s	T_m – 5 °C
Elongation		30 s / kb	72 °C
Final Extension		10 min	72 °C
Pause		10 min	4 °C

2.2.1.2 Genomic DNA extraction of *C. elegans*

During this work, *C. elegans* genomic DNA was extracted for genotyping or for cloning purposes, both applications consist of the same steps. First, 2.5 µl (or 5 µl for 2 PCR reactions, if the genotyping of 2 genomic regions was necessary) single egg-worm lysis buffer (SEWLB) with 2 % Proteinase K was pipetted into a PCR tube. 1-5 animals were picked into the tube, which was incubated at - 80 °C for at least 30 minutes (or overnight). Next, the sample was lysed at 60 °C for 1 hour, which was followed by the Proteinase K inactivation step (95 °C, 15 minutes). The obtained lysate was directly used as template DNA, the desired DNA fragment was amplified by PCR.

2.2.1.3 Site-directed mutagenesis

Two primers were designed in a way, that the desired point-mutation was inserted into the middle of the oligonucleotide sequences, thus, there were at least 9 bp complementary nucleotides on both sides of the primers. The oligonucleotides (forward and reverse) were completely overlapping, the obtained PCR product was the copy of the whole original plasmid with the point-mutation. Next, the PCR product was purified and digested by DpnI (according to the manufacturer's protocol), which aimed to remove the template plasmid. After inactivation of the enzyme (80 °C, 20 min), 5 µl of the mixture was transformed into *E. coli*.

2.2.1.4 Agarose gel electrophoresis

Agarose gel electrophoresis of DNA is a method which enables the separation of DNA fragments by its length. Under an electrical field, the negatively charged DNA runs in the agarose matrix toward the anode, shorter sequences run faster than large ones.
1 % gels were prepared by dissolving the agarose powder in the 1 x TAE buffer by heating up the mixture in the microwave oven. After the solution cooled down to 50 °C, it was poured into the gel tray. Once the gel was solid, the tray was moved to the gel chamber, and 1 x TAE buffer was poured over the gel. DNA samples were mixed with the loading dye (6x) and were pipetted into the pockets. DNA fragment separation was performed under a voltage of 150 V for 50-60 minutes. After this, the gel was stained in an ethidium bromide bath (0.1% (w/v) EtBr in dH_2O) for 20 minutes. Gel images were taken upon UV light exposure, for the visualization of the images the Argus X1 V.3 program was used.

2.2.1.5 DNA gel extraction

For DNA fragment extraction, the QiAquick Gel Extraction Kit was used. The extraction was performed according to the protocol with the following modifications. All centrifugation steps were carried out at 10000 x g in a table-top microcentrifuge. For the elution 30 µl Buffer EB was used, the incubation time was increased to 5 min.

2.2.1.6 PCR product purification

For PCR product purification, the QIAquick PCR & Gel Cleanup Kit was used. The extraction was performed according to the manufacturer's protocol with the following modifications. All centrifugation steps were carried out at 10000 x g in a table-top microcentrifuge. For the elution 30 µl Buffer EB was used, the incubation time was increased to 5 min.

2.2.1.7 DNA restriction digest

DNA restriction digest enables cutting a larger DNA fragment into smaller pieces, it can be used for analytical or for cloning purposes.
Restriction sites of the DNA were searched via the Clone Manager 9 software. The exact components and the optimal temperatures for the digest and for the heat-inactivation were looked up using the online NEBcloner program[1]. For analytical purposes 200-500 ng DNA was used with a final volume of 25 µl, whereas for cloning purposes much more 2-10 µg DNA was digested, if possible, using less enzyme but for an extended time[1] (if the final volume was maximal 50 µl, the mixture was aliquoted, if necessary).
[1] - https://international.neb.com/tools-and-resources/usage-guidelines/restriction-endonucleases-survival-in-a-reaction

2.2.1.8 DNA dephosphorylation

For the dephosphorylation of the 5'-ends of DNA, the Antarctic Phosphatase was used. All steps were carried out according to manufacturer's protocol.

2.2.1.9 DNA fragment ligation

Linear DNA fragments with sticky or blunt ends obtained by PCR or restriction digest, can be ligated together, thus, new circular constructs can be produced.
During this work two different ligases were used, the T4 DNA ligase and the Quick ligase. Both enzymes were used according to the manufacturer's protocol, the ligation components were always supplemented with additional ATP (0.5 µl, 100mM ddH_20 solution). For the

calculation of the insert:vector ratios, which varied between 3:1 and 6:1, the online NEBioCalculator was used (vector DNA mess was 50-100 ng). Samples were incubated either for 15 minutes at 25 °C (Quick ligase), or overnight at the 16 °C incubator (T4 DNA ligase). Heat-inactivation was applied, if necessary (T4 DNA ligase). Last, competent cells were transformed with 5 µl of the reaction.

2.2.1.10 Heat-shock transformation of *E. coli* cells

Heat-shock transformation of competent *E. coli* cells enables the amplification of newly synthetised, recombinant plasmids. During this work, calcium competent DH5α *E. coli* cells were used.

For the transformation, one vial (100 µl competent cells) was taken out from the - 80 °C freezer and was thawed on ice for about 30 minutes. Next, 5 µl of ligation mix, or 2 µl of plasmid solution was pipetted to the vial. After gently mixed, it was incubated on ice for 30 minutes. This was followed by a heat-shock step, where the mixture was placed for 45 s on a pre-heated 42 °C heat-block. Next, the vial was incubated on ice for 2 minutes, and after this, 1 ml RT LB was added, and the mixture was incubated in the 37 °C shaker incubator for an hour. The cells were centrifuged at 3000 g for 2 minutes, 950 µl medium was removed, and the bacteria was re-suspended. *E. coli* cells were plated on LB plates supplemented with respective antibiotics (the plasmid contained the antibiotics resistance gene), which allows the selection of the transformed cells. The plates were incubated overnight at 37 °C, single colonies were screened on the next day, plates were stored at 4 °C.

2.2.1.11 Plasmid DNA preparation

For plasmid DNA extraction, two kits were used. For analytical purposes (miniprep) the Roti-Prep Plasmid Mini kit was used, whereas for constructs, needed in larger amounts (midiprep), or in higher purity (such as *C. elegans* micro injection) the NucleoBond PC 100 was used. Single colonies were picked into 5 (miniprep) or 150 ml (midiprep) LB medium supplemented with the suitable antibiotics, the culture flasks were incubated overnight at 37 °C in the shaker incubator. Plasmid preparation was performed according to the manufacturer's recommendations.

2.2.1.12 DNA sequencing

DNA sequencing assignments were sent to the company Eurofins MWG GmbH. The samples were pre-mixed according to the company's recommendations (15 µl DNA solution mixed with 2 µl 10 µM sequencing primer). The results were compared to the originally planned sequences with the Clone Manager 9 software.

2.2.1.13 Cloning strategies

Most of the plasmids were created using the traditional restriction-enzyme-based cloning. For one construct (pJB10) the Gibson Assembly was used (all the steps were carried out according to the manufacturer's protocol), and there is another construct (pJB29), which was obtained using the TOPO cloning kit. In all the cases, fragments were obtained by PCR amplification or restriction digest, using plasmid DNA or genomic *C. elegans* DNA as a template.

pJB10 (*punc-17::syntintron::sng-1::unc-54-3'UTR::AmpR*): Three fragments were amplified by PCR: for AmpR::*punc-17*::syntintron the pRM348 plasmid, for *sng-1* the pAG52 plasmid and for *unc-54-3'UTR* the pAH03 plasmid was used as a template. The fragments were ligated together via Gibson Assembly.

pJB16 (*primb-1::GFP::AmpR*): *primb-1* was amplified by PCR from genomic *C. elegans* DNA with oBJ 76 and 77 primers, PCR product was digested with SapI. This was ligated into the vecor pCS179, which was previously digested by SapI and PsiI enzymes.

pJB17 (*punc-17::mCherry::AmpR*): *punc-17* was amplified by PCR from the pRM348 plasmid with oBJ 78 and 79 primers. The obtained PCR product was digested by SapI, and ligated into pCS178, which was previously digested by SapI and PsiI enzymes.

pJB24 (*pDisplay::pHuji**): the whole plasmid was amplified by PCR from the pJB22 plasmid with oBJ104 and 105 primers. After DpnI incubation and PCR purification, 5 ml from the obtained mixture was transformed to *E. coli* for getting the new plasmid.

pJB25 (*punc-17::syntintron::sng-1-pHuji*::unc-54-3'UTR::Amp*): *pHuji** was amplified by PCR from the pJB24 plasmid with oBJ107 and oBJ108 primers. The obtained PCR product was digested by BbsI and ligated intp pJB10, which was previously also digested by BbsI.

pJB26 *(punc-17::ChR-2(H134R)::myc*): *ChR-2(H134R)::myc* was amplified by PCR from the pmyo-3::myc::ChR2 plasmid with primers oBJ113 and oBJ114. The obtained PCR product and the pRM348 plasmid were both digested by NheI and the two parts were ligated together.

pJB29 (TOPO vector::*pHuji*): pHuji** was amplified by PCR from the pJB24 plasmid with primers oBJ107 and oBJ108 (primers contain BbsI restriction sites), then inserted into the TOPO vector using the TOPO cloning kit.

2.2.2 *C. elegans* methods

2.2.2.1 Cultivation of *C. elegans*

C. elegans strains were cultivated on 5.5 cm petri dishes filled with 8.2 ml Nematode Growth Medium (NGM). The plates were seeded with about 200 µl of OP50-1, the food-source of *C. elegans*, and were kept at RT. Once the bacteria have dried, animals were picked to the plates using a platinum wire, sterilized beforehand by heat. In some cases, a larger amount of animals were moved to a new plate, this was done by cutting out a piece of NGM agar of an old *C. elegans* plate (this is the so-called 'chunking'), which was done by a metal spatula, also sterilized by heat. For some experiments, it is advantageous picking the animals without any additional bacteria, for this an eyelash-pick was used, cleaned beforehand by ethanol. The strains were kept in the 16 °C or 20 °C incubator, the plates were sealed with parafilm. For some experiment plates were seeded with OP50-1 supplemented with ATR. These plates were prepared by pipetting 320 µl bacteria mixed with 0.64 µl ATR solution (100mM dissolved in ethanol) and were kept in dark by wrapping them with aluminium foil.

2.2.2.2 Male generation and crosses

C. elegans males were generated by heat-shock. L4 animals were picked to OP50-1 seeded NGM plates (6 animals/plate, 5 plates in total), which were incubated at 30 °C for 4-6 hours.

Males were picked from the next generation. In case the number of the generated males were not high enough, males were backcrossed with hermaphrodites from the same phenotype.
For the crosses, OP50-1 bacterial lawn was moved in donut-shape (diameter was 7-8 mm) into a centre of a fresh NGM plate using a platinum wire. 3-4 L4 hermaphrodites and 10-12 L4/adult males were picked into the middle of the plate, which was incubated overnight at RT. On the next day, hermaphrodites were singled to seeded NGM plates. Once the next generation appeared, plates were screened for males, which made sure that the cross worked effectively. The plate with the most F1 males was chosen, from this, 2-3 F1 hermaphrodites were singled. Next, from one of these plates 10-20 F2 animals were singled, and once the eggs were visible, these single animals were genotyped. In case further genotyping was necessary, this was either carried out by testing single animals, or the genotype of a plate with multiple animals were assessed by genotyping 4-5 random worms.
To verify the genotype of a crossed strain, at the end, 10 single animals were tested for the mutation(s) or transgene(s).

2.2.2.3 Genotyping

For genotyping a strain, genomic DNA was extracted from *C. elegans* (see chapter Genomic DNA extraction of *C. elegans*). The obtained PCR product was either purified (see chapter PCR product purification) and sent to sequencing (see chapter DNA sequencing), or an agarose gel electrophoresis (see chapter Agarose gel electrophoresis) was performed, and the images were directly analysed.

2.2.2.4 Decontamination

In case, *C. elegans* plates were infected by yeast, mold or bacteria, a decontamination was performed. For this, 15 ml bleach solution (see Table 4) was pipetted into a seeded NGM plate next to the bacterial lawn and 5-6 adult animals, with a lot of eggs, were picked into the fluid. On the next day, L1/L2 animals were picked to another seeded NGM plate which was checked regularly during the next days. Decontamination was repeated, if necessary.

2.2.2.5 Microinjection into *C. elegans*

Microinjection is an essential method in *C. elegans* research, that enables producing new transgenic strains with inheritable extrachromosomal arrays.

First, the injection mix was prepared (Table 15). The final DNA concentration was at least 110 ng/µl, this was reached by adding extra DNA (DNA ladder) to the solution, if necessary. During this work fluorescent markers were used as co-injection markers; this enables the selection of the transgenic animals. The final volume of the mix was 30 µl, the solution was centrifuged at 13000 x g for 10 minutes. Next, 15 µl from the supernatant was pipetted into a new Eppendorf tube and used for injection.

Table 15: Components of injection mix

Substance	Volume
Injection buffer	3 µl
Plasmid DNA	variable
Marker DNA	variable
DNA ladder	add to 110 ng/l, if necessary
ddH_2O	add to 30 µl

Glass capillaries were pulled with the micropipette puller. The obtained injection needles were placed vertically and were filled with approximately 0.5 µl injection mix. An injection pad (a coverslip with a dry agar pad - 2% (w/v) agar in ddH2O) was fixed to a microscope slide and was placed in the Zeiss Axiovert 40 CFL. The filled needle was inserted to the air pressure outlet and the needle was opened by the combination of applying air pressure and gently pushing it to the edge of the agar pad.

Next, a droplet of halocarbon oil was pipetted on the top of the agar pad. 1-2 young adult hermaphrodite *C. elegans*-es were picked into the oil, removed from it and placed near to the droplet. With the help of the micromanipulator the needle was positioned next to one of the distal arms of the gonads and the stage was moved in the direction of the needle, thus the tip of the needle get into the worm. For the injection, air pressure was applied, next, the injection needle was removed, and the other gonad was also injected. A drop of ddH_2O was pipetted on the top of the animal that was transferred to a seeded NGM plate. 5-6 injected animals were placed on the same plate, in total 30-40 animals were injected. Plates were cultivated on RT; in 2-3 days they were screened for transgenic animals, which were singled to seeded NGM plates, and the progeny was checked for fluorescence again.

2.2.2.6 *C. elegans* behavioural and pharmacological assays

C. elegans strains, which were tested in behavioural or pharmacological assays, were raised at 20 °C.

During the behavioural assays, transgenic animals which express Channelrhodopsin-2 (ChR2) (Liewald et al., 2008), were frequently used. For preparing these experiments, worms were raised in the presence of all-trans retinal (ATR – the co-factor of ChR2); animals were picked to ATR/non-ATR plates ~ 18 h prior to these assays. ChR2 was stimulated by blue light, as light source a 50 W mercury lamp was used which was filtered through a 450-490 nm GFP excitation filter. Contraction-assays and the light-stimulation swimming assays were performed using a Zeiss Axiovert 40 microscope equipped with a 10 x or 4 x objective, respectively. Illumination-length was defined by a computer-controlled shutter, videos were taken with a Powershot G9 digital camera at 640 x 480 resolution with 30 fps.

2.2.2.7 Swimming assay

96-well plates were filled with 100 ml NGM and 100 ml M9 buffer. Worms were picked into the fluid 15 minutes before the assay, the swimming behaviour was recorded for 60 s. In some cases, the behaviour was analysed before and after light stimulation (blue light intensity: 0.53 mW/mm^2), in these experiments photostimulation was applied for 90 s and after an additional 90 s incubation time, another 60 s was filmed. The swimming cycles (the worm's body bends twice per cycle) were counted manually.

2.2.2.8 Contraction assay

A single worm was picked with an eyelash-pick on the middle of a non-seeded RT NGM plate, which was placed in the Zeiss Axiovert 40 microscope. The video recording was started, and after a few seconds, the animal was stimulated with blue-light (1.4 mW/mm^2).

The videos were analysed as previously described (Erbguth et al., 2012). The before light stimulation length values were averaged, and next, all the length values were normalized using this number. Normalization was performed for each worm. Values below 0.8 were excluded, after this, the average length values were counted for each strain.

For the assay with the strains which contained the heat-sensitive *chc-1* allele (*b1025ts*), a heat-shock protocol was used. Animals were raised at 15 °C, and for the heat-shock (14 minutes, 30 °C), pre-warmed (at least 3 minutes at 30 °C) plates were used. After the heat-shock, worms were incubated at RT for 4 minutes.

2.2.2.9 Aldicarb and levamisole assays

For aldicarb assays 1.5 mM aldicarb plates (Mahoney et al., 2006), for levamisole assays 2 mM tetramisole plates (a racemic mixture, corresponding to 1 mM levamisole concentration) were prepared (different strains were tested on the same batch of dishes on the same day). One hour before the experiment, the middle of the plates was seeded with 4 µl OP50-1 bacteria. Young adults were transferred to this and animals were tested (by three gentle touches using a hair pick) every 30 minutes whether they are paralyzed. The pharmacological assays were carried out blinded.

2.2.3 Microscopy

2.2.3.1 Stereo microscopy

For *C. elegans* cultivation and during the preparation of some experiments a Nikon SMZ 645 stereo microscope was used.

2.2.3.2 Fluorescence microscopy

Strains, carrying extrachromosomal arrays and fluorescent co-injections markers, were screened and cultivated using a Leica MZ 16F fluorescence stereomicroscope.
For expression pattern analysis either a Zeiss Axiovert 200 microscope or a Zeiss Cell Observer SD spinning disc confocal microscope was used. Quantitative analysis of fluorescent signals was carried out using a Zeiss Axio Observer Z1, or a Zeiss Cell Observer SD spinning disc confocal microscope. The pOpsicle assays were carried out with a Zeiss Axio Observer Z1 microscope.

2.2.3.2.1 Expression pattern analysis of ERP-1 and RIMB-1

Animals were transferred onto 10 % agarose pads in M9 buffer and were immobilized with 0.1 µm Polystyrene beads.

For the ERP-1 analysis, the p*erp-1*::GFP (strain BC12478) and the p*unc-17*::ChR2(H134R)::YFP (strain ZX460) strains were analysed using the Zeiss Axiovert 200 microscope. This was supplemented with a 40x/0.25 Zeiss oil objective and a GFP filter set (Ex 470/40, Em 525/50 nm). Images were taken with an ORCA-Flash4.0 digital sCMOS camera.

The expression pattern of RIMB-1 was analysed by comparing the fluorescent signals of *primb-1*::GFP and p*unc-17*::mCherry (strain ZX2474). For this, a Zeiss Cell Observer SD spinning disc confocal microscope was used equipped with a 40x/0.6 Zeiss air objective, a LED-based illumination system (excitation wavelengths 488 nm and 561 nm) and a Zeiss double band pass emission filter (DBP 527/54 + 645/60). Images were obtained with a Rolera EM-C2 EMCCD camera.

2.2.3.2.2 Quantitative analysis of GFP::UNC-2

Single animals (from the strains ZX2691, ZX2824, ZX2825 and ZM9583) were picked onto 10 % agarose pads in M9 buffer and were immobilized with 1 µl 20 mM tetramisole hydrochloride. The fluorescent intensity of the GFP::UNC-2 signal in the nerve ring was analysed with a Zeiss Axio Observer Z1 microscope and also with a Zeiss Cell Observer SD spinning disc confocal microscope.

The Zeiss Axio Observer Z1 microscope was used for widefield fluorescence imaging, for this, a 40x/1.3 Zeiss oil objective, a 460 nm LED and a GFP filter cube (Ex 470/40, Em 520/35 nm) was used. The micrographs were obtained with an Evolve 512 Delta EMCCD camera, for controlling the gain (68) and the exposure time (50 ms) the Micro Manager software was used. The desired observation site was searched using only the transmission light. A series of images were taken, fluorescent light was turned on after a few seconds. The second frame with visible fluorescence of each image series was analysed using the FIJI software.

The Zeiss Cell Observer SD spinning disc confocal microscope was used for taking Z-stacks of the nerve ring. The equipment of the microscope consisted of a 63x /1.4 Zeiss oil objective, a 488 nm LED, and a 520/35 nm emission filter. The ZEN 2 blue software was used for

controlling the gain (150) and the exposure time (1000 ms), images were taken with a Rolera EM-C2 EMCCD camera. The nerve ring was located using the transmission light, Z-stacks were obtained using a NanoScanZ Piezo Z stage. In total 40 images per animal were taken with a 0.5 µm spacing, these were afterwards z-projected and analysed with the FIJI software.
Using the FIJI software, the nerve ring was selected by placing a ROI around it, and mean fluorescence intensity was calculated. A background intensity, measured in the worm's head close to the nerve ring, was used for background correction.

2.2.3.2.3 pOpsicle assay

L4 animals of the strain ZX2742 were transferred to ATR/non-ATR plates ~ 18 h before the experiment. 10 % agarose pads in M9 buffer were prepared, single worms were picked onto this and were immobilized with 1 µl 20 mM tetramisole hydrochloride. The experiment was performed using a Zeiss Axio Observer Z1 microscope equipped with a 100x/1.4 Zeiss oil objective, two LEDs (460 nm for ChR2 stimulation and 590 nm for pHuji visualization), and a filter cube (double band pass Ex: 479 and 585 nm combined with a 605 nm beam splitter and a 647 nm emission filter). The Micro Manager software was used for controlling the gain (68) and the exposure time (50 ms). Videos were acquired with an Evolve 512 Delta EMCCD camera.
The desired observation site (distal part of the dorsal nerve chord close to the tail of the animals) was searched by briefly turning on the 590 nm LED. After a short incubation time in the dark, the measurement was started. The 590 nm LED was turned on (10 s before light stimulation), after 10 s the 460 nm LED was also turned on (10 s light stimulation), finally the recording was continued for an additional 60 s using only the 590 nm LED (60 s after light stimulation). The image sequences were analysed using the FIJI software. A ROI was placed on the top of the dorsal nerve chord, for this the segmented line tool (line width: 8) was used. A second ROI was selected inside of the worm very close to the first one, that was used for the background correction. From the background corrected numbers, the $\Delta F\text{-}F_0/F_0$ values were calculated for single worms (where F_0 was the average mean grey value before light stimulation). These were then averaged to get the final graphs for the with/wo ATR groups.

2.2.3.3 Electronmicroscopy of *C. elegans* – performed mainly by Dr. Szi-chieh Yu

Electronmicroscopy was carried out based on previously described methods (Kittelmann et al., 2013; Rostaing et al., 2004; Weimer, 2006). NGM plates were seeded with OP50-1 supplemented with/wo ATR (0.1 mM), transgenic L4 worms were transferred onto these 1-2 days prior to the high-pressure freezing (HPF). For the HPF, 10-40 young adult animals and some extra OP50-1 +/- ATR were picked into an aluminium carrier, which was covered with a sapphire disc and a spacer ring. All these steps were carried out in the dark room under a red light, that should prevent the ChR2 pre-activation. Next, worms were illuminated continuously for 30 s using a blue laser (~20 mW/mm^2), which was followed by the manual sample insertion into the freezer (~6 s) and the HPF. In some experiments, the *chc-1* mutants (*b1025ts*) were used, these animals were kept constantly at 15 °C before HPF (worms were loaded into the carrier at RT and were frozen immediately, some of the groups were heat-shocked before at 30 °C for 14 minutes).

This was continued by the freeze substitution. Samples were kept under liquid nitrogen, and they were brought to the Reichert AFS machine. Samples were covered with a tannic acid solution (0.1 % in dry acetone) and they were incubated at -90 °C for 100 hours. This was followed by washing, and then the samples were incubated in an OsO_4 solution (2 % in dry acetone) at slowly increasing temperatures for 39.5 hours. In the following steps the samples were kept at RT. For embedding, an epoxy resin was used. The starter concentration of this was 50 % (in dry acetone), which was stepwise increased to 100 %. Last, samples were covered with 100 % epoxy resin, and they were dried at 60 °C for at least 48 hours.

In the next step, samples were cross-sectioned using the EM UC6 ultramicrotome, and the 40-nm-thick sections were transferred to the TEM grids. These were then stained with a 2.5 % aqueous uranyl acetate solution for 4 minutes, washed with distilled water, stained with a Reynolds lead citrate solution for 2 minutes, and finally washed again with distilled water.

The ventral nerve chord of the animals was searched using a Philips CM12 transmission electron microscope (operated at 80 kV), micrographs were obtained with an Erlangshen ES500W CCD camera. The images were blind analysed using the ImageJ software. The plasma membrane of the neuron was saved as a ROI and was quantified according to previously described methods (Steuer Costa et al., 2017). To compare the different parameters in the different groups, the number of the docked synaptic vesicles (DSVs) was normalized using an average value which represent the mean synaptic perimeter (1548 nm) of all the analysed

images. For the normalization of the number of synaptic vesicles (SVs) or large vesicles (LVs), the average synaptic area (164100 nm^2) was used (Steuer Costa et al., 2017). For the scoring of the SVs, randomly selected single images per synapse or 3 to 10 middle images of randomly selected synapses were used for each group. Typically, 2-3 worms with 10-19 synapses per group were analysed.

2.2.4 Electrophysiology of *C. elegans* – performed by Dr. Jana F. Liewald

Electrophysiological recordings were performed from body wall muscle cells of *C. elegans* in immobilized and dissected animals as described previously (Liewald et al., 2008). For immobilization, a Histoacryl glue was used. To access neuromuscular junctions along the anterior ventral nerve cord, a lateral incision was made. For enzymatically removing the basement membrane overlying body wall muscles, the samples were incubated in 0.5 mg/ml collagenase for 10 s. Prior to the recording the integrity of body wall muscle cells and nerve cord was visually examined using DIC microscopy. Recordings were acquired at 20-22 °C, using an EPC-10 amplifier equipped with Patchmaster software. The head stage was connected to a standard HEKA pipette holder for fire-polished borosilicate pipettes of of 4-9 MΩ resistance, recordings were sampled at 3.33 kHz.

The extracellular bath solution consisted of 150 mM NaCl, 5 mM KCl, 5 mM CaCl2, 1 mM MgCl2, 10 mM glucose, 5 mM sucrose, and 15 mM HEPES (pH 7.3 with NaOH,~330 mOsm). The internal/patch pipette solution consisted of K-gluconate 115 mM, KCl 25 mM, CaCl2 0.1 mM, $MgCl_2$ 5 mM, BAPTA 1 mM, HEPES 10 mM, Na_2ATP 5 mM, Na_2GTP 0.5 mM, cAMP 0.5 mM, and cGMP 0.5 mM (pH 7.2 with KOH,~320 mOsm). With these solutions, reversal potentials are about +20 mV for nicotinic ACh receptors (nAChRs) and -30 mV for GABAA receptors (Maro et al., 2015). Holding potential was −60 mV, where nAChR- related currents (EPSCs) and GABAA receptor-related currents (IPSCs) both display as inward currents.

For the photoactivation a LED lamp was used (470 nm, 8 mW/mm^2) which was controlled by the Patchmaster software. Subsequent analysis was also carried out with the Patchmaster software. For analyzing the mPSCs (frequency, amplitude) and to acquire the time to peak parameter, the MiniAnalysis software was used.

2.2.5 Voltage imaging of *C. elegans* – performed by Amelie Bergs

One day before the experiments, L4 animals were transferred onto ATR plates (final ATR concentration: 0.01 mM). On the next day, young adults were transferred onto 10 % agarose pads (in M9 buffer) and were immobilized with 0.1 μm polystyrene beads. ChR2(H134R) was stimulated by a monochromator at 300 $\mu W/mm^2$, while voltage-dependent fluorescence of Arch(D95N) was excited with a 637 nm red laser at 1.8 W/mm^2 and imaged at 700 nm (700/75 ET bandpass filter, integrated in Cy5 filter cube). For the imaging, a Zeiss Axio Observer Z1 microscope was used, equipped with a 40x/1.3 Zeiss oil immersion objective, a laser beam splitter, a galilean beam expander and an Evolve 512 Delta EMCCD camera.

2.2.6 Statistical analysis

All quantitative data visualized on the graphs are mean ± SEM values, if not mentioned otherwise. 'N' represents the number of the replicates (typically 2-3) and 'n' the number of the analysed worms. The reported significances were calculated using the two-tailed Student's t-test combined with the Bonferroni correction after one-way ANOVA, or two-way ANOVA combined with Bonferroni, Tukey, Dunnett or Kruskal-Wallis post-hoc test. For some pharmacological assays the data was compared across the duration of the experiment, in these cases the Log-Rank test was used with Bonferroni correction. The respective statistics and the p-values are represented in the figure legends, but generally * means $p<0.05$, ** $p<0.01$ and ***$p<0.001$. For the analysis and the plotting, the GraphPad Prism, Excel and OriginPro2015 softwares were used.

3. Results

3.1 Characterization of synaptic vesicle recycling factors

Synaptic vesicles (SVs) undergo a constant cycle of biogenesis, fusion, and recycling to sustain a fast and repeated neurotransmitter release. After docking and priming, neurotransmitter is released via Ca^{2+} triggered SV exocytosis, which is followed by SV endocytosis and recycling (Südhof, 2004). This cycle is modulated by numerous proteins, some of which are well-known players, however, there are a lot of proteins with unclear roles. In a previous publication (Wabnig et al., 2015) putative synaptic vesicle recycling factors were identified through a high-throughput all-optical analysis. After cluster analysis, the most promising candidates (*eel-1, let-60, sad-1, inx-8, inx-10, itsn-1*) were chosen (Figure 10) and the respective *C. elegans* mutants (*ok1575, sy93, ky289, gk42, ok2714, ok268*) were screened via behavioural assays.

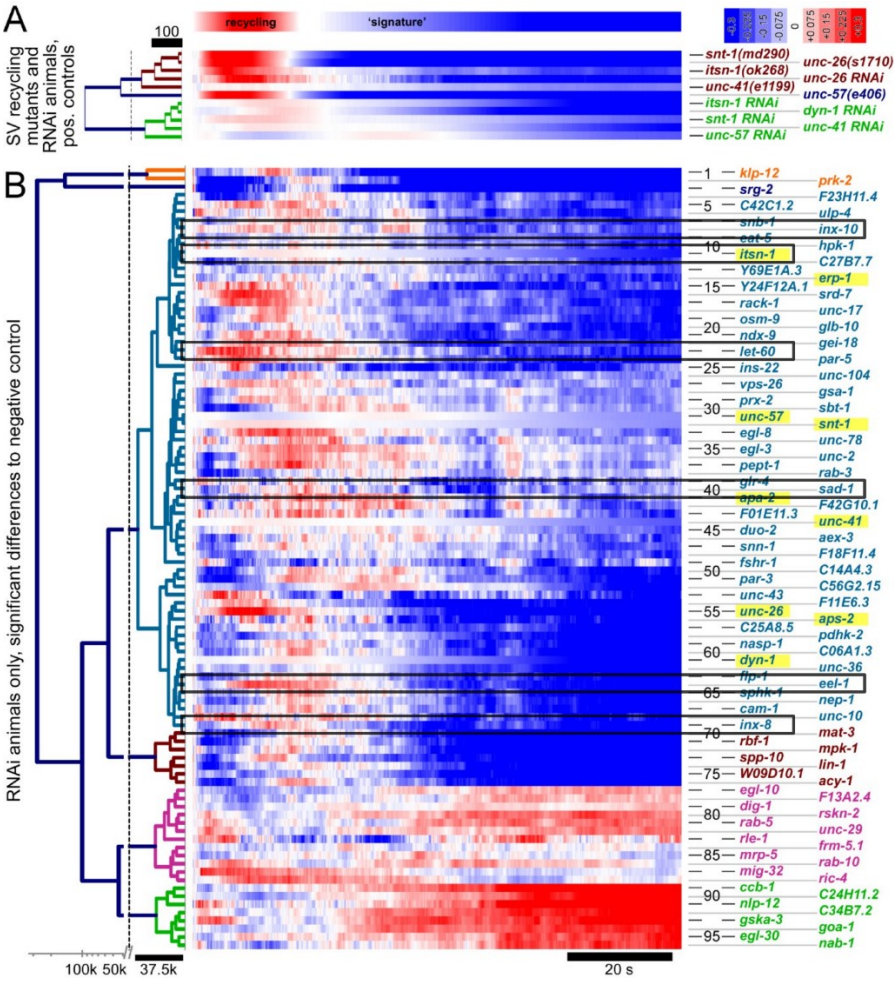

Figure 10: Putative synaptic vesicle (SV) recycling factors were identified in a previous high-throughput all-optical analysis (modified from: (Wabnig et al., 2015)). Motoneuron photostimulation combined with muscular Ca^{2+} imaging enables to detect SV recycling factors by their typical Ca^{2+} pattern. **(A)** Positive controls. **(B)** Cluster analysis of 96 genes, which showed significantly altered Ca^{2+} dynamics in the above-mentioned assay.

The most promising candidates (*eel-1, let-60, sad-1, inx-8, inx-10, itsn-1* - marked with a black frame) were further analysed via behavioural assay in this work.

3.1.1 *sad-1*

SAD-1 is a serin/threonine kinase, which has a role in presynaptic differentiation and SV clustering (Crump et al., 2001) and showed a recycling phenotype in the previously mentioned study (Wabnig et al., 2015). *sad-1 (ky289)* mutants were tested in the well-established swimming- (also called trashing-) assay. For this, animals were picked into M9 buffer and after a 15-minutes-long initial incubation time, a 60-s-long video was recorded. The frequency of the swimming movements (swimming cycles/min) was counted manually. Wild type animals show rapid swimming behaviour, while animals with mutations that affect the SV cycle in cholinergic neurons, typically swim with reduced speed, or they do not swim at all (Schultheis, Brauner, et al., 2011). The swimming activity of animals lacking SAD-1 was decreased significantly compared to wild type animals (Figure 11).

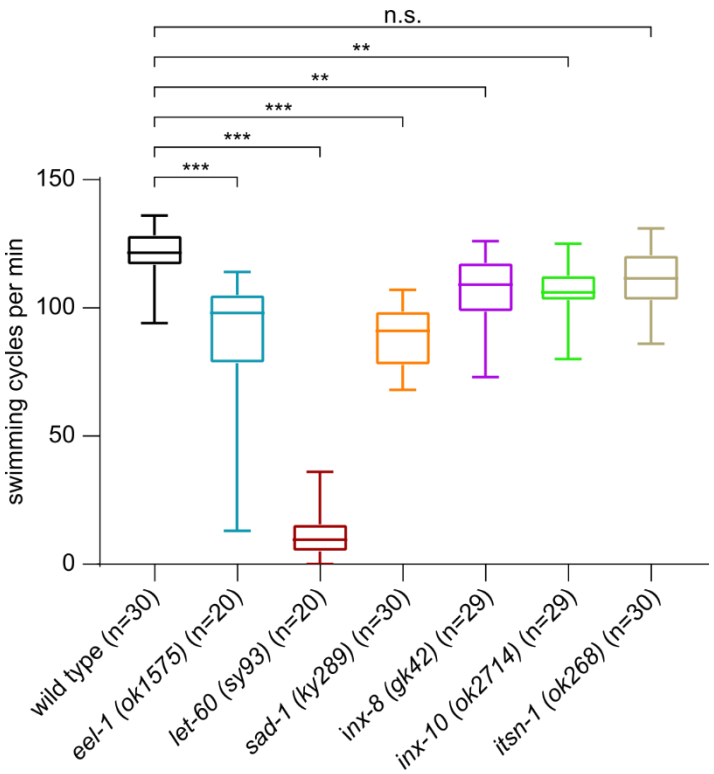

Figure 11: Swimming assay in putative synaptic vesicle recycling factor mutant strains. The total number of tested animals is indicated as n numbers, the assay was repeated 2-3 times (on different days, with different animal populations). Data shown as median and 25/75 quartiles, min to max. Statistical significance given as **p<0.01, ***p<0.001 after one-way ANOVA and Bonferroni post-hoc test.

3.1.2 *eel-1*

EEL-1 is involved in several processes, such as the regulation of early embryonic development (Page et al., 2007; Zahreddine et al., 2010) and is expressed in the nervous system including GABAergic and cholinergic motor neurons (Opperman et al., 2017). Besides, *eel-1* mutants showed altered, recycling-phenotype-like Ca^{2+} dynamics in body wall muscles (Wabnig et al., 2015)(Figure 10). Thus, *eel-1 (ok1575)* mutants were probed in swimming assay (Figure 11). The average number of swimming cycles was around 100/60 s, whereas for wild type animals it was about 125/60 s. This difference is statistically significant.

3.1.3 *let-60*

Another putative recycling factor is LET-60 (Wabnig et al., 2015), an ortholog of human HRAS. *let-60* is widely expressed in *C. elegans* also in the nervous system (Dent & Han, 1998) and is involved among others in vulval development (Beitel et al., 1990; M. Han & Sternberg, 1990), learning and memory (Gyurkó et al., 2015). *let-60* mutants showed a strong phenotype in swimming assay (Figure 11). The number of the swimming cycles was at about 10/60 s, which is strongly decreased compared to wild type animals. This low rate indicates that let-60/ras mutants likely have multiple phenotypes that contribute to locomotion in different cell types and pathways. Identifying an SV recycling related phenotype would require perform cell-specific knockdown in cholinergic neurons.

3.1.4 *inx-8, inx-10*

INX-8 and INX-10 are members of the innexin (intervertebrate gap junction subunits) family in *C. elegans.* Both genes are expressed in neurons (Z. F. Altun et al., 2009) and the knockdown of these genes caused recycling-mutant-type Ca^{2+} traces (Wabnig et al., 2015) (Figure 10).
First, *inx-8 (gk42)* and *inx-10 (ok2714)* mutants were probed in swimming assay (Figure 11). Both genotypes showed around 110 swimming cycles/60 s, which is a significant decrease compared to wild type animals. Next, animals were tested in contraction assays, which enables to measure the rate of cholinergic transmission indirectly. Animals expressing ChR2 in the cholinergic neurons, show - in the presence of all-trans retinal (ATR - the co-factor of ChR2,

which renders this protein functional)-, rapid body contraction during blue-light-illumination (Liewald et al., 2008). Wild type animals can keep the level of the contraction for prolonged periods, whereas (SV) recycling mutants show typically a progressive relaxation, also called 'recycling phenotype' (Wabnig et al., 2015). Animals carrying ChR2 (variant C128S) in the form of the integrated *zxIs58* transgene, were raised with/without ATR. As expected, wild type animals raised in the presence of ATR contracted upon blue light stimulation immediately and kept this contracted state during and after illumination (Figure 12, 13) (Wabnig et al., 2015). Wild type animals raised without ATR did not show any contraction. There was no altered phenotype visible for the *inx-8* mutants (Figure 12), whereas *inx-10* mutants showed also a wild-type-like contraction profile, however, a slightly increased contraction was visible in this group (Figure 13).

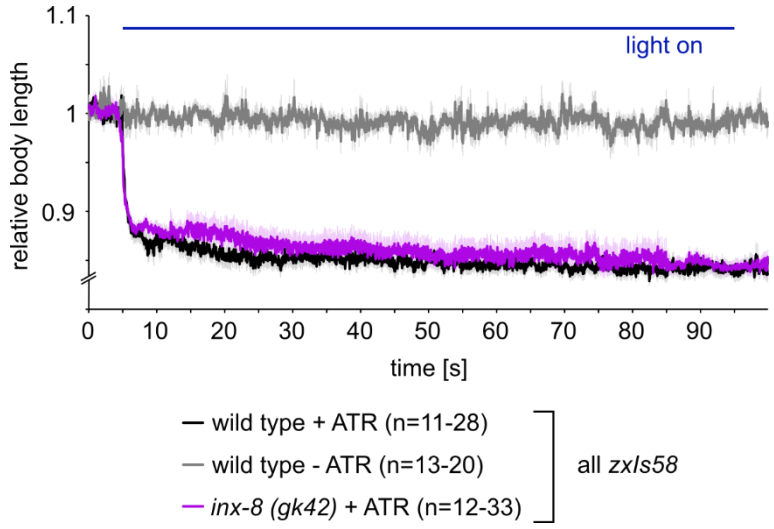

Figure 12: *inx-8* mutants did not show a phenotype upon optogenetically induced muscle contraction. Wild type animals and *inx-8* mutants (both expressing ChR2 in cholinergic neurons in form of the *zxIs58* transgene) were probed in a contraction assay. Animals were raised with/without ATR (all-trans retinal – the co-factor of ChR2) as indicated. In the presence of ATR animals contracted during the blue light illumination. The n numbers are indicated, where the smaller number represents the minimum number of animals (coiling animals were excluded in the time window while they coiled), whereas the bigger number indicates the number of the tested animals. Blue light stimulation was used to activate the cholinergic transmission, the length of the illumination was 60 s, started after a 5-s-long initial dark period.

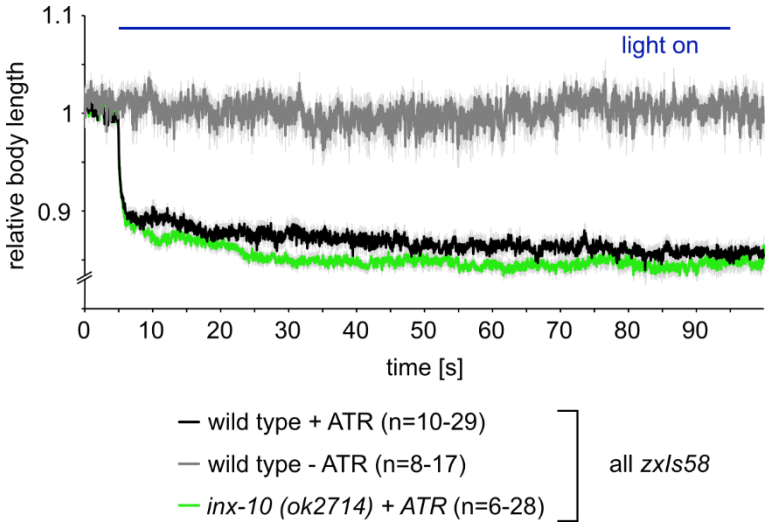

Figure 13: *inx-10* mutants showed slightly increased contraction than wild type animals. Wild type animals and *inx-10* mutants were tested in contraction assay. Experiment conditions as in Fig. 12.

3.1.5 *itsn-1*

ITSN-1 is responsible for the regulation of SV endocytosis and actin assembly (W. Wang et al., 2008). As expected, *istn-1* mutants showed the SV recycling Ca^{2+} pattern in the above mentioned high-throughput all-optical analysis (Wabnig et al., 2015), however, according to previous publications it was not clear yet whether ITSN-1 promotes (W. Wang et al., 2008) or inhibits (Rose et al., 2007) the endocytic events. To investigate this, behavioural experiments were performed.

In the swimming assay, there was no significant difference between wild type animals and *itsn-1* mutants (Figure 11). Next, a contraction assay was carried out (Figure 14). Again, *itsn-1* mutants did not show any difference compared to wild type animals. During blue light stimulation both groups raised with ATR contracted initially at about 10 % and they kept this contracted state until the very end of illumination. After this, a pharmacological assay was performed (Figure 15). Cholinergic transmission can be probed using the aldicarb assay. Aldicarb is an acetylcholinesterase inhibitor, the presence of which leads to acetylcholine accumulation in the synaptic cleft. This results in the over-activation of the acetylcholine receptors, that manifests in hyper-contraction of the muscles, ongoing paralysis, and death. Mutants with altered cholinergic transmission show faster or slower paralysis than wild type animals (Mahoney et al., 2006; K. G. Miller et al., 1996). 1 mM aldicarb plates were prepared, animals were placed onto these, and their locomotion ability was controlled every 30 minutes. *itsn-1* mutants appeared to show a clear aldicarb resistant phenotype, however, the difference

between wild type animals and *itsn-1* mutants was not statistically significant. Since these results were inconclusive, analysis of *itsn-1* was not further pursued.

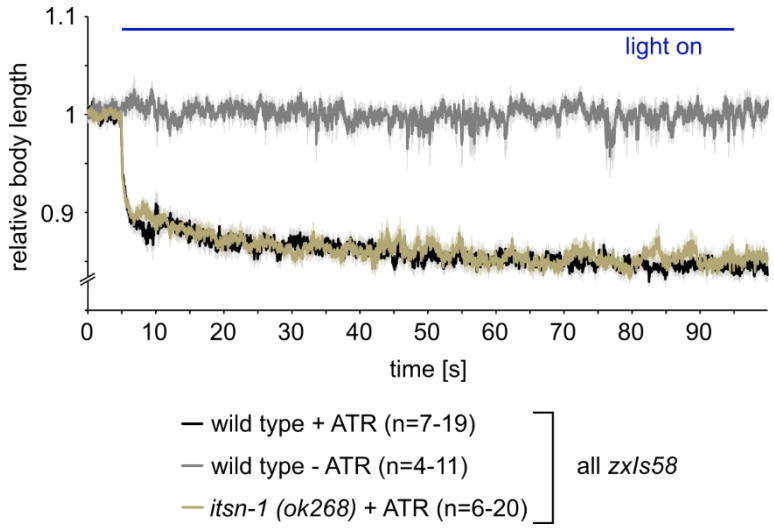

Figure 14: *itsn-1* mutants and wild type animals showed the same contraction pattern. Wild type animals and *itsn-1* mutants (both expressing ChR2 in cholinergic neurons in form of the *zxIs58* transgene) were tested in contraction assay. Animals were raised with/without ATR (all-trans retinal – the co-factor of ChR2), in the presence of ATR animals contracted during the blue light illumination. The n numbers are indicated, where the smaller number represents the minimum number of animals (coiling animals were excluded in the time window while they coiled), whereas the bigger number indicates the number of the tested animals. Blue light stimulation was used to activate the cholinergic transmission, the length of the illumination was 90 s, started after a 5-s-long initial period.

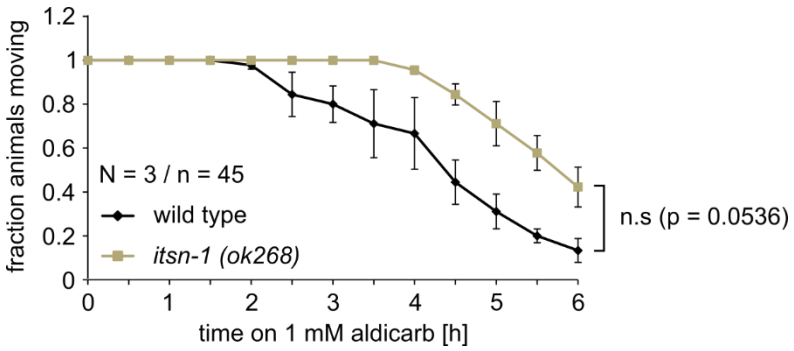

Figure 15: Mutants lacking ITSN-1 showed an aldicarb resistant phenotype. Aldicarb assay with 1 mM aldicarb plates. The indicated genotypes were tested and scored 3 times (on 3 different days, with worms from 3 different populations). The averaged graphs show that *itsn-1* mutants paralyzed slower than wild type animals. Shown are means ± SEM. n.s after Log-Rank test with Bonferroni correction.

Although some mutant phenotypes were visible in the above-described experiments, these were not as pronounced as we wished, thus it was not possible to draw proper conclusions. Swimming assay is a common test for measuring *C. elegans* motility, but this behaviour is driven by a complex neuromuscular network, thus, it serves only as a first hint in the identification of recycling genes. Aldicarb assay is a more direct test for investigating

cholinergic mutants. Aldicarb-resistant animals possess either a presynaptic defect in neurotransmitter release, or a postsynaptic defect, which can be distinguished using another pharmacological test (Mahoney et al., 2006). However, all presynaptic genes, that influence the SV cycle may affect the phenotype, thus, it is not possible to select the recycling genes. With the help of the contraction assay it is possible to find genes, which probably influence the SV recycling due to the characteristic contraction pattern (Liewald et al., 2008). Nonetheless, this is also an indirect assay, influenced by feedback mechanisms, which can complicate the interpretation of the results. Therefore, we changed our strategy. Instead of choosing 2-3 genes based on the behavioural results and use the respective *C. elegans* mutants for further extensive analysis (electrophysiology, transmission electron microscopy etc.), we concentrated on the investigation of two other candidate proteins: ERP-1 and RIMB-1. Furthermore, we aimed to create an assay, which enables the visualisation of released neurotransmitter and the direct analysis of the SV recycling process.

3.2 A novel player in SV recycling: endophilin B cooperates with endophilin A and clathrin to promote the regeneration of SVs

Endophilin-A (encoded by *unc-57* in *C. elegans*) has a crucial role in SV endocytosis: it recruits other essential proteins (Schuske et al., 2003; Sundborger et al., 2011) and has a membrane-bending function (Bai et al., 2010). Endophilin-B (encoded by *erp-1* in *C. elegans)* was recently identified as an SV recycling factor (Wabnig et al., 2015), but its possible contribution to SV endocytosis was not investigated yet. Clathrin (clathrin heavy chain encoded by *chc-1* in *C. elegans*) has a role in clathrin-mediated-endocytosis (Heuser & Reese, 1973) and also in ultrafast endocytosis, where it plays a role not at the plasma membrane (PM) but at the level of the endosomes and supports the regeneration of SVs (Watanabe et al., 2014).
During this project the function and a possible cooperation of UNC-57, ERP-1 and CHC-1 was investigated, with a special emphasis on the site of action (at the PM or at the membrane of the LVs) of these proteins. For this, behavioural, pharmacological, optogenetic, electrophysiological and ultrastructural assays were performed using *C. elegans*.

3.2.1 ERP-1 is expressed in cholinergic motor neurons

To investigate the localization of ERP-1, the expression pattern of P*erp-1*::GFP (strain BC12478, obtained from the CGC) was analysed (Figure 16). This was compared with the P*unc-17*::ChR2::YFP cholinergic marker strain, in which cholinergic neurons express YFP. The focus was on the ventral nerve chord (VNC) that consists of GABAergic and cholinergic motor neurons (White et al., 1976). As shown in Figure 16, the Perp-1::GFP animals possessed many more bright spots along the VNC than the control strain, thus ERP-1 is expressed not only in cholinergic but also in the GABAergic motor neurons. For further verifying this concept, motor neuron cell bodies were tentatively assigned.

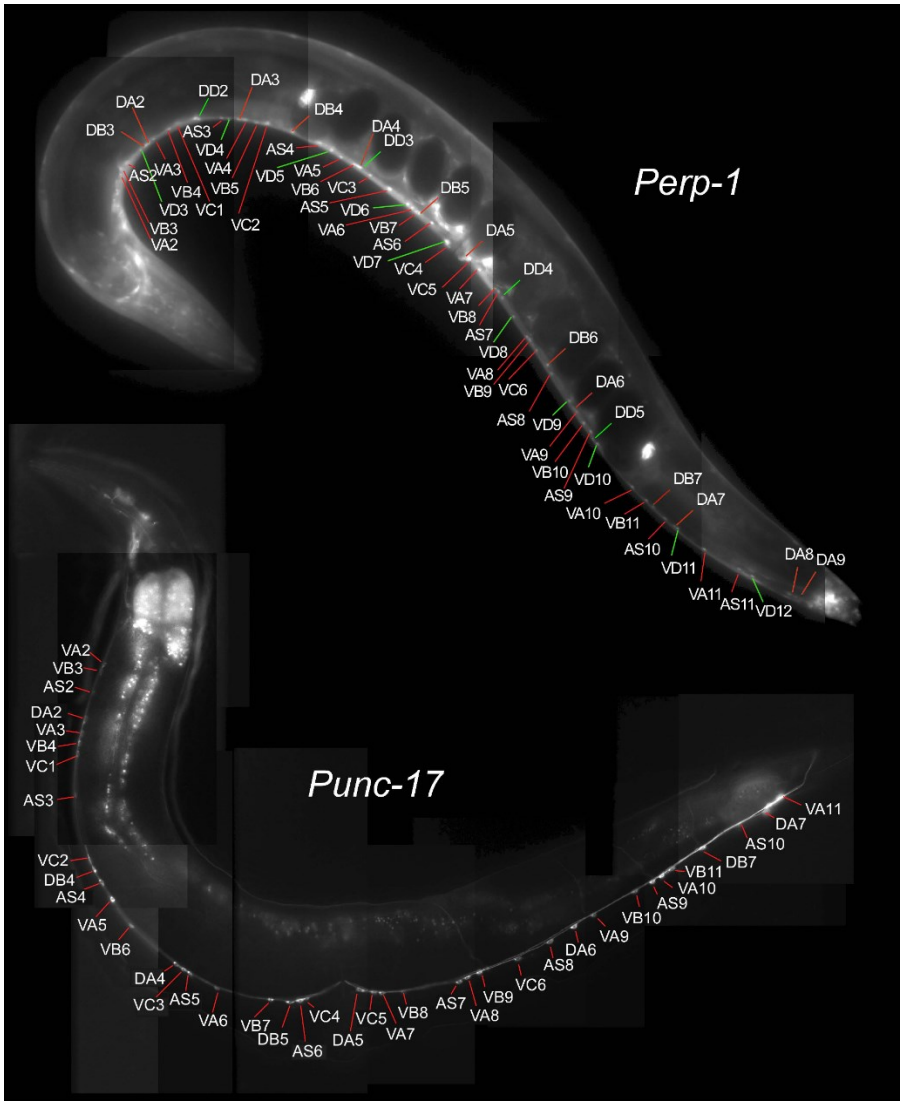

Figure 16: ERP-1 is expressed in cholinergic and GABAergic motor neurons. Representative images comparing the Perp-1::GFP (above) with the Punc-17::ChR2::YFP (Punc-17 is a cholinergic specific promoter - below) expression patterns along the ventral nerve chord in *C. elegans*. Cholinergic motor neurons are marked with red, whereas GABAergic motor neurons are marked with green lines. The fluorescent micrographs were compiled from smaller images.

3.2.2 *erp-1* mutants exhibit reduced cholinergic transmission

As a next step, cholinergic transmission of *erp-1(ok462)*, *unc-57(e406)* and *erp-1(ok462); unc-57(e406)* mutants were tested by pharmacological and behavioural assays. First, an aldicarb assay was performed.

The different genotypes were probed 5 hours long on 1.5 mM aldicarb plates (Figure 17). Wild type animals were almost completely paralyzed at the end of the assay, whereas about half of the *erp-1* mutants still moved at this point. The other three genotypes, *unc-57* (endophilin A) mutants, *erp-1; unc-57* double mutants and the positive control *unc-10* (RIM) mutants, showed

a very strong aldicarb resistant phenotype. This was also confirmed by the statistical analysis, which showed that these mutants differ significantly compared to the wild type group.
This assay showed that the lack of ERP-1 results in decreased acetylcholine transmission, whereas the lack of UNC-57 results in an even more pronounced reduction.

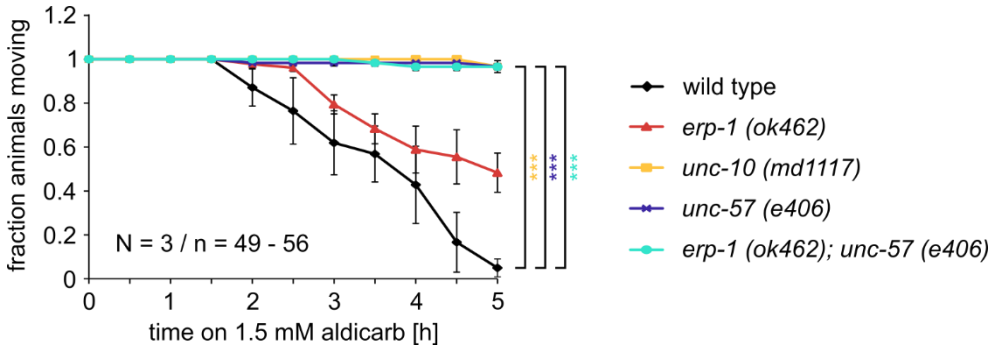

Figure 17: Mutants that lack ERP-1 showed aldicarb resistant phenotypes. Aldicarb assay with 1.5 mM aldicarb plates. The indicated genotypes were tested and scored 3 times (on 3 different days, with worms from 3 different populations). The averaged graphs depict that *erp-1* mutants paralyzed slower than the wild type animals, whereas *unc-57* mutants and the *erp-1; unc-57* double mutants showed an even stronger aldicarb resistant phenotype such as the positive control *unc-10* mutants. Shown are means ± SEM. ***p<0.001, after Log-Rank test with Bonferroni correction.

For further investigating the cholinergic function of *erp-1* mutants, a swimming assay was carried out. Animals expressing ChR2 in cholinergic cells (via the *zxIs6* transgene) were probed in a two-round swimming assay (Figure 18). First, swimming behaviour was investigated after the initial incubation time, and next, a 90-s-long blue light illumination was applied, which aimed to activate the cholinergic transmission. After this, animals were kept in dark for another 90 s, which was followed by the second swimming assay. Under standard conditions (without ATR, before light stimulation), *erp-1* mutants showed a slightly, but significantly reduced swimming rate. Wild type animals showed no difference in the swimming behaviour after the optogenetic stimulation, regardless of whether they were raised with or without the ChR2 co-factor all-trans retinal (ATR). Contrarily, mutants lacking ERP-1 showed a statistically significant decrease in the second swimming assay compared to the first one. Thus, photostimulation caused an exercise-induced fatigue in the swimming behaviour of *erp-1* mutants, probably caused by reduced cholinergic transmission.

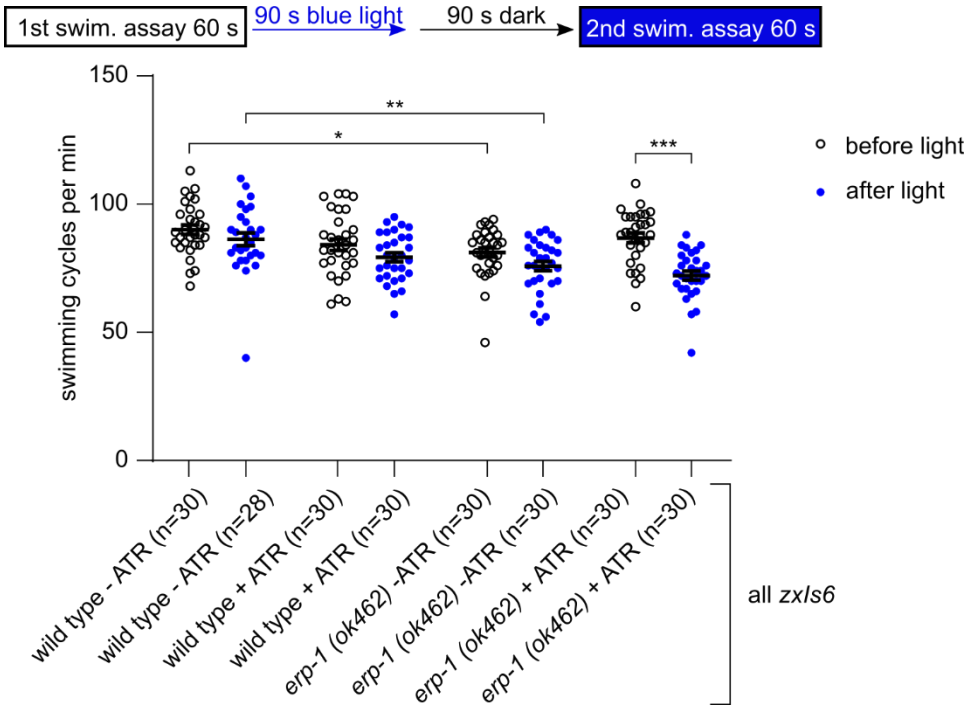

Figure 18: *erp-1* mutants showed exercise-induced fatigue in a swimming assay. Wild type animals and *erp-1* mutants (both expressing ChR2 in form of the *zxIs6* transgene) were compared in a two-round swimming assay under different conditions. After the first round of swimming assay, a 90-s-long blue light illumination was used to activate the cholinergic transmission. Animals were incubated in dark for 90 s (the time after the swimming cycles of wild type animals reverted to normal) and the second round of swimming assay was recorded. Wild type animals showed no difference in the swimming behaviour after this treatment, whereas there was a significant reduction in the swimming cycles/min for the *erp-1* mutants. The total number of tested animals is indicated as n numbers, the assay was repeated 3 times (on different days, with different animal populations). Animals were raised with/without ATR (all-trans retinal – the co-factor of ChR2). Scatter plot with mean ± SEM. *p<0.05, **p<0.001, ***p<0.001, after two-way ANOVA with Bonferroni post-hoc test.

The rate of cholinergic transmission can be indirectly measured via the contraction assay. Wild type animals and *erp-1* mutants were filmed for 130 s, blue light illumination was started after an initial 5 s. As expected, wild type animals raised without ATR did not show any contraction (Figure 19). In the presence of ATR, wild type animals contracted by about 6 % of their body length, and this did not change during the whole length of photostimulation. On the other hand, *erp-1* mutants also contracted by about 6 % at the beginning of the illumination, however, the level of the contraction decreased progressively; at the end of the photostimulation it was only about 3 %. This difference was also statistically significant. Thus, mutants lacking ERP-1 showed the typical SV recycling phenotype.

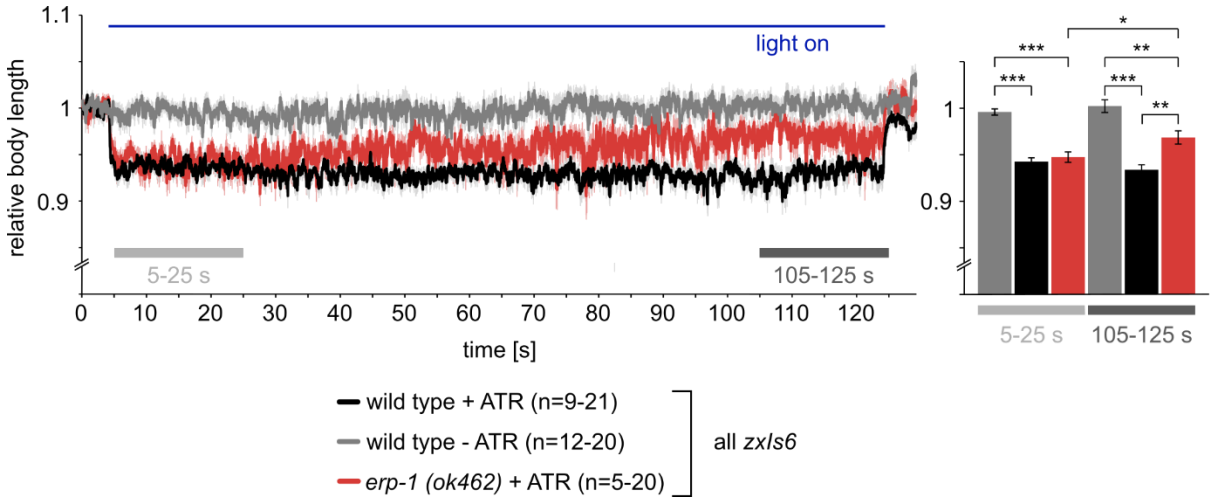

Figure 19: Mutants that lack ERP-1 showed progressive relaxation in the contraction assay. Wild type animals and *erp-1* mutants (both expressing ChR2 in cholinergic neurons in form of the *zxIs6* transgene) were probed in contraction assay. Animals were raised with/without ATR (all-trans retinal – the co-factor of ChR2), in the presence of ATR animals contracted during the blue light illumination. The n numbers are indicated, where the smaller number represents the minimum number of animals (coiling animals were excluded in the time window while they coiled), whereas the bigger number indicates the number of the tested animals. Blue light stimulation was used to activate the cholinergic transmission, the length of the illumination was 120 s, started after a 5-s-long initial period. **Left panel:** Contraction assay. **Right panel:** Relative body lengths were compared at the beginning (5-25 s) and at the end (105-125 s) of the stimulation. Shown are means of means ± SEM. *p<0.05, **<0.01, ***p<0.001, after one-way ANOVA with Bonferroni (for same period) or two-way ANOVA with Bonferroni (for different time periods).

3.2.3 ERP-1 participates in the same pathway as UNC-57

To investigate whether UNC-57 and ERP-1 participate in the same or in different pathways, double mutants were tested in contraction assays. The same protocol as described above was used again with a 60-s-long optogenetic stimulation, started after a 5-s-long initial period. Wild type animals raised without ATR did not show any contraction (Figure 20), whereas wild type animals and *erp-1* mutants raised in the presence of ATR contracted again by about 6 % of their body length. Since the length of the light stimulation was shorter as in the previous assay, only a slight tendency of the recycling phenotype was visible for *erp-1* mutants. *unc-57* and *unc-57; erp-1* double mutants showed a strong initial contraction (about 12 % of their body length) and a pronounced progressive relaxation. This increased contraction is, due to compensatory mechanisms in the body wall muscle, typical for animals with defective acetylcholine transmission (Liewald et al., 2008). The phenotype of the double mutants was not exacerbated, rather, it was completely dominated by the *unc-57* mutation. This shows that there is still a somehow functional synaptic vesicle cycle in double mutants, thus, there must be an additional pathway, which is able to compensate the lack of these two proteins.

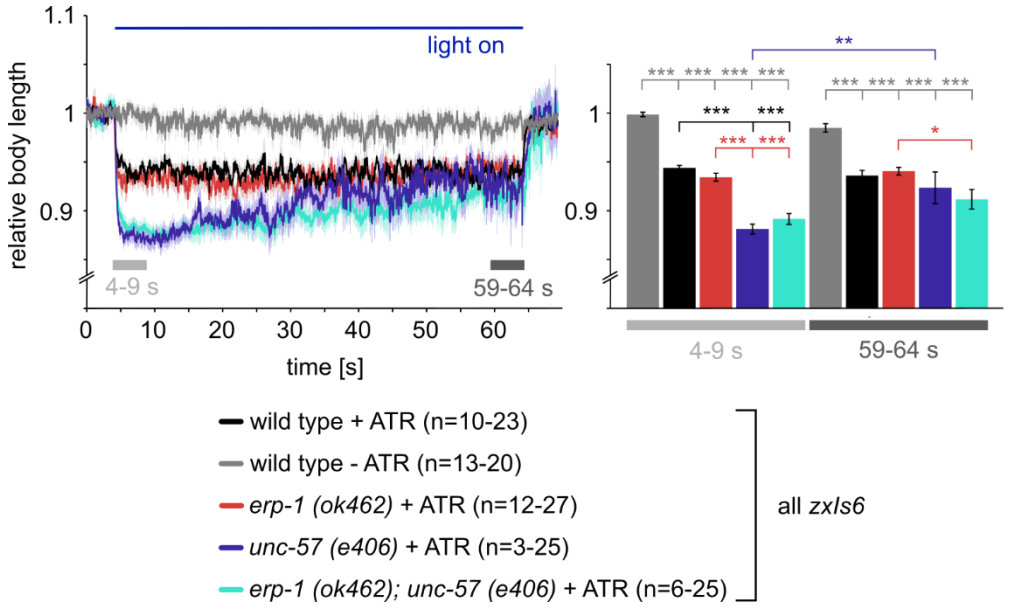

Figure 20: *erp-1; unc-57* double mutants showed no exacerbated phenotype compared to *unc-57* mutants in contraction assay. Indicated genotypes (all expressing ChR2 in cholinergic neurons in form of the *zxIs6* transgene) were tested in contraction assays. Animals were raised with or without ATR. In the presence of ATR, animals contracted during the blue light illumination. The n numbers are indicated, where the smaller number represents the minimum number of animals (coiling animals were excluded in the time window while they coiled), whereas the bigger number indicates the number of the tested animals. Blue light stimulation was used to activate the cholinergic transmission, the length of the illumination was 60 s, started after a 5-s-long initial period. **Left panel:** Contraction assay. **Right panel:** Relative body lengths were compared at the beginning (4-9 s) and at the end (59-64 s) of the stimulation. Shown are means of means ± SEM. *p<0.05, **<0.01, ***p<0.001, after one-way ANOVA with Bonferroni (for same period) or two-way ANOVA with Bonferroni (for different time periods).

To further analyse this, mutants were tested by electrophysiology (Figure 21, data provided by Dr. Jana F. Liewald). Measuring the spontaneous (miniature postsynaptic currents - mPSCs) and optogenetically evoked (evoked postsynaptic currents - ePSCs) transmission at the neuromuscular junction of *C. elegans* is a powerful method to detect SV recycling defects (Liewald et al., 2008). First, basal activity was measured. There was no difference, neither of the amplitude, nor of the frequency of mPSCs, between wild type animals and *erp-1* mutants (Figure 21, A, B). The frequency of the mPSCs was decreased significantly in *unc-57* and *erp-1; unc-57* mutants, furthermore there was a slight reduction of amplitudes in *unc-57* mutants. Next, cholinergic neurons were stimulated at 0.5 Hz. This evoked strong currents in wild type animals, while ePSCs in *erp-1* mutants were significantly smaller (ca. 2/3 of wild type) (Figure 21, C). *unc-57* mutants and *erp-1; unc-57* double mutants showed a similar phenotype: the first stimulus caused a small ePSC (ca. 15% of wild type) in both groups, which got even smaller (almost immeasurable) during the following stimuli. According to these results, ERP-1 has also a function in SV recycling, however, the role of UNC-57 seems to be essential, while mutants that lack ERP-1 showed only mild defects.

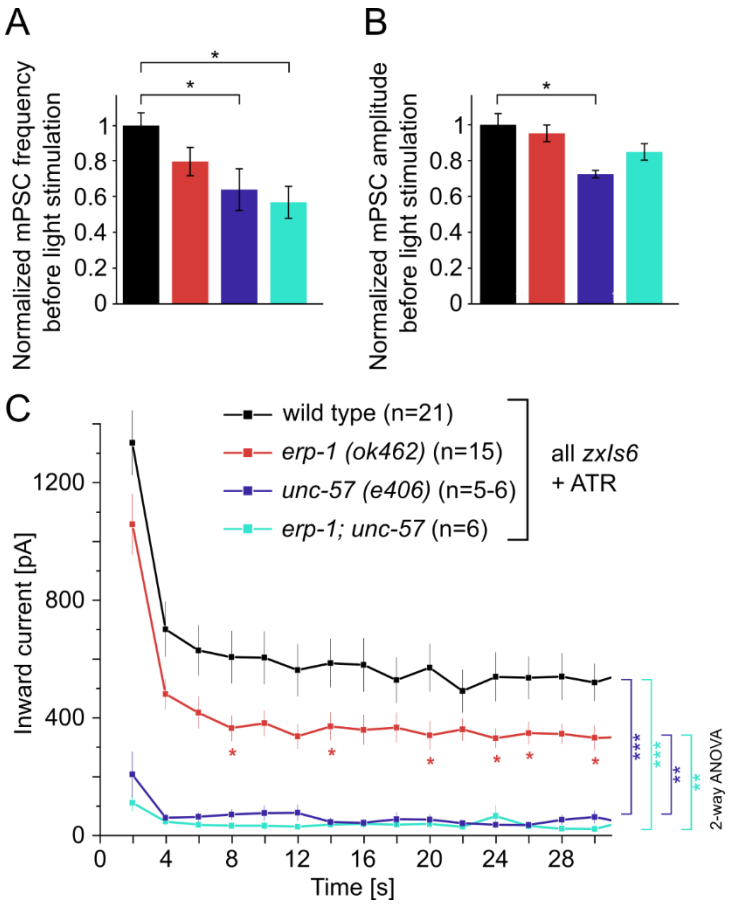

Figure 21: Spontaneous and evoked postsynaptic currents at the NMJ of *erp-1*, *unc-57* and *erp-1; unc-57* double mutants. Animals of the indicated genotypes were raised in the presence of ATR and analysed by patch-clamp electrophysiology. Evoked postsynaptic currents (ePSCs) were measured using blue light stimulation, spontaneous currents (mPSCs) were measured 30 s long before first light stimulus. **(A)** Mean, normalized mPSC frequencies and **(B)** amplitudes ± SEM. One-way ANOVA, Dunnett's multiple comparison test. **(C)** ePSCs, mean ± SEM. One-way ANOVA with Bonferroni correction test for individual stimuli; two-way ANOVA to compare entire datasets. Statistical significance given as *p<0.05, **p<0.01, ***p<0.001. Data provided by Dr. Jana F. Liewald.

3.2.4 Animals that lack both ERP-1 and UNC-57 are still capable of SV recycling

Flash and freeze EM and the ultrastructural analysis of cholinergic *en passant* synapses (Kittelmann et al., 2013; Watanabe, Liu, et al., 2013) enable to analyse the site of action (the plasma membrane or the large vesicles) of ERP-1 and UNC-57. For this, animals expressing ChR2 in cholinergic neurons were illuminated with blue light for 30 s, transferred to the freezing chamber and cryoimmobilized via high-pressure-freezing (HPF). After freeze-substitution and heavy-metal staining the animals were cross-sectioned and 40 nm thin samples were investigated under the transmission electron microscope (Figure 22, data provided by Dr. Szi-chieh Yu).

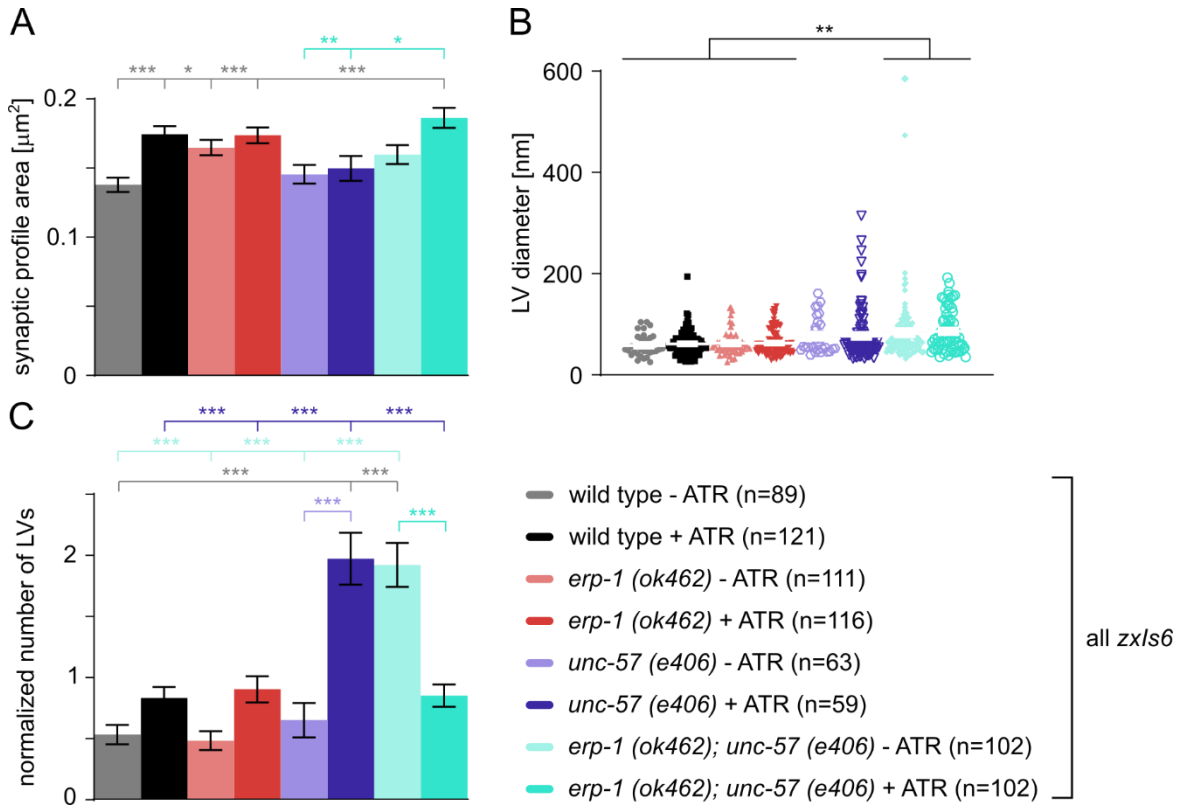

Figure 22: Large vesicle (LV) analysis via transmission electron microscopy (TEM) in *erp-1*, *unc-57* and *erp-1; unc-57* mutants. Indicated genotypes were raised with/without ATR and were photostimulated for 30 s prior to HPF. The number of the analysed profiles is depicted as n numbers (analysed profiles are the single photographs of synapses, taken at the TEM; in total, 9-19 synapses in 2-3 animals/genotypes were analysed). For the *erp-1; unc-57* double mutants two technical replicates were prepared and analysed. **(A)** Synaptic profile areas, shown are means ± SEM. **(B)** Diameter of the large vesicles. Shown are means ± SEM with scatter plots, depicting the largest diameter of the observed (single) LVs. **(C)** Number of large vesicles normalized to a typical synaptic profile area. Shown are means ± SEM. *p<0.05, **<0.01, ***p<0.001, after one-way ANOVA with Tukey post-hoc test. Data provided by Dr. Szi-chieh Yu.

As expected, blue light stimulation activated the cholinergic synaptic transmission in animals raised with ATR, which is noticeable trough the changes of different parameters. Once an increased number of synaptic vesicles is released, the area of the presynaptic membrane (the equivalent of the plasma membrane surface in the 2D images is termed synaptic profile perimeter) grows excessively, hence this extra membrane needs to be retrieved in a fast manner. One of these recycling mechanisms is the bulk endocytosis which enables the endocytosis of large parts of the plasma membrane and leads to the generation of so-called large vesicles (LVs) in the pre-synapse (Kittelmann et al., 2013). The synaptic profile area was significantly increased in wild type animals raised with ATR compared to the non-ATR group (Figure 22, A), and an elevated number of LVs were also visible in the ATR group (Figure 22, C). In *erp-1* mutants, the synaptic profile area was increased, also in animals raised without ATR, which can be an indicator of ineffective SV recycling. The LV profile was similar to the wild type

group, in animals raised with ATR there were more LVs visible than in the non-ATR mutants. The synaptic profile area of the *unc-57* mutants has not changed in animals raised with ATR compared to the without ATR ones, however, the number of the LVs drastically increased in the ATR group. The *erp-1; unc-57* double mutants showed an increased synaptic profile area in the animals raised in the presence of ATR, which demonstrates that some SVs were released upon stimulation. In contrast to all the other groups, the number of the LVs was strongly increased in the animals raised without ATR and, surprisingly, this number was significantly reduced in the ATR group. Furthermore, the size of the LVs was significantly increased compared to the wild type and *erp-1* mutant groups (Figure 22, B). All this evidence showed that ERP-1 and UNC-57 both contribute to the formation of SVs. The site of action of ERP-1 is not clear yet, whereas UNC-57 has an essential role in the breakdown of the large vesicles. Furthermore, the analysis of the double mutants demonstrated that in animals lacking both ERP-1 and UNC-57, (an)other back-up mechanism(s) can be activated, which enable some basal SV recycling via alternative pathways.

3.2.5 *chc-1* mutants have a moderate SV recycling defect

Next, animals with mutant clathrin heavy chain protein (*chc-1*) were investigated. Clathrin is known to act at the plasma membrane in clathrin-mediated endocytosis (Heuser & Reese, 1973), but it was shown that after stimulation and ultrafast endocytosis, it also participates at the break-down of large vesicles in mammalian synapses (Watanabe et al., 2014).

For the experiments a heat-sensitive allele, the *chc-1(b1025ts)* was used. In this *C. elegans* strain, the level of CHC-1 is drastically reduced already at permissive temperature (15 °C), but keeping the worms at non-permissive temperature further decreases the protein level and results in exacerbated phenotypes (Sato et al., 2009). First, *chc-1* mutants were probed in contraction assays. For this, animals were prepared as usually (genotypes were raised with or without ATR), but an additional heat-shock step was performed (14 minutes at 30 °C) prior to the experiment, as indicated (Figure 23). Wild type animals raised in the presence of ATR contracted by about 6 % of their body length, while *chc-1* mutants showed initially a similar level of contraction, but at the end of the illumination it was only about 5 %. After the heat-shock treatment, there was an increase in the level of contraction in both genotypes. An obvious exacerbated phenotype was not visible for mutants lacking CHC-1; however, a mild progressive relaxation was visible irrespective of the heat-shock, thus, these animals possess a

moderate defect in SV recycling.

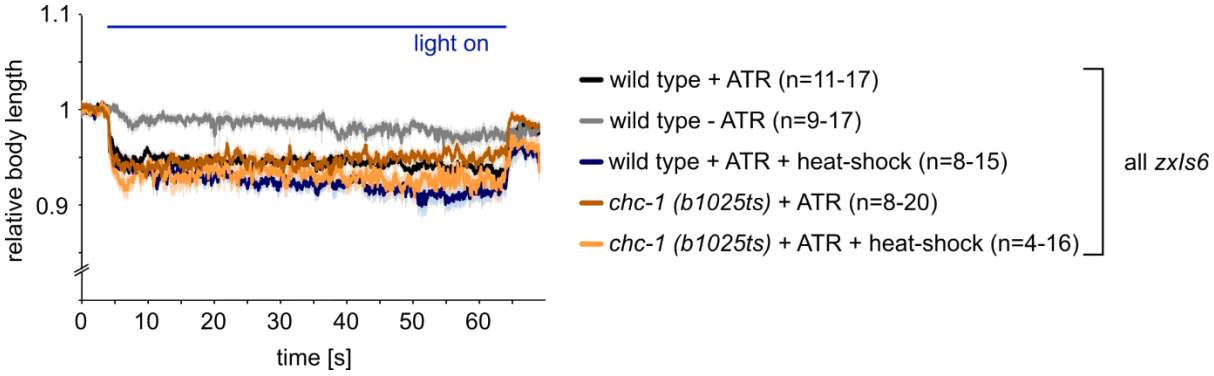

Figure 23: *chc-1* mutants showed a mild recycling phenotype in contraction assay. Wild type animals and *chc-1* mutants (both expressing ChR2 in cholinergic neurons in form of the *zxIs6* transgene) were tested in contraction assay. *chc-1(b1025ts)* is a heat-sensitive allele; thus all the strains were raised at permissive temperature (15 °C), heat-shock (30°C – 14 minutes) was started 15 minutes before the experiment. Animals were raised with/without ATR (all-trans retinal – the co-factor of ChR2), in the presence of ATR animals contracted during the blue light illumination. The n numbers are indicated, where the smaller number represents the minimum number of animals (coiling animals were excluded in the time window while they coiled), whereas the bigger number indicates the number of the tested animals. Blue light stimulation was used to activate the cholinergic transmission, the length of the illumination was 60 s, started after a 5-s-long initial period.

3.2.6 CHC-1 has a role in the breakdown of large endosomal vesicles

chc-1 mutants were further analysed via transmission electron microscopy. Animals were raised in permissive temperature and were/were not heat-shocked before the HPF as indicated (Figure 24, data provided by Dr. Szi-chieh Yu). The synaptic profile area increased significantly after light stimulation in both wild type and *chc-1* mutant groups, regardless of the heat-shock (Figure 24, A). The number of LVs was significantly larger in *chc-1* mutants after heat-shock, also in animals which were raised without ATR (Figure 24, C). Furthermore, the diameter of the LVs in heat-shocked animals lacking CHC-1 was significantly increased (Figure 24, B). These results indicate that CHC-1 is not necessary for the SV fusion at the plasma membrane, but rather has a role in the breakdown of large vesicles after bulk endocytosis.

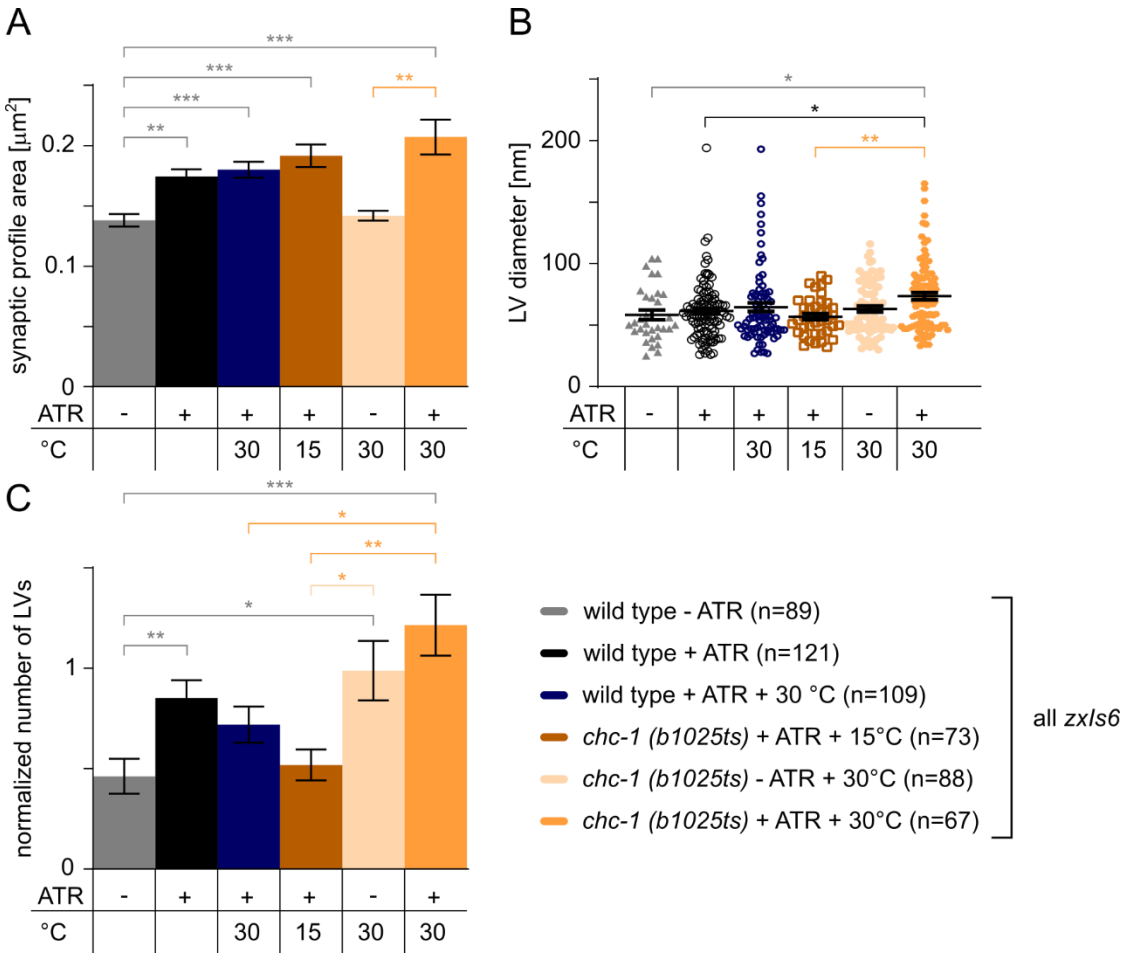

Figure 24: Large vesicle (LV) analysis in mutants lacking CHC-1 indicates a role in the breakdown of synaptic endosomes during SV recycling. Genotypes were raised at 15 °C or at RT with/without ATR and were (marked as '+ 30 °C') /were not heat-shocked as indicated. Heat-shock (30°C – 14 minutes) was started 15 minutes prior to the 30-s-long photostimulation, which was followed by HPF. The number of the analysed profiles is depicted as n numbers (analysed profiles are the single photographs of synapses, taken at the TEM, in total 11-19 synapses in 2-3 animals/genotypes were analysed). **(A)** Synaptic profile areas, shown are means ± SEM. **(B)** Diameter of large vesicles. Shown are means ± SEM with scatter plots, depicting the largest diameter of the observed (single) LVs. **(C)** Number of large vesicles normalized to a typical synaptic profile area. Shown are means ± SEM. *p<0.05, **<0.01, ***p<0.001, after one-way ANOVA with Tukey post-hoc test. Data provided by Dr. Szi-chieh Yu.

3.2.7 The cooperation of endophilins and CHC-1 enables SV recycling

Since *erp-1; unc-57* double mutants still showed some basal SV recycling activity, there must be another pathway which enables the production of new SVs. It was previously shown in rodent neurons that clathrin acts at the plasma membrane at non-physiological temperatures, or as a back-up mechanism when ultrafast endocytosis fails (Watanabe et al., 2014). To investigate whether CHC-1 functions similar in *C. elegans, erp-1; chc-1* and *unc-57; chc-1* double mutants were analysed.

First, the double mutants were tested in the contraction assay. For this, different genotypes

were prepared as indicated (Figure 25, 26). Wild type animals (without heat-shock) contracted by about 6 % of their body length and a progressive relaxation was not visible during illumination. *erp-1; chc-1* double mutants showed a similar contraction profile, however, at the beginning of the light stimulation the level of the contraction was slightly increased (Figure 25). This difference became more pronounced in the groups which were tested after heat-shock. *unc-57; chc-1* animals showed an obvious recycling phenotype, already without heat-shock (Figure 26). These double mutants contracted at the beginning by about 10 % of their body length, but at the end of the illumination it was only about 8 %. Interestingly in the heat-shock group this difference became smaller, which can be a hint, that an additional back-up mechanism was activated.

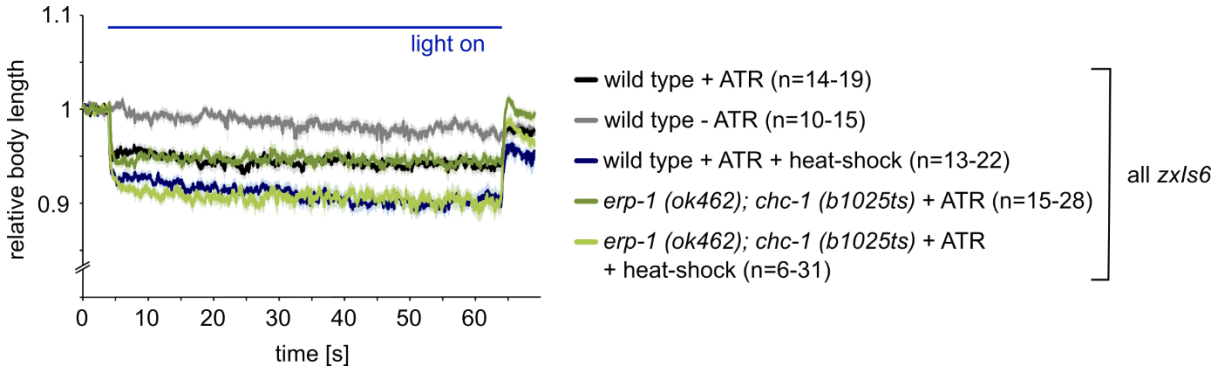

Figure 25: *erp-1; chc-1* double mutants showed wild-type-like phenotype in contraction assay. Wild type animals and *erp-1; chc-1* double mutants (both expressing ChR2 in cholinergic neurons in form of the *zxIs6* transgene) were probed in contraction assay. *chc-1 (b1025ts)* is a heat-sensitive allele; thus, all the strains were raised at permissive temperature (15 °C), heat-shock (30°C – 14 minutes) was started 15 minutes before the experiment. Animals were raised with/without ATR (all-trans retinal – the co-factor of ChR2), in the presence of ATR animals contracted during the blue-light-illumination. The n numbers are indicated, where the smaller number represents the minimum number of animals (coiling animals were excluded in the time window while they coiled), whereas the bigger number indicates the number of the tested animals. Blue light stimulation was used to activate the cholinergic transmission, the length of the illumination was 60 s, started after a 5-s-long initial period.

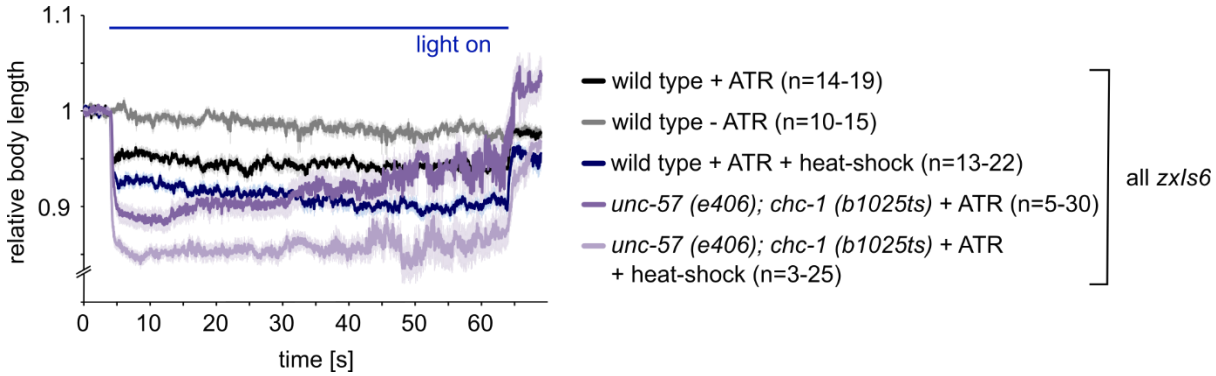

Figure 26: *unc-57; chc-1* double mutants showed a strong recycling phenotype in contraction assay. Wild type animals and *unc-57; chc-1* double mutants (both expressing ChR2 in cholinergic neurons in form of the *zxIs6* transgene) were tested in contraction assay. Experiment conditions as in Fig. 25.

For comparing the contraction patterns among all the genotypes, the average level of contraction was counted at the beginning (4-9 s) and at the end (59-64 s) of illumination (Table 16). Mutants lacking UNC-57 showed the most pronounced recycling phenotype, whereas *erp-1; unc-57* double mutants still showed a progressive relaxation, but this was milder compared to *unc-57* single mutants. The temperature sensitive *chc-1* mutants showed a mild recycling phenotype without heat-shock, but not after heat-shock. In the further experiments, all genotypes (wild type, *erp-1; chc-1* and *unc-57; chc-1* mutants) showed progressive increases in the level of contractions during illumination, which was most likely caused by technical issues during these measurements. However, it is still possible to compare the contraction patterns. The *erp-1; chc-1* groups showed wild-type-like contraction pattern irrespective of a heat-shock, whereas *unc-57; chc-1* double mutants without heat-shock showed a similar level of relaxation as the *erp-1; unc-57* mutants. This pronounced recycling phenotype disappeared in animals after heat-shock.

All these results show that UNC-57 and CHC-1 are the main players while ERP-1 has comparably a less essential role in SV recycling at the first glance. However, it is suitable to activate back-up mechanisms (which is most obvious in the *erp-1; unc-57* double mutants), and most probably can serve itself as a back-up in mutants lacking both UNC-57 and CHC-1 (SV release and recycling is still functioning in a basal level in *unc-57; chc-1* double mutants after heat-shock).

Table 16: Level of contraction in the different genotypes kept at the indicated temperatures at the beginning (4-9 s) and at the end of (59-64 s) illumination.

Genotype (all *zxIs6*)	**Average contraction (4-9 s)**	**Average contraction (59-64 s)**	**Difference**
wild type + ATR (RT)	0,944	0,936	0,008
erp-1 + ATR (RT)	0,934	0,94	- 0,006
unc-57 + ATR (RT)	0,881	0,924	- 0,043
erp-1; unc-57 + ATR (RT)	0,892	0,912	- 0,02
chc-1 + ATR (15 °C)	0,948	0,950	- 0,002
chc-1 + ATR (30 °C)	0,933	0,927	0,006
wild type + ATR (15 °C)	0,954	0,939	0,015
wild type + ATR (30 °C)	0,928	0,901	0,027

erp-1; chc-1 + ATR (15 °C)	0,950	0,943	0,007
erp-1; chc-1 + ATR (30 °C)	0,923	0,898	0,025
unc-57; chc-1 + ATR (15 °C)	0,900	0,919	- 0,019
unc-57; chc-1 + ATR (30 °C)	0,858	0,861	0,03

Next, *erp-1; chc-1* and *unc-57; chc-1* double mutants were analysed under the TEM. For this, animals were raised at permissive temperature and were/were not heat-shocked before light stimulation and HPF, as indicated (Figure 27, data provided for the most part by Dr. Szi-chieh Yu). As in the contraction assays, *erp-1; chc-1* mutants showed comparably milder phenotypes and these were dominated by the loss of UNC-57, such as the synaptic profile area values which were very close to the *unc-57* single mutant values (Figure 27, A). The size of the LVs was significantly increased in the *unc-57; chc-1* double mutants under all the conditions (Figure 27, B) and in the heat-shocked group raised with ATR the number of the LVs was strongly increased (Figure 27, C) similar to the *chc-1* (although this was less pronounced) and the *unc-57* single mutants. These results showed again that CHC-1 or UNC-57 are the main players (since mutants lacking these proteins showed the strongest phenotypes), but these two proteins with ERP-1 serve as mutual back-up mechanisms in SV endocytosis and release.

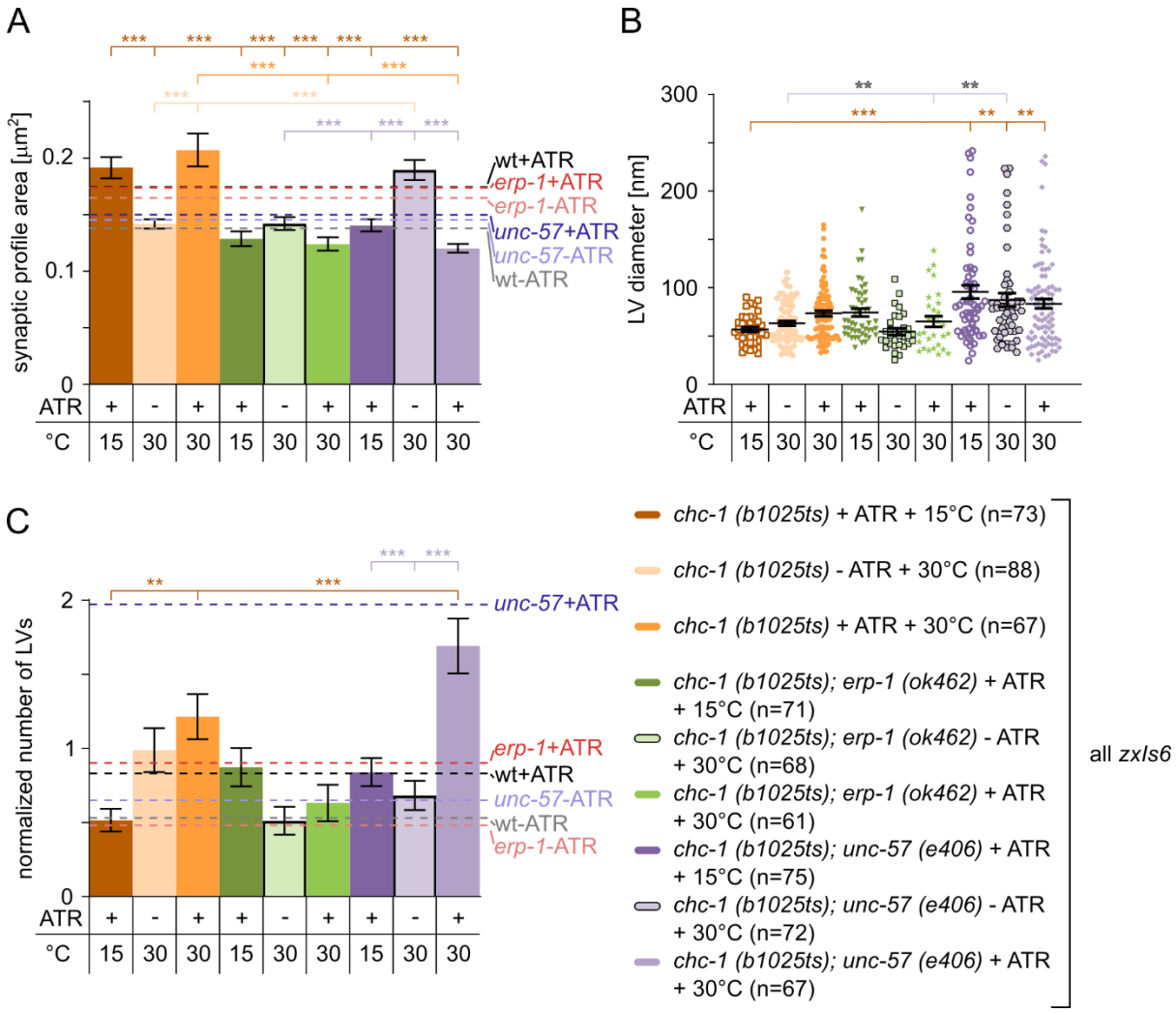

Figure 27: Large vesicle (LV) analysis via transmission electron microscopy (TEM) in *chc-1*, *chc-1; erp-1*, and *chc-1; unc-57* mutants. Genotypes were raised at 15 °C with/without ATR and were (marked as '+ 30 °C') /were not heat-shocked as indicated. Heat-shock (30°C – 14 minutes) was started 15 minutes prior to the 30-s-long photostimulation, which was followed by HPF. The number of the analysed profiles is depicted as n numbers (analysed profiles are the single photographs of synapses, taken at the TEM, in total 9-13 synapses in 2 animals/genotypes were analysed). **(A)** Synaptic profile areas, shown are means ± SEM. **(B)** Diameter of the large vesicles. Shown are means ± SEM with scatter plots, depicting the largest diameter of the observed (single) LVs. **(C)** Number of large vesicles normalized to a typical synaptic profile area. Shown are means ± SEM. On **(A)** and **(C)** the dashed lines depict the respective mean values of the other genotypes (see **Figure 22**). **p<0.01, ***p<0.001, after one-way ANOVA with Tukey post-hoc test. Data provided for the most part by Dr. Szi-chieh Yu.

3.3 New insights into a known player: RIMB-1 affects the localization of VGCCs and the excitation/inhibition balance in *C. elegans*

The evolutionarily conserved active zone protein, RIM-binding protein (RIM-BP) consist of three *src*-homology type III (SH3) (one N, and two C-terminal ones), and three fibronectin type III (FN3)(localized in the middle of the protein) domains (Hibino et al., 2002)(Figure 28, A). SH3 domains directly interact with RIM (Y. Wang et al., 2000) and with N, P/Q and also L-type Ca^{2+} channels (Hibino et al., 2002)(Figure 28, B). During the past years, several publications aimed to describe the function of RIM-BP (Acuna et al., 2015, 2016; Davydova et al., 2014; Grauel et al., 2016; Hibino et al., 2002; Krinner et al., 2017; Kushibiki et al., 2019; K. S. Y. Liu et al., 2011; Müller et al., 2015), however, a lot of questions remained unclear and an extensive analysis of RIMB-1 (the *C. elegans* ortholog of RIM-BP) including an electrophysiological and electron microscopical analysis does not exist yet.

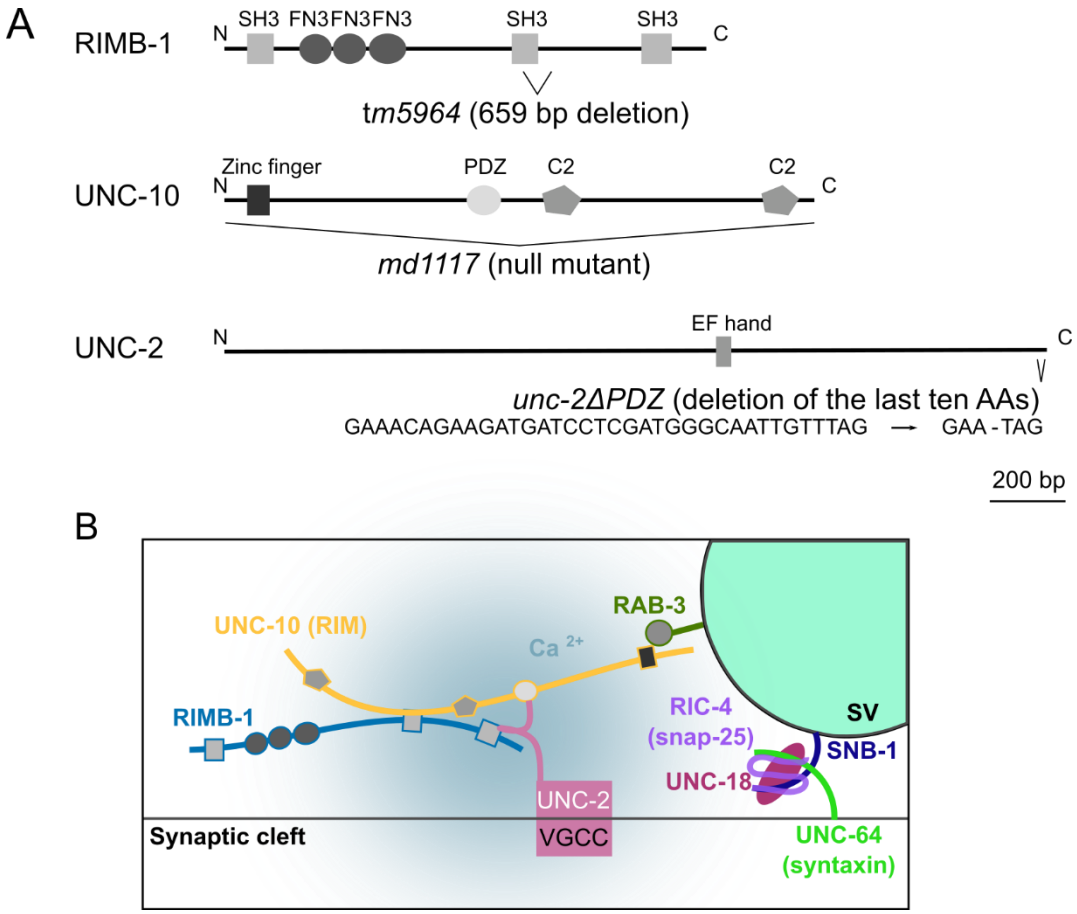

Figure 28: Structures and interactions of RIMB-1, UNC-10/RIM and UNC-2/VGCC. (A) Domains are indicated as: SH3: src homology type III, FN3: fibronectin type III, PDZ: PDZ domain, C2: Ca^{2+} and phospholipid binding domain. Brackets indicate the deletion sites of alleles used in this work. **(B)** The interactions between RIMB-1, UNC-10 and UNC-2 enable the precise localization of SVs in the vicinity of VGCCs. SV: synaptic vesicle, VGCC: voltage gated Ca^{2+} channel.

During this project, the synaptic function of RIMB-1 and its interaction with UNC-10 (*C. elegans* ortholog of RIM) and UNC-2 (*C. elegans* ortholog of the CaV2 α1 subunit) was investigated through behavioural, pharmacological, optogenetic, electrophysiological and ultrastructural assays using *C. elegans*.

3.3.1 RIMB-1 is expressed in cholinergic and GABAergic motor neurons

For investigating the expression pattern of RIMB-1, animals expressing the *Primb-1::GFP* (*rimb-1* promoter defined as 3 kb upstream of the ATG) and the *Punc-17::mCherry* (expressed specifically in cholinergic neurons) constructs, were analysed under the fluorescence microscope. GFP was widely expressed in the nervous system and along the ventral nerve cord, whereas mCherry expression along the ventral nerve cord was only visible in a subset of neurons, overlapping with the GFP signal (Figure 29). Thus, RIMB-1 is expressed most probably pan-neuronally and at the neuromuscular junction in cholinergic and GABAergic motor neurons.

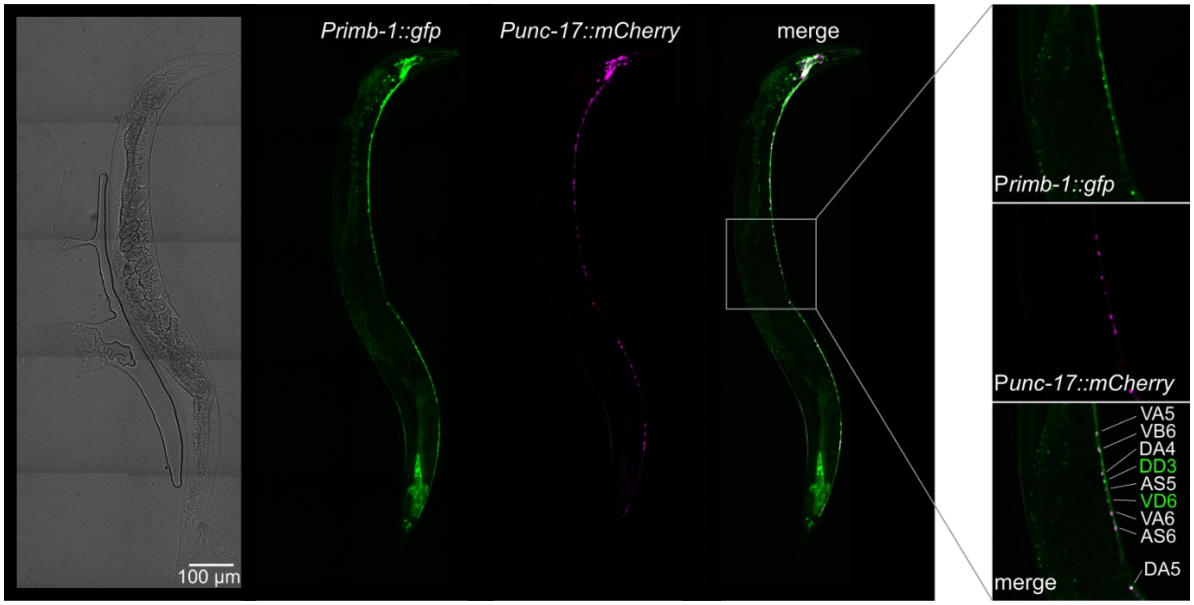

Figure 29: RIMB-1 is expressed in GABAergic and cholinergic motor neurons. *C. elegans*, expressing GFP from the *rimb-1* promoter (green) and mCherry from the *punc-17* promoter (cholinergic neurons - magenta), was investigated under the fluorescent microscope. The merged images show that RIMB-1 is expressed not only in the cholinergic, but also in GABAergic motor neurons along the ventral nerve chord. Right panel, merge image: Cell bodies along the ventral nerve chord are tentatively assigned, cholinergic cell bodies are marked with white, GABAergic ones with green colour.

3.3.2 Cholinergic transmission is reduced in *rimb-1* mutants

For the experiments the *rimb-1(tm5964)* mutant was used. This has a 659 bp deletion at exon 14, which results in a deletion of the second SH3 domain and in an additional frameshift and early stop codon. Whether this is a null allele is not known, but the binding sites of UNC-10 and UNC-2 (second and third SH3 domains (Davydova et al., 2014; Y. Wang et al., 2000)) are definitely affected, thus using this mutant enabled us to investigate the protein interactions of our interest with a possibility to keep other protein-protein interactions intact.

Cholinergic transmission was probed by pharmacological assays. First, an aldicarb assay was performed. Aldicarb is an acetylcholinesterase inhibitor, the presence of which leads to acetylcholine accumulation in the synaptic cleft, and this causes postsynaptic receptor hyperactivation and progressive muscle paralysis (Mahoney et al., 2006; K. G. Miller et al., 1996). The different genotypes were placed on 2 mM aldicarb plates, and the fraction of moving animals was assessed every 30 minutes (Figure 30). Wild type animals were completely paralyzed after 6 hours, whereas at this time-point about 40 % of the *rimb-1* mutants were still not paralyzed, thus these animals showed a pronounced aldicarb-resistant phenotype. *unc-10* mutants and *rimb-1; unc-10* double mutants were even more resistant to aldicarb; after 6 hours almost all these animals were still capable of moving, which indicates a strong reduction of SV release, or a strong deficit of postsynaptic receptor function. Testing the latter hypothesis, another pharmacological assay, the levamisole-assay was carried out with the *rimb-1* mutants. Levamisole is an agonist of the main postsynaptic nicotinic acetylcholine receptor (nAChR) in *C. elegans*, thus it causes muscle hyperactivation and paralysis (Lewis et al., 1980). *unc-38* encodes an AChR subunit and is known as a levamisole-resistance gene, therefore mutants lacking UNC-38 were used in the assay as positive controls (Figure 31). Animals were placed on 2 mM tetramisole hydrochloride (corresponding to 1 mM levamisole concentration) plates, and moving worms were counted every 30 minutes. As excepted, *unc-38* mutants were resistant to tetramisole hydrochloride, after 5 hours all the animals were still able to move. Wild type animals started to paralyze after 30-, *rimb-1* mutants after 90 minutes, however, the progression of the paralysis was similar in these two groups and there was no significant difference between them. This showed that the postsynaptic receptors are unaffected in *rimb-1* mutants, thus the aldicarb resistant phenotype is caused by a presynaptic defect, which manifests in reduced SV release.

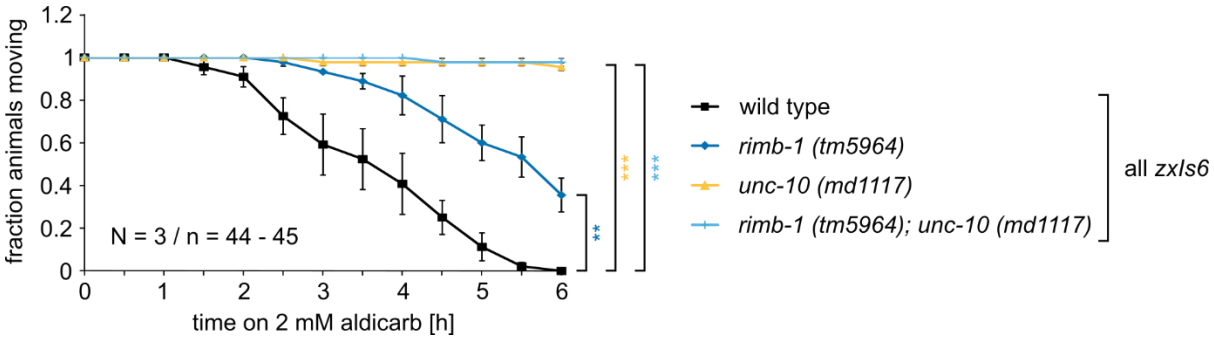

Figure 30: *rimb-1* mutants showed an aldicarb resistant phenotype. Aldicarb assay with 2 mM aldicarb plates. The indicated genotypes were tested and scored 3 times (on 3 different days, with worms from 3 different populations). Around 40 % of the *rimb-1* mutants were still capable of moving after spending 6 hours on 2 mM aldicarb plates. *unc-10* and *rimb-1; unc-10* double mutants showed an even stronger aldicarb resistant phenotype; almost none of these animals were paralyzed at the end of the assay. Shown are means ± SEM. **p<0.01, ***p<0.001, after Log-Rank test with Bonferroni correction.

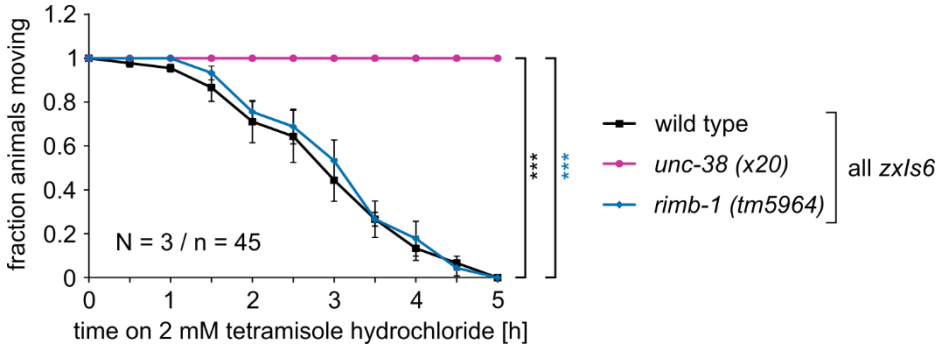

Figure 31: Postsynaptic nAChRs are unaffected in *rimb-1* mutants. Levamisole assay with 2 mM tetramisole hydrochloride (corresponding to 1 mM levamisole) plates. The indicated genotypes were tested and scored 3 times (on 3 different days, with worms from 3 different populations). The positive control *unc-38* mutants were completely levamisole resistant; after 5 hours none of the animals were paralysed. Wild type animals and *rimb-1* mutants started to paralyze after 30 and 90 minutes respectively, however, there was no significant difference between these genotypes. Shown are means ± SEM.
***p<0.001, after Log-Rank test with Bonferroni correction.

Next, animals were tested in a trashing assay (Figure 32). For this, animals were placed into M9 buffer and after 15 minutes incubation time, the recording was started. The number of the trashes were counted manually. *rimb-1* mutants showed a significant reduction in the trashing behaviour compared to wild type, whereas the swimming rate of *unc-10* mutants and *rimb-1; unc-10* double mutants decreased even more. There was a significant difference between *unc-10* and *unc-10; rimb-1* groups; the mutation of *rimb-1* resulted in an exacerbated phenotype in the double mutants.

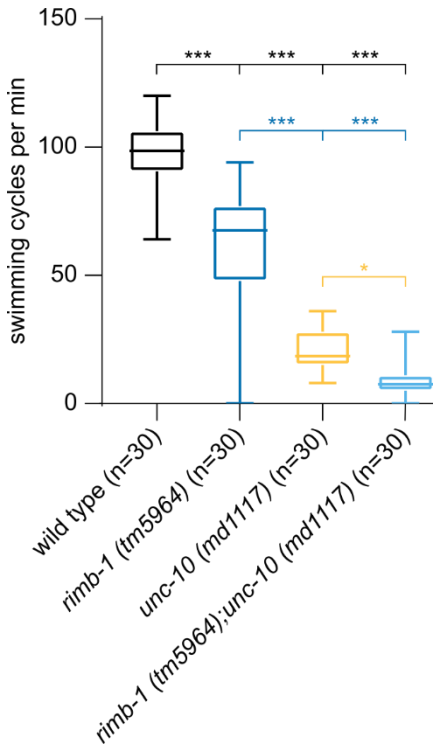

Figure 32: *rimb-1* mutants showed reduced swimming rates. The indicated mutant strains and wild type animals were probed in a swimming assay. *rimb-1, unc-10* and *rimb-1; unc-10* mutants all showed a significant reduction in the number of the swimming cycles compared to wild type. *unc-10* mutants were hardly capable of swimming and this reduction became even more pronounced in the double mutants. The total number of tested animals is indicated as n numbers, the assay was repeated 3 times (on different days, with different animal populations). Data shown as median and 25/75 quartiles, min to max.
*p<0.05, ***p<0.001, after one-way ANOVA and Bonferroni post-hoc test.

After this, cholinergic function was probed using the contraction assay. Animals with an integrated *zxIs6* transgene (ChR2 in the cholinergic neurons) were raised with/without ATR were placed into fresh plates and were filmed for 70 s. Video recording was started, and after 5 s the animals were illuminated with blue light for 60 s. The control groups behaved as expected: the initial relative body length of wild type animals did not significantly differ from the length at the end of the illumination (Figure 33). Wild type animals raised without ATR showed no contraction at all, whereas in the + ATR group animals contracted by about 10 % of their body length. *rimb-1* mutants contracted by about 6 % initially, but there was a mild progressive relaxation, thus at the end of the illumination this was about 5 % of their body length. The contraction patterns of *unc-10* mutants and *rimb-1; unc-10* double mutants were similar: animals from these genotypes contracted at the beginning of the light stimulation wild-type-like, about 10 % of their body length, but they showed a recycling phenotype (Liewald et al., 2008) and after 60 s illumination the contraction was about 6 %. Typically, SV release mutants show initially increased contraction compared to wild type animals due to a homeostatic, compensatory mechanism, which is followed by the continuous relaxation that

manifests in body elongation. However, the contraction pattern of *rimb-1* mutants was different, thus in the next step these mutants were tested in another contraction assay.

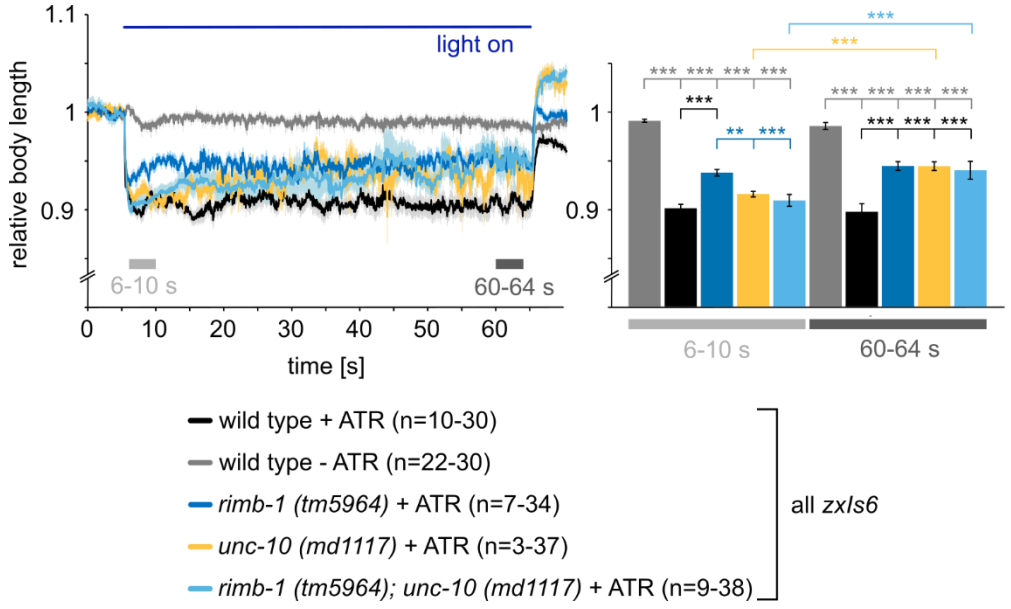

Figure 33: *rimb-1* mutants showed decreased initial contraction followed by a progressive relaxation in contraction assay. Indicated genotypes (all expressing ChR2 in cholinergic neurons in form of the *zxIs6* transgene) were tested in contraction assay. Animals were raised with/without ATR (all-trans retinal – the co-factor of ChR2), in the presence of ATR animals contracted during the blue light illumination. The n numbers are indicated, where the smaller number represents the minimum number of animals (coiling animals were excluded in the time window while they coiled), whereas the bigger number indicates the number of the tested animals. Blue light stimulation was used to activate the cholinergic transmission, the length of the illumination was 60 s, started after a 5-s-long initial period. **Left panel:** Contraction assay. **Right panel:** Relative body lengths were compared at the beginning (6-10 s) and at the end (60-64 s) of the stimulation. Shown are means of means ± SEM. **p<0.01, ***p<0.001, after one-way ANOVA with Bonferroni (for same period) or two-way ANOVA with Bonferroni (for different time periods).

Wild type animals, *rimb-1* mutants and as SV release mutant control, *snb-1* (synaptobrevin) mutants were crossed with a strain in which ChR2 was integrated in the postsynaptic muscle cells, thus, upon illumination muscle cells can be directly stimulated. These *snb-1* mutants contracted significantly more than wild type animals in a previous study (Liewald et al., 2008) and here, *rimb-1* mutants were compared with these mutants to test postsynaptic excitability. The strains were prepared before the experiment as explained before, i.e. animals were raised with/without ATR as indicated (Figure 34). Animals were illuminated with blue light for 60 s after a 5 s initial period. Wild type animals raised without ATR did not contract at all, whereas animals from the same genotype raised in the presence of ATR contracted at about 13 % of their body length. *snb-1* mutants contracted significantly more than wild type animals; however, this was not the case for *rimb-1* mutants which behaved in this assay in a wild-type-

like manner. This shows that the excitability of the postsynaptic muscle cells is not affected in *rimb-1* mutants, thus the fact that this genotype behaves in a different way than the typical SV release mutants, is most probably due to a presynaptic defect. Jointly with the results of the aldicarb assay, these results also indicate a possible difference in presynaptic mutants affected the SV fusion machinery, as opposed to mutants affecting localization of VGCCs and docked SVs.

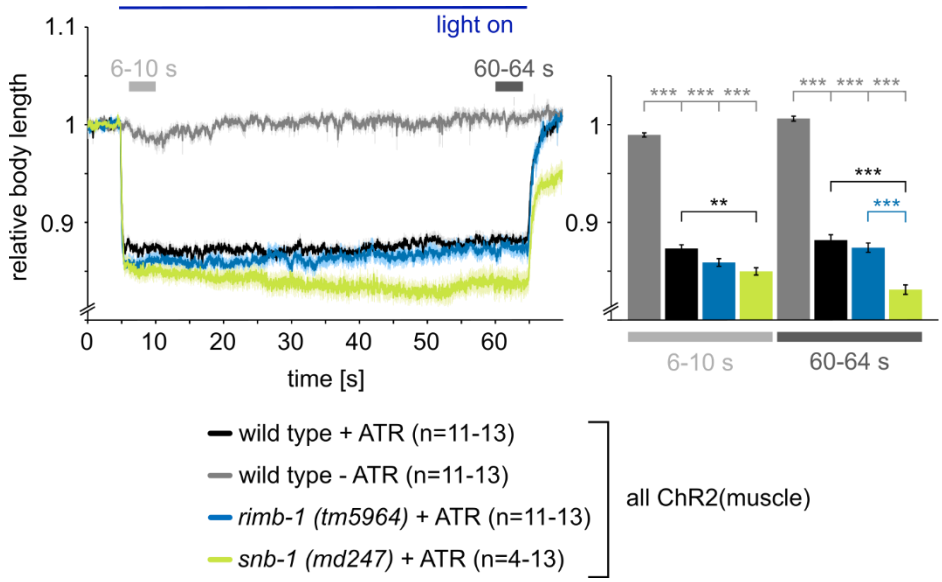

Figure 34: The excitability in the postsynaptic muscle cells is unaffected in *rimb-1* mutants. Contraction assay with animals which express ChR2 in the postsynaptic muscle cells. Indicated genotypes were raised with/without ATR (all-trans retinal – the co-factor of ChR2), in the presence of ATR animals contracted during the blue light illumination. The n numbers are indicated, where the smaller number represents the minimum number of animals (coiling animals were excluded in the time window while they coiled), whereas the bigger number indicates the number of the tested animals. Blue light stimulation was used to activate the cholinergic transmission, the length of the illumination was 60 s, started after a 5-s-long initial period. **Left panel:** Contraction assay. **Right panel:** Relative body lengths were compared at the beginning (6-10 s) and at the end (60-64 s) of the stimulation. Shown are means of means ± SEM. **p<0.01, ***p<0.001, after one-way ANOVA with Bonferroni (for same period) or two-way ANOVA with Bonferroni (for different time periods).

3.3.3 Unexpectedly, *rimb-1* mutants exhibit increased evoked postsynaptic currents

Cholinergic transmission of *rimb-1* mutants was further analysed by electrophysiology (Figure 35, data provided by Dr. Jana F. Liewald). Spontaneous (miniature postsynaptic currents - mPSCs) and evoked (evoked postsynaptic currents - ePSCs) currents were measured at the neuromuscular junction (NMJ) (Liewald et al., 2008). mPSC frequencies of *unc-10* and *rimb-1; unc-10* mutants were significantly decreased, while the rate of currents for *rimb-1* animals tended to be decreased, though this difference was not statistically significant (Figure 35, A).

mPSC amplitudes were similar in all groups (Figure 35, B). Cholinergic neurons that express ChR2 via the *zxIs6* transgene (Liewald et al., 2008), were stimulated using blue light at 0.5 Hz (Figure 35, C). This evoked strong currents in *rimb-1* mutants; the first peak was ca. 1.5 times that of wild type animals and the currents stayed increased during the whole stimulus train. On the contrary, in *unc-10* and *rimb-1; unc-10* mutants ePSCs were significantly decreased. These results were unexpected, since according to previous experiments (aldicarb assay, trashing assay, and contraction assay) *rimb-1* animals exhibit decreased cholinergic transmission. To unravel this conflict, parameters of the first ePSC were analyzed and, indeed, time to peak values were delayed in *rimb-1; unc-10* double mutants (Figure 35, D). These results show that, jointly, RIMB-1 and UNC-10 are required for effective, timely acute and fast synaptic transmission, following depolarization, at the NMJ of *C. elegans*.

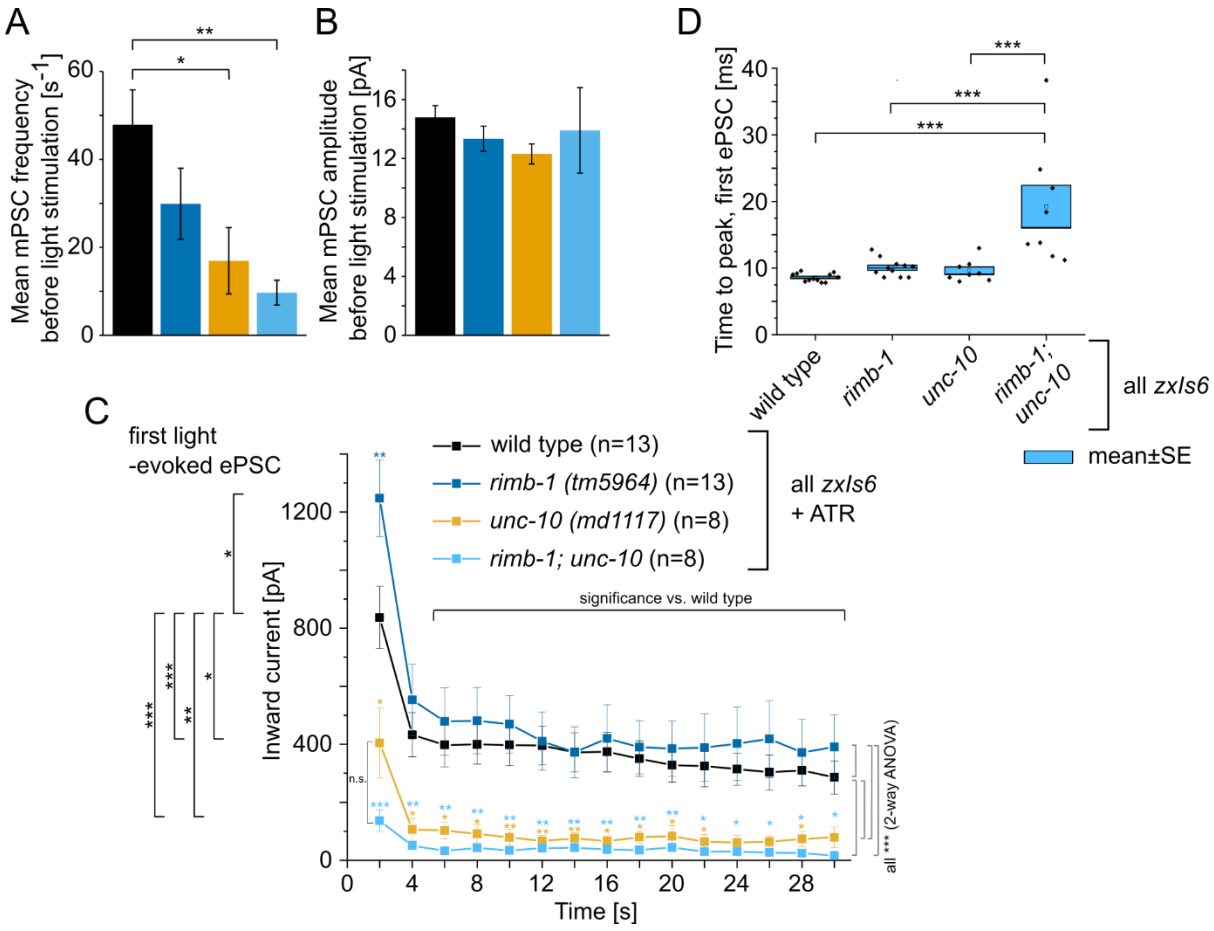

Figure 35: *rimb-1* mutants exhibit increased evoked postsynaptic currents at the NMJ. Indicated genotypes were raised in the presence of ATR and analysed by electrophysiology. Evoked postsynaptic currents (ePSCs) were measured using blue light stimulation, spontaneous currents (mPSCs) were measured 30 s long before first light stimulus. **(A)** mPSC frequencies and **(B)** amplitudes. One-way ANOVA, Kruskal-Wallis test. **(C)** ePSCs. One-way ANOVA with Tukey test in first light-evoked ePSC analysis and for indivicual stimuli; two-way ANOVA to compare entire datasets. **(D)** Time (from light onset) to peak analysis of first ePSC. One-way ANOVA and Tukey test. Data shown as mean ± SEM in A-C, statistical significance given as *p<0.05, **p<0.01, ***p<0.001. Data provided by Dr. Jana F. Liewald.

The next question was whether this delay of ePSCs could affect the postsynaptic activity. For investigating this, a voltage-imaging experiment was carried out (Figure 36, data provided by Amelie Bergs). The archaerhodopsin variant D95N is a genetically encoded voltage indicator which shows voltage dependent fluorescence changes (Azimi Hashemi et al., 2019). Wild type animals and *rimb-1* mutants, expressing ChR2 in the cholinergic neurons and archaerhodopsin D95N in the muscle cells, were photostimulated for 8 s. This stimulation, indeed, led to reduced muscle depolarization in *rimb-1* mutants, thus in spite of the larger currents, SV release of *rimb-1* mutants is ineffective, which influences the muscle contraction in a negative way.

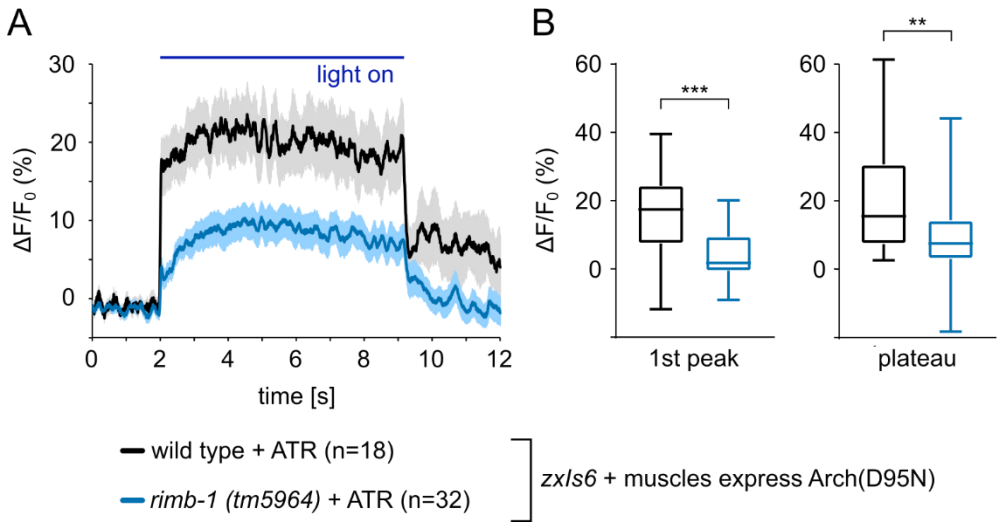

Figure 36: Photostimulation of cholinergic neurons led to reduced muscle depolarization in *rimb-1* mutants. Voltage imaging of muscle depolarisation. Animals that express ChR2 in cholinergic neurons (via the *zxIs6* transgene) and Arch(D95N) in muscle cells, were raised with ATR. Total number of tested animals is indicated as n numbers. **(A)** Blue light stimulation was started 2 s after the beginning of the voltage imaging, fluorescence increased during photostimulation. **(B)** 1st peak and plateau shown as median and 25/75 quartiles, min to max. **p<0.01, ***p<0.001, after unpaired t-test. Data provided by Amelie Bergs.

3.3.4 Direct stimulation of GABAergic neurons led to decreased ePSCs in *rimb-1* mutants

When *C. elegans* is placed on an agar plate, the animal shows a characteristic, sinusoidal locomotion, which is regulated by the GABAergic and cholinergic motor neurons, located in the ventral nerve cord (VNC) of the animal. The network of motor neurons is built up in a way that once a cholinergic motor neuron is activated, it stimulates the GABAergic motor neuron, which inhibits the reciprocal muscle cells. Thus, if the dorsal muscles are activated the ventral muscles are inhibited and vica versa (White et al., 1978).

As a next step, a contraction assay was performed to investigate the role of RIMB-1 in GABAergic neurons (Figure 37). For this, *rimb-1* mutants were crossed with a strain expressing ChR2 in the GABAergic neurons (as the integrated *zxIs3* transgene) (Liewald et al., 2008). Animals were raised with or without ATR and placed onto unseeded agar plates. Animals were illuminated with blue light for 60 s after a 5-s-long initial period. Upon stimulation, animals raised with ATR showed body elongation (Figure 37). Both wild type animals and *rimb-1* mutants showed a 5 % increase in the body length. This relaxed state was kept only for a few seconds, after 2-3 s the level of elongation started to decrease and after 10 s, the original length was reached again. As expected, animals raised without ATR did not show any elongation at all. The results show that the mutant RIMB-1 affects GABAergic and cholinergic motor neurons in a different way. When the stimulation directly targets GABAergic neurons, *rimb-1* mutants do not exhibit any mutant phenotype at the behavioural level.

Next, wild type animals and *rimb-1* mutants carrying the *zxIs3* transgene, were photostimulated and ePSCs were measured (Figure 38, data provided by Dr. Jana F. Liewald). These were significantly smaller in *rimb-1* mutants (Figure 38, A). Furthermore, the time to peak value was also delayed in these animals compared to wild type (Figure 38, B). Thus, stimulation of GABAergic or cholinergic neurons affected *rimb-1* mutants in different ways: during cholinergic stimulation there were larger ePSCs while GABAergic stimulation resulted in smaller ePSCs, however, the SV transmission was delayed in both cases.

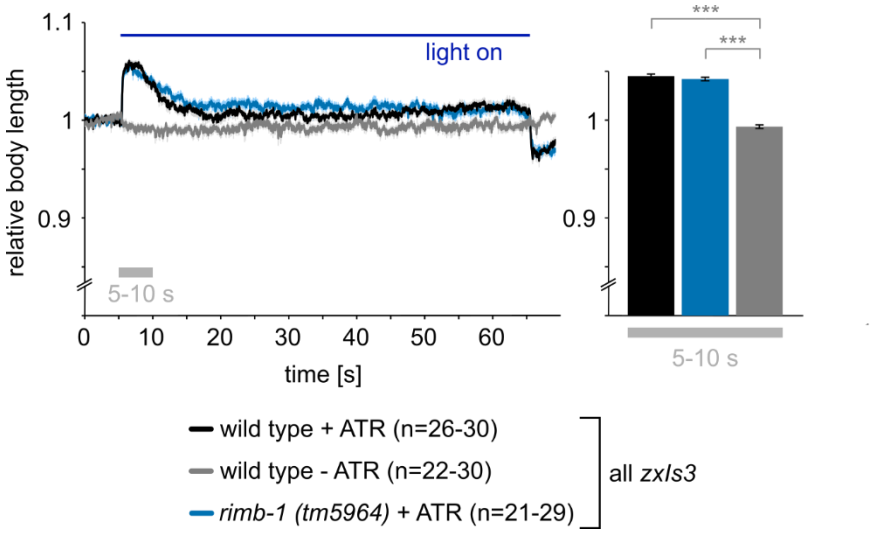

Figure 37: The stimulation of GABAergic neurons in *rimb-1* mutants resulted in wild-type-like elongation profile. Indicated genotypes (all expressing ChR2 in GABAergic neurons in form of the *zxIs3* transgene) were tested in contraction assay. Animals were raised with/without ATR (all-trans retinal – the co-factor of ChR2), in the presence of ATR animals elongated during the blue light illumination. The n numbers are indicated, where the smaller number represents the minimum number of animals (coiling animals were excluded in the time window while they coiled), whereas the bigger number indicates the number of the tested animals. Blue light stimulation was used to activate GABAergic transmission, the length of the illumination was 60 s, started after a 5-s-long initial

period. **Left panel:** Contraction assay. **Right panel:** Relative body lengths were compared at the beginning (5-10 s) of the stimulation. Shown are means of means ± SEM. ***p<0.001, after one-way ANOVA with Bonferroni.

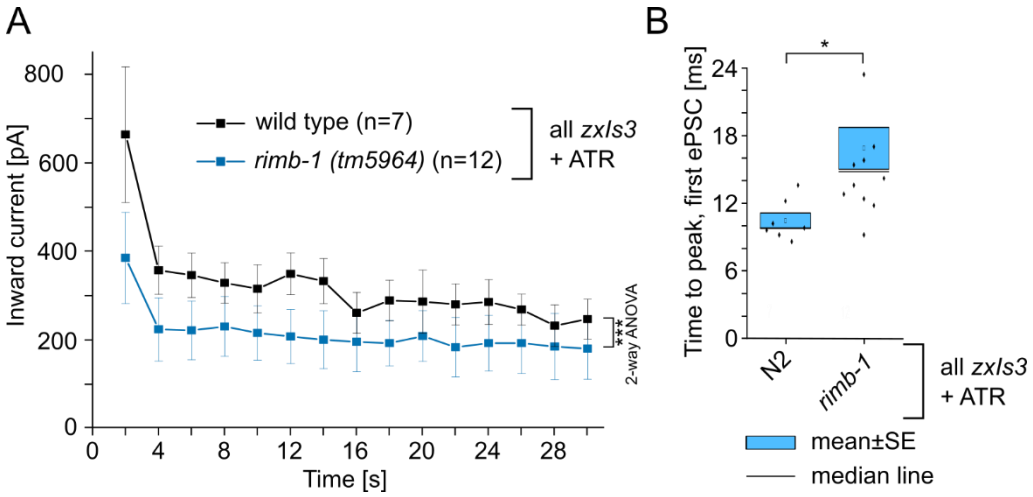

Figure 38: Photostimulation of GABAergic neurons resulted in reduced postsynaptic currents in *rimb-1* mutants. Indicated genotypes were raised in the presence of ATR and analysed by electrophysiology. **(A)** Evoked postsynaptic currents (ePSCs) were measured using blue light stimulation. Two-way ANOVA. **(B)** Time (from light onset) to peak analysis of first ePSC. One-way ANOVA and Tukey test. Data shown as mean ± SEM in A, statistical significance given as *p<0.05, ***p<0.001. Data provided by Dr. Jana F. Liewald.

3.3.5 Increased ePSCs of *rimb-1* mutants are gone in the absence of GABA transmission

The role of RIMB-1 in GABAergic neurons was further investigated using the *unc-47* mutants, which animals lack the vesicular GABA transporter (vGAT). Animals of the respective genotypes were prepared as indicated (Figure 39), the length of blue light stimulation was again 60 s after a 5-s-long initial period. *unc-47* mutants contracted significantly stronger than wild type animals, which was expected due to the complete lack of inhibitory transmission. *rimb-1; unc-47* double mutants contracted at the beginning of the illumination at about the similar level as wild type animals raised with ATR, but this was followed by an ongoing relaxation (i.e., a recycling phenotype), which was more pronounced than for the *rimb-1* mutants. These results highlight the importance of RIMB-1 in cholinergic neurons and strengthens the hypothesis that RIMB-1 affects cholinergic and GABAergic neurons in a different way. Furthermore, it appears to affect recycling of SVs, in an unknown way.

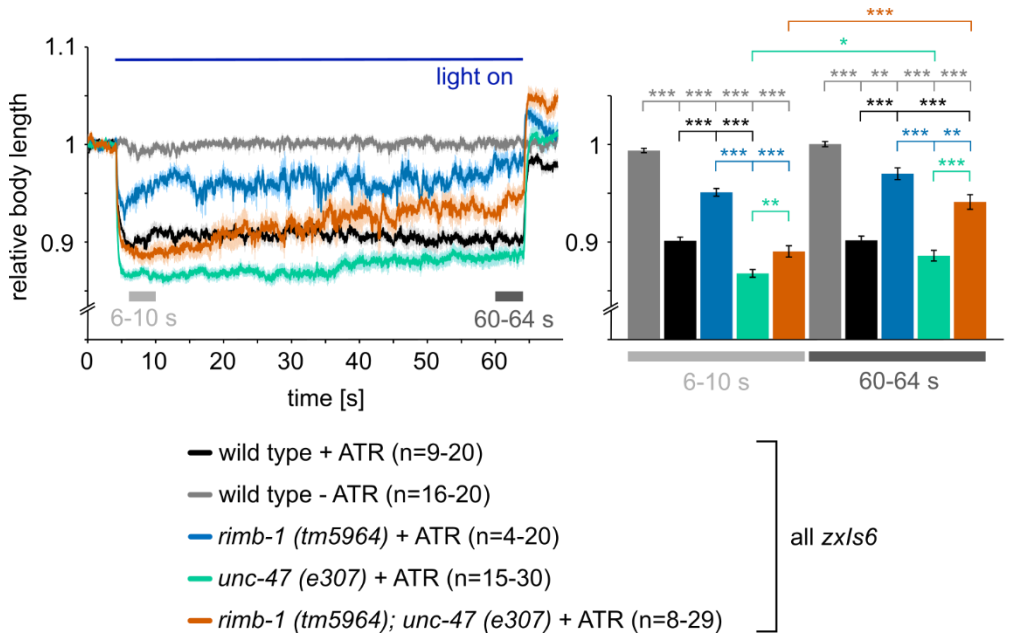

Figure 39: *rimb-1; unc-47* double mutants showed a more pronounced recycling phenotype than *rimb-1* mutants. Indicated genotypes (all expressing ChR2 in cholinergic neurons in form of the *zxIs6* transgene) were tested in contraction assay. Animals were raised with/without ATR (all-trans retinal – the co-factor of ChR2), in the presence of ATR animals contracted during the blue light illumination. The n numbers are indicated, where the smaller number represents the minimum number of animals (coiling animals were excluded in the time window while they coiled), whereas the bigger number indicates the number of the tested animals. Blue light stimulation was used to activate the cholinergic transmission, the length of the illumination was 60 s, started after a 5-s-long initial period. **Left panel:** Contraction assay. **Right panel:** Relative body lengths were compared at the beginning (6-10 s) and at the end (60-64 s) of the stimulation. Shown are means of means ± SEM. *p<0.05, **p<0.01, ***p<0.001, after one-way ANOVA with Bonferroni (for same period), or two-way ANOVA with Bonferroni (for different time periods).

These strains were further analysed via electrophysiology (Figure 40, data provided by Dr. Jana F. Liewald). *unc-47* mutants exhibited significantly reduced mPSC frequencies compared to wild type animals (Figure 40, A). The reduction was even more pronounced in *rimb-1; unc-47* double mutants, furthermore, mPSC amplitudes were also significantly reduced in this group (Figure 40, B). Next, photoevoked cholinergic PSCs were analysed (Figure 40, C). As seen before, *rimb-1* mutants exhibited increased ePSCs compared to wild type, while this was not the case for the other groups. During the first ePSC there was no significant difference between *unc-47* mutants, *rimb-1; unc-47* double mutants and wild type animals, thus the increased ePSCs of the *rimb-1* mutant were compensated or counterbalanced in the double mutants. This shows that muscle currents measured during these experiments are dominantly influenced by cholinergic inputs, whereas GABA contribution seems to be not present, possibly due to damaging of cholinergic-GABAergic connections during the dissection. Therefore, our hypothesis is that enlarged cholinergic ePSCs of *rimb-1* mutants represent a homeostatic compensatory response as far as excitation-inhibition balance is intact. Once it is disturbed,

there is no further need for a homeostatic increase of cholinergic transmission, thus the larger currents are no longer observable.

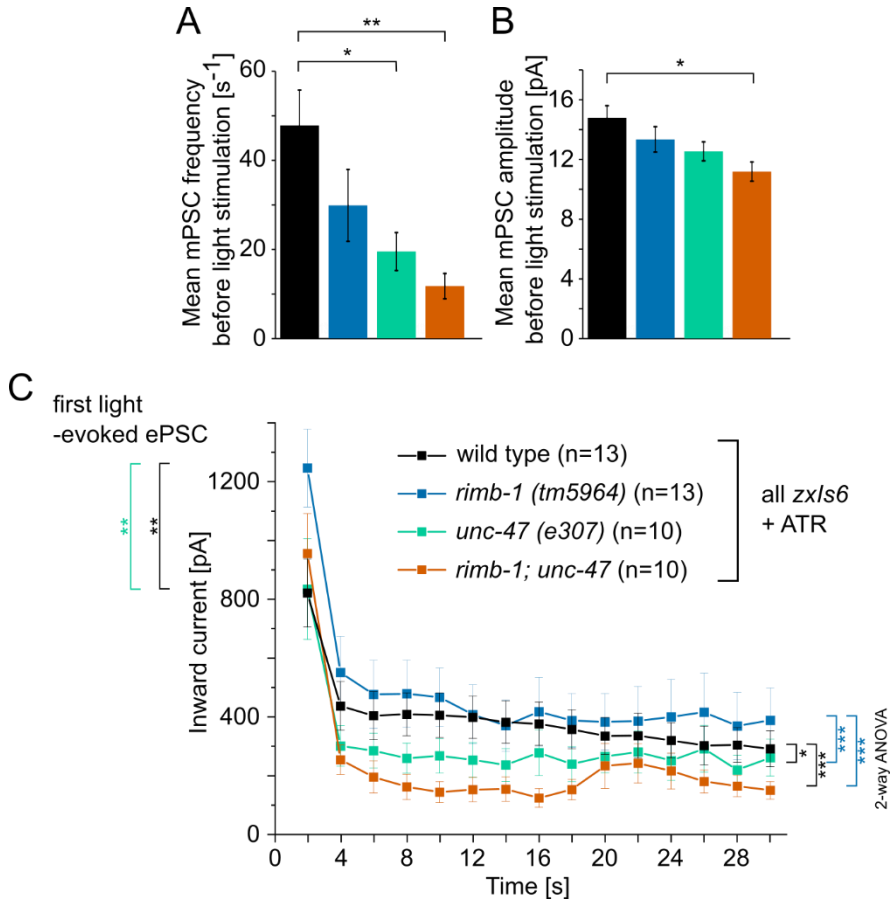

Figure 40: Increased ePSCs of *rimb-1* mutants are gone in *rimb-1; unc-47* double mutants. Indicated genotypes were raised in the presence of ATR and analysed by electrophysiology. Evoked postsynaptic currents (ePSCs) were measured using blue light stimulation, spontaneous currents (mPSCs) were measured 30 s long before first light stimulus. **(A)** mPSC frequencies and **(B)** amplitudes. One-way ANOVA, Tukey test. **(C)** ePSCs. One-way ANOVA with Tukey test in first light-evoked ePSC analysis; two-way ANOVA to compare entire datasets. Data shown as mean ± SEM, statistical significance given as *p<0.05, **p<0.01, ***p<0.001. Data provided by Dr. Jana F. Liewald.

3.3.6 RIMB-1 and ELKS-1 do not have redundant functions

The exocytosis of SVs is mediated by a group of proteins which together constitute a structure known as the cytomatrix of active zone (CAZ), or dense projection (DP). Five proteins of these - RIM, Munc13, RIM-BP, α-liprin and ELKS (in *C. elegans* UNC-10, UNC-13, RIMB-1, SYD-2, and ELKS-1 respectively) -, are the evolutionary conserved core proteins. Among others, these are responsible for the docking and priming of SVs and for the precise localization of voltage-gated Ca^{2+} channels which ensure an efficient neurotransmission upon

depolarisation (Südhof, 2012). In the previous experiments the function of RIMB-1 and UNC-10 was already addressed, thus I next investigated a possibly redundant role of RIMB-1 and ELKS-1.

It is known that there is a direct interaction between ELKS-1 and the PDZ domain of UNC-10 (Ohtsuka et al., 2002), however, the loss of ELKS-1 does not result in any strong phenotype in *C. elegans* (Deken et al., 2005). Previous publications showed that SH3 domains of RIM-BP bind to the prolin-rich regions of RIM (Y. Wang et al., 2000), and I showed that the mutation of *rimb-1* exacerbates the phenotype of *unc-10* mutants (see for example the swimming assay results of *rimb-1; unc-10*). If ELKS-1 and RIMB-1 were redundant proteins, mutants that lack ELKS-1 might not necessarily exhibit strong mutant phenotypes, however, *rimb-1; elks-1* double mutants should do so.

To investigate this hypothesis, *rimb-1(tm5964)* mutants were crossed with *elks-1(js816)* animals, and *rimb-1; elks-1* double mutants were probed in swimming assay (Figure 41). Animals were placed into M9 buffer and after a 15-minute-long incubation time, 60-s-long videos were recorded. Afterwards, the videos were analysed, the number of the trashes were counted manually.

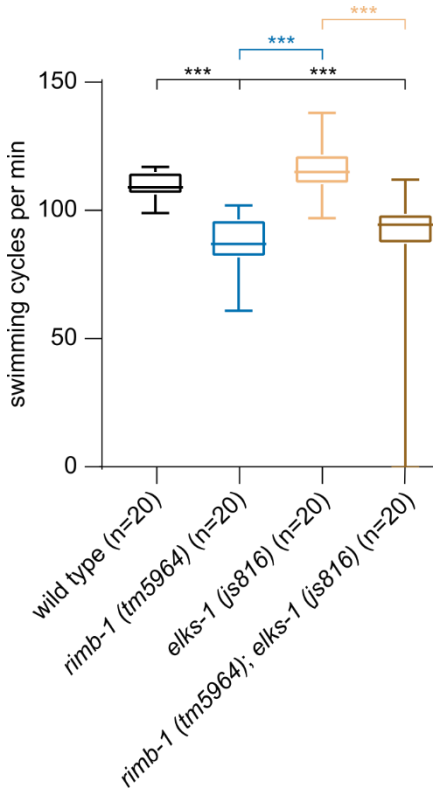

Figure 41: *rimb-1; elks-1* double mutants and *rimb-1* mutants performed similarly in swimming assay. The indicated mutant strains and wild type animals were probed in swimming assay. *rimb-1* and *rimb-1; elks-1* mutants showed a significant reduction in the number of the swimming cycles compared to wild type, however, there was no difference between these two mutant genotypes. The total number of tested animals is indicated as n numbers, the assay was repeated 2 times (on different days, with different animal populations). Data shown as median and 25/75 quartiles, min to max. ***p<0.001, after one-way ANOVA and Bonferroni post-hoc test.

Wild type animals showed at about 110 trashes per minute, and as already showed before, there was a significant reduction in the *rimb-1* mutant. Mutants lacking ELKS-1 did not show any phenotype, and the number of the swimming cycles in the double mutants were at about the same level as for *rimb-1* animals. Thus, there is no redundant relationship between RIMB-1 and ELKS-1.

3.3.7 RIMB-1 is essential for the precise localisation of SV release

It was previously published that RIM-BP has an essential role in organizing the AZ scaffold in *Drosophila* (K. S. Y. Liu et al., 2011), thus, this structure may also be effected in *rimb-1* mutants in *C. elegans*. For investigating this, serial sections of synapses were analysed under the transmission electron microscope (TEM) (Kittelmann et al., 2013).

Wild type animals and *rimb-1* mutants were raised with/without ATR as indicated (Figure 42, data provided by Dr. Szi-chieh Yu) and were illuminated with a blue laser for 30 s. After high-pressure freezing (HPF), freeze-substitution, sectioning and staining, the samples were analysed by TEM.

The total number of SVs was significantly decreased in *rimb-1* mutants already in animals raised without ATR. Moreover, illumination of the + ATR groups led to a drastic reduction of the SVs in *rimb-1* mutants, whereas there was a less significant decrease in the number of SVs in wild type animals (Figure 42, A). This was not expected according to the behavioural experiments; however, it is in line with the strong ePSCs measured in *rimb-1* mutants (Figure 35). Next, the number of the docked vesicles was analysed, which was significantly decreased in *rimb-1* mutants, both in animals raised with or without ATR (Figure 42, B). Thus, RIMB-1 is necessary for SV docking. Since RIMB-1 plays a role in the precise localization of VGCCs, possibly, these channels are not perfectly anchored at the dense projection (DP) in *rimb-1* mutants. This could have an influence on the distribution of the docked SVs along the presynaptic plasma membrane. Therefore, this hypothesis was investigated by counting the distance of the docked SVs and the DP, and indeed, *rimb-1* mutants showed an altered distribution. Most of the docked SVs were found within 33 nm to the DP in both genotypes (Figure 42, C), but the number of these was significantly smaller in *rimb-1* mutants. At first glance, there was no difference between the two genotypes at other distances, but this data was re-analysed in a different way (Figure 42, D). A single genotype-specific value was calculated for the different distances in a way that the number of the docked vesicles in the + ATR group

were subtracted from the number of the – ATR group. With this, it is possible to visualize the hypothetical number of the released SVs, and this showed that there was an altered distribution of released SVs in *rimb-1* mutants: most of the released SVs were found in the 66 nm and not in the 33 nm bin, and there was some SV exocytosis at greater distances as well, whereas in wild type animals beyond the 99 nm bin practically no SVs were released.

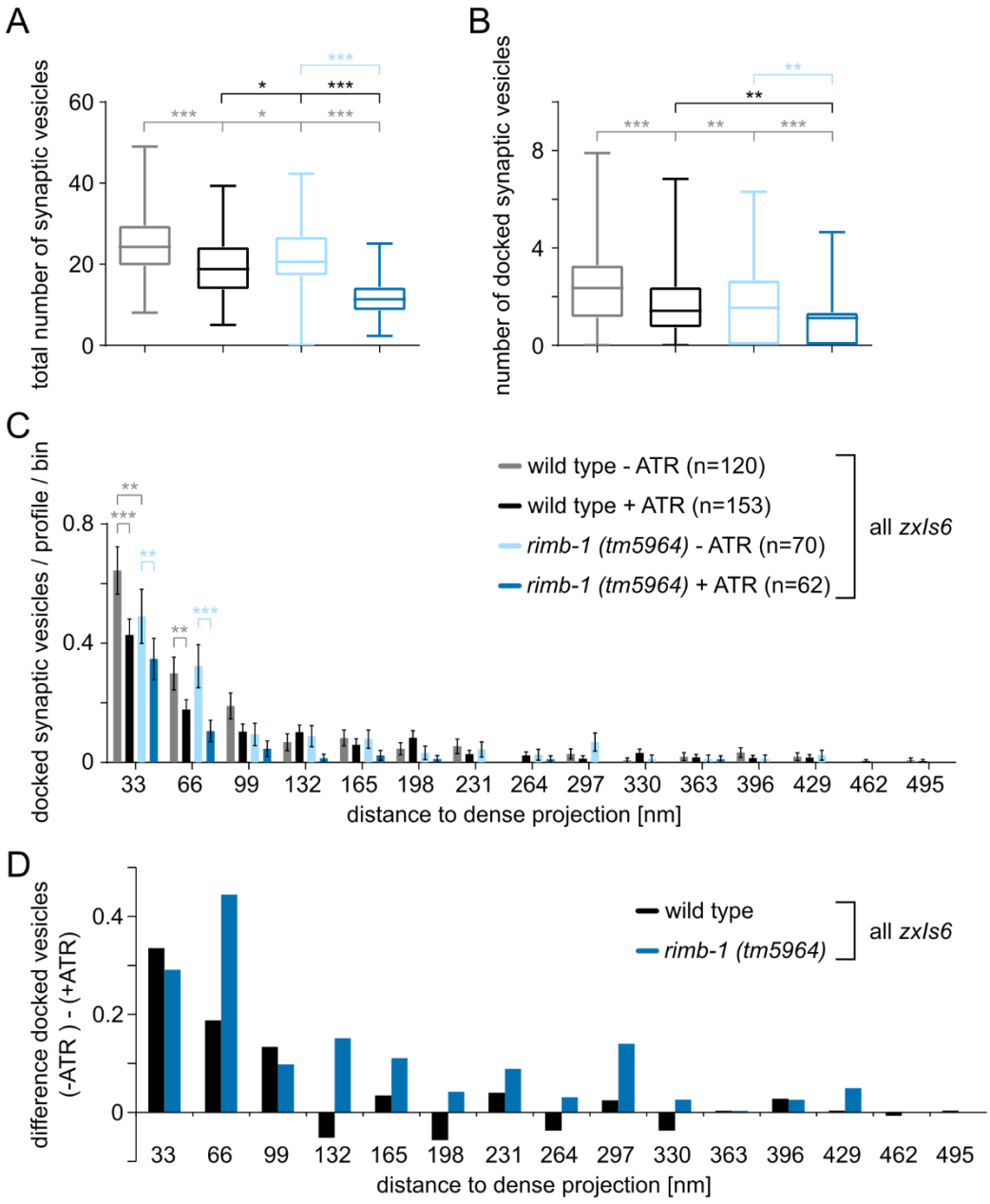

Figure 42: Electron microscopy analysis of photostimulated, cholinergic synapses in *rimb-1* mutants. Indicated genotypes were raised with/without ATR and were photostimulated for 30 s prior to HPF. The number of the analysed profiles is depicted as n numbers (analysed profiles are the single photographs of synapses, taken at the TEM, in total 10-16 synapses in 2-4 animals/genotypes were analysed). **(A-B)** Quantification of the number of the total (A) and docked (B) synaptic vesicles. Data shown as median and 25/75 quartiles, min to max. *p<0.05, **p<0.01, ***p<0.001, after one-way ANOVA and Bonferroni post-hoc test. **(C)** Analysis of the distance between docked synaptic vesicles and dense projection, along the plasma membrane. For the quantification 33 nm bins

were used. **p<0.01, ***p<0.001, after two-way ANOVA and Bonferroni post-hoc test (within bins, between groups). **(D)** Genotype-specific docked synaptic vesicle (DSV) values. Numbers depicted in (C) were normalized to the -ATR groups at the 33 nm bin, genotype-specific values were generated by subtracting the number of the DSVs of the +ATR group from the DSVs of the -ATR group. This shows the genotype-specific, hypothetical number of the released SVs, per bin. Data provided by Dr. Szi-chieh Yu.

3.3.8 Unfastening VGCCs affects cholinergic transmission and counterweights the mutation of RIMB-1

The altered distribution of released SVs in *rimb-1* mutant implies an altered distribution of the voltage gated Ca^{2+} channels as well. It was shown before in other organisms, that the C-terminal of the CaV2 α1 subunit (UNC-2) is anchored at the DP by the SH3 domains of RIM-BP (RIMB-1) (Hibino et al., 2002) and the PDZ domain of RIM (UNC-10) (Kaeser et al., 2011). In the previous experiments *rimb-1(tm5964)* and *unc-10(md1117)* mutants were already analysed; one could see that *rimb-1* mutants showed rather mild phenotypes, whereas *unc-10 (md1117)* mutants showed strong defects in the assays, which is expected since this protein has other functions besides Ca^{2+} channel tethering (Südhof, 2012). Since the phenotypes of *rimb-1; unc-10* double mutants are dominated by the *unc-10* mutation, the analysis of these mutants is not suitable to investigate the pure effect of the de-anchoring of VGCCs. Theerefore, a reverse strategy was used. *unc-2* mutants with a C-terminal deletion (the last ten amino-acids – the site of the PDZ domain ligand-, were deleted) were ordered from the SunyBiotech company (from now on called as UNC-2-ΔPDZ mutants) and were crossed with *rimb-1(tm5964)* mutants. In these animals, the dual tethering of UNC-2 to both, RIMB-1 and UNC-10 should be abolished. For investigating the cholinergic transmission in these double mutants, first, an aldicarb-assay was performed (Figure 43).

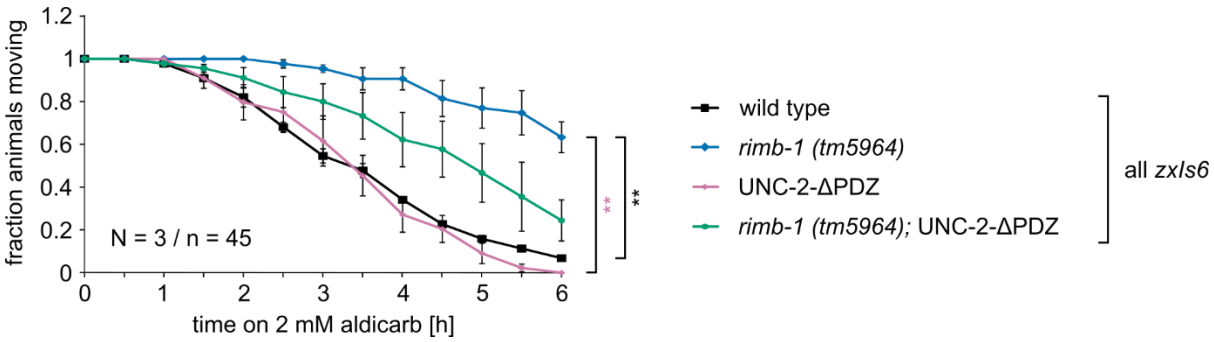

Figure 43: *rimb-1;* UNC-2 ΔPDZ mutants showed a mild aldicarb-resistant phenotype. Aldicarb assay with 2 mM aldicarb plates. The indicated genotypes were tested and scored 3 times (on 3 different days, with worms from 3 different populations). Around 40 % and 25 % of the *rimb-1 and* the rimb-1; UNC-2 ΔPDZ mutants respectively, were still capable of moving after spending 6 hours on 2 mM aldicarb plates, whereas almost all wild type animals and UNC-2 ΔPDZ mutants were paralyzed at the end of the assay. Shown are means ± SEM. **p<0.01 after Log-Rank test with Bonferroni correction.

As already seen before, *rimb-1(tm5964)* single mutants showed an aldicarb-resistant phenotype compared to wild type animals. The UNC-2-ΔPDZ single mutants behaved in a wild-type-like manner, whereas the *rimb-1(tm5964)*; UNC-2-ΔPDZ double mutants showed an intermediate, mild aldicarb-resistant phenotype.

Next, a swimming assay was carried out (Figure 44). As expected according to previous experiments, the number of swimming cycles was significantly decreased for the *rimb-1* mutants. Similar to the results of the aldicarb assay, the UNC-2-ΔPDZ mutants did not show any difference compared to wild type animals, while the double mutants showed again an intermediate phenotype: the number of the swimming cycles was more than for the *rimb-1* mutants and less than for wild type animals. However, this latter difference was not statistically significant.

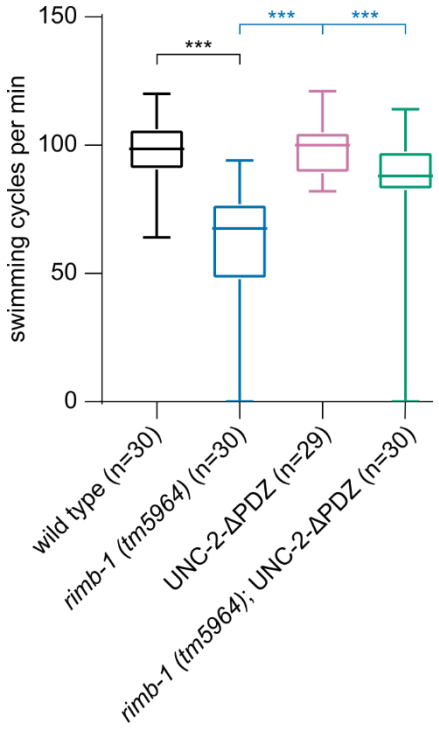

Figure 44: *rimb-1;* UNC-2 ΔPDZ double mutants showed an increased swimming activity compared to *rimb-1* mutants. The indicated mutant strains and wild type animals were probed in swimming assay. *rimb-1* mutants showed a significant reduction in the number of the swimming cycles compared to wild type animals, however, there was no significant difference between the UNC-2 ΔPDZ, *rimb-1;* UNC-2 ΔPDZ and wild type animals. The total number of tested animals is indicated as n numbers, the assay was repeated 3 times (on different days, with different animal populations). Data shown as median and 25/75 quartiles, min to max. ***p<0.001, after one-way ANOVA and Bonferroni post-hoc test.

The third assay for testing the cholinergic transmission was the contraction assay. Animals of the different genotypes were prepared as indicated (Figure 45) and photostimulated for 60 s using a blue light after a 5 s initial period. At the beginning of the illumination, *rimb-1* mutants contracted significantly less than wild type animals raised with ATR, whereas UNC-2-ΔPDZ

mutants contracted significantly stronger, at about 12 % of their initial body length. The level of contraction stayed at the same level for wild type animals and UNC-2-ΔPDZ mutants, while the *rimb-1* mutants and *rimb-1*; UNC-2-ΔPDZ double mutants showed a statistically significant progressive relaxation of the body length (Figure 45, right panel). The initial level of contraction was at about 11 % for the double mutants, which is not significantly different compared to ~ 10 % of wild type animals. However, the detailed analysis of the last 5 s of the illumination showed that there was a significant difference between these two groups: after the progressive relaxation, the level of the contraction was at about 8 % for the double mutants.

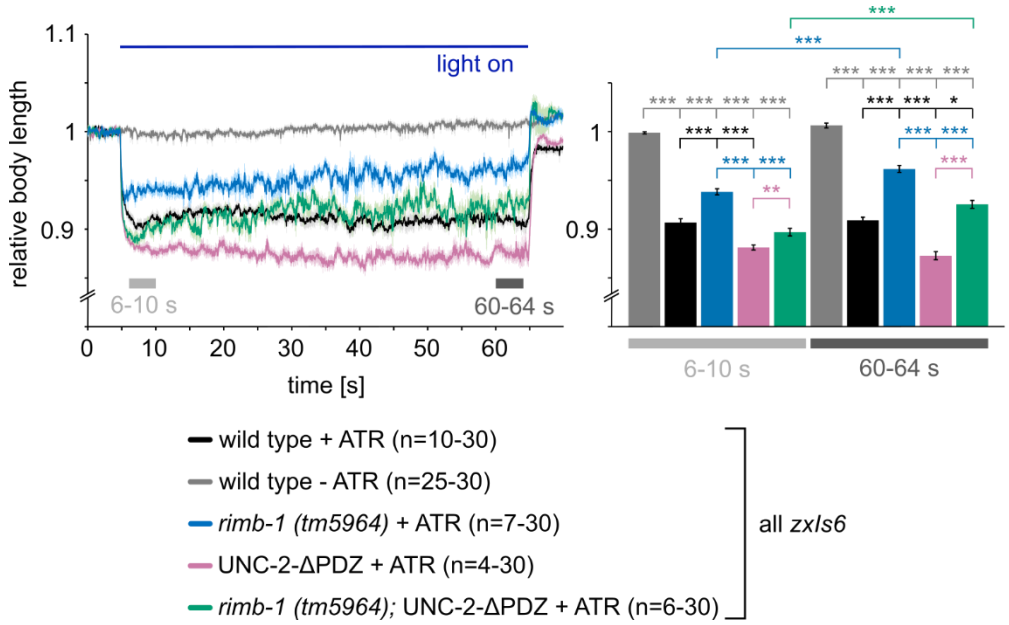

Figure 45: *rimb-1;* UNC-2-ΔPDZ double mutants contracted more than *rimb-1* single mutants and showed a recycling phenotype. Indicated genotypes (all expressing ChR2 in cholinergic neurons in form of the *zxIs6* transgene) were tested in contraction assay. Animals were raised with/without ATR (all-trans retinal – the co-factor of ChR2), in the presence of ATR animals contracted during the blue light illumination. The n numbers are indicated, where the smaller number represents the minimum number of animals (coiling animals were excluded in the time window while they coiled), whereas the bigger number indicates the number of the tested animals. Blue light stimulation was used to activate the cholinergic transmission, the length of the illumination was 60 s, started after a 5-s-long initial period. **Left panel:** Contraction assay. **Right panel:** Relative body lengths were compared at the beginning (6-10 s) and at the end (60-64 s) of the stimulation. Shown are means of means ± SEM.
*p<0.05, **p<0.01, ***p<0.001, after one-way ANOVA with Bonferroni.

All these results did not really show what we expected. The original expectation was rather that the UNC-2-ΔPDZ mutants would show a mutant phenotype: since the binding site of UNC-10 should not be functional anymore, the VGCCs could not be perfectly anchored at the active zone, thus the SV release should be ineffective, and less neurotransmitter should be released. Instead, we did not see any mutant phenotype in the behavioural assays without light stimulation for UNC-2-ΔPDZ mutants, whereas in the contraction assay there was seen a stronger contraction compared to wild type animals. This latter experiment could mean, that

the VGCCs, indeed, could not be perfectly tethered, thus, upon strong stimulation the Ca^{2+} microdomains cannot be perfectly centralized at the active zone and more SVs can be released -also in greater distance to the active zone-, than in wild type animals. However, we did not see any exacerbated phenotype in the *rimb-1*; UNC-2-ΔPDZ double mutants compared to *rimb-1* single mutants, on the contrary, there was an intermediate phenotype seen in all three experiments. This could mean that in case the binding sites of UNC-10 and RIMB-1 are both missing, other redundant proteins may compensate for this.

In the next step, synaptic transmission was analysed by electrophysiology (Figure 46, data provided by Dr. Jana F. Liewald). For this, animals of the indicated genotypes were raised with ATR, spontaneous (mPSCs) and evoked currents (ePSCs) were measured in the body wall muscles of *C. elegans* before and during photostimulation, respectively.

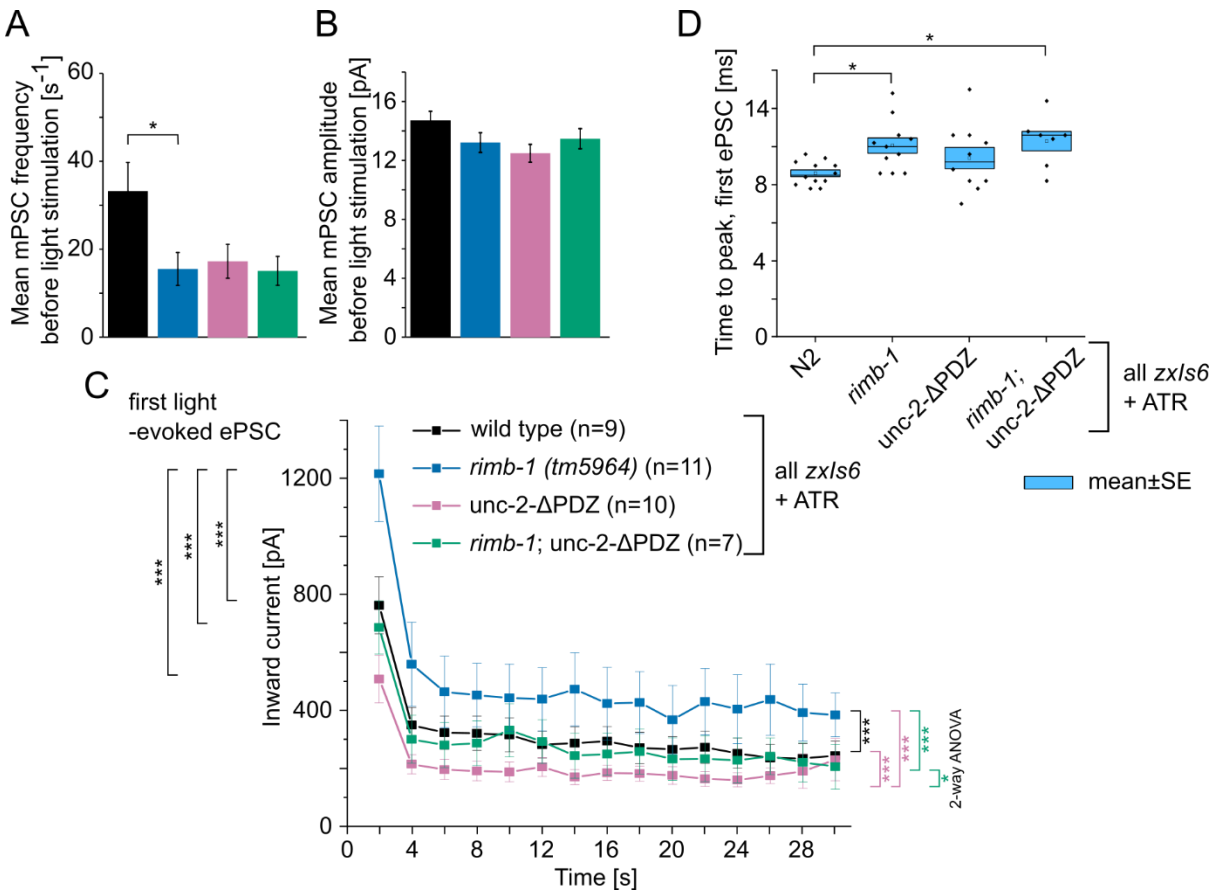

Figure 46: UNC-2-ΔPDZ mutants exhibited altered synaptic transmission in electrophysiological experiments. Indicated genotypes were raised in the presence of ATR and analysed by electrophysiology. Evoked postsynaptic currents (ePSCs) were measured using blue light stimulation, spontaneous currents (mPSCs) were measured 30 s long before first light stimulus. **(A)** mPSC frequencies and **(B)** amplitudes. One-way ANOVA, Tukey test. **(C)** Photoevoked PSC amplitudes. One-way ANOVA with Newman-Keuls test in first light-evoked ePSC analysis; two-way ANOVA to compare entire datasets. **(D)** Time (from light onset) to peak analysis of first ePSC. One-way ANOVA and Kruskall-Wallis test. Data shown as mean ± SEM in A-C, statistical significance given as *p<0.05, ***p<0.001. Data provided by Dr. Jana F. Liewald.

mPSC amplitudes were similar in all four groups (Figure 46, B). There was no significant difference between UNC-2-ΔPDZ and wild type animals regarding the mPSC frequency, but in the double mutants, UNC-2-ΔPDZ slightly reverted the significantly reduced value of *rimb-1* single mutants (Figure 46, A). This was in line with the previous results: the deletion of the PDZ binding domain of UNC-2 has not a negative effect on spontaneous SV release. However, UNC-2-ΔPDZ mutants exhibited strongly reduced ePSCs during photostimulation compared to wild type and *rimb-1* animals (Figure 46, C). Thus, although UNC-2-ΔPDZ animals are still able to present normal spontaneous activity, this is not the case during evoked activity, where the precise coupling of UNC-2 and docked vesicles is crucial. Time to peak was delayed in *rimb-1 (t5964)*; UNC-2-ΔPDZ double mutants, which is also a sign of imperfect coupling (Figure 46, D).

As a control experiment, *unc-2(pk95::Tc1)* loss-of-function mutants were also tested in contraction assays (Figure 47). The phenotype of these animals was similar to *rimb-1;* UNC-2-ΔPDZ double mutants: they showed decreased contraction at the beginning of the illumination compared to wild type animals, which was followed by an ongoing relaxation. Thus, the defects caused by the different mutations (*unc-2(pk95::Tc1) vs. rimb-1;* UNC-2-ΔPDZ) are comparable, however, using the double mutants additional details could be clarified.

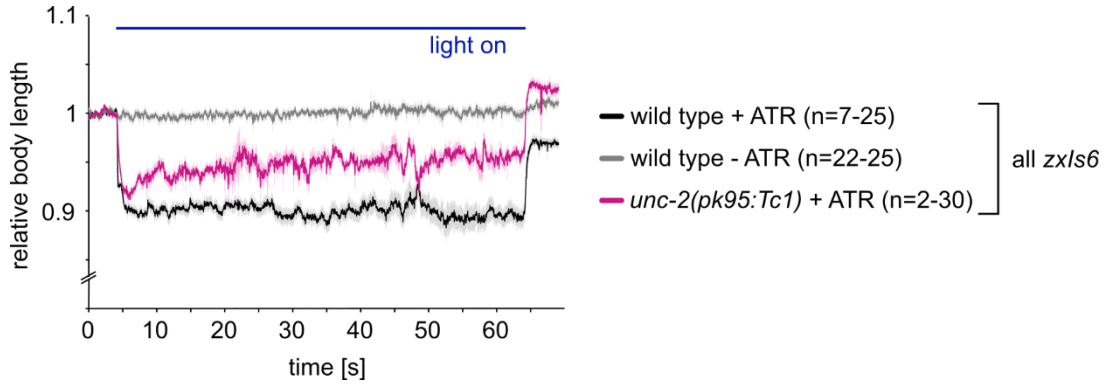

Figure 47: *unc-2(pk95:Tc1)* mutants showed decreased initial contraction followed by an ongoing relaxation. Indicated genotypes (all expressing ChR2 in cholinergic neurons in form of the *zxIs6* transgene) were tested in contraction assay. Animals were raised with/without ATR (all-trans retinal – the co-factor of ChR2), in the presence of ATR animals contracted during the blue light illumination. The n numbers are indicated, where the smaller number represents the minimum number of animals (coiling animals were excluded in the time window while they coiled), whereas the bigger number indicates the number of the tested animals. Blue light stimulation was used to activate the cholinergic transmission, the length of the illumination was 60 s, started after a 5-s-long initial period.

3.3.9 VGCC distribution is strongly altered in animals lacking both RIMB-1 and the PDZ ligand of UNC-2

Deleting the PDZ domain ligand of UNC-2 should have an effect on the mobility of this protein, thus, UNC-2-ΔPDZ mutants may have an altered VGCC distribution. This was analysed by fluorescence and confocal microscopy, using a strain in which the GFP sequence was inserted in-frame at the N-terminal domain of UNC-2 via CRISPR (a gift of Mei Zhen; (Gao et al., 2018) (from now on called as GFP::UNC-2 mutants). These animals were used for a further CRISPR-mediated editing of the *unc-2* locus (performed by the SunyBiotech company), where, again, the last ten amino-acids – the site of the PDZ domain ligand-, were deleted (from now on called as GFP::UNC-2-ΔPDZ strain). Both strains were crossed with the *rimb-1(tm5964)* mutants generating in total four strains, which were used for the analysis of GFP::UNC-2 fluorescence in the nerve ring.

It was known before that there is a GFP expression in the nerve ring (NR) of the GFP::UNC-2 mutants (Gao et al., 2018), thus, to assess the VGCC distribution, the fluorescence level of this region was compared (Figure 48). First, animals were analysed under an epi-fluorescence microscope (Figure 48, B). GFP::UNC-2 animals showed the strongest GFP expression, while there was a slight, not significant reduction in the GFP::UNC-2; *rimb-1(tm5964)* and the GFP:: UNC-2-ΔPDZ strains. GFP::UNC-2-ΔPDZ; *rimb-1(tm5964)* mutants showed a statistically significant reduction compared to all the other strains, which is also visible on the representative images (Figure 48, A). The experiment was repeated under the confocal microscope (Figure 48, C), where the same tendencies were seen. This shows that in mutants lacking both RIMB-1 and UNC-2 PDZ ligand, the VGCC distribution is indeed altered, whereas in mutants lacking only RIMB-1 or UNC-2 PDZ ligand, this effect is not such prominent. Thus, RIMB-1 and the UNC-2 PDZ ligand are very important players and are together responsible for the correct tethering of VGCC channels.

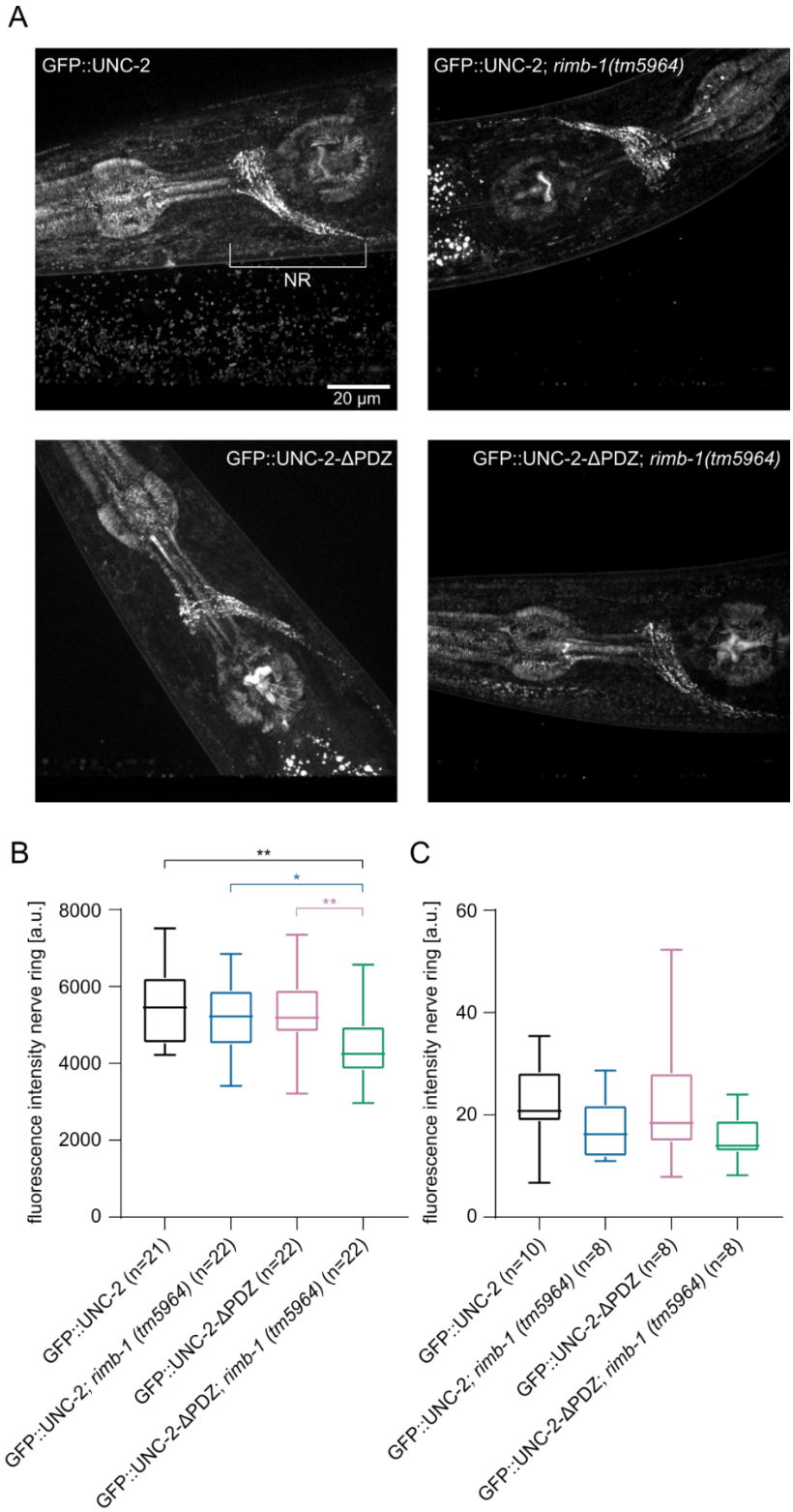

Figure 48: UNC-2/CaV2 channels are reduced in synapses lacking both RIMB-1 and UNC-2 PDZ domain. **(A)** Representative images of GFP::UNC-2 expression. Indicated genotypes were analysed under the confocal microscope, shown are Z-projections of the nerve ring (NR). **(B)** Quantification of fluorescent intensity of the nerve ring. Animals were photographed using an epi-fluorescence microscope. The total number of tested animals is indicated as n numbers, the assay was repeated three times (on different days, with different animal populations). Data shown as median and 25/75 quartiles, min to max. *p<0.05, **p<0.01, after one-way ANOVA and Bonferroni post-hoc test. **(C)** Quantification of fluorescent intensity of the nerve ring, using confocal Z-projections. The total number of tested animals is indicated as n numbers, the assay was repeated two times (on different days, with different animal populations). Data shown as median and 25/75 quartiles, min to max.

3.4 A new method for directly assessing synaptic vesicle fusion and recycling events

In the synaptic vesicle (SV) cycle, SVs undergo docking and priming, which is followed by the Ca^{2+} triggered exocytosis and the recycling of SVs (Südhof, 2004). There are numerous proteins which may play a role at the SV cycle (Wabnig et al., 2015), however, it is not clear yet what the exact functions of these are, or in which step of the cycle they are participating at. For identifying proteins, that participate at the SV recycling phase, there are indirect assays available. Putative SV recycling factors can be probed for example in the contraction assay, and as published before, SV recycling proteins such as synaptojanin (*unc-26*) mutants show a characteristic phenotype (Liewald et al., 2008), which enables to identify novel players as well. However, this is an indirect assay, thus, indirect factors such as compensatory feedback mechanisms can influence the results and the conclusions. To overcome this hurdle, a new all-optical analysis was established in *C. elegans*, which enables the direct analysis of mutants lacking putative recycling factors.

3.4.1 The construct of the new tool – the pOpsicle method

Synaptogyrin (*sng-1*) is a conserved, synaptic tetraspan vesicle membrane protein, which is in *C. elegans* strongly expressed in cholinergic motor neurons, moreover, mutants, lacking SNG-1 show only mild phenotypes (Abraham et al., 2006, 2011), making this protein a perfect candidate for inserting a marker inside the SV lumen. pHuji, the pH sensitive red fluorescent protein (Shen et al., 2014) was inserted into the second intravesicular loop of SNG-1. Once excited by yellow light, upon SV release, a fluorescent signal is visible due to the local pH rise, while during SV recycling the pH decreases and the fluorescent signal is quenched again. Thus, SV recycling can be directly visualized in neurons expressing this construct. For confining the expression to the cholinergic neurons, the *unc-17* promoter (Alfonso et al., 1993) was used. ChR2 was co-injected for enhancing the pHuji signal, thus, SV release can be activated with blue light and SV recycling can be investigated after turning off the blue light.

Worms were injected with the combination of the *Punc-17::sng-1-pHuji*, *Punc-17::ChR2(H134R)* and an additional co-marker (*Pmyo-2::CFP*) plasmids . The progeny of these animals was screened for transgenics under the fluorescence microscope, transgenic lines were maintained separately by picking fluorescent L4 animals to fresh NGM plates.

3.4.2 First microscopy results

One day before the experiment, transgenic L4 worms (carrying SNG-1::pHuji and ChR2 in the cholinergic neurons, furthermore the co-marker as extrachromosal arrays) were placed to fresh plates supplemented with/without ATR. These animals were probed next day under the fluorescence microscope.

Single worms were immobilized, observation site (distal part of the dorsal nerve cord – Figure 49, A) was searched by briefly turning on the yellow light, which was followed by a short incubation time in the dark. The measurement was started by turning on the yellow light again, blue light stimulation (ChR2 activation) was started after 9 s. Blue light was turned off after 7 s and the recording was continued.

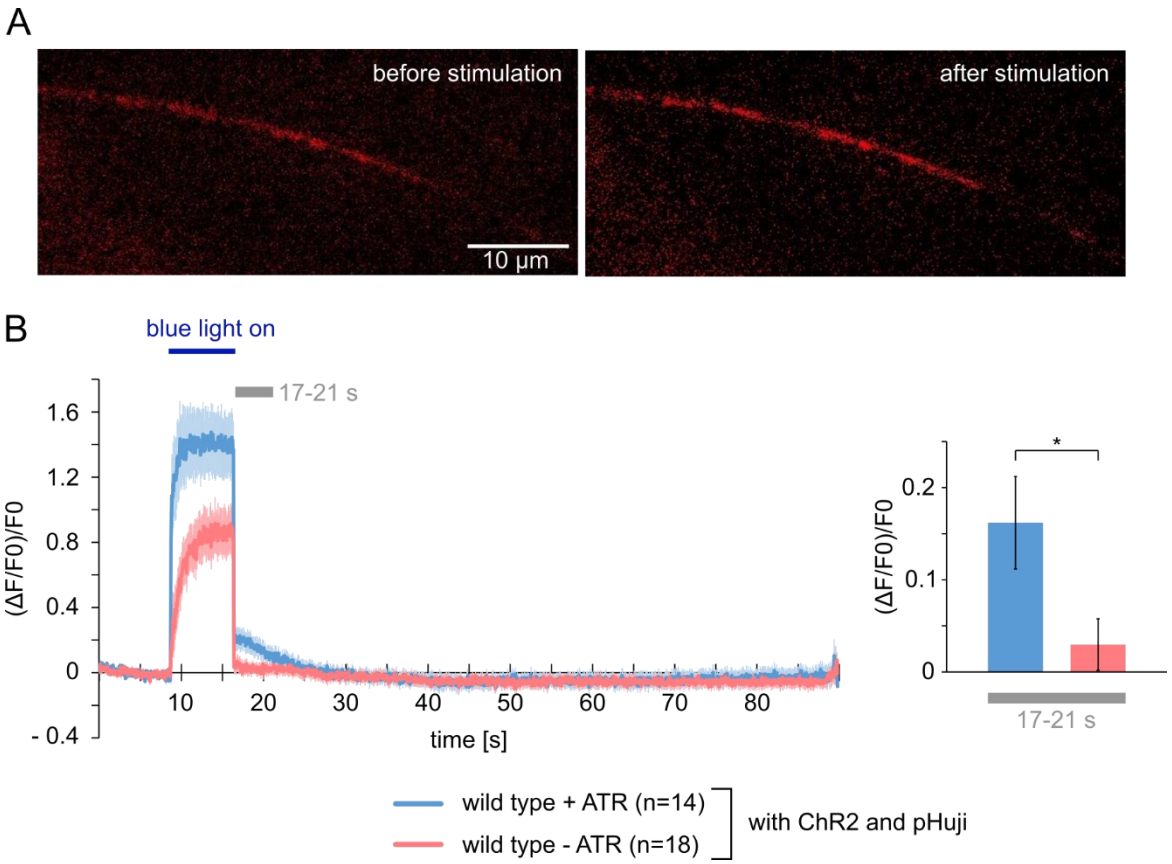

Figure 49: Synaptic vesicle release visualized by co-expressing ChR2 and pHuji in cholinergic neurons. (A) Representative images of pHuji (*punc-17::sng-1-pHuji)* expression in cholinergic neurons before and after blue-light-stimulation. The depicted observation site is at the distal part of the dorsal nerve chord close to the tail of the animals. The level of fluorescence increased after stimulation. **(B)** Quantitative analysis of pHuji fluorescence in animals raised with/w.o. ATR, as indicated. Analysed videos were recorded as depicted in (A). The total number of tested animals is indicated as n numbers, the assay was repeated two times (on different days, with different animal populations). **Left panel:** Blue light stimulation was started after 9 s, total length of the recordings was 90 s. pHuji fluorescence increased during and after light stimulation in animals raised with ATR. **Right panel:** Statistical analysis of fluorescence intensity after blue light stimulation as depicted at panel left. *p<0.05 after t-test.

Animals cultivated on ATR supplemented plates showed a significantly increased pHuji fluorescence not only during blue light administration, but also about 10-s-long after that (Figure 49, B). Thus, in these animals an increased number of SVs was released and the recycling of these lasts about 10 s. At later times, there was no difference between the two groups.

4. Discussion

SV recycling is crucial for a proper neuronal function, thus the investigation of factors affecting this process is necessary for understanding this complex system but also for identifying novel therapeutic targets. RIM-BPs seem to be implicated in autism spectrum disorders (Bucan et al., 2009; Corominas et al., 2014; Pinto et al., 2010), whereas ERP-1/endophilin-B is involved in Alzheimer's disease (D. B. Wang et al., 2015) and Parkinson's disease (A. S. L. Wong et al., 2011), thus, understanding the molecular function of these proteins is indispensable.

In this work, the role of ERP-1 and RIMB-1 in synaptic transmission was analysed investigating the cholinergic NMJs of the nematode *C. elegans.* It was shown that ERP-1 cooperates with UNC-57 and CHC-1 during SV recycling. While UNC-57 is the main player and functions both at the plasma membrane and at the endosome, ERP-1 acts also at both membrane systems but has rather a minor role and acts as a back-up protein. CHC-1 functions in the first place at the endosome, but it can compensate for the loss of UNC-57 and acts as a back-up protein at the plasma membrane.

In this work I demonstrated that RIMB-1 – in cooperation with UNC-10-, contributes to the precise localization of the VGCCs at the pre-synapse in *C. elegans*. Furthermore, I could show that RIMB-1 plays distinct roles in cholinergic and GABAergic neurons and with this, supports a proper excitation/inhibition balance.

There are numerous optogenetic assays available which enable the indirect analysis of putative synaptic recycling factors, but direct assays are more informative and thus highly desired. During this work, an optogenetic tool, the pOpsicle assay was described, which enables the direct visualization of SV exo-, and endocytosis events, and with this the identification of novel SV recycling proteins.

4.1 ERP-1 supports SV recycling at the PM and at the LV membrane in cooperation with UNC-57 and CHC-1

ERP-1, the *C. elegans* ortholog of endophilin B, was recently identified as a potential SV recycling factor (Wabnig et al., 2015), its possible contribution to SV endocytosis was not investigated before. In vertebrates there are two endophilin isoforms present: Endophilin A (UNC-57 in *C. elegans*) has an essential role in SV endocytosis and recycling, while the

function of endophilin B (ERP-1) was less well understood. During this work, ERP-1 was identified as an SV recycling protein, which contributes to SV endocytosis and regeneration through its cooperation with UNC-57 and CHC-1. Activity-dependent bulk endocytosis (ADBE) enables to retrieve SV membrane and proteins in a fast manner during intense stimulation (Clayton et al., 2008), resulting in bulk endosomes (also called as 'large vesicles', LVs) (Kittelmann et al., 2013), from which SVs are reformed via budding. This project had a special emphasis on the site of action of ERP-1, UNC-57, and CHC-1; whether they act at the plasma membrane (PM) or at the LV membrane. UNC-57 acts at the PM and at the LV membrane, while CHC-1 functions at the LV membrane in the presence of UNC-57. Once UNC-57 is missing, CHC-1 can compensate its loss, also at the PM. ERP-1 has a minor role compared to the other two proteins, however, it enables a basal level of SV recycling also if UNC-57 and CHC-1 are both missing, and it functions both at the PM and at LV membrane.

Endophilin A is proven to be involved in clathrin-mediated vesicle- (Gad et al., 2000; Milosevic et al., 2011; Ringstad et al., 1999; Sundborger et al., 2011) and clathrin-independent receptor endocytosis (Boucrot et al., 2015). It was shown that this protein contributes to fast clathrin-independent vesicle retrieval (Llobet et al., 2011) and bulk endocytosis (Laporte et al., 2022), however the site of its function remained controversial. ADBE suits well for investigating this: it begins with a clathrin-independent membrane retrieval at the PM which is followed by a clathrin-dependent SV budding at the LV membrane, thus it is possible to distinguish the two sites of action of endophilin A. In our ultrastructural analysis, very large synaptic endosomes were seen in *unc-57* and *unc-57; erp-1* mutants, which suggests that UNC-57/endophilin A is not absolutely necessary for the LV formation at the PM, and that clathrin can compensate for its loss.

LV formation is expected during high-frequency stimulation when ADBE is activated. During our experiments, we analysed stimulated *C. elegans* strains expressing ChR2 in its cholinergic neurons, raised both with and without ATR (all-trans retinal). ATR renders ChR2 active, thus animals raised without this represent the "unstimulated" controls, typically with very few LVs. However, *unc-57; erp-1* double mutants showed an unexpected phenotype regarding the LV formation: unstimulated animals produced numerous LVs whereas this was not the case for stimulated animals. In Endophilin A triple knockout (there are three endophilin A genes in mouse, instead of the one in *C. elegans*) mouse mutants ultrafast endocytosis was drastically slowed, but remained functional (Watanabe et al., 2018). In stimulated wild type animals, SV membrane is retrieved via ultrafast endocytosis, however, the loss of both UNC-57 and ERP-1 drastically slows this pathway down, or perhaps SV recycling happens via an originally

slower pathway, the clathrin-mediated endocytosis (CME). This may be sufficient for maintaining a close to normal size synaptic profile area and recovering the drastically reduced number of SVs (through the slow resolution of LVs) of unstimulated double mutants. However, following stimulation this pathway is not able to retrieve the excess membrane in a fast manner, thus the synaptic profile area is enlarged, and the number of LVs is reduced compared to the unstimulated double mutants (Figure 50.) (S. Yu et al., 2018).

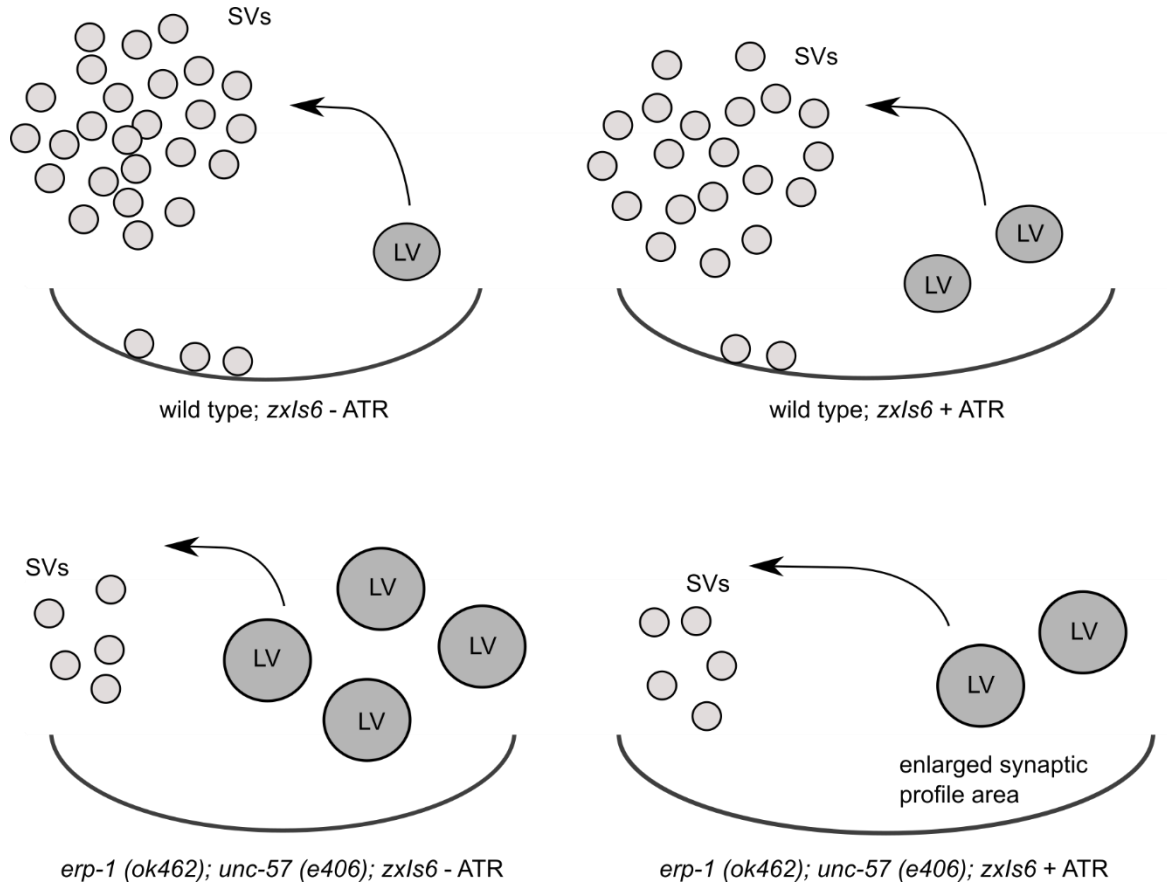

Figure 50: Schematic comparing the presynapse of wild type animals and *erp-1; unc-57* double mutants. Animals raised with ATR represent the 'stimulated' group whereas -ATR animals show the normal state of the synapse. 'Stimulated' wild type animals show decreased SVs and an increased number of LVs. On the contrary, 'unstimulated' *erp-1; unc-57* mutants had more LVs than the 'stimulated' double mutants. This shows that there must be an activity-dependent mechanism which enables some synaptic recycling in 'stimulated' animals but indicates also that the recycling pathway is drastically slowed compared to wild type animals. The enlarged synaptic profile area of stimulated *erp-1; unc-57* mutants indicates that the excess membrane cannot be retrieved and shows that recycling of these animals is insufficient. **ATR**: all-trans retinal - the co-factor of ChR2; ***zxIs6*** transgene: ChR2 in cholinergic neurons; **SVs**: synaptic vesicles, **LV**: large vesicle. For the detailed TEM analysis see (S. . Yu et al., 2018).

In stimulated *erp-1* mutants the number of LVs was increased, but only to a similar extent as in wild type animals. However, the enlarged synaptic profile area of unstimulated *erp-1* animals shows that ERP-1 is involved in SV recycling at the PM. Furthermore, the number of the SVs was also significantly decreased (S. Yu et al., 2018), which proves that ERP-1 contributes also to the reformation of SVs at the LV membrane. LV analysis of *erp-1; chc-1* and *unc-57; chc-*

1 verified that ERP-1 has only a minor role in SV recycling: the number of the LVs was slightly decreased in stimulated *erp-1; chc-1* animals compared to stimulated *erp-1* mutants. On the contrary, in stimulated *unc-57; chc-1* double mutants the number of the LVs significantly increased, although not as drastically as in stimulated *unc-57* mutants. This shows that in case UNC-57 and CHC-1 are both missing, other back-up proteins, such as ERP-1, can be activated. The milder phenotypes of *erp-1* compared to *unc-57* mutants can be explained through its function. While the major function of UNC-57/Endophilin-A is the contribution to SV recycling, ERP-1/Endophilin-B seems to be responsible in the first place for intracellular trafficking (J. Li et al., 2016; Modregger et al., 2003) and the regulation of autophagy (Hernandez-Diaz et al., 2022; D. B. Wang et al., 2015; A. S. L. Wong et al., 2011) and appears to be involved in SV recycling only as a back-up protein. It needs to be mentioned that also endophilin A and clathrin have functions beyond the SV endocytosis. Endophilin A is not only present at the presynaptic terminals but also at the ER/Golgi apparatus, endosomes, lysosomes and mitochondria (Kjaerulff et al., 2011), furthermore it is also necessary for synapse formation (Rikhy et al., 2002). CHC-1 is known to be responsible for the intracellular membrane trafficking (Brodsky et al., 2001) but is also involved in mitosis (Royle et al., 2005). Thus, it is not surprising that these mutations cause drastic phenotypes also in *C. elegans*.

A previous publication described the role of CHC-1 in ultrafast endocytosis. Whereas this protein functions at the PM in CME, in ultrafast endocytosis (at physiological temperatures) CHC-1 contributes to SV recycling rather at the LV membrane (Watanabe et al., 2014). This could be verified with our experiments: not only the number but also the size of LVs was strongly increased in stimulated *chc-1* mutants (at non-permissive temperature), thus CHC-1 acts mainly at the LV membrane in ADBE as well.

Clathrin triskelia consist of 3 light,- and 3 heavy chains. In *C. elegans* there is one gene encoding heavy-, (*chc-1*) and at least one gene (*clic-1*) encoding light chains (L. Wang & Audhya, 2014). Loss of CHC-1 induces embryonic lethality (Grant & Hirsh, 1999), whereas loss of CLIC-1 does not affect viability (Sato et al., 2009; L. Wang & Audhya, 2014), however, this protein does not seem to play an essential role in CME (Huang et al., 2004). Thus, during our experiments we worked with a temperature-sensitive allele of CHC-1, the *chc-1(b1025ts)* strain (Sato et al., 2009). These mutants need to be raised at permissive temperature (15 °C), and animal development is blocked at restrictive temperature (25 °C). CHC-1 level is drastically reduced in these mutants also at permissive temperature (4.5 % of wild type), however, this can be further decreased (to 2 %) by keeping the animals at 25 °C. *chc-1(b1025ts)* mutants showed decreased performance in thrashing assay, which further declined after

keeping the worms at 25°C for 24 h or at 30°C for 10 min. Unexpectedly, the number of SV was not significantly altered in *chc-1(b1025ts)* mutants, however, they were smaller than in wild type animals.

To sum it up, during this project ERP-1 was identified as a novel player in SV recycling. Behavioural, electrophysiological, and ultrastructural assays led to the conclusion, that ERP-1 cooperates with UNC-57 and CHC-1 during this process. The cooperation of these proteins results in a robust system: once two proteins are missing, the third one can compensate this, enabling sufficient synaptic activity and survival.

4.2 RIMB-1 is responsible for the precise localization of VGCCs and for maintaining the excitation-inhibition balance between cholinergic and GABAergic neurons

In the second project, the function of RIMB-1, the *C. elegans* ortholog of RIM-BP, was extensively characterized, focusing on the tripartite complex of RIMB-1, UNC-10/RIM and UNC-2/VGCC. Previous publications described before that RIM-BP and RIM participate in the precise localization of VGCCs in different organisms (Acuna et al., 2015, 2016; Davydova et al., 2014; Hibino et al., 2002; Krinner et al., 2017; Kushibiki et al., 2019, 2019; K. S. Y. Liu et al., 2011; Müller et al., 2015; Oh et al., 2021). However, an extensive analysis regarding the behavioural, electrophysiological, and ultrastructural aspects of the respective mutant strains *(rimb-1*, *unc-10*, *unc-2*) in *C. elegans*, was not available before.

rimb-1(tm5964) mutants showed mild behavioural defects in swimming and aldicarb assays, similar to the results presented before (Kushibiki et al., 2019), and a mild recycling phenotype in the contraction assay. At this point it needs to be mentioned, that based on our results published in this work, RIMB-1 does not seem to have a direct role in the SV recycling pathway. The name of this phenotype comes from previous experiments, in which mutants lacking known recycling proteins showed this type of contraction pattern with an ongoing relaxation (Liewald et al., 2008; Wabnig et al., 2015), thus it was termed as recycling phenotype.

Cholinergic deficits, detected in the behavioural experiments, were not visible in the electrophysiological experiments, where cholinergic stimulation through ChR2 resulted in increased transmission in *rimb-1* mutants. However, reduced depolarisation values of *rimb-1*

mutants in muscle voltage imaging could verify our previous interpretation based on the behavioural assays. The overall ACh release of *rimb-1* mutants was not reduced but delayed and most likely not as synchronous as required to evoke muscular currents (P. Liu et al., 2013). In order to balance this, an increased amount of ACh was released, but due to the imprecise timing, muscular depolarisation was ineffective, which was demonstrated by the reduced postsynaptic muscle contraction of *rimb-1* mutants.

This was not the case in *rimb-1* mutants lacking GABA, where ACh release was not as upregulated as in *rimb-1* single mutants. Furthermore, direct stimulation of GABAergic neurons of *rimb-1* mutants did not lead to any behavioural defects, however, electrophysiological measurements showed that muscles in these animals exhibit reduced ePSCs and neuronal SV release was delayed. The enlarged cholinergic ePSCs of *rimb-1* mutants most probably represent a homeostatic compensatory response; *rimb-1* mutants lacking GABA possess a lower homeostatic drive to balance the cholinergic-GABAergic system through upregulation of ACh release, thus the enlarged currents are gone in these mutants. All these point out the fact that RIMB-1 plays different roles in GABAergic and cholinergic synapses and that this protein contributes to the normal excitation/inhibition balance at the neuromuscular junction (NMJ) of *C. elegans*. It is not surprising that a presynaptic protein plays different roles in different types of synapses. Another presynaptic protein, Munc-13 plays an essential role in SV priming in glutamatergic and GABAergic hippocampal neurons, its absence blocked SV transmission completely (Varoqueaux et al., 2002). However, Munc-13 deficient cholinergic synapses were still capable of SV release (Varoqueaux et al., 2005). The fact that SV fusion of cholinergic and GABAergic synapses are differentially regulated in *C. elegans* was also described before (H. Liu et al., 2018), thus it is well possible that proteins such as RIMB-1, contribute to the inhibition/excitation balance through playing distinct roles in the different types of synapses.

Not only the electrophysiological experiments of *rimb-1* mutants, but also the ultrastructural analysis indicated an altered SV transmission in these animals. Docked SVs showed an altered distribution in *rimb-1* mutants; these were visible not only in close proximity to the dense projection, but also at greater distances. Comparison of the animals raised with or without ATR, furthermore larger evoked currents indicate that these distal SVs were also released; optogenetic stimulation is much stronger than a physiological one (Liewald et al., 2008; Q. Liu et al., 2009), and results in larger Ca^{2+} domains with the possibility to reach more docked SVs. Optogenetically-induced SV fusion events at distal sites were reported before (Watanabe, Liu, et al., 2013), however, *rimb-1* mutants released significantly more SVs compared to wild type

animals. Voltage-gated Ca^{2+} channels (VGCCs) are recruited to the active zone in wild type animals, thus SV release is only possible at the close proximity of this region (Ackermann et al., 2015; Südhof, 2012). SV transmission outside of the active zone indicates that VGCC localization is disturbed, which indicates that RIMB-1 has a role in the recruitment of these. The loss of RIM-BP resulted in an altered distribution of VGCCs in other organisms as well (Acuna et al., 2015; Grauel et al., 2016), we could verify these findings via ultrastructural analysis in *C. elegans*.

It is worth to mention that neither *rimb-1* nor *unc-10* single mutants showed the compensatory stronger contraction, typically seen in synaptic transmission mutants in contraction assay (Liewald et al., 2008). Synaptic transmission mutants, tested previously in contraction assay, are required for SV fusion, thus this special phenotype without compensatory contraction may be a specific feature of mutants lacking proteins that affect VGCC channel localization.

Indeed, according to another publication, the presynaptic protein UNC-10/RIM is responsible for anchoring VGCCs to the active zone (Kaeser et al., 2011). During this project we compared *rimb-1* mutants with *rimb-1; unc-10* double mutants, however, animals lacking UNC-10 are known to have serious defects (Koushika et al., 2001), and the phenotypes of the double mutants were dominated by these. There were only two experiments in which *rimb-1; unc-10* double mutants exhibited an exacerbated phenotype compared to *unc-10* single mutants. First, the number of the swimming cycles of *rimb-1; unc-10* animals was decreased even more than in *unc-10* mutants, which is consistent with previously published results (Kushibiki et al., 2019). Second, in electrophysiology the time to peak value of the first ePSC was drastically increased in double mutants compared to *unc-10* or *rimb-1* single mutants. These result show that RIMB-1 and UNC-10 cooperate, but the strong mutant phenotypes in animals lacking UNC-10 mask the phenotype caused solely by the imperfect localization of UNC-2. A new approach aimed to unmask these phenotypes. RIM binds to the C termini of VGCCs via its PDZ domain, whereas its N-terminal domain is required for SV priming (Kaeser et al., 2011). The analysis of UNC-2-ΔPDZ mutants enabled us to investigate the contribution of UNC-10 to the recruitment of VGCCs, keeping UNC-10 completely intact.

UNC-2-ΔPDZ mutants showed partly less (aldicarb assay), partly more (contraction assay) severe phenotypes than *rimb-1* mutants, however, in double mutants the phenotypes counteracted each other in almost all experiments. The phenotypes of the UNC-2-ΔPDZ mutants can be explained through additional protein-interactions. During the contraction assay and the electrophysiological experiments, UNC-2-ΔPDZ mutants showed phenotypes, which

are typical for SV fusion or priming mutants (Liewald et al., 2008). It is known that voltage-gated calcium channels directly interact with SV docking and priming proteins, such as syntaxin (Sheng et al., 1994), SNAP-25 (Rettig et al., 1996), synaptotagmin (Sheng et al., 1997) or Munc13 (Calloway et al., 2015). Thus, it is well possible, that the slight mis-localization of voltage-gated calcium channels impairs the binding ability of the priming factors, resulting in phenotypes which are typical for these mutants. The rather unexpected intermediate phenotypes of the *rimb-1*; UNC-2-ΔPDZ mutants can be explained by redundant protein interactions. It is possible that UNC-2 is tethered by more than two (RIMB-1 and UNC-10) proteins. Indeed, the deletion of Bruchpilot (BRP), the *Drosophila* ortholog of CAST/ELKS, resulted in reduced Ca^{2+} channel levels in the neuromuscular junction (Kittel et al., 2006) and it was shown that there is direct interaction between the N-terminus of BRP and the C-terminal $Ca_v\alpha_1$ subunit (Fouquet et al., 2009). Moreover, mammalian ELKS/CAST also directly interacts with β_4 or a_1 subunits of CaV2 (Kiyonaka et al., 2012). I addressed the question whether there is a redundant relationship between ELKS-1 and RIMB-1, however, only a single swimming assay was performed. Since there was no exacerbated phenotype in *rimb-1; elks-1* double mutants, we concluded that these proteins are not redundant. Although a previous publication (Oh et al., 2021) showed that ELKS-1 contributes to UNC-2 localization, it was found that it plays rather a minor role causing visible phenotypes only in *rimb-1; elks-1; unc-10* triple mutants. Their finding that UNC-10 and RIMB-1 (but not ELKS-1), are the proteins which play a critical role in UNC-2 localization, is consistent with our results.

It can be mentioned that the unexpected wild-type-like phenotypes of UNC-2-ΔPDZ mutants could be due to an imperfect degradation of the PDZ-binding domain of UNC-2, however, this option is not very likely. It was shown before that the PDZ domain of RIM interacts directly with the C-termini of presynaptic N and P/Q type $Ca2^{+}$ channels (Kaeser et al., 2011). The C-termini of UNC-2 shows the classical PDZ binding motif (Oh et al., 2021) and a previous study showed that PDZ domains of *C. elegans* bind to C-terminal sequences by recognizing the last seven ligand positions (Tonikian et al., 2008). In the UNC-2-ΔPDZ mutants the last ten amino-acids were deleted using CRISPR, which removed most probably the complete PDZ recognition site. The intermediate phenotypes of *rimb-1*; UNC-2-ΔPDZ and the fact that the contraction assay pattern of these animals was similar to the pattern of the *unc-2(pk95:Tc1)* mutants, further verify the complete degradation of the PDZ binding site. However, it must be mentioned, that there are fifteen different UNC-2 isoforms in *C. elegans*. The last ten amino acids are identical in fourteen of them (which were removed in the UNC-2-ΔPDZ mutants),

but one isoform ('isoform a') is a shorter one with a different ending. Yet there is no study analysing the function of the different isoforms, thus, it cannot be ruled out that the intact 'isoform a' acts as a back-up protein and partly rescues the phenotype.

In mutants lacking both RIMB-1 and UNC-2 PDZ ligand, fluorescent intensity of GFP::UNC-2 was significantly decreased, whereas single mutants showed wild-type-like intensities. This is consistent with the results of another paper (Oh et al., 2021), in which the peak intensity of GFP::UNC-2 was measured in different mutant backgrounds: there was a significant decrease in animals lacking both RIMB and UNC-10, compared to the *unc-10* single mutants. This proves further that the degradation of the PDZ binding site was successful and showed that RIMB-1 and UNC-10 are both necessary for the precise localization of VGCCs.

During the experiments the *rimb-1(tm5964)* strain was used, which contains a 659 bp deletion site including exon 14 and the preceding intron, resulting in the deletion of the second SH3 domain and a frameshift mutation with an early stop codon. Whether this represents a null mutant, is not known, however, this mutant is expected to express a truncated protein, which misses at least the last 482 amino acid, including the second and third SH3 domains, which are essential for the interaction with UNC-10/RIM (Y. Wang et al., 2000) and UNC-2/VGCC (Davydova et al., 2014; Petzoldt et al., 2020). Previously, additional *rimb-1* alleles were described: *gk452845* and *ce828* (Edwards et al., 2018), resulting in a premature stop codon after amino acid 113 or at codon 18, respectively. *rimb-1(gk452845)* mutants showed aldicarb-resistant phenotype and reduced swimming activity compared to wild type animals (Kushibiki et al., 2019), similar to our results analysing the *rimb-1(tm5964)* allele. On the contrary, *rimb-1(gk452845)* animals did not show reduced thrashing rates (Oh et al., 2021). However, the other two alleles express truncated proteins, thus it is possible that some (undefined) protein interaction sites remained intact in these, whereas this is very unlikely in animals carrying the *ce828* allele. A previous publication showed indeed that the N-terminal domain of the *Drosophila* RIM-BP is crucial for the AZ scaffold organization and SV recruitment, but not for SV/VGCC coupling or VGCC localization (Petzoldt et al., 2020). Other papers also mentioned a contribution of RIM-BP to SV recruitment (Krinner et al., 2017; Müller et al., 2015). Further work is required to investigate this in *C. elegans*, but the comparison of the different mutant alleles can serve as a good starting point.

4.3 pOpsicle enables the direct visualization of SV recycling

The pOpsicle assay enables the direct visualization of SV recycling by monitoring the pH of the SV lumen using pHuji (Shen et al., 2014), a pH sensitive fluorescent protein. pHuji was inserted into the second intravesicular loop of synaptogyrin (SNG-1), a tetraspan SV membrane protein (Abraham et al., 2006, 2011).

Previous studies which aimed to monitor synaptic activity in *C. elegans*, frequently used the pHlourin-synaptobrevin (SNB-1) fusion construct (Dittman & Kaplan, 2006; Oda et al., 2011). However, this transgene is suited rather to investigate steady-state synaptic features, since around 30 % of SNB-1 resides in the PM (Dittman & Kaplan, 2006), thus the comparison of the different SV recycling mutants would be impossible. Glutamatergic neurons can be visualized using the vesicular glutamate transporter(VGLUT)-pHluorin (Ventimiglia & Bargmann, 2017; M. Wang et al., 2021). This construct is optimal for the analysis of SV dynamic due to VGLUT's minimal residence time in the PM (Ventimiglia & Bargmann, 2017). Synaptic specialization of the *C. elegans* were visualized before using the synaptobrevin-GFP and synaptogyrin-GFP constructs (Nonet, 1999). SNG-1 is expressed in cholinergic motor neurons, whereas *sng-1* mutants show only mild phenotypes (Abraham et al., 2006, 2011), thus we decided to insert the fluorescent marker inside of this protein.

pHluorins are the most frequently used pH-sensitive green fluorescent proteins for visualizing synaptic activity (Miesenböck et al., 1998; Sankaranarayanan et al., 2000). However, it is not possible to use this in combination with the well-established optogenetic stimulation of cholinergic motor neurons trough ChR2 (Liewald et al., 2008), thus a red pH-sensitive fluorescent protein was needed. pHuji (Shen et al., 2014) with its highly pH sensitive property, seemed to be optimal. In the meanwhile another pOpsicle variant has been established, in which pHlourin is combined with the novel red-shifted ChR ChrimsonSA (Seidenthal et al., 2022).

4.4 Outlook

Fur future investigation of the cooperation of ERP-1, UNC-57 and CHC-1 and to uncover further back-up mechanisms and proteins, the analysis of an another CHC-1 mutant *C. elegans* could be beneficial. Inserting a photosensitive degron (PSD) (Hermann et al., 2015) right before the stop codon of CHC-1, would enable the acute degradation of this protein by illuminating the animals with blue light. The simultaneous loss of ERP-1, UNC-57 and CHC-

1 would definitely result in embryonic lethality, however, by crossing the CHC-1::PSD strain with *erp-1; unc-57* double mutants, a triple mutant strain could be perhaps investigated.

It was shown that RIMB-1 affects cholinergic and GABAergic neurons in a different way. Future work is required to continue the investigation of this. A cell-specific deletion of RIMB-1 would enable to compare the cell-specific functions of this protein. Another interesting aspect could be to investigate how RIMB-1 contributes to SV recruitment in *C. elegans*. Recently, the N-terminal region (NTR) of RIMB-1 was found to be specifically responsible for this in *Drosophila* (Petzoldt et al., 2020). CRISPR enables the partial deletion of a protein, thus it would be possible to create mutant strains, which miss one or another domain. With this, the domain specific molecular interactions could be defined as precisely as never before and the enigmatic function of the NTR could be specifically investigated. In this work, we concluded that ELKS-1 has not an important role in the precise localization of UNC-2, however, a recent paper (Oh et al., 2021) measuring the GFP::UNC-2 peak intensity in different mutant backgrounds, found an exacerbated phenotype in *rimb-1; elks-1; unc-10* triple mutants. The extensive behavioural, electrophysiological, and ultrastructural analysis of this triple mutant strain would be beneficial, and future work is required to unravel the function of ELKS-1.

Here, the first successful experiment of pOpsicle was presented. During this, a transgenic *C. elegans* strain, with extrachromosomal constructs, was used. In the meanwhile, a strain with integrated constructs is available (Seidenthal et al., 2022). Crossing this with numerous mutant strains enables to screen many putative SV recycling mutants, contributes to the identification of novel SV recycling proteins and helps to broaden our current knowledge about the SV cycle.

References

Abraham, C., Bai, L., & Leube, R. E. (2011). Synaptogyrin-dependent modulation of synaptic neurotransmission in Caenorhabditis elegans. *Neuroscience*, *190*, 75–88. https://doi.org/10.1016/j.neuroscience.2011.05.069

Abraham, C., Hutter, H., Palfreyman, M. T., Spatkowski, G., Weimer, R. M., Windoffer, R., Jorgensen, E. M., & Leube, R. E. (2006). Synaptic tetraspan vesicle membrane proteins are conserved but not needed for synaptogenesis and neuronal function in *Caenorhabditis elegans*. *Proceedings of the National Academy of Sciences*, *103*(21), 8227–8232. https://doi.org/10.1073/pnas.0509400103

Ackermann, F., Schink, K. O., Bruns, C., Izsvák, Z., Hamra, F. K., Rosenmund, C., & Garner, C. C. (2019). Critical role for Piccolo in synaptic vesicle retrieval. *ELife*, *8*, e46629. https://doi.org/10.7554/eLife.46629

Ackermann, F., Waites, C. L., & Garner, C. C. (2015). Presynaptic active zones in invertebrates and vertebrates. *EMBO Reports*, *16*(8), 923–938. https://doi.org/10.15252/embr.201540434

Acuna, C., Liu, X., Gonzalez, A., & Südhof, T. C. (2015). RIM-BPs Mediate Tight Coupling of Action Potentials to Ca 2+ -Triggered Neurotransmitter Release. *Neuron*, *87*(6), 1234–1247. https://doi.org/10.1016/j.neuron.2015.08.027

Acuna, C., Liu, X., & Südhof, T. C. (2016). How to Make an Active Zone: Unexpected Universal Functional Redundancy between RIMs and RIM-BPs. *Neuron*, *91*(4), 792–807. https://doi.org/10.1016/j.neuron.2016.07.042

Alfonso, A., Grundahl, K., Duerr, J. S., Han, H.-P., & Rand, J. B. (1993). The Caenorhabditis elegans unc-17 Gene: A Putative Vesicular Acetylcholine Transporter. *Science*, *261*(5121), 617–619. https://doi.org/10.1126/science.8342028

Altun, Z. (2017). WormAtlas Embryo Handbook—Nervous System in the Embryo—Nerve Ring Development. *WormAtlas*. https://doi.org/10.3908/wormatlas.4.2

Altun, Z. F., Chen, B., Wang, Z.-W., & Hall, D. H. (2009). High resolution map of Caenorhabditis elegans gap junction proteins. *Developmental Dynamics*, *238*(8), 1936–1950. https://doi.org/10.1002/dvdy.22025

Altun, Z. F., & Hall, D. H. (2005). WormAtlas Hermaphrodite Handbook—Nervous System—General Description. *WormAtlas*. https://doi.org/10.3908/wormatlas.1.18

Altun, Z. F., & Hall, D. H. (2006). WormAtas Hermaphrodite Handbook—Introduction. *WormAtlas*. https://doi.org/10.3908/wormatlas.1.1

Aravanis, A. M., Pyle, J. L., & Tsien, R. W. (2003). Single synaptic vesicles fusing transiently and successively without loss of identity. *Nature*, *423*(6940), 643–647. https://doi.org/10.1038/nature01686

Atias, M., Tevet, Y., Sun, J., Stavsky, A., Tal, S., Kahn, J., Roy, S., & Gitler, D. (2019). Synapsins regulate α-synuclein functions. *Proceedings of the National Academy of Sciences*, *116*(23), 11116–11118. https://doi.org/10.1073/pnas.1903054116

Atluri, P. P., & Ryan, T. A. (2006). The kinetics of synaptic vesicle reacidification at hippocampal nerve terminals. *The Journal of Neuroscience: The Official Journal of the Society for Neuroscience*, *26*(8), 2313–2320. https://doi.org/10.1523/JNEUROSCI.4425-05.2006

Augustin, I., Rosenmund, C., Südhof, T. C., & Brose, N. (1999). Munc13-1 is essential for fusion competence of glutamatergic synaptic vesicles. *Nature*, *400*(6743), 457–461. https://doi.org/10.1038/22768

Azimi Hashemi, N., Bergs, A. C. F., Schüler, C., Scheiwe, A. R., Steuer Costa, W., Bach, M., Liewald, J. F., & Gottschalk, A. (2019). Rhodopsin-based voltage imaging tools for use in muscles and neurons of Caenorhabditis elegans. *Proceedings of the National*

Academy of Sciences, *116*(34), 17051–17060. https://doi.org/10.1073/pnas.1902443116

Bai, J., Hu, Z., Dittman, J. S., Pym, E. C. G., & Kaplan, J. M. (2010). Endophilin Functions as a Membrane-Bending Molecule and Is Delivered to Endocytic Zones by Exocytosis. *Cell*, *143*(3), 430–441. https://doi.org/10.1016/j.cell.2010.09.024

Barrett, P. L., Fleming, J. T., & Göbel, V. (2004). Targeted gene alteration in Caenorhabditis elegans by gene conversion. *Nature Genetics*, *36*(11), 1231–1237. https://doi.org/10.1038/ng1459

Beitel, G. J., Clark, S. G., & Horvitz, H. R. (1990). Caenorhabditis elegans ras gene let-60 acts as a switch in the pathway of vulval induction. *Nature*, *348*(6301), 503–509. https://doi.org/10.1038/348503a0

Bergs, A., Schultheis, C., Fischer, E., Tsunoda, S. P., Erbguth, K., Husson, S. J., Govorunova, E., Spudich, J. L., Nagel, G., Gottschalk, A., & Liewald, J. F. (2018). Rhodopsin optogenetic toolbox v2.0 for light-sensitive excitation and inhibition in Caenorhabditis elegans. *PLOS ONE*, *13*(2), e0191802. https://doi.org/10.1371/journal.pone.0191802

Berndt, A., Yizhar, O., Gunaydin, L. A., Hegemann, P., & Deisseroth, K. (2009). Bi-stable neural state switches. *Nature Neuroscience*, *12*(2), 229–234. https://doi.org/10.1038/nn.2247

Bessereau, J.-L., Wright, A., Williams, D. C., Schuske, K., Davis, M. W., & Jorgensen, E. M. (2001). Mobilization of a Drosophila transposon in the Caenorhabditis elegans germ line. *Nature*, *413*(6851), 70–74. https://doi.org/10.1038/35092567

Betz, A., Thakur, P., Junge, H. J., Ashery, U., Rhee, J.-S., Scheuss, V., Rosenmund, C., Rettig, J., & Brose, N. (2001). Functional Interaction of the Active Zone Proteins Munc13-1 and RIM1 in Synaptic Vesicle Priming. *Neuron*, *30*(1), 183–196. https://doi.org/10.1016/S0896-6273(01)00272-0

Bloom, O., Evergren, E., Tomilin, N., Kjaerulff, O., Löw, P., Brodin, L., Pieribone, V. A., Greengard, P., & Shupliakov, O. (2003). Colocalization of synapsin and actin during synaptic vesicle recycling. *Journal of Cell Biology*, *161*(4), 737–747. https://doi.org/10.1083/jcb.200212140

Bonifacino, J. S., & Traub, L. M. (2003). Signals for Sorting of Transmembrane Proteins to Endosomes and Lysosomes. *Annual Review of Biochemistry*, *72*(1), 395–447. https://doi.org/10.1146/annurev.biochem.72.121801.161800

Bonnycastle, K., Davenport, E. C., & Cousin, M. A. (2021). Presynaptic dysfunction in neurodevelopmental disorders: Insights from the synaptic vesicle life cycle. *Journal of Neurochemistry*, *157*(2), 179–207. https://doi.org/10.1111/jnc.15035

Boucrot, E., Ferreira, A. P. A., Almeida-Souza, L., Debard, S., Vallis, Y., Howard, G., Bertot, L., Sauvonnet, N., & McMahon, H. T. (2015). Endophilin marks and controls a clathrin-independent endocytic pathway. *Nature*, *517*(7535), 460–465. https://doi.org/10.1038/nature14067

Boyden, E. S., Zhang, F., Bamberg, E., Nagel, G., & Deisseroth, K. (2005). Millisecond-timescale, genetically targeted optical control of neural activity. *Nature Neuroscience*, *8*(9), 1263–1268. https://doi.org/10.1038/nn1525

Bozza, T., McGann, J. P., Mombaerts, P., & Wachowiak, M. (2004). In Vivo Imaging of Neuronal Activity by Targeted Expression of a Genetically Encoded Probe in the Mouse. *Neuron*, *42*(1), 9–21. https://doi.org/10.1016/S0896-6273(04)00144-8

Brenner, S. (1974). The Genetics Of *Caenorhabditis Elegans*. *Genetics*, *77*(1), 71–94. https://doi.org/10.1093/genetics/77.1.71

Brodsky, F. M., Chen, C.-Y., Knuehl, C., Towler, M. C., & Wakeham, D. E. (2001). Biological Basket Weaving: Formation and Function of Clathrin-Coated Vesicles. *Annual Review*

of Cell and Developmental Biology, *17*(1), 517–568. https://doi.org/10.1146/annurev.cellbio.17.1.517

Brose, N., Hofmann, K., Hata, Y., & Südhof, T. C. (1995). Mammalian Homologues of Caenorhabditis elegans unc-13 Gene Define Novel Family of C2-domain Proteins. *Journal of Biological Chemistry*, *270*(42), 25273–25280. https://doi.org/10.1074/jbc.270.42.25273

Brunger, A. T., Leitz, J., Zhou, Q., Choi, U. B., & Lai, Y. (2018). Ca2+-Triggered Synaptic Vesicle Fusion Initiated by Release of Inhibition. *Trends in Cell Biology*, *28*(8), 631–645. https://doi.org/10.1016/j.tcb.2018.03.004

Bucan, M., Abrahams, B. S., Wang, K., Glessner, J. T., Herman, E. I., Sonnenblick, L. I., Alvarez Retuerto, A. I., Imielinski, M., Hadley, D., Bradfield, J. P., Kim, C., Gidaya, N. B., Lindquist, I., Hutman, T., Sigman, M., Kustanovich, V., Lajonchere, C. M., Singleton, A., Kim, J., … Hakonarson, H. (2009). Genome-wide analyses of exonic copy number variants in a family-based study point to novel autism susceptibility genes. *PLoS Genetics*, *5*(6), e1000536. https://doi.org/10.1371/journal.pgen.1000536

Burkhardt, P., Hattendorf, D. A., Weis, W. I., & Fasshauer, D. (2008). Munc18a controls SNARE assembly through its interaction with the syntaxin N-peptide. *The EMBO Journal*, *27*(7), 923–933. https://doi.org/10.1038/emboj.2008.37

Byerly, L., Cassada, R. C., & Russell, R. L. (1976). The life cycle of the nematode Caenorhabditis elegans. *Developmental Biology*, *51*(1), 23–33. https://doi.org/10.1016/0012-1606(76)90119-6

Calloway, N., Gouzer, G., Xue, M., & Ryan, T. A. (2015). The active-zone protein Munc13 controls the use-dependence of presynaptic voltage-gated calcium channels. *ELife*, *4*, e07728. https://doi.org/10.7554/eLife.07728

Cassada, R. C., & Russell, R. L. (1975). The dauerlarva, a post-embryonic developmental variant of the nematode Caenorhabditis elegans. *Developmental Biology*, *46*(2), 326–342. https://doi.org/10.1016/0012-1606(75)90109-8

Ceccarelli, B., Hurlbut, W. P., & Mauro, A. (1973). Turnover of transmitter and synaptic vesicles at the frog neuromusuclar junction. *Journal of Cell Biology*, *57*(2), 499–524. https://doi.org/10.1083/jcb.57.2.499

Chanaday, N. L., Cousin, M. A., Milosevic, I., Watanabe, S., & Morgan, J. R. (2019). The Synaptic Vesicle Cycle Revisited: New Insights into the Modes and Mechanisms. *The Journal of Neuroscience*, *39*(42), 8209–8216. https://doi.org/10.1523/JNEUROSCI.1158-19.2019

Chase, D. L., & Koelle, M. R. (2007). Biogenic amine neurotransmitters in C. elegans. *WormBook*. https://doi.org/10.1895/wormbook.1.132.1

Cheng, Y., Wang, J., Wang, Y., & Ding, M. (2015). Synaptotagmin 1 directs repetitive release by coupling vesicle exocytosis to the Rab3 cycle. *ELife*, *4*, e05118. https://doi.org/10.7554/eLife.05118

Chi, P., Greengard, P., & Ryan, T. A. (2001). Synapsin dispersion and reclustering during synaptic activity. *Nature Neuroscience*, *4*(12), 1187–1193. https://doi.org/10.1038/nn756

Clayton, E. L., Evans, G. J. O., & Cousin, M. A. (2008). Bulk Synaptic Vesicle Endocytosis Is Rapidly Triggered during Strong Stimulation. *Journal of Neuroscience*, *28*(26), 6627–6632. https://doi.org/10.1523/JNEUROSCI.1445-08.2008

Conte, D., MacNeil, L. T., Walhout, A. J. M., & Mello, C. C. (2015). RNA Interference in *Caenorhabditis elegans*. *Current Protocols in Molecular Biology*, *109*(1). https://doi.org/10.1002/0471142727.mb2603s109

Coppola, T., Magnin-Lüthi, S., Perret-Menoud, V., Gattesco, S., Schiavo, G., & Regazzi, R. (2001). Direct Interaction of the Rab3 Effector RIM with Ca2+Channels, SNAP-25, and Synaptotagmin. *Journal of Biological Chemistry*, *276*(35), 32756–32762. https://doi.org/10.1074/jbc.M100929200

Corominas, R., Yang, X., Lin, G. N., Kang, S., Shen, Y., Ghamsari, L., Broly, M., Rodriguez, M., Tam, S., Trigg, S. A., Fan, C., Yi, S., Tasan, M., Lemmens, I., Kuang, X., Zhao, N., Malhotra, D., Michaelson, J. J., Vacic, V., … Iakoucheva, L. M. (2014). Protein interaction network of alternatively spliced isoforms from brain links genetic risk factors for autism. *Nature Communications*, *5*, 3650. https://doi.org/10.1038/ncomms4650

Corsi, A. K., Wightman, B., & Chalfie, M. (2015). A Transparent Window into Biology: A Primer on *Caenorhabditis elegans*. *Genetics*, *200*(2), 387–407. https://doi.org/10.1534/genetics.115.176099

Corti, C., Aldegheri, L., Somogyi, P., & Ferraguti, F. (2002). Distribution and synaptic localisation of the metabotropic glutamate receptor 4 (mGluR4) in the rodent CNS. *Neuroscience*, *110*(3), 403–420. https://doi.org/10.1016/S0306-4522(01)00591-7

Crump, J. G., Zhen, M., Jin, Y., & Bargmann, C. I. (2001). The SAD-1 Kinase Regulates Presynaptic Vesicle Clustering and Axon Termination. *Neuron*, *29*(1), 115–129. https://doi.org/10.1016/S0896-6273(01)00184-2

Dai, Y., Taru, H., Deken, S. L., Grill, B., Ackley, B., Nonet, M. L., & Jin, Y. (2006). SYD-2 Liprin-alpha organizes presynaptic active zone formation through ELKS. *Nature Neuroscience*, *9*(12), 1479–1487. https://doi.org/10.1038/nn1808

Davydova, D., Marini, C., King, C., Klueva, J., Bischof, F., Romorini, S., Montenegro-Venegas, C., Heine, M., Schneider, R., Schröder, M. S., Altrock, W. D., Henneberger, C., Rusakov, D. A., Gundelfinger, E. D., & Fejtova, A. (2014). Bassoon Specifically

Controls Presynaptic P/Q-type Ca2+ Channels via RIM-Binding Protein. *Neuron*, *82*(1), 181–194. https://doi.org/10.1016/j.neuron.2014.02.012

De Camilli, P., Harris, S. M., Huttner, W. B., & Greengard, P. (1983). Synapsin I (Protein I), a nerve terminal-specific phosphoprotein. II. Its specific association with synaptic vesicles demonstrated by immunocytochemistry in agarose-embedded synaptosomes. *Journal of Cell Biology*, *96*(5), 1355–1373. https://doi.org/10.1083/jcb.96.5.1355

Deken, S. L., Vincent, R., Hadwiger, G., Liu, Q., Wang, Z.-W., & Nonet, M. L. (2005). Redundant Localization Mechanisms of RIM and ELKS in Caenorhabditis elegans. *Journal of Neuroscience*, *25*(25), 5975–5983. https://doi.org/10.1523/JNEUROSCI.0804-05.2005

Dent, J. A., & Han, M. (1998). Post-embryonic expression pattern of C. elegans let-60 ras reporter constructs. *Mechanisms of Development*, *72*(1–2), 179–182. https://doi.org/10.1016/S0925-4773(98)00026-4

Dickinson, D. J., Ward, J. D., Reiner, D. J., & Goldstein, B. (2013). Engineering the Caenorhabditis elegans genome using Cas9-triggered homologous recombination. *Nature Methods*, *10*(10), 1028–1034. https://doi.org/10.1038/nmeth.2641

Dimitrov, D., He, Y., Mutoh, H., Baker, B. J., Cohen, L., Akemann, W., & Knöpfel, T. (2007). Engineering and Characterization of an Enhanced Fluorescent Protein Voltage Sensor. *PLoS ONE*, *2*(5), e440. https://doi.org/10.1371/journal.pone.0000440

Dittman, J. S., & Kaplan, J. M. (2006). Factors regulating the abundance and localization of synaptobrevin in the plasma membrane. *Proceedings of the National Academy of Sciences*, *103*(30), 11399–11404. https://doi.org/10.1073/pnas.0600784103

Dong, W., Radulovic, T., Goral, R. O., Thomas, C., Suarez Montesinos, M., Guerrero-Given, D., Hagiwara, A., Putzke, T., Hida, Y., Abe, M., Sakimura, K., Kamasawa, N., Ohtsuka, T., & Young, S. M. (2018). CAST/ELKS Proteins Control Voltage-Gated Ca2+

Channel Density and Synaptic Release Probability at a Mammalian Central Synapse. *Cell Reports*, *24*(2), 284-293.e6. https://doi.org/10.1016/j.celrep.2018.06.024

Dulubova, I., Lou, X., Lu, J., Huryeva, I., Alam, A., Schneggenburger, R., Südhof, T. C., & Rizo, J. (2005). A Munc13/RIM/Rab3 tripartite complex: From priming to plasticity? *The EMBO Journal*, *24*(16), 2839–2850. https://doi.org/10.1038/sj.emboj.7600753

Edwards, S. L., Morrison, L. M., Manning, L., Stec, N., Richmond, J. E., & Miller, K. G. (2018). Sentryn Acts with a Subset of Active Zone Proteins To Optimize the Localization of Synaptic Vesicles in *Caenorhabditis elegans*. *Genetics*, *210*(3), 947–968. https://doi.org/10.1534/genetics.118.301466

Erbguth, K., Prigge, M., Schneider, F., Hegemann, P., & Gottschalk, A. (2012). Bimodal Activation of Different Neuron Classes with the Spectrally Red-Shifted Channelrhodopsin Chimera C1V1 in Caenorhabditis elegans. *PLoS ONE*, *7*(10), e46827. https://doi.org/10.1371/journal.pone.0046827

Farsad, K., Ringstad, N., Takei, K., Floyd, S. R., Rose, K., & De Camilli, P. (2001). Generation of high curvature membranes mediated by direct endophilin bilayer interactions. *Journal of Cell Biology*, *155*(2), 193–200. https://doi.org/10.1083/jcb.200107075

Fielenbach, N., & Antebi, A. (2008). *C. elegans* dauer formation and the molecular basis of plasticity. *Genes & Development*, *22*(16), 2149–2165. https://doi.org/10.1101/gad.1701508

Fire, A., Xu, S., Montgomery, M. K., Kostas, S. A., Driver, S. E., & Mello, C. C. (1998). Potent and specific genetic interference by double-stranded RNA in Caenorhabditis elegans. *Nature*, *391*(6669), 806–811. https://doi.org/10.1038/35888

Fouquet, W., Owald, D., Wichmann, C., Mertel, S., Depner, H., Dyba, M., Hallermann, S., Kittel, R. J., Eimer, S., & Sigrist, S. J. (2009). Maturation of active zone assembly by

Drosophila Bruchpilot. *The Journal of Cell Biology*, *186*(1), 129–145. https://doi.org/10.1083/jcb.200812150

Frézal, L., & Félix, M.-A. (2015). C. elegans outside the Petri dish. *ELife*, *4*, e05849. https://doi.org/10.7554/eLife.05849

Gad, H., Ringstad, N., Löw, P., Kjaerulff, O., Gustafsson, J., Wenk, M., Di Paolo, G., Nemoto, Y., Crum, J., Ellisman, M. H., De Camilli, P., Shupliakov, O., & Brodin, L. (2000). Fission and Uncoating of Synaptic Clathrin-Coated Vesicles Are Perturbed by Disruption of Interactions with the SH3 Domain of Endophilin. *Neuron*, *27*(2), 301–312. https://doi.org/10.1016/S0896-6273(00)00038-6

Gan, Q., & Watanabe, S. (2018). Synaptic Vesicle Endocytosis in Different Model Systems. *Frontiers in Cellular Neuroscience*, *12*, 171. https://doi.org/10.3389/fncel.2018.00171

Gandini, M. A., & Zamponi, G. W. (2022). Voltage-gated calcium channel nanodomains: Molecular composition and function. *The FEBS Journal*, *289*(3), 614–633. https://doi.org/10.1111/febs.15759

Gao, S., Guan, S. A., Fouad, A. D., Meng, J., Kawano, T., Huang, Y.-C., Li, Y., Alcaire, S., Hung, W., Lu, Y., Qi, Y. B., Jin, Y., Alkema, M., Fang-Yen, C., & Zhen, M. (2018). Excitatory motor neurons are local oscillators for backward locomotion. *ELife*, *7*, e29915. https://doi.org/10.7554/eLife.29915

Garção, P., Oliveira, C. R., Cunha, R. A., & Agostinho, P. (2014). Subsynaptic localization of nicotinic acetylcholine receptor subunits: A comparative study in the mouse and rat striatum. *Neuroscience Letters*, *566*, 106–110. https://doi.org/10.1016/j.neulet.2014.02.018

Gendrel, M., Atlas, E. G., & Hobert, O. (2016). A cellular and regulatory map of the GABAergic nervous system of C. elegans. *ELife*, *5*, e17686. https://doi.org/10.7554/eLife.17686

Geppert, M., Goda, Y., Hammer, R. E., Li, C., Rosahl, T. W., Stevens, C. F., & Südhof, T. C. (1994). Synaptotagmin I: A major Ca2+ sensor for transmitter release at a central synapse. *Cell*, *79*(4), 717–727. https://doi.org/10.1016/0092-8674(94)90556-8

Giovedì, S., Vaccaro, P., Valtorta, F., Darchen, F., Greengard, P., Cesareni, G., & Benfenati, F. (2004). Synapsin Is a Novel Rab3 Effector Protein on Small Synaptic Vesicles. *Journal of Biological Chemistry*, *279*(42), 43760–43768. https://doi.org/10.1074/jbc.M403293200

Grant, B., & Hirsh, D. (1999). Receptor-mediated Endocytosis in the *Caenorhabditis elegans* Oocyte. *Molecular Biology of the Cell*, *10*(12), 4311–4326. https://doi.org/10.1091/mbc.10.12.4311

Grauel, M. K., Maglione, M., Reddy-Alla, S., Willmes, C. G., Brockmann, M. M., Trimbuch, T., Rosenmund, T., Pangalos, M., Vardar, G., Stumpf, A., Walter, A. M., Rost, B. R., Eickholt, B. J., Haucke, V., Schmitz, D., Sigrist, S. J., & Rosenmund, C. (2016). RIM-binding protein 2 regulates release probability by fine-tuning calcium channel localization at murine hippocampal synapses. *Proceedings of the National Academy of Sciences*, *113*(41), 11615–11620. https://doi.org/10.1073/pnas.1605256113

Guo, J., Ge, J., Hao, M., Sun, Z., Wu, X., Zhu, J., Wang, W., Yao, P., Lin, W., & Xue, L. (2015). A Three-Pool Model Dissecting Readily Releasable Pool Replenishment at the Calyx of Held. *Scientific Reports*, *5*(1), 9517. https://doi.org/10.1038/srep09517

Gyurkó, M. D., Csermely, P., Sőti, C., & Steták, A. (2015). Distinct roles of the RasGAP family proteins in C. elegans associative learning and memory. *Scientific Reports*, *5*(1), 15084. https://doi.org/10.1038/srep15084

Han, M., & Sternberg, P. W. (1990). Let-60, a gene that specifies cell fates during C. elegans vulval induction, encodes a ras protein. *Cell*, *63*(5), 921–931. https://doi.org/10.1016/0092-8674(90)90495-Z

Han, X., & Boyden, E. S. (2007). Multiple-Color Optical Activation, Silencing, and Desynchronization of Neural Activity, with Single-Spike Temporal Resolution. *PLoS ONE*, *2*(3), e299. https://doi.org/10.1371/journal.pone.0000299

Hata, Y., Butz, S., & Sudhof, T. (1996). CASK: A novel dlg/PSD95 homolog with an N-terminal calmodulin-dependent protein kinase domain identified by interaction with neurexins. *The Journal of Neuroscience*, *16*(8), 2488–2494. https://doi.org/10.1523/JNEUROSCI.16-08-02488.1996

He, L., Wu, X.-S., Mohan, R., & Wu, L.-G. (2006). Two modes of fusion pore opening revealed by cell-attached recordings at a synapse. *Nature*, *444*(7115), 102–105. https://doi.org/10.1038/nature05250

Held, R. G., Liu, C., & Kaeser, P. S. (2016). ELKS controls the pool of readily releasable vesicles at excitatory synapses through its N-terminal coiled-coil domains. *ELife*, *5*, e14862. https://doi.org/10.7554/eLife.14862

Hermann, A., Liewald, J. F., & Gottschalk, A. (2015). A photosensitive degron enables acute light-induced protein degradation in the nervous system. *Current Biology: CB*, *25*(17), R749-750. https://doi.org/10.1016/j.cub.2015.07.040

Hernandez-Diaz, S., Ghimire, S., Sanchez-Mirasierra, I., Montecinos-Oliva, C., Swerts, J., Kuenen, S., Verstreken, P., & Soukup, S.-F. (2022). Endophilin-B regulates autophagy during synapse development and neurodegeneration. *Neurobiology of Disease*, *163*, 105595. https://doi.org/10.1016/j.nbd.2021.105595

Heuser, J. E., & Reese, T. S. (1973). EVIDENCE FOR RECYCLING OF SYNAPTIC VESICLE MEMBRANE DURING TRANSMITTER RELEASE AT THE FROG NEUROMUSCULAR JUNCTION. *Journal of Cell Biology*, *57*(2), 315–344. https://doi.org/10.1083/jcb.57.2.315

Hibino, H., Pironkova, R., Onwumere, O., Vologodskaia, M., Hudspeth, A. J., & Lesage, F. (2002). RIM Binding Proteins (RBPs) Couple Rab3-Interacting Molecules (RIMs) to Voltage-Gated Ca2+ Channels. *Neuron*, *34*(3), 411–423. https://doi.org/10.1016/S0896-6273(02)00667-0

Hinshaw, J. E., & Schmid, S. L. (1995). Dynamin self-assembles into rings suggesting a mechanism for coated vesicle budding. *Nature*, *374*(6518), 190–192. https://doi.org/10.1038/374190a0

Hodgkin, J., & Barnes, T. M. (1991). More is not better: Brood size and population growth in a self-fertilizing nematode. *Proceedings of the Royal Society of London. Series B: Biological Sciences*, *246*(1315), 19–24. https://doi.org/10.1098/rspb.1991.0119

Hodgkin, J., & Doniach, T. (1997). Natural Variation and Copulatory Plug Formation in *Caenorhabditis elegans*. *Genetics*, *146*(1), 149–164. https://doi.org/10.1093/genetics/146.1.149

Holderith, N., Lorincz, A., Katona, G., Rózsa, B., Kulik, A., Watanabe, M., & Nusser, Z. (2012). Release probability of hippocampal glutamatergic terminals scales with the size of the active zone. *Nature Neuroscience*, *15*(7), 988–997. https://doi.org/10.1038/nn.3137

Huang, F., Khvorova, A., Marshall, W., & Sorkin, A. (2004). Analysis of Clathrin-mediated Endocytosis of Epidermal Growth Factor Receptor by RNA Interference. *Journal of Biological Chemistry*, *279*(16), 16657–16661. https://doi.org/10.1074/jbc.C400046200

Husson, S. J., Gottschalk, A., & Leifer, A. M. (2013). Optogenetic manipulation of neural activity in *C. elegans*: From synapse to circuits and behaviour. *Biology of the Cell*, *105*(6), 235–250. https://doi.org/10.1111/boc.201200069

Husson, S. J., Liewald, J. F., Schultheis, C., Stirman, J. N., Lu, H., & Gottschalk, A. (2012). Microbial Light-Activatable Proton Pumps as Neuronal Inhibitors to Functionally

Dissect Neuronal Networks in C. elegans. *PLoS ONE*, *7*(7), e40937. https://doi.org/10.1371/journal.pone.0040937

Iseki, M., Matsunaga, S., Murakami, A., Ohno, K., Shiga, K., Yoshida, K., Sugai, M., Takahashi, T., Hori, T., & Watanabe, M. (2002). A blue-light-activated adenylyl cyclase mediates photoavoidance in Euglena gracilis. *Nature*, *415*(6875), 1047–1051. https://doi.org/10.1038/4151047a

Kaeser, P. S., Deng, L., Wang, Y., Dulubova, I., Liu, X., Rizo, J., & Südhof, T. C. (2011). RIM Proteins Tether Ca2+ Channels to Presynaptic Active Zones via a Direct PDZ-Domain Interaction. *Cell*, *144*(2), 282–295. https://doi.org/10.1016/j.cell.2010.12.029

Kittel, R. J., Wichmann, C., Rasse, T. M., Fouquet, W., Schmidt, M., Schmid, A., Wagh, D. A., Pawlu, C., Kellner, R. R., Willig, K. I., Hell, S. W., Buchner, E., Heckmann, M., & Sigrist, S. J. (2006). Bruchpilot Promotes Active Zone Assembly, Ca $^{2+}$ Channel Clustering, and Vesicle Release. *Science*, *312*(5776), 1051–1054. https://doi.org/10.1126/science.1126308

Kittelmann, M., Liewald, J. F., Hegermann, J., Schultheis, C., Brauner, M., Steuer Costa, W., Wabnig, S., Eimer, S., & Gottschalk, A. (2013). In vivo synaptic recovery following optogenetic hyperstimulation. *Proceedings of the National Academy of Sciences*, *110*(32), E3007–E3016. https://doi.org/10.1073/pnas.1305679110

Kiyonaka, S., Nakajima, H., Takada, Y., Hida, Y., Yoshioka, T., Hagiwara, A., Kitajima, I., Mori, Y., & Ohtsuka, T. (2012). Physical and functional interaction of the active zone protein CAST/ERC2 and the β-subunit of the voltage-dependent Ca(2+) channel. *Journal of Biochemistry*, *152*(2), 149–159. https://doi.org/10.1093/jb/mvs054

Kjaerulff, O., Brodin, L., & Jung, A. (2011). The Structure and Function of Endophilin Proteins. *Cell Biochemistry and Biophysics*, *60*(3), 137–154. https://doi.org/10.1007/s12013-010-9137-5

Ko, J., Na, M., Kim, S., Lee, J.-R., & Kim, E. (2003). Interaction of the ERC Family of RIM-binding Proteins with the Liprin-α Family of Multidomain Proteins. *Journal of Biological Chemistry*, *278*(43), 42377–42385. https://doi.org/10.1074/jbc.M307561200

Koch, H., Hofmann, K., & Brose, N. (2000). Definition of Munc13-homology-domains and characterization of a novel ubiquitously expressed Munc13 isoform. *Biochemical Journal*, *349*(1), 247–253. https://doi.org/10.1042/bj3490247

Kogo, N., Dalezios, Y., Capogna, M., Ferraguti, F., Shigemoto, R., & Somogyi, P. (2004). Depression of GABAergic input to identified hippocampal neurons by group III metabotropic glutamate receptors in the rat. *European Journal of Neuroscience*, *19*(10), 2727–2740. https://doi.org/10.1111/j.0953-816X.2004.03394.x

Koushika, S. P., Richmond, J. E., Hadwiger, G., Weimer, R. M., Jorgensen, E. M., & Nonet, M. L. (2001). A post-docking role for active zone protein Rim. *Nature Neuroscience*, *4*(10), 997–1005. https://doi.org/10.1038/nn732

Krinner, S., Butola, T., Jung, S., Wichmann, C., & Moser, T. (2017). RIM-Binding Protein 2 Promotes a Large Number of CaV1.3 Ca2+-Channels and Contributes to Fast Synaptic Vesicle Replenishment at Hair Cell Active Zones. *Frontiers in Cellular Neuroscience*, *11*, 334. https://doi.org/10.3389/fncel.2017.00334

Kuhara, A., Ohnishi, N., Shimowada, T., & Mori, I. (2011). Neural coding in a single sensory neuron controlling opposite seeking behaviours in Caenorhabditis elegans. *Nature Communications*, *2*(1), 355. https://doi.org/10.1038/ncomms1352

Kushibiki, Y., Suzuki, T., Jin, Y., & Taru, H. (2019). RIMB-1/RIM-Binding Protein and UNC-10/RIM Redundantly Regulate Presynaptic Localization of the Voltage-Gated Calcium Channel in *Caenorhabditis elegans*. *The Journal of Neuroscience*, *39*(44), 8617–8631. https://doi.org/10.1523/JNEUROSCI.0506-19.2019

LaConte, L. E. W., Chavan, V., Liang, C., Willis, J., Schönhense, E.-M., Schoch, S., & Mukherjee, K. (2016). CASK stabilizes neurexin and links it to liprin-α in a neuronal activity-dependent manner. *Cellular and Molecular Life Sciences*, *73*(18), 3599–3621. https://doi.org/10.1007/s00018-016-2183-4

Lai, C.-H., Chou, C.-Y., Ch'ang, L.-Y., Liu, C.-S., & Lin, W. (2000). Identification of Novel Human Genes Evolutionarily Conserved in *Caenorhabditis elegans* by Comparative Proteomics. *Genome Research*, *10*(5), 703–713. https://doi.org/10.1101/gr.10.5.703

Lai, Y., Choi, U. B., Leitz, J., Rhee, H. J., Lee, C., Altas, B., Zhao, M., Pfuetzner, R. A., Wang, A. L., Brose, N., Rhee, J., & Brunger, A. T. (2017). Molecular Mechanisms of Synaptic Vesicle Priming by Munc13 and Munc18. *Neuron*, *95*(3), 591-607.e10. https://doi.org/10.1016/j.neuron.2017.07.004

Laporte, M. H., Chi, K. I., Caudal, L. C., Zhao, N., Schwarz, Y., Rolland, M., Martinez-Hernandez, J., Martineau, M., Chatellard, C., Denarier, E., Mercier, V., Lemaître, F., Blot, B., Moutaux, E., Cazorla, M., Perrais, D., Lanté, F., Bruns, D., Fraboulet, S., … Sadoul, R. (2022). Alix is required for activity-dependent bulk endocytosis at brain synapses. *PLoS Biology*, *20*(6), e3001659. https://doi.org/10.1371/journal.pbio.3001659

Lewis, J. A., Wu, C. H., Berg, H., & Levine, J. H. (1980). The genetics of levamisole resistance in the nematode Caenorhabditis elegans. *Genetics*, *95*(4), 905–928.

Li, J., Barylko, B., Eichorst, J. P., Mueller, J. D., Albanesi, J. P., & Chen, Y. (2016). Association of Endophilin B1 with Cytoplasmic Vesicles. *Biophysical Journal*, *111*(3), 565–576. https://doi.org/10.1016/j.bpj.2016.06.017

Li, L., Bischofberger, J., & Jonas, P. (2007). Differential Gating and Recruitment of P/Q-, N-, and R-Type Ca2+ Channels in Hippocampal Mossy Fiber Boutons. *Journal of*

Neuroscience, *27*(49), 13420–13429. https://doi.org/10.1523/JNEUROSCI.1709-07.2007

Li, Y., & Tsien, R. W. (2012). PHTomato, a red, genetically encoded indicator that enables multiplex interrogation of synaptic activity. *Nature Neuroscience*, *15*(7), 1047–1053. https://doi.org/10.1038/nn.3126

Liewald, J. F., Brauner, M., Stephens, G. J., Bouhours, M., Schultheis, C., Zhen, M., & Gottschalk, A. (2008). Optogenetic analysis of synaptic function. *Nature Methods*, *5*(10), 895–902. https://doi.org/10.1038/nmeth.1252

Lin, M. Z., & Schnitzer, M. J. (2016). Genetically encoded indicators of neuronal activity. *Nature Neuroscience*, *19*(9), 1142–1153. https://doi.org/10.1038/nn.4359

Lints, R., & Hall, D. H. (2004). WormAtlas Male Handbook—Introduction. *WormAtlas*. https://doi.org/10.3908/wormatlas.2.1

Liu, H., Li, L., Wang, W., Gong, J., Yang, X., & Hu, Z. (2018). Spontaneous Vesicle Fusion Is Differentially Regulated at Cholinergic and GABAergic Synapses. *Cell Reports*, *22*(9), 2334–2345. https://doi.org/10.1016/j.celrep.2018.02.023

Liu, K. S. Y., Siebert, M., Mertel, S., Knoche, E., Wegener, S., Wichmann, C., Matkovic, T., Muhammad, K., Depner, H., Mettke, C., Buckers, J., Hell, S. W., Muller, M., Davis, G. W., Schmitz, D., & Sigrist, S. J. (2011). RIM-Binding Protein, a Central Part of the Active Zone, Is Essential for Neurotransmitter Release. *Science*, *334*(6062), 1565–1569. https://doi.org/10.1126/science.1212991

Liu, P., Chen, B., & Wang, Z.-W. (2013). Postsynaptic current bursts instruct action potential firing at a graded synapse. *Nature Communications*, *4*(1), 1911. https://doi.org/10.1038/ncomms2925

Liu, Q., Hollopeter, G., & Jorgensen, E. M. (2009). Graded synaptic transmission at the *Caenorhabditis elegans* neuromuscular junction. *Proceedings of the National Academy of Sciences*, *106*(26), 10823–10828. https://doi.org/10.1073/pnas.0903570106

Llobet, A., Gallop, J. L., Burden, J. J. E., Çamdere, G., Chandra, P., Vallis, Y., Hopkins, C. R., Lagnado, L., & McMahon, H. T. (2011). Endophilin drives the fast mode of vesicle retrieval in a ribbon synapse. *The Journal of Neuroscience: The Official Journal of the Society for Neuroscience*, *31*(23), 8512–8519. https://doi.org/10.1523/JNEUROSCI.6223-09.2011

Luján, R., Shigemoto, R., Kulik, A., & Juiz, J. M. (2004). Localization of the GABA $_B$ receptor 1a/b subunit relative to glutamatergic synapses in the dorsal cochlear nucleus of the rat: Distribution of GABA $_B$ Receptors in the DCN. *Journal of Comparative Neurology*, *475*(1), 36–46. https://doi.org/10.1002/cne.20160

Lyons, L. C., & Hecht, R. M. (1997). Acute ethanol exposure induces nondisjunction of hte X chromosome during spermatogenesis. *Worm Breeders Gazette*, *14*, 52.

Mahoney, T. R., Luo, S., & Nonet, M. L. (2006). Analysis of synaptic transmission in Caenorhabditis elegans using an aldicarb-sensitivity assay. *Nature Protocols*, *1*(4), 1772–1777. https://doi.org/10.1038/nprot.2006.281

Maro, G. S., Gao, S., Olechwier, A. M., Hung, W. L., Liu, M., Özkan, E., Zhen, M., & Shen, K. (2015). MADD-4/Punctin and Neurexin Organize C. elegans GABAergic Postsynapses through Neuroligin. *Neuron*, *86*(6), 1420–1432. https://doi.org/10.1016/j.neuron.2015.05.015

Maruyama, I. N., & Brenner, S. (1991). A phorbol ester/diacylglycerol-binding protein encoded by the unc-13 gene of Caenorhabditis elegans. *Proceedings of the National Academy of Sciences*, *88*(13), 5729–5733. https://doi.org/10.1073/pnas.88.13.5729

Maycox, P. R., Deckwerth, T., Hell, J. W., & Jahn, R. (1988). Glutamate uptake by brain synaptic vesicles. Energy dependence of transport and functional reconstitution in proteoliposomes. *Journal of Biological Chemistry*, *263*(30), 15423–15428. https://doi.org/10.1016/S0021-9258(19)37605-7

McIntire, S. L., Jorgensen, E., Kaplan, J., & Horvitz, H. R. (1993). The GABAergic nervous system of Caenorhabditis elegans. *Nature*, *364*(6435), 337–341. https://doi.org/10.1038/364337a0

McMahon, H. T., Missler, M., Li, C., & Südhof, T. C. (1995). Complexins: Cytosolic proteins that regulate SNAP receptor function. *Cell*, *83*(1), 111–119. https://doi.org/10.1016/0092-8674(95)90239-2

McPherson, P. S., Garcia, E. P., Slepnev, V. I., David, C., Zhang, X., Grabs, D., Sossini, W. S., Bauerfeind, R., Nemoto, Y., & De Camilli, P. (1996). A presynaptic inositol-5-phosphatase. *Nature*, *379*(6563), 353–357. https://doi.org/10.1038/379353a0

Miesenböck, G., De Angelis, D. A., & Rothman, J. E. (1998). Visualizing secretion and synaptic transmission with pH-sensitive green fluorescent proteins. *Nature*, *394*(6689), 192–195. https://doi.org/10.1038/28190

Miller, K. G., Alfonso, A., Nguyen, M., Crowell, J. A., Johnson, C. D., & Rand, J. B. (1996). A genetic selection for Caenorhabditis elegans synaptic transmission mutants. *Proceedings of the National Academy of Sciences*, *93*(22), 12593–12598. https://doi.org/10.1073/pnas.93.22.12593

Miller, T. M., & Heuser, J. E. (1984). Endocytosis of synaptic vesicle membrane at the frog neuromuscular junction. *Journal of Cell Biology*, *98*(2), 685–698. https://doi.org/10.1083/jcb.98.2.685

Milosevic, I., Giovedi, S., Lou, X., Raimondi, A., Collesi, C., Shen, H., Paradise, S., O'Toole, E., Ferguson, S., Cremona, O., & De Camilli, P. (2011). Recruitment of Endophilin to

Clathrin-Coated Pit Necks Is Required for Efficient Vesicle Uncoating after Fission. *Neuron*, *72*(4), 587–601. https://doi.org/10.1016/j.neuron.2011.08.029

Mittelstaedt, T., & Schoch, S. (2007). Structure and evolution of RIM-BP genes: Identification of a novel family member. *Gene*, *403*(1–2), 70–79. https://doi.org/10.1016/j.gene.2007.08.004

Modregger, J., Schmidt, A. A., Ritter, B., Huttner, W. B., & Plomann, M. (2003). Characterization of Endophilin B1b, a Brain-specific Membrane-associated Lysophosphatidic Acid Acyl Transferase with Properties Distinct from Endophilin A1. *Journal of Biological Chemistry*, *278*(6), 4160–4167. https://doi.org/10.1074/jbc.M208568200

Monier, S., Jollivet, F., Janoueix-Lerosey, I., Johannes, L., & Goud, B. (2002). Characterization of Novel Rab6-Interacting Proteins Involved in Endosome-to-TGN Transport: **Novel Rab6-Interacting Proteins**. *Traffic*, *3*(4), 289–297. https://doi.org/10.1034/j.1600-0854.2002.030406.x

Morgan, J. R., Prasad, K., Hao, W., Augustine, G. J., & Lafer, E. M. (2000). A Conserved Clathrin Assembly Motif Essential for Synaptic Vesicle Endocytosis. *The Journal of Neuroscience*, *20*(23), 8667–8676. https://doi.org/10.1523/JNEUROSCI.20-23-08667.2000

Mukherjee, K., Yang, X., Gerber, S. H., Kwon, H.-B., Ho, A., Castillo, P. E., Liu, X., & Südhof, T. C. (2010). Piccolo and bassoon maintain synaptic vesicle clustering without directly participating in vesicle exocytosis. *Proceedings of the National Academy of Sciences*, *107*(14), 6504–6509. https://doi.org/10.1073/pnas.1002307107

Muller, H. J. (1927). Artificial Transmutation of the Gene. *Science*, *66*(1699), 84–87. https://doi.org/10.1126/science.66.1699.84

Müller, M., Genç, Ö., & Davis, G. W. (2015). RIM-Binding Protein Links Synaptic Homeostasis to the Stabilization and Replenishment of High Release Probability Vesicles. *Neuron*, *85*(5), 1056–1069. https://doi.org/10.1016/j.neuron.2015.01.024

Nagel, G., Brauner, M., Liewald, J. F., Adeishvili, N., Bamberg, E., & Gottschalk, A. (2005). Light Activation of Channelrhodopsin-2 in Excitable Cells of Caenorhabditis elegans Triggers Rapid Behavioral Responses. *Current Biology*, *15*(24), 2279–2284. https://doi.org/10.1016/j.cub.2005.11.032

Nagel, G., Szellas, T., Huhn, W., Kateriya, S., Adeishvili, N., Berthold, P., Ollig, D., Hegemann, P., & Bamberg, E. (2003). Channelrhodopsin-2, a directly light-gated cation-selective membrane channel. *Proceedings of the National Academy of Sciences*, *100*(24), 13940–13945. https://doi.org/10.1073/pnas.1936192100

Nakata, T., Kitamura, Y., Shimizu, K., Tanaka, S., Fujimori, M., Yokoyama, S., Ito, K., & Emi, M. (1999). Fusion of a novel gene,ELKS, toRET due to translocation t(10;12)(q11;p13) in a papillary thyroid carcinoma. *Genes, Chromosomes and Cancer*, *25*(2), 97–103. https://doi.org/10.1002/(SICI)1098-2264(199906)25:2<97::AID-GCC4>3.0.CO;2-L

Nigon, V. (1949). Les modalites de la reproduction et le determinisme du sexe chez quelques nematodes libres. *Annales de Sciences Naturelles - Zool. Biol. Anim.*, *11*, 1–132.

Nonet, M. L. (1999). Visualization of synaptic specializations in live C. elegans with synaptic vesicle protein-GFP fusions. *Journal of Neuroscience Methods*, *89*(1), 33–40. https://doi.org/10.1016/S0165-0270(99)00031-X

Oda, S., Tomioka, M., & Iino, Y. (2011). Neuronal plasticity regulated by the insulin-like signaling pathway underlies salt chemotaxis learning in *Caenorhabditis elegans*. *Journal of Neurophysiology*, *106*(1), 301–308. https://doi.org/10.1152/jn.01029.2010

Oh, K. H., Krout, M. D., Richmond, J. E., & Kim, H. (2021). UNC-2 CaV2 Channel Localization at Presynaptic Active Zones Depends on UNC-10/RIM and SYD-

2/Liprin-α in *Caenorhabditis elegans*. *The Journal of Neuroscience*, *41*(22), 4782–4794. https://doi.org/10.1523/JNEUROSCI.0076-21.2021

Ohtsuka, T., Takao-Rikitsu, E., Inoue, E., Inoue, M., Takeuchi, M., Matsubara, K., Deguchi-Tawarada, M., Satoh, K., Morimoto, K., Nakanishi, H., & Takai, Y. (2002). Cast: A novel protein of the cytomatrix at the active zone of synapses that forms a ternary complex with RIM1 and munc13-1. *Journal of Cell Biology*, *158*(3), 577–590. https://doi.org/10.1083/jcb.200202083

Okazaki, A., Sudo, Y., & Takagi, S. (2012). Optical Silencing of C. elegans Cells with Arch Proton Pump. *PLoS ONE*, *7*(5), e35370. https://doi.org/10.1371/journal.pone.0035370

Opperman, K. J., Mulcahy, B., Giles, A. C., Risley, M. G., Birnbaum, R. L., Tulgren, E. D., Dawson-Scully, K., Zhen, M., & Grill, B. (2017). The HECT Family Ubiquitin Ligase EEL-1 Regulates Neuronal Function and Development. *Cell Reports*, *19*(4), 822–835. https://doi.org/10.1016/j.celrep.2017.04.003

Page, B. D., Diede, S. J., Tenlen, J. R., & Ferguson, E. L. (2007). EEL-1, a Hect E3 ubiquitin ligase, controls asymmetry and persistence of the SKN-1 transcription factor in the early *C. elegans* embryo. *Development*, *134*(12), 2303–2314. https://doi.org/10.1242/dev.02855

Pang, Z. P., & Südhof, T. C. (2010). Cell biology of Ca2+-triggered exocytosis. *Current Opinion in Cell Biology*, *22*(4), 496–505. https://doi.org/10.1016/j.ceb.2010.05.001

Paquin, N., Murata, Y., Froehlich, A., Omura, D. T., Ailion, M., Pender, C. L., Constantine-Paton, M., & Horvitz, H. R. (2016). The Conserved VPS-50 Protein Functions in Dense-Core Vesicle Maturation and Acidification and Controls Animal Behavior. *Current Biology*, *26*(7), 862–871. https://doi.org/10.1016/j.cub.2016.01.049

Pavlos, N. J., & Jahn, R. (2011). Distinct yet overlapping roles of Rab GTPases on synaptic vesicles. *Small GTPases*, *2*(2), 77–81. https://doi.org/10.4161/sgtp.2.2.15201

Pereira, L., Kratsios, P., Serrano-Saiz, E., Sheftel, H., Mayo, A. E., Hall, D. H., White, J. G., LeBoeuf, B., Garcia, L. R., Alon, U., & Hobert, O. (2015). A cellular and regulatory map of the cholinergic nervous system of C. elegans. *ELife*, *4*, e12432. https://doi.org/10.7554/eLife.12432

Perin, M. S., Fried, V. A., Mignery, G. A., Jahn, R., & Südhof, T. C. (1990). Phospholipid binding by a synaptic vesicle protein homologous to the regulatory region of protein kinase C. *Nature*, *345*(6272), 260–263. https://doi.org/10.1038/345260a0

Petrov, A. M., Zakirjanova, G. F., Kovyazina, I. V., Tsentsevitsky, A. N., & Bukharaeva, E. A. (2022). Adrenergic receptors control frequency-dependent switching of the exocytosis mode between "full-collapse" and "kiss-and-run" in murine motor nerve terminal. *Life Sciences*, *296*, 120433. https://doi.org/10.1016/j.lfs.2022.120433

Petzoldt, A. G., Götz, T. W. B., Driller, J. H., Lützkendorf, J., Reddy-Alla, S., Matkovic-Rachid, T., Liu, S., Knoche, E., Mertel, S., Ugorets, V., Lehmann, M., Ramesh, N., Beuschel, C. B., Kuropka, B., Freund, C., Stelzl, U., Loll, B., Liu, F., Wahl, M. C., & Sigrist, S. J. (2020). RIM-binding protein couples synaptic vesicle recruitment to release sites. *Journal of Cell Biology*, *219*(7), e201902059. https://doi.org/10.1083/jcb.201902059

Pinto, D., Pagnamenta, A. T., Klei, L., Anney, R., Merico, D., Regan, R., Conroy, J., Magalhaes, T. R., Correia, C., Abrahams, B. S., Almeida, J., Bacchelli, E., Bader, G. D., Bailey, A. J., Baird, G., Battaglia, A., Berney, T., Bolshakova, N., Bölte, S., … Betancur, C. (2010). Functional impact of global rare copy number variation in autism spectrum disorders. *Nature*, *466*(7304), 368–372. https://doi.org/10.1038/nature09146

Putrenko, I., Zakikhani, M., & Dent, J. A. (2005). A Family of Acetylcholine-gated Chloride Channel Subunits in Caenorhabditis elegans. *Journal of Biological Chemistry*, *280*(8), 6392–6398. https://doi.org/10.1074/jbc.M412644200

Qin, X., Tsien, R. W., & Park, H. (2019). Real-time three-dimensional tracking of single synaptic vesicles reveals that synaptic vesicles undergoing kiss-and-run fusion remain close to their original fusion site before reuse. *Biochemical and Biophysical Research Communications*, *514*(3), 1004–1008. https://doi.org/10.1016/j.bbrc.2019.05.043

Rettig, J., Sheng, Z. H., Kim, D. K., Hodson, C. D., Snutch, T. P., & Catterall, W. A. (1996). Isoform-specific interaction of the alpha1A subunits of brain Ca2+ channels with the presynaptic proteins syntaxin and SNAP-25. *Proceedings of the National Academy of Sciences*, *93*(14), 7363–7368. https://doi.org/10.1073/pnas.93.14.7363

Rikhy, R., Kumar, V., Mittal, R., & Krishnan, K. S. (2002). Endophilin Is Critically Required for Synapse Formation and Function in *Drosophila melanogaster*. *The Journal of Neuroscience*, *22*(17), 7478–7484. https://doi.org/10.1523/JNEUROSCI.22-17-07478.2002

Ringstad, N., Gad, H., Löw, P., Di Paolo, G., Brodin, L., Shupliakov, O., & De Camilli, P. (1999). Endophilin/SH3p4 Is Required for the Transition from Early to Late Stages in Clathrin-Mediated Synaptic Vesicle Endocytosis. *Neuron*, *24*(1), 143–154. https://doi.org/10.1016/S0896-6273(00)80828-4

Rizzoli, S. O., & Betz, W. J. (2005). Synaptic vesicle pools. *Nature Reviews. Neuroscience*, *6*(1), 57–69. https://doi.org/10.1038/nrn1583

Rizzoli, S. O., & Jahn, R. (2007). Kiss-and-run, Collapse and 'Readily Retrievable' Vesicles. *Traffic*, *8*(9), 1137–1144. https://doi.org/10.1111/j.1600-0854.2007.00614.x

Rose, S., Malabarba, M. G., Krag, C., Schultz, A., Tsushima, H., Di Fiore, P. P., & Salcini, A. E. (2007). Caenorhabditis elegans Intersectin: A Synaptic Protein Regulating Neurotransmission. *Molecular Biology of the Cell*, *18*(12), 5091–5099. https://doi.org/10.1091/mbc.e07-05-0460

Rostaing, P., Weimer, R. M., Jorgensen, E. M., Triller, A., & Bessereau, J.-L. (2004). Preservation of immunoreactivity and fine structure of adult C. elegans tissues using high-pressure freezing. *The Journal of Histochemistry and Cytochemistry: Official Journal of the Histochemistry Society*, *52*(1), 1–12. https://doi.org/10.1177/002215540405200101

Royle, S. J., Bright, N. A., & Lagnado, L. (2005). Clathrin is required for the function of the mitotic spindle. *Nature*, *434*(7037), 1152–1157. https://doi.org/10.1038/nature03502

Saheki, Y., & De Camilli, P. (2012). Synaptic Vesicle Endocytosis. *Cold Spring Harbor Perspectives in Biology*, *4*(9), a005645–a005645. https://doi.org/10.1101/cshperspect.a005645

Sankaranarayanan, S., De Angelis, D., Rothman, J. E., & Ryan, T. A. (2000). The Use of pHluorins for Optical Measurements of Presynaptic Activity. *Biophysical Journal*, *79*(4), 2199–2208. https://doi.org/10.1016/S0006-3495(00)76468-X

Sato, K., Ernstrom, G. G., Watanabe, S., Weimer, R. M., Chen, C.-H., Sato, M., Siddiqui, A., Jorgensen, E. M., & Grant, B. D. (2009). Differential requirements for clathrin in receptor-mediated endocytosis and maintenance of synaptic vesicle pools. *Proceedings of the National Academy of Sciences*, *106*(4), 1139–1144. https://doi.org/10.1073/pnas.0809541106

Schoch, S., Castillo, P. E., Jo, T., Mukherjee, K., Geppert, M., Wang, Y., Schmitz, F., Malenka, R. C., & Südhof, T. C. (2002). RIM1α forms a protein scaffold for regulating neurotransmitter release at the active zone. *Nature*, *415*(6869), 321–326. https://doi.org/10.1038/415321a

Schröder-Lang, S., Schwärzel, M., Seifert, R., Strünker, T., Kateriya, S., Looser, J., Watanabe, M., Kaupp, U. B., Hegemann, P., & Nagel, G. (2007). Fast manipulation of cellular

cAMP level by light in vivo. *Nature Methods*, *4*(1), 39–42. https://doi.org/10.1038/nmeth975

Schultheis, C., Brauner, M., Liewald, J. F., & Gottschalk, A. (2011). Optogenetic analysis of GABA B receptor signaling in Caenorhabditis elegans motor neurons. *Journal of Neurophysiology*, *106*(2), 817–827. https://doi.org/10.1152/jn.00578.2010

Schultheis, C., Liewald, J. F., Bamberg, E., Nagel, G., & Gottschalk, A. (2011). Optogenetic Long-Term Manipulation of Behavior and Animal Development. *PLoS ONE*, *6*(4), e18766. https://doi.org/10.1371/journal.pone.0018766

Schuske, K. R., Richmond, J. E., Matthies, D. S., Davis, W. S., Runz, S., Rube, D. A., van der Bliek, A. M., & Jorgensen, E. M. (2003). Endophilin Is Required for Synaptic Vesicle Endocytosis by Localizing Synaptojanin. *Neuron*, *40*(4), 749–762. https://doi.org/10.1016/S0896-6273(03)00667-6

Seidenthal, M., Jánosi, B., Rosenkranz, N., Schuh, N., Elvers, N., Willoughby, M., Zhao, X., & Gottschalk, A. (2022). *pOpsicle: An all-optical reporter system for synaptic vesicle recycling combining pH-sensitive fluorescent proteins with optogenetic manipulation of neuronal activity* [Preprint]. Neuroscience. https://doi.org/10.1101/2022.12.20.521193

Serrano-Saiz, E., Poole, R. J., Felton, T., Zhang, F., De La Cruz, E. D., & Hobert, O. (2013). Modular Control of Glutamatergic Neuronal Identity in C. elegans by Distinct Homeodomain Proteins. *Cell*, *155*(3), 659–673. https://doi.org/10.1016/j.cell.2013.09.052

Serra-Pagès, C., Kedersha, N. L., Fazikas, L., Medley, Q., Debant, A., & Streuli, M. (1995). The LAR transmembrane protein tyrosine phosphatase and a coiled-coil LAR-interacting protein co-localize at focal adhesions. *The EMBO Journal*, *14*(12), 2827–2838.

Shaner, N. C., Lin, M. Z., McKeown, M. R., Steinbach, P. A., Hazelwood, K. L., Davidson, M. W., & Tsien, R. Y. (2008). Improving the photostability of bright monomeric orange and red fluorescent proteins. *Nature Methods*, *5*(6), 545–551. https://doi.org/10.1038/nmeth.1209

Shaye, D. D., & Greenwald, I. (2011). OrthoList: A Compendium of C. elegans Genes with Human Orthologs. *PLoS ONE*, *6*(5), e20085. https://doi.org/10.1371/journal.pone.0020085

Shen, Y., Rosendale, M., Campbell, R. E., & Perrais, D. (2014). PHuji, a pH-sensitive red fluorescent protein for imaging of exo- and endocytosis. *Journal of Cell Biology*, *207*(3), 419–432. https://doi.org/10.1083/jcb.201404107

Sheng, Z.-H., Rettig, J., Takahashi, M., & Catterall, W. A. (1994). Identification of a syntaxin-binding site on N-Type calcium channels. *Neuron*, *13*(6), 1303–1313. https://doi.org/10.1016/0896-6273(94)90417-0

Sheng, Z.-H., Yokoyama, C. T., & Catterall, W. A. (1997). Interaction of the synprint site of N-type Ca $^{2+}$ channels with the C2B domain of synaptotagmin I. *Proceedings of the National Academy of Sciences*, *94*(10), 5405–5410. https://doi.org/10.1073/pnas.94.10.5405

Shigemoto, R., Kulik, A., Roberts, J. D. B., Ohishi, H., Nusser, Z., Kaneko, T., & Somogyi, P. (1996). Target-cell-specific concentration of a metabotropic glutamate receptor in the presynaptic active zone. *Nature*, *381*(6582), 523–525. https://doi.org/10.1038/381523a0

Silverman, G. A., Luke, C. J., Bhatia, S. R., Long, O. S., Vetica, A. C., Perlmutter, D. H., & Pak, S. C. (2009). Modeling Molecular and Cellular Aspects of Human Disease Using the Nematode Caenorhabditis elegans. *Pediatric Research*, *65*(1), 10–18. https://doi.org/10.1203/PDR.0b013e31819009b0

Söllner, T., Bennett, M. K., Whiteheart, S. W., Scheller, R. H., & Rothman, J. E. (1993). A protein assembly-disassembly pathway in vitro that may correspond to sequential steps of synaptic vesicle docking, activation, and fusion. *Cell*, *75*(3), 409–418. https://doi.org/10.1016/0092-8674(93)90376-2

Söllner, T., Whiteheart, S. W., Brunner, M., Erdjument-Bromage, H., Geromanos, S., Tempst, P., & Rothman, J. E. (1993). SNAP receptors implicated in vesicle targeting and fusion. *Nature*, *362*(6418), 318–324. https://doi.org/10.1038/362318a0

Spangler, S. A., & Hoogenraad, C. C. (2007). Liprin-α proteins: Scaffold molecules for synapse maturation. *Biochemical Society Transactions*, *35*(5), 1278–1282. https://doi.org/10.1042/BST0351278

Spangler, S. A., Schmitz, S. K., Kevenaar, J. T., de Graaff, E., de Wit, H., Demmers, J., Toonen, R. F., & Hoogenraad, C. C. (2013). Liprin-α2 promotes the presynaptic recruitment and turnover of RIM1/CASK to facilitate synaptic transmission. *Journal of Cell Biology*, *201*(6), 915–928. https://doi.org/10.1083/jcb.201301011

Steuer Costa, W., Yu, S.-C., Liewald, J. F., & Gottschalk, A. (2017). Fast cAMP Modulation of Neurotransmission via Neuropeptide Signals and Vesicle Loading. *Current Biology: CB*, *27*(4), 495–507. https://doi.org/10.1016/j.cub.2016.12.055

Stevens, D. R., Wu, Z.-X., Matti, U., Junge, H. J., Schirra, C., Becherer, U., Wojcik, S. M., Brose, N., & Rettig, J. (2005). Identification of the Minimal Protein Domain Required for Priming Activity of Munc13-1. *Current Biology*, *15*(24), 2243–2248. https://doi.org/10.1016/j.cub.2005.10.055

Südhof, T. C. (2004). THE SYNAPTIC VESICLE CYCLE. *Annual Review of Neuroscience*, *27*(1), 509–547. https://doi.org/10.1146/annurev.neuro.26.041002.131412

Südhof, T. C. (2012). The Presynaptic Active Zone. *Neuron*, *75*(1), 11–25. https://doi.org/10.1016/j.neuron.2012.06.012

Sulston, J. E., & Horvitz, H. R. (1977). Post-embryonic cell lineages of the nematode, *Caenorhabditis elegans*. *Developmental Biology*, *56*(1), 110–156. https://doi.org/10.1016/0012-1606(77)90158-0

Sulston, J., & Hodgkin, J. (1988). *Methods. In The Nematode Caenorhabditis elegans, W. B. Wood, ed. (New York: Cold Spring Harbor Laboratory)* (p. 592).

Sun, J.-Y., Wu, X.-S., & Wu, L.-G. (2002). Single and multiple vesicle fusion induce different rates of endocytosis at a central synapse. *Nature*, *417*(6888), 555–559. https://doi.org/10.1038/417555a

Sundborger, A., Soderblom, C., Vorontsova, O., Evergren, E., Hinshaw, J. E., & Shupliakov, O. (2011). An endophilin–dynamin complex promotes budding of clathrin-coated vesicles during synaptic vesicle recycling. *Journal of Cell Science*, *124*(1), 133–143. https://doi.org/10.1242/jcs.072686

Tang, J., Maximov, A., Shin, O.-H., Dai, H., Rizo, J., & Südhof, T. C. (2006). A Complexin/Synaptotagmin 1 Switch Controls Fast Synaptic Vesicle Exocytosis. *Cell*, *126*(6), 1175–1187. https://doi.org/10.1016/j.cell.2006.08.030

Tantama, M., Hung, Y. P., & Yellen, G. (2011). Imaging Intracellular pH in Live Cells with a Genetically Encoded Red Fluorescent Protein Sensor. *Journal of the American Chemical Society*, *133*(26), 10034–10037. https://doi.org/10.1021/ja202902d

Taru, H., & Jin, Y. (2011). The Liprin homology domain is essential for the homomeric interaction of SYD-2/Liprin-α protein in presynaptic assembly. *The Journal of Neuroscience: The Official Journal of the Society for Neuroscience*, *31*(45), 16261–16268. https://doi.org/10.1523/JNEUROSCI.0002-11.2011

Teng, H., Lin, M. Y., & Wilkinson, R. S. (2007). Macroendocytosis and endosome processing in snake motor boutons: Endosome processing in boutons. *The Journal of Physiology*, *582*(1), 243–262. https://doi.org/10.1113/jphysiol.2007.130989

The *C. elegans* Sequencing Consortium*. (1998). Genome Sequence of the Nematode *C. elegans*: A Platform for Investigating Biology. *Science*, *282*(5396), 2012–2018. https://doi.org/10.1126/science.282.5396.2012

Thompson, O., Edgley, M., Strasbourger, P., Flibotte, S., Ewing, B., Adair, R., Au, V., Chaudhry, I., Fernando, L., Hutter, H., Kieffer, A., Lau, J., Lee, N., Miller, A., Raymant, G., Shen, B., Shendure, J., Taylor, J., Turner, E. H., … Waterston, R. H. (2013). The million mutation project: A new approach to genetics in *Caenorhabditis elegans*. *Genome Research*, *23*(10), 1749–1762. https://doi.org/10.1101/gr.157651.113

Tolstenkov, O., Van der Auwera, P., Steuer Costa, W., Bazhanova, O., Gemeinhardt, T. M., Bergs, A. C., & Gottschalk, A. (2018). Functionally asymmetric motor neurons contribute to coordinating locomotion of Caenorhabditis elegans. *ELife*, *7*, e34997. https://doi.org/10.7554/eLife.34997

Tonikian, R., Zhang, Y., Sazinsky, S. L., Currell, B., Yeh, J.-H., Reva, B., Held, H. A., Appleton, B. A., Evangelista, M., Wu, Y., Xin, X., Chan, A. C., Seshagiri, S., Lasky, L. A., Sander, C., Boone, C., Bader, G. D., & Sidhu, S. S. (2008). A Specificity Map for the PDZ Domain Family. *PLoS Biology*, *6*(9), e239. https://doi.org/10.1371/journal.pbio.0060239

Varoqueaux, F., Sigler, A., Rhee, J.-S., Brose, N., Enk, C., Reim, K., & Rosenmund, C. (2002). Total arrest of spontaneous and evoked synaptic transmission but normal synaptogenesis in the absence of Munc13-mediated vesicle priming. *Proceedings of the National Academy of Sciences*, *99*(13), 9037–9042. https://doi.org/10.1073/pnas.122623799

Varoqueaux, F., Sons, M. S., Plomp, J. J., & Brose, N. (2005). Aberrant Morphology and Residual Transmitter Release at the Munc13-Deficient Mouse Neuromuscular Synapse.

Molecular and Cellular Biology, *25*(14), 5973–5984. https://doi.org/10.1128/MCB.25.14.5973-5984.2005

Ventimiglia, D., & Bargmann, C. I. (2017). Diverse modes of synaptic signaling, regulation, and plasticity distinguish two classes of C. elegans glutamatergic neurons. *ELife*, *6*, e31234. https://doi.org/10.7554/eLife.31234

von Mollard, G. F., Südhof, T. C., & Jahn, R. (1991). A small GTP-binding protein dissociates from synaptic vesicles during exocytosis. *Nature*, *349*(6304), 79–81. https://doi.org/10.1038/349079a0

Wabnig, S., Liewald, J. F., Yu, S., & Gottschalk, A. (2015). High-Throughput All-Optical Analysis of Synaptic Transmission and Synaptic Vesicle Recycling in Caenorhabditis elegans. *PLOS ONE*, *10*(8), e0135584. https://doi.org/10.1371/journal.pone.0135584

Wang, D. B., Kinoshita, Y., Kinoshita, C., Uo, T., Sopher, B. L., Cudaback, E., Keene, C. D., Bilousova, T., Gylys, K., Case, A., Jayadev, S., Wang, H.-G., Garden, G. A., & Morrison, R. S. (2015). Loss of endophilin-B1 exacerbates Alzheimer's disease pathology. *Brain*, *138*(7), 2005–2019. https://doi.org/10.1093/brain/awv128

Wang, L., & Audhya, A. (2014). In vivo imaging of C. elegans endocytosis. *Methods*, *68*(3), 518–528. https://doi.org/10.1016/j.ymeth.2014.03.028

Wang, M., Witvliet, D., Wu, M., Kang, L., & Shao, Z. (2021). Temperature regulates synaptic subcellular specificity mediated by inhibitory glutamate signaling. *PLOS Genetics*, *17*(1), e1009295. https://doi.org/10.1371/journal.pgen.1009295

Wang, W., Bouhours, M., Gracheva, E. O., Liao, E. H., Xu, K., Sengar, A. S., Xin, X., Roder, J., Boone, C., Richmond, J. E., Zhen, M., & Egan, S. E. (2008). ITSN-1 Controls Vesicle Recycling at the Neuromuscular Junction and Functions in Parallel with DAB-1. *Traffic*, *9*(5), 742–754. https://doi.org/10.1111/j.1600-0854.2008.00712.x

Wang, Y., Liu, X., Biederer, T., & Südhof, T. C. (2002). A family of RIM-binding proteins regulated by alternative splicing: Implications for the genesis of synaptic active zones. *Proceedings of the National Academy of Sciences*, *99*(22), 14464–14469. https://doi.org/10.1073/pnas.182532999

Wang, Y., Okamoto, M., Schmitz, F., Hofmann, K., & Südhof, T. C. (1997). Rim is a putative Rab3 effector in regulating synaptic-vesicle fusion. *Nature*, *388*(6642), 593–598. https://doi.org/10.1038/41580

Wang, Y., & Südhof, T. C. (2003). Genomic definition of RIM proteins: Evolutionary amplification of a family of synaptic regulatory proteins☆☆Sequence data from this article have been deposited with the GenBank Data Library under Accession Nos. AF548738 and AF548739. *Genomics*, *81*(2), 126–137. https://doi.org/10.1016/S0888-7543(02)00024-1

Wang, Y., Sugita, S., & Südhof, T. C. (2000). The RIM/NIM Family of Neuronal C2 Domain Proteins. *Journal of Biological Chemistry*, *275*(26), 20033–20044. https://doi.org/10.1074/jbc.M909008199

Watanabe, S., Liu, Q., Davis, M. W., Hollopeter, G., Thomas, N., Jorgensen, N. B., & Jorgensen, E. M. (2013). Ultrafast endocytosis at Caenorhabditis elegans neuromuscular junctions. *ELife*, *2*, e00723. https://doi.org/10.7554/eLife.00723

Watanabe, S., Mamer, L. E., Raychaudhuri, S., Luvsanjav, D., Eisen, J., Trimbuch, T., Söhl-Kielczynski, B., Fenske, P., Milosevic, I., Rosenmund, C., & Jorgensen, E. M. (2018). Synaptojanin and Endophilin Mediate Neck Formation during Ultrafast Endocytosis. *Neuron*, *98*(6), 1184-1197.e6. https://doi.org/10.1016/j.neuron.2018.06.005

Watanabe, S., Rost, B. R., Camacho-Pérez, M., Davis, M. W., Söhl-Kielczynski, B., Rosenmund, C., & Jorgensen, E. M. (2013). Ultrafast endocytosis at mouse

hippocampal synapses. *Nature*, *504*(7479), 242–247. https://doi.org/10.1038/nature12809

Watanabe, S., Trimbuch, T., Camacho-Pérez, M., Rost, B. R., Brokowski, B., Söhl-Kielczynski, B., Felies, A., Davis, M. W., Rosenmund, C., & Jorgensen, E. M. (2014). Clathrin regenerates synaptic vesicles from endosomes. *Nature*, *515*(7526), 228–233. https://doi.org/10.1038/nature13846

Wei, Z., Zheng, S., Spangler, S. A., Yu, C., Hoogenraad, C. C., & Zhang, M. (2011). Liprin-Mediated Large Signaling Complex Organization Revealed by the Liprin-α/CASK and Liprin-α/Liprin-β Complex Structures. *Molecular Cell*, *43*(4), 586–598. https://doi.org/10.1016/j.molcel.2011.07.021

Weimer, R. M. (2006). Preservation of C. elegans tissue via high-pressure freezing and freeze-substitution for ultrastructural analysis and immunocytochemistry. *Methods in Molecular Biology (Clifton, N.J.)*, *351*, 203–221. https://doi.org/10.1385/1-59745-151-7:203

Weissenberger, S., Schultheis, C., Liewald, J. F., Erbguth, K., Nagel, G., & Gottschalk, A. (2011). PACα- an optogenetic tool for in vivo manipulation of cellular cAMP levels, neurotransmitter release, and behavior in Caenorhabditis elegans: Optogenetic manipulation of cAMP levels using PACα. *Journal of Neurochemistry*, *116*(4), 616–625. https://doi.org/10.1111/j.1471-4159.2010.07148.x

Wen, X., Saltzgaber, G. W., & Thoreson, W. B. (2017). Kiss-and-Run Is a Significant Contributor to Synaptic Exocytosis and Endocytosis in Photoreceptors. *Frontiers in Cellular Neuroscience*, *11*, 286. https://doi.org/10.3389/fncel.2017.00286

White, J. G., Albertson, D. G., & Anness, M. A. R. (1978). Connectivity changes in a class of motoneurone during the development of a nematode. *Nature*, *271*(5647), 764–766. https://doi.org/10.1038/271764a0

White, J. G., Southgate, E., Thomson, J. N., & Brenner, S. (1976). The structure of the ventral nerve cord of *Caenorhabditis elegans*. *Philosophical Transactions of the Royal Society of London. B, Biological Sciences*, *275*(938), 327–348. https://doi.org/10.1098/rstb.1976.0086

White, J. G., Southgate, E., Thomson, J. N., & Brenner, S. (1986). The structure of the nervous system of the nematode Caenorhabditis elegans. *Philosophical Transactions of the Royal Society of London. Series B, Biological Sciences*, *314*(1165), 1–340. https://doi.org/10.1098/rstb.1986.0056

Witvliet, D., Mulcahy, B., Mitchell, J. K., Meirovitch, Y., Berger, D. R., Wu, Y., Liu, Y., Koh, W. X., Parvathala, R., Holmyard, D., Schalek, R. L., Shavit, N., Chisholm, A. D., Lichtman, J. W., Samuel, A. D. T., & Zhen, M. (2021). Connectomes across development reveal principles of brain maturation. *Nature*, *596*(7871), 257–261. https://doi.org/10.1038/s41586-021-03778-8

Wong, A. S. L., Lee, R. H. K., Cheung, A. Y., Yeung, P. K., Chung, S. K., Cheung, Z. H., & Ip, N. Y. (2011). Cdk5-mediated phosphorylation of endophilin B1 is required for induced autophagy in models of Parkinson's disease. *Nature Cell Biology*, *13*(5), 568–579. https://doi.org/10.1038/ncb2217

Wong, M. Y., Liu, C., Wang, S. S. H., Roquas, A. C. F., Fowler, S. C., & Kaeser, P. S. (2018). Liprin-α3 controls vesicle docking and exocytosis at the active zone of hippocampal synapses. *Proceedings of the National Academy of Sciences*, *115*(9), 2234–2239. https://doi.org/10.1073/pnas.1719012115

Wood, A. J., Lo, T.-W., Zeitler, B., Pickle, C. S., Ralston, E. J., Lee, A. H., Amora, R., Miller, J. C., Leung, E., Meng, X., Zhang, L., Rebar, E. J., Gregory, P. D., Urnov, F. D., & Meyer, B. J. (2011). Targeted Genome Editing Across Species Using ZFNs and TALENs. *Science*, *333*(6040), 307–307. https://doi.org/10.1126/science.1207773

Wu, X., Cai, Q., Shen, Z., Chen, X., Zeng, M., Du, S., & Zhang, M. (2019). RIM and RIM-BP Form Presynaptic Active-Zone-like Condensates via Phase Separation. *Molecular Cell*, *73*(5), 971-984.e5. https://doi.org/10.1016/j.molcel.2018.12.007

Wu, X.-S., Lee, S. H., Sheng, J., Zhang, Z., Zhao, W.-D., Wang, D., Jin, Y., Charnay, P., Ervasti, J. M., & Wu, L.-G. (2016). Actin Is Crucial for All Kinetically Distinguishable Forms of Endocytosis at Synapses. *Neuron*, *92*(5), 1020–1035. https://doi.org/10.1016/j.neuron.2016.10.014

Xuan, Z., Manning, L., Nelson, J., Richmond, J. E., Colón-Ramos, D. A., Shen, K., & Kurshan, P. T. (2017). Clarinet (CLA-1), a novel active zone protein required for synaptic vesicle clustering and release. *ELife*, *6*, e29276. https://doi.org/10.7554/eLife.29276

Yizhar, O., Fenno, L. E., Davidson, T. J., Mogri, M., & Deisseroth, K. (2011). Optogenetics in Neural Systems. *Neuron*, *71*(1), 9–34. https://doi.org/10.1016/j.neuron.2011.06.004

Yu, D., & Davis, R. L. (2012). Functional Imaging of Antennal Lobe Neurons in Drosophila with Synapto-pHluorin. In J.-R. Martin (Ed.), *Genetically Encoded Functional Indicators* (Vol. 72, pp. 71–81). Humana Press. https://doi.org/10.1007/978-1-62703-014-4_4

Yu, S., Jánosi, B., Liewald, J. F., Wabnig, S., & Gottschalk, A. (2018). Endophilin A and B Join Forces With Clathrin to Mediate Synaptic Vesicle Recycling in Caenorhabditis elegans. *Frontiers in Molecular Neuroscience*, *11*, 196. https://doi.org/10.3389/fnmol.2018.00196

Zahreddine, H., Zhang, H., Diogon, M., Nagamatsu, Y., & Labouesse, M. (2010). CRT-1/Calreticulin and the E3 Ligase EEL-1/HUWE1 Control Hemidesmosome Maturation in C. elegans Development. *Current Biology*, *20*(4), 322–327. https://doi.org/10.1016/j.cub.2009.12.061

Zhang, F., Wang, L.-P., Brauner, M., Liewald, J. F., Kay, K., Watzke, N., Wood, P. G., Bamberg, E., Nagel, G., Gottschalk, A., & Deisseroth, K. (2007). Multimodal fast optical interrogation of neural circuitry. *Nature*, *446*(7136), 633–639. https://doi.org/10.1038/nature05744

Zhang, Q., Li, Y., & Tsien, R. W. (2009). The Dynamic Control of Kiss-And-Run and Vesicular Reuse Probed with Single Nanoparticles. *Science*, *323*(5920), 1448–1453. https://doi.org/10.1126/science.1167373

Zhang, S., Li, F., Zhou, T., Wang, G., & Li, Z. (2020). Caenorhabditis elegans as a Useful Model for Studying Aging Mutations. *Frontiers in Endocrinology*, *11*, 554994. https://doi.org/10.3389/fendo.2020.554994

Zhao, Y., Araki, S., Wu, J., Teramoto, T., Chang, Y.-F., Nakano, M., Abdelfattah, A. S., Fujiwara, M., Ishihara, T., Nagai, T., & Campbell, R. E. (2011). An Expanded Palette of Genetically Encoded Ca^{2+} Indicators. *Science*, *333*(6051), 1888–1891. https://doi.org/10.1126/science.1208592

Zhen, M., & Jin, Y. (1999). The liprin protein SYD-2 regulates the differentiation of presynaptic termini in C. elegans. *Nature*, *401*(6751), 371–375. https://doi.org/10.1038/43886

Zhen, M., & Samuel, A. D. T. (2015). C. elegans locomotion: Small circuits, complex functions. *Current Opinion in Neurobiology*, *33*, 117–126. https://doi.org/10.1016/j.conb.2015.03.009

List of Publications

Yu SC, **Jánosi B**, Liewald JF, Wabnig S, Gottschalk A. Endophilin A and B join forces with clathrin to mediate synaptic vesicle recycling in Caenorhabditis elegans. Frontiers in molecular neuroscience. 2018 Jun 14;11:196. (equal first author)

Jánosi B, Liewald JF, Yu SC, Umbach S, Alcantara IC, Bergs AC, Schneider M, Shao J, Gottschalk A. RIM and RIM-binding protein localize synaptic Cav2 channels in a differential manner to regulate transmission in neuronal circuits. bioRxiv. 2021 Feb 2:2021-02. (preprint publication)

Seidenthal M, **Jánosi B**, Rosenkranz N, Schuh N, Elvers N, Willoughby M, Zhao X, Gottschalk A. pOpsicle: An all-optical reporter system for synaptic vesicle recycling combining pH-sensitive fluorescent proteins with optogenetic manipulation of neuronal activity. Frontiers in Cellular Neuroscience. 2023 Mar 31;17:1120651.

Acknowledgements

I spent almost five years in the Gottschalk Lab, and it was sometimes wonderful, sometimes stressful but every day was a great experience. During these years I learned a lot of methods, I got to know excellent people and I had a chance to work in a great international atmosphere; I am very thankful for all of these things.

Alexander, thank you for the opportunity to work in your Lab and especially thank you for your support and all the time that you spent on our discussions. I found it really good, that you always had an open ear for new ideas and an open door for spontaneous meetings. I liked a lot when you told us stories about your PhD and career, and it was great to have a supervisor who is truly enthusiastic about science.

Jana, thank you that you were always ready to help in any kind of projects and thank you for all your advice. I appreciate our nice lunches and conference days, which we spent together, a lot.

Szi-chieh, thank you for teaching me the TEM methods and for the interesting conversations during the long freezing sessions.

Wagner, thank you for the motivating discussions and for your never-ending patience.

Thilo, Frank, Max, Amelie, Marcial and Dennis, thank you for being the very best PhD colleagues for a long time.

Marius and Simon, thank you for showing me, how motivating it is to work with motivated master students.

Alexandra, Negin, Liese and Bojana, thank you for the delicious salad lunches during the first couple of years. I always felt welcome, although back than my german knowledge was not yet the best.

Tina, thank you for showing me, that a scientific career is also possible with a child.

Franzi, Oleg, Petrus, Martin, Jiajie, Holger, Heike and every other former or present Lab member and student who I might have forgotten, thank you for contributing to the nice atmosphere of the Lab.

Last, but not least I would like to say a big thank to my family: my father, who introduced me into science already as a child and always supported my scientific career, my mother who always helped me during my studies and career, my husband, who always believed in me and my little daughter, who reminds me every day what the real values in life are.